Electrical and Optical Properties of Novel Phthalocyanine Compounds for Sensor Devices

James Richard Exley

A thesis submitted in partial fulfilment of the requirements of
Sheffield Hallam University
for the degree of Doctor of Philosophy

November 1995

Any pages, tables, figures or photographs, missing from this digital copy, have been excluded at the request of the university.

PAGE

NUMBERING

AS ORIGINAL

BEST COPY

AVAILABLE

TEXT IN ORIGINAL IS CLOSE TO THE EDGE OF THE PAGE

Contents

Acknowledgements

I should briefly like to acknowledge the large number of people who have contributed a great deal to this programme of work in various manners.

Firstly, sincere thanks are due to Professor A K Ray, without whom, as the saying goes, none of this would have been possible; and whose continued support and guidance over the past three years have proven invaluable; also to Drs. J. Silver and S C Thorpe for supplying a greatly appreciated combination of experimental materials and advice. Thanks are also due to my colleagues within the Electronics and Fibre-Optics Research Group, who through their combination of advice, friendship and good humour have contributed greatly to my time here in many ways. I am particularly grateful to my parents for their support at all stages of the work.

I feel obliged also to mention my three specimens of *N. hollandicus*, as they have unfailingly caused me a great deal of welcome amusement and diversion whilst working at home. Long may they continue to do so.

Abstract

Abstract

UV/visible spectrophotometry measurements, together with measurement of the temperature dependence of ac parameters G (conductance), C (capacitance) and tan (dielectric loss) for 20Hz<f<1MHz, and dc conduction, for 77K<T<300K, are performed for a number of vacuum-sublimed phthalocyanine compounds.

Steady state electrical measurements and optical absorption experiments were performed on samples of sublimed heavy fraction rare-earth element, fluorochromium and lutetium bisphthalocyanine films. From the Arrhenius plot of ln(T) (where (T) is the conductivity at temperature T) it is found that two conduction regimes exist. The activation energy in the order 0.2eV at high temperatures (T > 162K) relates to the distance of singlet states below the conduction band. The low temperature activation energy indicates hopping conduction between localised states close to the Fermi level..

Visible optical absorption and transmission spectra are obtained for 50nm thick sublimed films of heavy fraction rare-earth [HF(pc)(pc*)], gadolinium [Gd(pc)(pc*)] and thulium [Tm(pc)(pc*)] bisphthalocyanine compounds when they have undergone the post-deposition treatments of voltage-cycling to blue, voltage cycling to red and annealing at 393K for one hour; also for untreated fluorochromium phthalocyanine. The different post-deposition treatments produce different effects on the absorption spectra; in the case of annealing, this is attributed to the phase changes occurring in the films. The changes due to the voltage cycling are believed to be a result of oxidation processes taking place in the materials. Absorption data are also analysed in order to obtain information regarding the dispersion of refractive index and dielectric constants within optical frequency range. Absorption data are analysed in terms of a well known power law, and a value of 2.3eV is found for the optical gap E_0. in HF (pc)(pc*)

Chapter One

Introduction

Introduction

Phthalocyanines (Pc's) are organic dye materials. Metal-free phthalocyanine, H_2Pc ($C_{32}H_{18}N_8$) is a plane ring molecule consisting of four benzene rings symmetrically positioned about an inner porphyrin ring. (Fig. 2.1). The two central hydrogen atoms may be substituted with any metal in the Periodic Table. Pc's are generally thermally and chemically stable. They exhibit a variety of physical, electrical, p-type semiconductor and optical properties which render them of interest as gas and optical sensors, photovoltaic cells and other electronic devices. Various methods are available for their preparation into thin films. The structure and morphology of such films are dependent on the deposition conditions and method used, and affect the film properties considerably, offering wide scope for the manufacture of a thin-film device corresponding to individual requirements for use.

This project has been undertaken as a result of the current interest in "alternative" semiconductor technologies, with a view to improvement over, or expansion on, the capabilities of the more traditional lines of semiconductor materials, most obviously silicon and to a lesser extent gallium arsenide, germanium etc. Devices fabricated using organic semiconductor materials have already seen promising research into possible applications as sensors and transducers - electrophilic gas concentration and light intensity to current, and applied voltage to film colour.

Naturally before any such device may obtain a commercial or laboratory-based application, it is expedient that the properties of the semiconductor material involved should be fully characterised in the presence of whatever electrode materials and configurations be used. These data are necessary to ensure operational stability, reliability and reproducibility under all prospective conditions.

It is necessary to establish the behaviour of this type of material under many types of controlled conditions; temperature, humidity, oxygen content and presence of trace gases in its vicinity, together with intensity and wavelength of any illuminating radiation. However, the issue is further complicated by the fact that altering one environmental parameter of the material may modify its response to one or more of the others. For

example, the response of phthalocyanines to gas detection is influenced to a greater or lesser extent by the presence of oxygen in ambient, and the spectral photoresponse of a bisphthalocyanine film will be modified by voltage cycling-induced redox processes.

In order to use a device fabricated from such a material for a specified purpose, it follows that all parameters to which it is susceptible must either be strictly controlled, or else some associated electronics used whose purpose is to provide continuous compensation for effects of undesirable parameters. Obviously the latter proposition is the more practical, but requires a full and prior understanding of the material properties to implement.

A battery of tests has therefore been performed, the sum of which is to elucidate and quantify the electronic processes taking place in certain examples of the bisphthalocyanine family of materials. It is to be hoped that the information thus gained will be of value to future workers attempting to fabricate viable sensor or other electronic components from them.

Chapter Two discusses the current state of work in elucidating phthalocyanine compounds, and describes the results obtained by other workers in areas including the parameters investigated. This also allows comparison of our result with those previously published for similar compounds.

Chapter Three outlines the theoretical background to the work, and outlines the mathematical and physical methods by which the analysis of the results was obtained.

Chapter Four describes the design and construction of the experimental measurement system, and the principles of its operation, together with ancillary procedures relating to preparation and handling of the material samples used.

Chapter Five is dedicated to describing the results of the experiments and their analysis in terms of the theoretical work presented in Chapter Three. Detailed descriptions of the characterisations we have carried out are presented.

Chapter Six concludes the work with a discussion of our results and their relevance to present and further work.

Chapter 2

Literature Review

2.1. Introduction

In this Chapter, we shall investigate and describe some of the previous work performed upon phthalocyanines, in order to illustrate the properties so far elucidated, and to present our case for continuation of work on these materials. Manufacture, purification, thin-film deposition, electrical, optical and sensor properties will be discussed, together with the relevance of such properties to possible use in commercial devices. Properties which might hinder particular applications are also discussed, in order to draw attention to further characterisation which may be required before application of certain of the materials becomes feasible.

2.2 Synthesis

As a historical note, synthesis of phthalocyanine was originally performed by accident in 1928, during an attempt to prepare phthalimide, though much work has since been performed in determining appropriate methods of synthesis.

The most common method of preparing phthalocyanines (Nalwa and Vasudevan, 1983) is by reacting phthalonitrile and the chloride of the required metal at 573K, then extracting the product with ethanol to remove all traces of phthalonitrile. Purification may be effected by means of treatment with NaOH followed by HCl, then finally heating under vacuum at a temperature sufficient to sublime off all the impurities remaining, or by means of a sublimation furnace.

Preparation of metal-free Pc (Vincett *et. al.* 1981) may be achieved by first recrystallising dimethyl formamide and water to form phthalonitrile, then refluxing in 2-dimethylaminoethanol to give a 50% yield of β-phthalocyanine.

Cook *et. al.* (1987) report synthesis of hydrophilic chain substituted phthalocyanaines for specific use in Langmuir-Blodgett deposition, illustrating how readily particular variants of the standard metal-free phthalocyanine may be synthesised.

2.3. Bulk Crystalline Forms

There are three characterised forms of bulk metal-free phthalocyanine crystals (Eley and Parfitt 1955) referred to as α, β and γ. These are stable in differing temperature regions. The α and β forms have been characterised by means of X-ray diffraction (Lucia and Verderame, 1968) for H_2Pc, CuPc, NiPc, CoPc and ZnPc, Reversion to the β form takes place after annealing, confirming the αto be stable at "room temperature" but not at temperatures above the region of 393K.

α-phthalocyanine is reported to form randomly oriented microcrystallites, and has been shown by X-ray diffraction (Collins and Mohammed (1986)) to be polycrystalline in nature.

The crystal structure for the β form has been characterised as monoclinic (Robertson, 1935), with two molecules per unit cell. The monoclinic form exhibits "whisker growth" of long, needle-like crystals; these may be prepared by entrainer sublimation. Thicknesses obtained by this method are in the region of 0.1μm to several μm.

Triclinic or γ phthalocyanine is the third form. This may be converted to the β form by extensive milling in the presence of NaCl.

A fourth form of phthalocyanine crystal referred to as "x" has been claimed.

X-ray diffraction allows the elucidation of crystal structures by diagnosis of the intermolecular spacings present in the crystal. In addition to allowing differentiation of one crystalline form from another by measurement of these spacings, it is possible also to determine the crystal orientation in a thin film. Spacings of 12.8Å for α crystals and 12.4Å for the β form of phthalocyanine were reported by Lucia and Verderame (1968)

Preparation of the two forms was effected as follows. The α form may be prepared as a thin film by sublimation onto fused silica at 423-453K in vacuum of less than $3x10^{-5}$ torr, the β form by sublimation at 588-613K at 5-10 torr. The latter rarely yields pure β crystals so the process is usually followed by heat treatment at a temperature above 573K. The crystalline form may be determined by comparison of the transmission spectra for the two forms as follows:

Visible spectra for mixed crystals of the two forms often exhibit Davydov or observed exciton splitting (Davydov, 1962). This property is recognised by two (or more) peaks being present in the envelope of an absorption peak, and illustrates the difference in peak absorbed photon energy between the various forms, which occurs as a result of the variations in intermolecular forces resulting from differing spacing and structure of the molecular arrangement in the crystal types. The relative peak intensities can be used to give an idea of the relative proportion of the types either in solution or in a thin film

2.4. Thin Film Deposition Processes

For a number of reasons, it is often beneficial to deposit a thin film of phthalocyanine onto a suitable substrate for electrical or optical testing. The thinner a sample of material can be made, the higher the current density which may be induced through the thickness of the film. It is, for example, desirable in the photogeneration of carriers to present as high a field density as possible to the material; additionally, as will be described later, the ratio of film thickness to exciton diffusion length and depletion layer width is significant in the quantity of short-circuit photocurrent and open-circuit photovoltage observed.

The various deposition techniques in use are respectively suitable for manufacturing thin film samples of differing thickness, structure and macroscopic properties. By prior selection of a particular type of deposition and its associated conditions, is should be possible to manufacture a film to whatever criteria are required by the experimenter. However, it is possible that some materials lend themselves to deposition by particular processes better than others. The phthalocyanines, having high thermal stability, are almost universally suitable for vacuum and ion cluster beam deposition. However, owing to the lack of solubility of some classes of the group (for example H_2Pc) in organic solvents, it is not possible to carry out Langmuir-Blodgett deposition with many of them. An overview of the processes follows.

2.4.1 Vacuum Evaporation

Vacuum evaporation (otherwise known as vacuum sublimation or deposition) is a method of preparing a relatively thick film coating of phthalocyanine. It is possible on account of the thermal stability of the phthalocyanines up to ca. 750-800 K, as considerable heat is used in the sublimation process. The material must be chemically stable at temperatures in excess of that at which it sublimes under vacuum; this condition is here satisfied, as the temperatures necessary to evaporate phthalocyanines are commonly between 523K and 623K. The process is to place a crucible full of crystalline Pc within a tungsten or tantalum basket connected to a variable low-voltage (ca. 10V), high current supply (in the order of 25-100A). A light plug of glass wool is placed in the crucible to prevent the escape of large pieces of the compound which may be forcibly ejected ("spit") from the crucible by the expansion of trapped gaseous phthalocyanine during heating and contaminate the substrate. A clean substrate is placed above the crucible, at the maximum possible distance from the source. Approximately 10-20 cm is permissible in the average small laboratory system such as the apparatus used in this work, with a bell-jar of diameter approximately 40cm.

In the absence of any physical constraint, the ejection of evaporated material is omnidirectional, and film thickness will be uniform over the surface of a theoretical sphere whose centre is the evaporation source. It is therefore expedient to place the substrate as far away from the source as the chamber design will allow, in order that the radius of this "sphere" be so large that the flat surface of the substrate becomes a reasonable approximation to it. Additionally, it is easier to effect cooling of the substrate at a greater distance from the heat source of the boat.

Before deposition, it is necessary to ensure absolute cleanliness of the boat and substrate, so as to avoid contamination in the former case and inhomogeneous film quality in the latter. Cleaning methods will be described here, although they are equally applicable to those for Langmuir-Blodgett substrates. The substrate is ultrasonically cleaned in a variety of solvents; for example a sequence might consist of 1,1,1-trichloroethane, isopropanol and acetone. After each of these, the substrate is removed with forceps and

blown dry in a stream of dry nitrogen gas, and then ultrasonically washed in ultrapure ("Millipore") water and dried again. After the final rinse and dry, the substrate is placed in a dust-free environment until required for use. The cleaning process is schematically illustrated in Fig. 2.2.

This system is enclosed in a vacuum chamber which is then pumped down to approximately 10^{-5} torr. Current is then gradually applied to the basket, causing the phthalocyanine to sublime onto the substrate. The thickness of the evaporated film may be monitored by a quartz crystal monitor. This comprises a quartz wafer whose natural frequency of oscillation varies according to the thickness of layer present on its surface. Once deposition has occurred to the required thickness, the power is reduced to zero and the system left to cool for approximately 30 minutes whilst still under vacuum. Should air be injected before the system, boat and substrates have cooled to approximately room temperature, rapid oxidation of the hot surfaces may cause contamination throughout the system.

Air is now bled into the system, the bell jar removed and the substrates removed and stored for use. It is prudent to clean the system after each operation, so as to reduce the risk of contamination and also because compounds may bake onto the inside surface of the bell jar with successive usage. They are subsequently far more difficult to remove than freshly-deposited materials. The vacuum deposition system schematic is presented in Fig. 2.3.

The vacuum evaporation conditions should be carefully monitored and recorded; it will shortly become apparent that these conditions are important in all the structural, electrical and optical properties of the material film, and it must be borne in mind that there is no guarantee of reproducibility between samples of the same type if the evsporation parameters are not identical for the two.

The background pressure of the vacuum chamber and the evaporation rate were demonstrated to be important parameters in the *electronic properties* of copper phthalocyanine (Gould, 1986). Current density - temperature measurements were performed at constant voltage upon various films, evaporated at ratios of chamber pressure to deposition ratio of 2.6×10^{4} to 1.3×10^{9} Pa m-1s. There was a decrease in

mobility from 10^{-6} to 10^{-8} $m^2v^{-1}s^{-1}$ and an increase in trapping concentration from $5x10^{22}$ to $6x10^{24}$ m^{-3} as the pressure to evaporation rate ratio was increased. Results are presented in Fig. 2.4. The decrease in mobility was attributed to additional scattering of carriers in the film by the incorporation of impurity molecules, predominantly nitrogen and oxygen. Also the number of potential trapping centres increases. It is estimated that under the most favourable conditions, 40% impurity to Pc may arrive at the substrate, and under less favourable ones, the impurity may be four orders of magnitude more common than the Pc. This effect is largely independent of the type of phthalocyanine used, and the effect may reasonably be extrapolated to (at least) other members of this class of compounds.

The effect of deposition conditions upon the *crystalline composition* of films of H_2, Cu, Ni, Co and Zn Pc's has also been described (Lucia and Verderame, 1968). To obtain the α form, the sublimation was carried out at 523K-543K in vacuo of less than 10^{-5} torr. Sublimation in an inert gas atmosphere (Ar or N_2) at 5-10 torr, with the substrate maintained at 588-623K provided a mixture of α and β forms, complete conversion to β form being effected by holding the sample at T>573K and annealing for several hours. The relative quantities of α and β forms obtained in the film may be determined by Gaussian fitting of the absorption peaks. This method is discussed more fully in the relevant section of this Chapter.

2.4.2 Ion Cluster Beam Deposition

Copper phthalocyanine films have been prepared by ion cluster beam deposition (Fejfar and Biederman, 1992) with the main aim of characterising the effects of the beam energy on the films.

The principle of ion cluster beam deposition (proposed by Tagaki et. al. (1975) is to load the material to be deposited into a crucible which is then sealed, the only outlet being a nozzle of roughly 0.5mm diameter, and to heat the crucible under high vacuum in the order of 10^{-6} torr until the saturated vapour pressure reaches several torr. The vapour cools adiabatically as it passes through the nozzle, and the molecules condense

into weakly coupled clusters. This cluster beam is ionised by bombardment from an electron beam, and then accelerated by an electrostatic potential difference. (Fig. 2.5) When clusters hit the substrate, they disintegrate and the molecules participate in the film growth.

A number of factors in favour of this technique are presented by Ishida *et al.* (1976), notably that there is improved adhesion of the film to the substrate due to cleaning of the substrate surface by the ion bombardment, formation of an interfacial layer between film and substrate, and evaporation of contaminants due to the high substrate temperature achieved by the conversion of the bombarding ions' momentum to thermal energy. (It is possible to vary the substrate temperature by balancing the energy of bombardment and cooling water flow to the substrate.)

One notable disadvantage is the non-uniformity of large deposited areas, owing to the mechanism of deposition. Langmuir-Blodgett deposition gives, under optimum conditions, a perfectly uniform layer over the area deposited, and vacuum sublimation provides a good approximation to a homogeneous layer, with a tendency to be very marginally thicker in the centre. However, ICB by principle originates only a slightly divergent beam from the crucible nozzle, with the thickness deposited falling off dramatically outside the area subtended by the ion cluster beam. It is therefore difficult to provide uniform coverage of large areas with this method. This factor is however unimportant in manufacture of single small devices, in which case the advantages far outweigh the disadvantages.

A number of other factors in favour of this technique are presented by Ishida *et al.* (1976), notably that there is improved adhesion of the film to the substrate due to cleaning of the substrate surface by the ion bombardment, formation of an interfacial layer between film and substrate, and evaporation of contaminants due to the high substrate temperature achieved by the conversion of the bombarding ions' momentum to thermal energy.

With CuPc, it was found that with increasing energy the film colour changed (possibly due to the increased oxygen content reported) and the films became more durable (similar vacuum sublimed samples are soluble in xylene, but high energy ICB deposits are

not). Some cross linking of the molecules is proposed to have occurred. Morphology, structure and property investigation of the coatings showed that higher energy deposits tended to be smoother, more ordered and more finely crystalline. They were also seen to have increased oxygen content, but no chemical modification to the constituent molecules was readily observed. ICB deposition can therefore produce CuPc films in a very well defined way, and should it latterly be possible to characterise the effect of deposition energy on oxygen content, there is an application in gas sensing devices where the oxygen content of the material is in some cases a significant factor in response to other gases, and a known value would assist in their manufacture.

2.4.3 Langmuir-Blodgett Technique.

The principle of Langmuir-Blodgett (LB) film deposition depends upon the property of polar molecules to form a monolayer on the surface of a suitable subphase. The process is graphically presented in Fig. 2.6. The earliest recorded experiment in this area was that carried out by Benjamin Franklin in 1765, who applied a small quantity of oil to the surface of a lake, established the area covered by the monolayer and hence calculated one of the dimensions of the molecule.

The next reported experiment of this type was by Agnes Pockels (1891) who constrained a monolayer (reportedly in the kitchen sink) by means of a barrier system, pioneering the currently popular method of surface pressure maintenance.

Investigations on the effect of confining such a monolayer were then carried out by Irving Langmuir and Katharine Blodgett. Their first joint paper on the work was published in 1937, although both had independently published previous work; Langmuir in 1917 and Blodgett in 1934/5. The principles which they established for the operation of the Langmuir-Blodgett coating process were as follows. Beginning for the sake of argument with a crystalline material, first a solvent must be found in which the material should dissolve but not chemically react. It is also desirable that the solvent should be volatile ie. evaporate quickly after application to the subphase.

A solution of the material is made, and a suitable volume of this is spread onto the subphase surface and allowed to form a monolayer. The solvent evaporates and a monolayer of the pure compound remains.

The state of the monolayer at this point is usually described as a two-dimensional gas analogue. This is not suitable for deposition, which requires a tightly packed ordered layer of material at the air/subphase interface. The purpose of the Langmuir-Blodgett trough is to enable one to contain the monolayer and control its area and hence the surface pressure of the material. When the monolayer is compressed, the increase of the surface pressure is seen to obey three regimes, corresponding to phase changes in the two-dimensional analogue. The rate of increase of surface pressure with decrease of area increases as the material transfers from 2D gas to liquid to solid, and if constriction of the area continues, the surface pressure will fall off as the film collapses. Fig.2.7 illustrates a typical pressure-area isotherm for H_2Pc.

When a suitable surface pressure to produce the solid phase has been found, this pressure is maintained and a substrate introduced. This can take the form of a glass slide, which can be made either hydrophobic or hydrophilic by pretreatment. If the substrate is hydrophobic, then slowly lowering the substrate into the water with the surfaces perpendicular to the water surface will cause a monolayer of the material to attach to the substrate.

Advantages of the L-B method are that very thin, very ordered films (as thin as one molecular diameter) can be produced.

In order to prepare a film to particular requirements, it is necessary to examine the structural properties of the material prior to and after deposition. The pressure-area isotherm provides only a rough indication of subphase quality and cleanliness.

Fabrication of L-B films of phthalocyanines is described by (Mukhopadhyay and Ray, 1992) who ascertained that the electronic and optical properties were related to molecular orientation in the layer. Optical absorption of a polarised light source was used to investigate preferential ordering within the monolayers. Raw phthalocyanine is not suitable for L-B deposition, being insoluble or only slightly soluble in most of the solvents suitable for the process. However, certain substituted materials do prove to be

suitable; subsitution of alkyl sidechains to the phthalocyanine ring has been used to achieve better amphiphilicity.

L-B deposition characterisation of a large number of substituted amphiphilic phthalocyanines has been presented by Cook *et. al.* who investigated (1987) 1,4,8,11,15,18-hexa-alkyl-22,25-bis(carboxypropyl)phthalocyanines and (1988) a series of eight 1, 4, 8, 11, 13, 18, 22, 25 - octa-alkoxyphthalocyanines, designed specifically with Langmuir-Blodgett deposition in mind. The best film quality was seen for octabutyloxy and octapentyloxy chains. X-ray diffraction data corresponded well to the theoretical film structure obtained from the space-filling model. Cook et.al. (1994), in continuation of this work, presented data on a further family of newly-synthesised materials of the same type. This work illustrated the importance of amphiphilism of the molecule on viability of L-B deposition, together with effects of the substituent chain lengths on film ordering. Poor films were obtained from those materials with long sidechains, suggesting that these chains were disruptive to surface ordering. Conversely, where the chains were shorter, closer ordering was observed. In addition to this, consistently better deposition results were obtained for metallated derivatives than for metal-free materials.

The ordering in the films modified the broadness of the Q-band in the materials' optical absorption spectra, with more disordered films exhibiting a broadening in this band compared to the more ordered structures. It was suggested that close control of molecular packing in these materials could be effected by modification of these substituent chains, allowing selection of desirable gas sensing and optical absorption properties. The effects of the former are discussed more fully in the section of this Chapter concerning gas sensing, but the reasons for modification of the electronic absorption are rather less obvious. It is postulated that in future the matter may prove to be of note in laser-addressed data storage systems, allowing integration of multilayers, with each addressable by a specific wavelength which does not affect the remainder.

The structure and morphology of L-B films of Cu-t-Bu_4PC was elucidated by Brynda *et al.* (1993) by means of X-ray diffraction and transmission electron microscopy and diffraction. It was ascertained that preferential orientation of the molecules took place

perpendicular to the dipping direction, though their reported interlayer distance of 1.65nm., compared to the molecular dimension of 1.7nm in crystalline powder of the compound, suggests that the molecules are offset from the perpendicular. A stacking angle of 14° from the vertical is suggested from these data.

We see from these three deposition processes that it is possible with phthalocyanines to prepare a variety of film types suitable for many different applications. The quality of such films is demonstrated in the micrograph in Fig. 2.8 (Mukhopadhyay 1990). However, in summary each of these processes offers distinct advantages and disadvantages applicable to this type of compound:

(1) not all phthalocyanines may be deposited by the L-B technique, although very thin films of those suitable may be prepared. Disadvantages are that application of electrodes to this type of film where a through-plane structure is intended must be carried out very carefully, or destruction of the film may occur, causing an interelectrode short.

(2) Vacuum evaporation, although permissible for most phthalocyanines, and producing relatively thick layers, has the disadvantage that fouling of the deposited film by contaminants present in the chamber is very likely, especially when the material is evaporated gently rather than quickly. Further, there is a problem of pinholing in the films which is related to destructive thermal stressing of the film during cooling of the film and substrate from the evaporation process.

2.5. Electrical properties - d.c.

Various types of phthalocyanine have been studied in terms of their conduction properties. The interest in phthalocyanines arose because CuPc was found to have a hole mobility of 75 $cm^2/Vsec$, which is regarded as very high for an organic material.

By way of illustrating the progress made in this area, we shall now examine a selection of materials tested to illustrate the transport properties and methods of determination of these for various phthalocyanines.

Charge transport in NiPc crystals was studied by Abdel-Malik and Cox (1977), by measuring ohmic and space charge limited currents. A tentative energy band diagram for NiPc in vacuo (Fig. 2.9) was suggested, along with state densities. Measurement of drift mobilities of electrons and holes in single crystals of metal-free and lead phthalocyanine were carried out by Westgate and Warfield (1967). Two types of transient current measurement were used. For both types, a transparent gold electrode was evaporated onto the face of the crystal, and a silver paste one painted onto the opposite face. A microsecond flash from a mercury arc lamp was used to generate the injecting contact for carriers. Two types of carrier generation were observed, the first being direct if the voltage were applied shortly before flashing the light. Fast recombination was observed after holes and electrons were generated near the surface. If the voltage was present for a considerable time before applying the flash, excitation from surface traps took place. This was more efficient than the previous method. A band gap energy of 1.76 eV was found. Transient SCLC measurements provided voltage-time transients (Fig. 2.10), which enabled it to be ascertained that for several H_2Pc crystals, drift mobilities varied between .05 -.1cm^2/Vsec. for both holes and electrons, with a trapping time of 3 microseconds. For lead phthalocyanine, mobility was 0.6-4 cm^2/Vsec. Many deep traps are hypothesised, from the release time of approx. 1 sec, and the shape of the SCL transients. Many authors have characterised the trapping states for a variety of Pc materials. -ZnPc (Abdel-Malik *et al*, 1982) (Fig. 2.11) ,NiPc (Hassan and Gould, 1993), H_2Pc (Barbe and Westgate, 1970). The method of dark current-voltage curves as a function of temperature was employed; ohmic conduction was observed at low voltages, and space-charge limited at higher voltages. Treatment of log I vs. 1/T for fixed voltage gave for nickel phthalocyanine (in a sandwich configuration with gold electrodes) an ohmic activation energy of 0.41 eV (energetic position of an acceptor level) and 1 eV (for intrinsic conduction) below and above 350K were calculated for a fresh sample. For SCLC, 0.58eV was determined; this was thought to correspond to oxygen- induced trapping levels. For an annealed NiPc sample, 0.81eV was found for the ohmic activation energy. This is thought to be due to a phase transfer of some of the film from to states. The SCLC conduction curve was linear. Trap concentration of $4x10^{27}/m^3$ and

and mobility 2.33×10^{-7} $m^2V^{-1}s^{-1}$ were determined. For both ohmic and SCLC, very low activation energies at low temperature indicated hopping conduction. For CuPc, measurements of dark and photoconductivity in air, nitrogen and oxygen were performed. (Gas sensing *per se* is discussed in further detail in section 2.7.)

In order to determine the effect of traps and their energies upon the conduction regimes occurring in the material, Shafai and Gould (1992) performed dc I-V measurements of lead phthalocyanine films between aluminium and gold electrodes. Schottky and Poole-Frenkel properties were observed. The Poole-Frenkel effect is a lowering of the activation energies of impurity centres in the presence of an electric field.

Under forward and reverse bias (gold positive and negative respectively), the forward bias results showed a $J \propto V^n$ relationship with $n \approx 3.65$ at lower voltages and 2 at higher ones. The higher region suggests SCLC in an exponential trap distribution, whilst the lower suggests the same type of conduction controlled by a single trapping level.

Reverse bias measurements show a dependence of log J on $V^{0.5}$. Existence of a Schottky barrier at the aluminium electrode was decided by measuring capacitance-voltage characteristics of the junction.

Under reverse bias was observed a transition from Schottky to Poole-Frenkel effect, showing electrode-limited and bulk-limited conduction respectively.

These results were confirmed by the work of Ahmad and Collins (1991) who also performed very similar measurements on Au-PbPc-Al structures.

2.5.2 Photoelectric properties

Phthalocyanines, in common with other organic semiconductors, have become the subject of interest for applications in light sensitive devices because of their ability to photogenerate free charge carriers. The particular interest in thin films came about as a result of the relatively low quantum charge generation efficiency of the materials at low electric fields; it is easy to generate a very high electric field with a very thin film. Furthermore, LB films can be prepared where the whole film thickness encompasses the active charge generation region.

Considerable work has been undertaken concerning the photoelectric properties of various phthalocyanines in differing ambient environments (Brynda *et al* 1990, Brynda *et al* 1991, Yoneyama *et al* 1986, Takada *et al* 1992).

Yoneyama *et al* (1986) fabricated Schottky barrier photovoltaic cells using asymmetrically substituted CuPc sandwiched between a semitransparent Al electrode and a gold counter electrode. The resulting device is also known as a p-type Schottky diode. The short-circuit photocurrent was negative, as would be expected from such a device. When the L-B film was sufficiently thick (20 layers) a strong rectifying effect was observed. (Fig. 2.12) A short-circuit photocurrent of 10^{-8} A and an open circuit photovoltage of approx. 0.3V were obtained for irradiation intensity of $1000\mu Wcm^{-2}$. This was higher than for other known LB film photodiodes, attributed to the absence of long alkyl chains and to the ordered structure and close packing in the film.

2.5.3 Switching properties

Electronic switching properties have been observed in films of lead phthalocyanine by Hamann and Mrwa (1992) and Machida *et. al.* (1989)

This property was found to be strongly associated with the film structure employed. Voltage-controlled electrical switching/memory effect was found to occur; these effects were multistable indicating a number of intermediate switching states. If an electric field of between $3x10^4$ and $5x10^4$ Vcm^{-1} was applied to the film, the conductivity would increase by up to ten orders of magnitude. This could be reversed by applying short current pulses. The switching time was found to be less than 0.5 μs.

Specific resistivities of lead phthalocyanine for this process were determined as 10^{11} Ωcm at room temperature for "off" state or 0, and 10^9 - 10^4 Ωcm ofr the "on" or 1 state. Both these values are quoted at room temperature.

2.5.4. Thermally Stimulated Discharge

Thermally stimulated discharge (TSD) can provide information about the dielectric relaxation processes occurring in phthalocyanines. The principle of thermally stimulated discharge is to heat a sample of a compound so as to cause carrier formation (polarisation) by means of supplying thermal energy, followed by the application of a dc field. The material is then short circuited causing discharge and cooled, the effect being to prevent immediate release of the charge present from the polarisation. For clarity, it can be imagined that latent charge is "frozen" into the material. If the material sample is subsequently heated at a predetermined rate, and a current-temperature thermogram obtained, one or several peaks will be observed. In copper phthalocyanine (Das, Tripathi and Srivastava, 1983), a single peak was observed (Fig. 2.13), the temperature at which the current peak occurred being seen to depend upon the polarising field. For first order kinetics of the electret formation, the peak would depend on the activation energy and the relaxation time alone; it is hypothesised that the mechanism of electret formation is second order, since the initial polarising conditions are significant. There was also linear dependence of released charge and peak current on the polarising field. The transport mechanism was therefore suggested to be charge migration, with the recapture time being small by comparison with the lifetime in traps. This would lead to a dependence of the rate of decay of polarisation on the release rate from the traps.

2.6 A.C. Electrical Properties

Dielectric behaviour of phthalocyanines has been well characterised recently; CoPc (Nalwa, Vasudevan 1983), CuPc (Gould and Hassan 1993), ZnPc (Saleh, Gould and Hassan 1993), MoPc (James, Ray and Silver 1992). CoPc was examined in the form of pellets sandwiched between aluminium electrodes. The dielectric constant ε was obtained for frequencies of 0.5, 1, 5, 10 and 50 kHz by measurement of the ratio of the capacitance of the device to that of a similar device using air as the dielectric. ε was calculated by

$$\varepsilon = C_0 d / (\varepsilon_0 A) \qquad (1)$$

where $\varepsilon_0 = 8.85 \times 10^{-14}$ Fcm^{-1}. Variation of the dielectric constant as a function of temperature produced $5<\varepsilon<62$ at room temperature, with ε decreasing with increase in frequency. A dielectric peak was observed at ca. 423K at all frequencies. The frequency and temperature effects were attributed to (a) the number of free mobile charges increasing with temperature and (b) the decrease at higher temperatures being due to the conductivity increase making retention of charge more difficult.

Further to dielectric constant measurements, a.c. conductivity measurements can indicate something about the bulk nature of the material, even with an electrode-limited conduction process. CuPc as a vacuum sublimed film was studied from 173K-360K for 100 Hz - 20 kHz. The ac conductivity was found to obey $\sigma \propto \omega^s$ where $s \leq 1$. Hopping conduction was postulated at low temperatures and high frequencies; at higher temperatures and lower frequencies, free carrier conduction with a mean activation energy of 0.3eV was observed. Capacitance and dielectric loss decreased with frequency and increased with temperature.

Good qualitative agreement with the above was observed for ZnPc, but heat treatment above 430K additionally promoted a decrease in the conductivity, suggesting a partial phase change of the film from α to β form.

2.7. Optical properties

The transmission and absorption spectra of phthalocyanine thin films and solutions can be powerful tools in suggesting the electronic properties of the materials. With the addition of reflection spectra, it becomes possible to determine not only the real and imaginary parts of the complex refractive index, but also the corresponding values of dielectric constant in the optical frequency range. The complex refractive index N = n-ik, where n is the propagation constant and k the extinction coefficient of the material at a particular wavelength or photon energy.

Transmission data for H_2,C_2, Ni, Co and ZnPc's in sublimed films were characterised by Lucia and Verderame, (1968). (Fig. 2.14). They examined the spectral changes resulting

from the conversion of the α forms of these Pc's to β form by heat treatment. Sharp changes in the transmission spectra for the above compounds were observed as a result of annealing. Similar measurement for VOPc showed no effect; in the light of X-ray diffraction measurements, it was postulated that VOPc has a different crystalline structure to the other materials investigated.

The effect of metal substitution on the optical absorption spectrum of various metallophthalocyanines was characterised by Davidson (1982). The materials studied were H_2Pc, MgPc, FePc, ZnPc, CoPc, and CuPc.

2.8. Uses as Sensors

Much work has been undertaken regarding the sensitivity of phthalocyanines in varying degrees to light and the presence of electrophilic gases, also smart windows (electrochromic display devices) and possible "fuzzy logic" applications due to their possession of a number of discrete switching states.

2.8.1 Gas Sensing

A number of metal phthalocyanines can have their electrical conductivity modified by the presence of certain gases. Since they operate as p-type semiconductors, electrophilic gases like NO_2 can improve conductivity by injecting holes into the Pc, the effect for nucleophilic gases being to decrease the conductivity by electron injection. There are at present problems involved in the manufacture of a viable commercial sensor, because the dark- and photo-conductivity of the materials are dependent upon a variety of parameters which are undesirable - notably the film purity, effect of phase changes of the film structure, the rôle of oxygen in the sensitivity to other gases, and the trade-off in relevance of surface adsorption and bulk absorption of the gas. An ideal phthalocyanine gas sensor would be sensitive, selective (i.e. respond well to a particular gas without being affected by others) and exhibit a fast recovery time (desorption of gas should take

place reasonably quickly in the absence of ambient). It is also desirable that the relationship between conductivity and gas concentration should be linear, though this is not so important as the other properties mentioned.

Wilson and Collins (1986) put forward a theoretical model for the effect of gas adsorption on conductivity based on a modified Roginsky-Zeldovich equation, thus :

$$\log \sigma(m) = \frac{\gamma kT}{\beta} \log(t + t_0) = K' \qquad (5)$$

where (m) is electrical conductivity and m the amount adsorbed at time ($t+t_0$), γ and β constants at a given vapour pressure, k Boltzmann's constant, T absolute temperature and K' constant. The assumptions required for this model to operate in a satisfactory manner are that for a cell of given geometry and applied voltage, the dark conductivity is proportional to the sensor voltage, and hence log (σ(m)) can be replaced by log (i_S(m)), the dark current. On adsorption, the sensor current follows logarithmic behaviour. (Fig.. 2.15)

They also found evidence that bulk oxygen absorption affected device conductivity in CuPc and H_2Pc ammonia sensors. This was attributed to the adsorption of water vapour onto the sensor. With an Au-H_2Pc-Au device, a fall in sensor current was observed on the introduction of the ammonia-air mixture. Using indium as the electrode metal on H_2Pc, the sensor current fell by up to three orders of magnitude on the introduction of ammonia. Speed of response and recovery times were not consistent over different samples. Desorption was not complete upon subsequent runs, suggesting that the bulk properties of the film were significant, possibly as a result of the bulk absorbed oxygen. However, it was not possible to quantify this effect.

The effects of NO_2, NO, F_2, BCl_3, BF_3, NH_3, H_2S, SO_2 and HCl, present in concentrations of less than 1 ppm in air have been investigated. It has been found (Jones & Bott, 1986) that as the atomic weight of the metal substituent in phthalocyanines became heavier, increasing sensitivity to NO_2 was observed. This was determined by exposing H_2, Mg, Mn, Co, Ni, Fe, Zn, Na_2 and Ag phthalocyanines (as vacuum-

sublimed films, ca. 1 μm thick) to low concentrations of NO_2 in air. It was concluded that PbPc provided high sensitivity, along with good stability and reproducibility, to NO_2 in air, whilst MgPc was sensitive only to HCl, providing interest as a viable sensor for this gas alone without disturbance of the properties by other gases.

In addition to vacuum sublimed films, the applicability of Langmuir-Blodgett films of Pc's as gas sensors has been investigated by Baker, Roberts and Petty (1983), Cole, McIlroy, Thorpe, Cook, McMurdo and Ray (1993) and Jiang, Pang and Hua (1991) and reviewed by Honeybourne and O'Donnell (1991). Baker *et al* investigated dilithium phthalocyanine and tetra-tert-butyl phthalocyanine. The response and recovery times for NO_2 were found to be shorter than those previously reported for thin-film Pc devices fabricated by other means. This is thought to be a result of the more ordered nature of the LB film, allowing the gas to adsorb and desorb from the film surface more readily. O'Donnell (1990) describes NO_2 sensing with LB films including PPPcVO and PPPcCu, for various numbers of layers. Mostly, the plots of log σ : log (NO_x) were found to be linear, with a high degree of reversibility, particularly for PPPcVO. Both of these properties are most promising for working gas sensor applications, because the linearity allows easy characterisation of the gas concentration, whilst, more importantly, the high reversibility indicates that the device will readily desorb the gas and is applicable to prolonged use with no irreversible effects of the ambient NO_2. However, the issue of temperature effects upon conduction still requires attention in this type of instrument.

Bearing in mind the aforementioned problems, the method of surface plasmon resonance (Lloyd, Pearson and Petty,1988),(Vukusic and Sambles, 1992) is of current interest in detecting adsorbed gases. The method is advantageous compared to electrical processes, as there is no requirement to apply complex associated electronics to account for temperature dependence of the material's electrical properties. By means of the arrangement shown in Fig. 2.16, a surface plasmon can, by means of laser light, be excited on a thin metal film at a particular angle of incidence, θ. This angle is dependent upon the refractive index and thickness of the organic film. Any change of these due to

gas adsorption will result in a shift in the angle θ at which the resonance is observed (Fig. 2.17). Hence in practice it should be possible to fabricate a small integrated device of high stability, based on the system of a material film, a laser diode and detector, the signal from which does not require complicated post-transducer electronics to account for undesirable parameters in the sensor material.

2.8.2. Optical sensors

As described earlier, the photoelectric properties of Pc's are being characterised. This has been extended by some workers to the fabrication of practical photocells. Metal-free Pc sandwiched with various combinations of gold, lead and aluminium electrodes has been used (Hall, Bonham and Lyons 1978) but were found to be very inefficient. MgPc (Ghosh, Morel, Feng, Shaw, Rowe 1974) provided a photovoltaic efficiency of ca. 0.01% under illumination from a filament lamp. The highest reported for organic photovoltaic cells was about 1% for a merocyanine dye. Surfactant aluminium phthalocyanine (Belanger, Dodelet, Dao and Lombos 1984), a $C_{16}H_{33}$ chain bonded to aluminium phthalocyanine by a phosphate bridge, was investigated on both gold and doped SnO_2 electrodes. The former provided, at I = 10 $mWcm^{-2}$, an efficiency of about $2x10^{-3}$%, and the latter ca. $1x10^{-2}$%. Zinc phthalocyanine (Twarowski 1982) using "Nesatron" (ITO coated) glass as the base electrode and gold on top was used in an experiment to determine those factors which limit the conversion efficiency. This work showed for the first time that the Onsager mechanism for photocurrent generation applies to phthalocyanine thin films excited in the visible region. The quantum efficiency of the devices varies with the applied electric field, and it was proven that an upper limit for conversion efficiency would be ca. 1%. It was concluded that when a blocking contact was made to Pc thin films, other photogeneration methods might be introduced. Substituted silicon phthalocyanine between gold and ITO electrodes (Hua, Petty and Roberts 1987) as an LB film showed that the use of very thin films, in addition to permitting high electric fields, was useful, since the open circuit photovoltage and the short-circuit photocurrent both began to decrease when the film thickness became

greater than the sum of the depletion layer width and the exciton diffusion length. (Fig.2.19) It follows that a certain amount of work remains to be performed before commercial devices are viable.

(a)

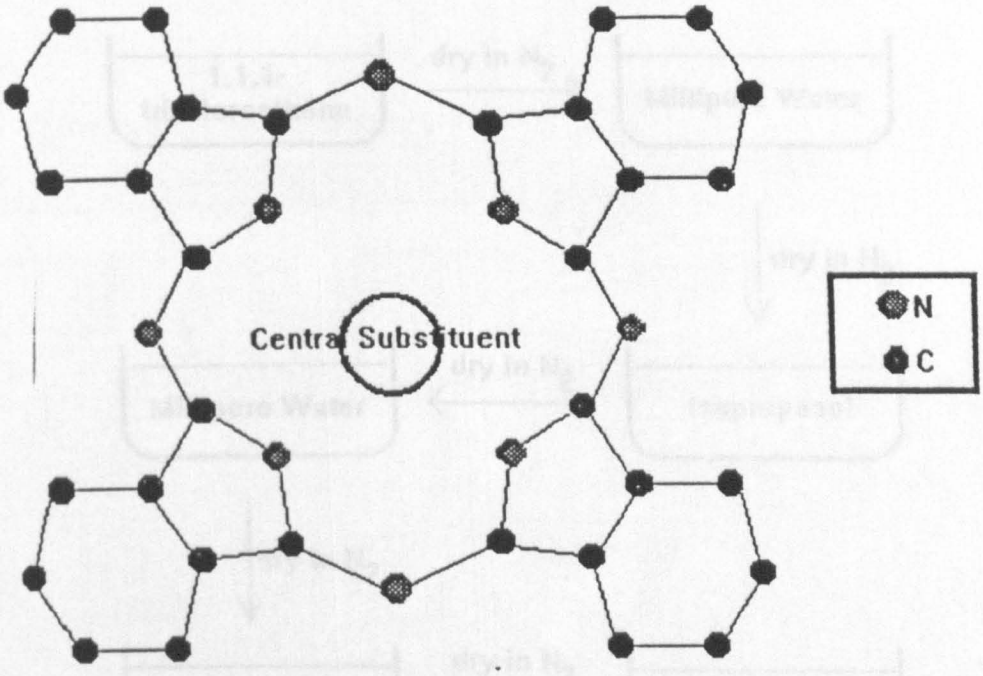

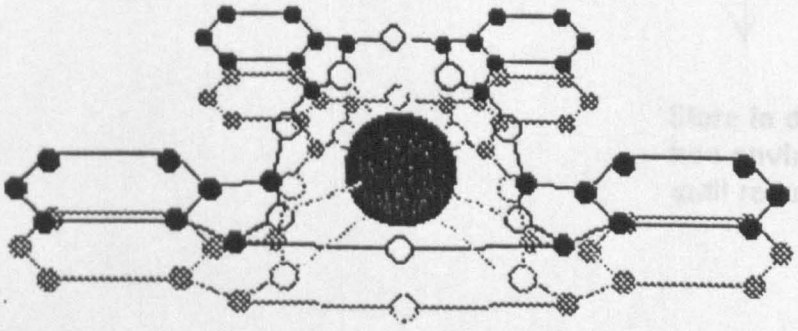

(b)

2.1. Schematic of (a) phthalocyanine, and (b) bisphthalocyanine molecules

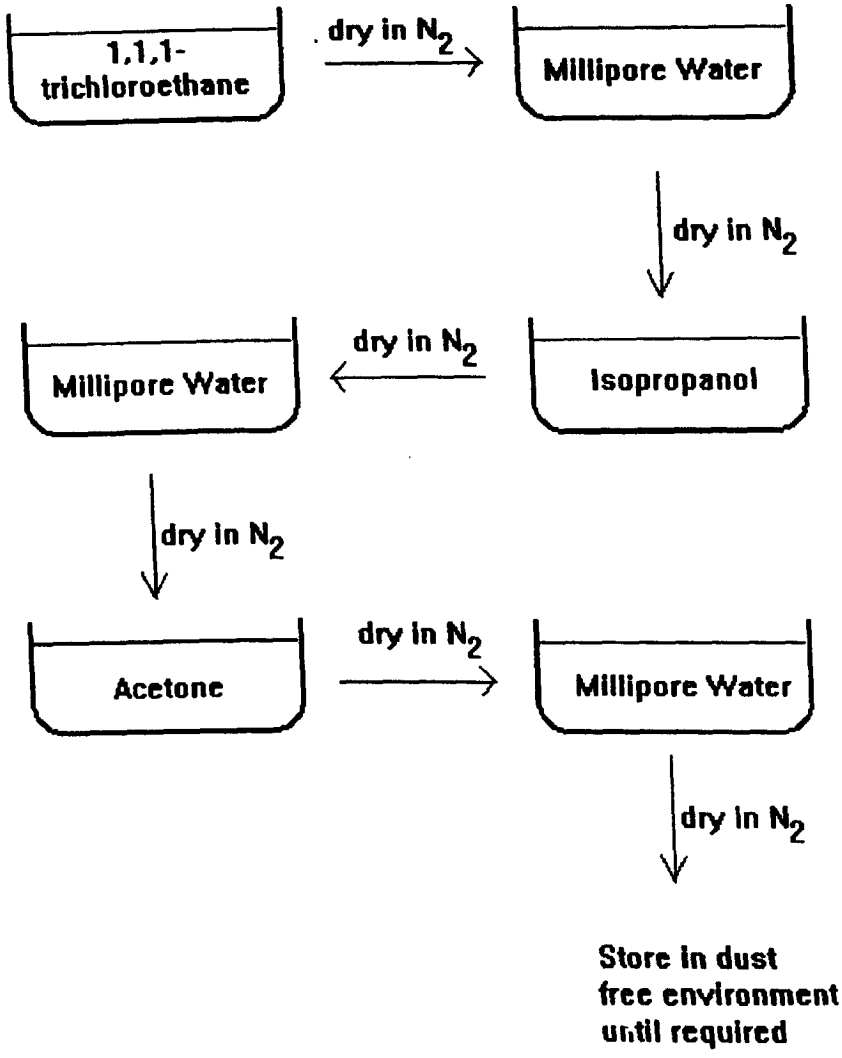

2.2. Cleaning Process for Deposition Substrates

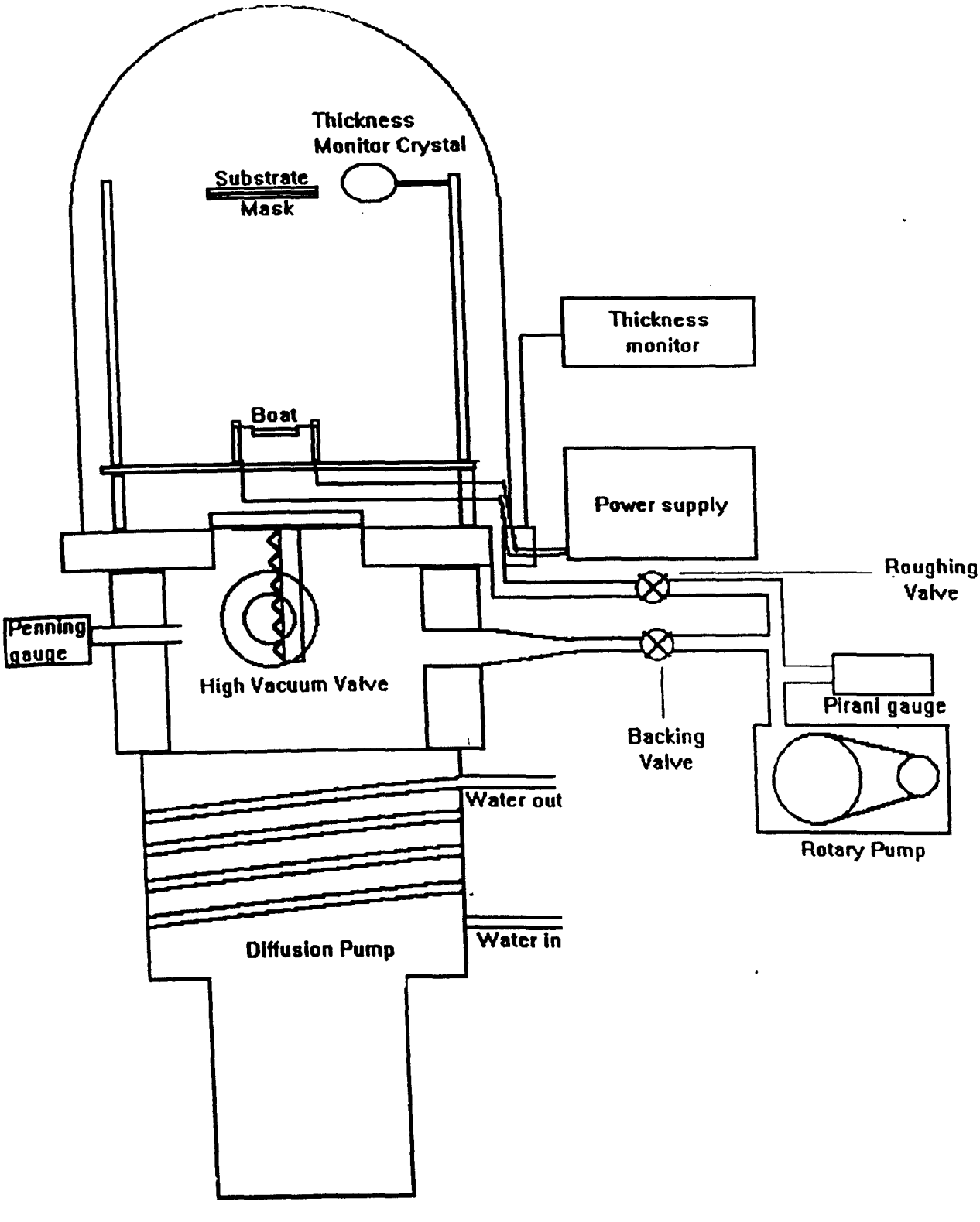

2.3 Vacuum Sublimation System Schematic

2.4 Carrier mobility in CuPc as a function of evaporation pressure and rate [Gould, 1986]

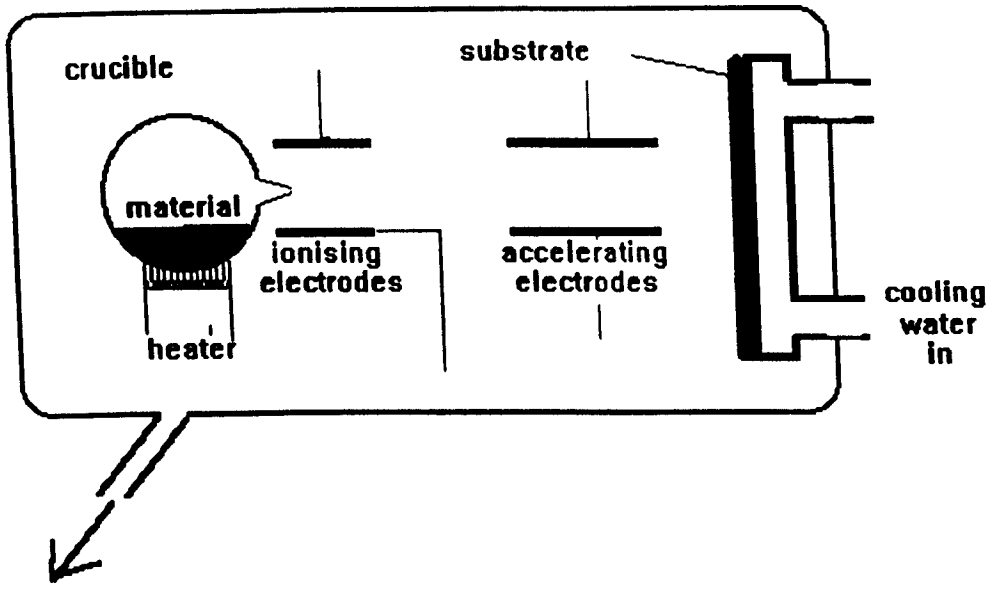

2.5. Ion Cluster Beam Deposition schematic

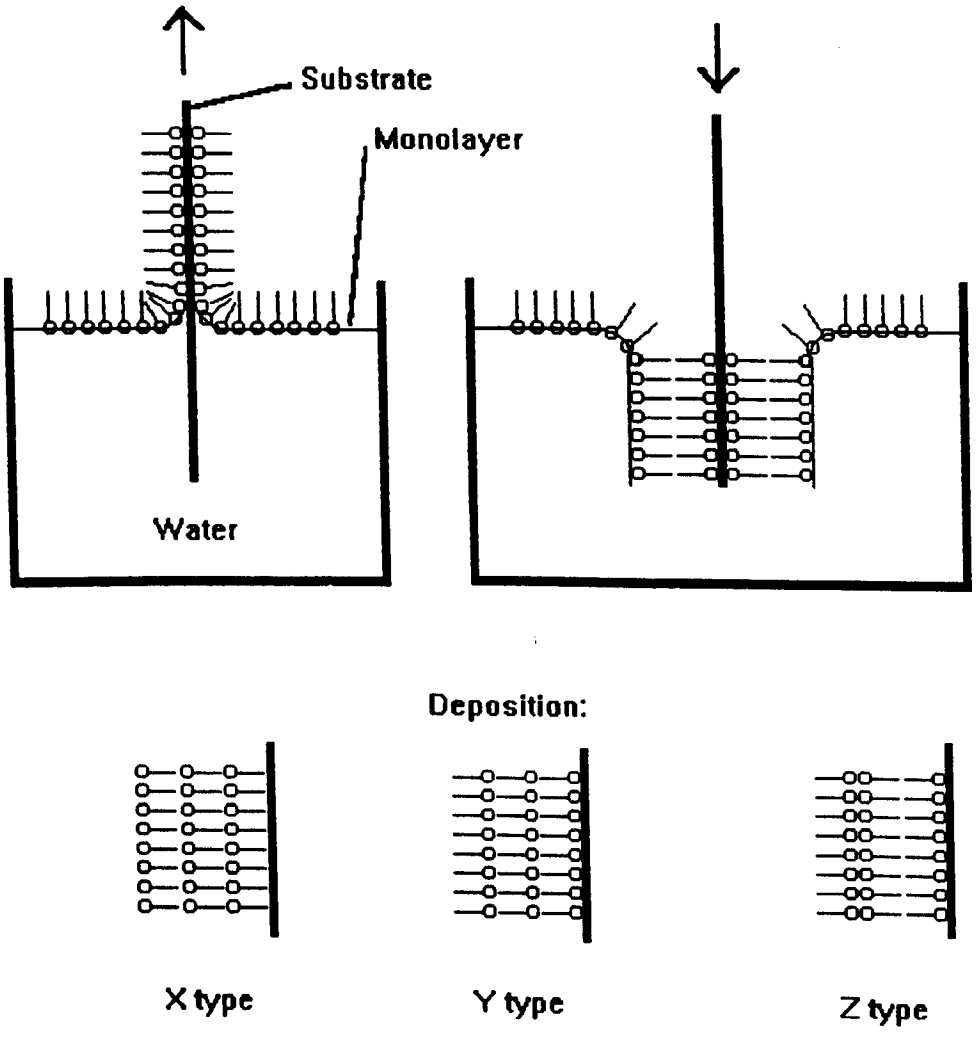

2.6 Langmuir-Blodgett deposition process

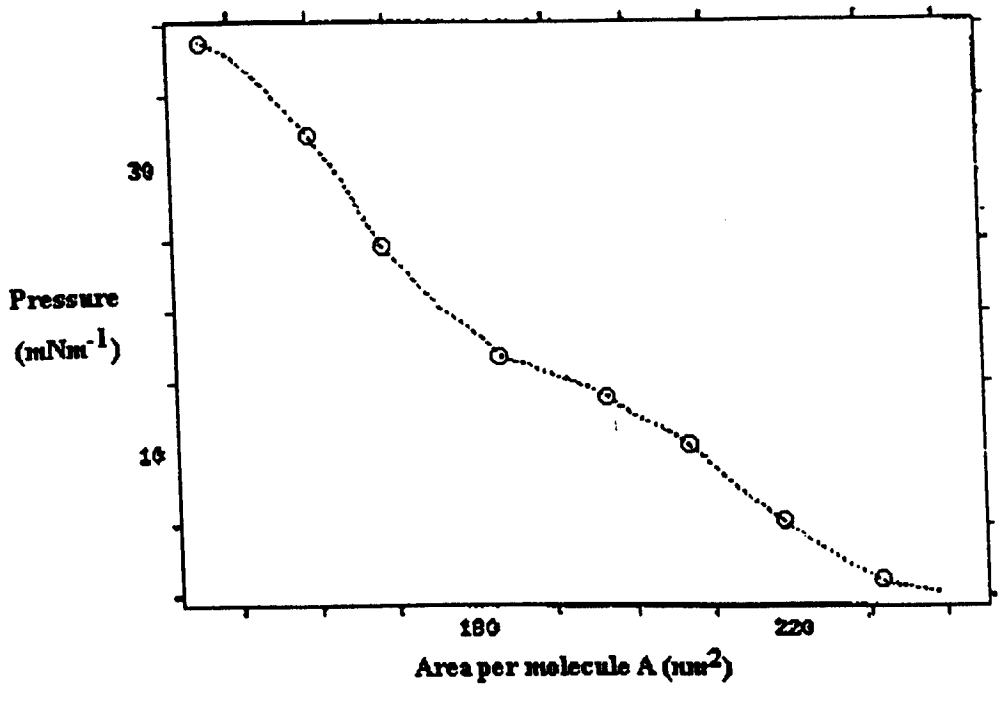

2.7 Pressure-area isotherm for solution of H_2Pc on water at 298K

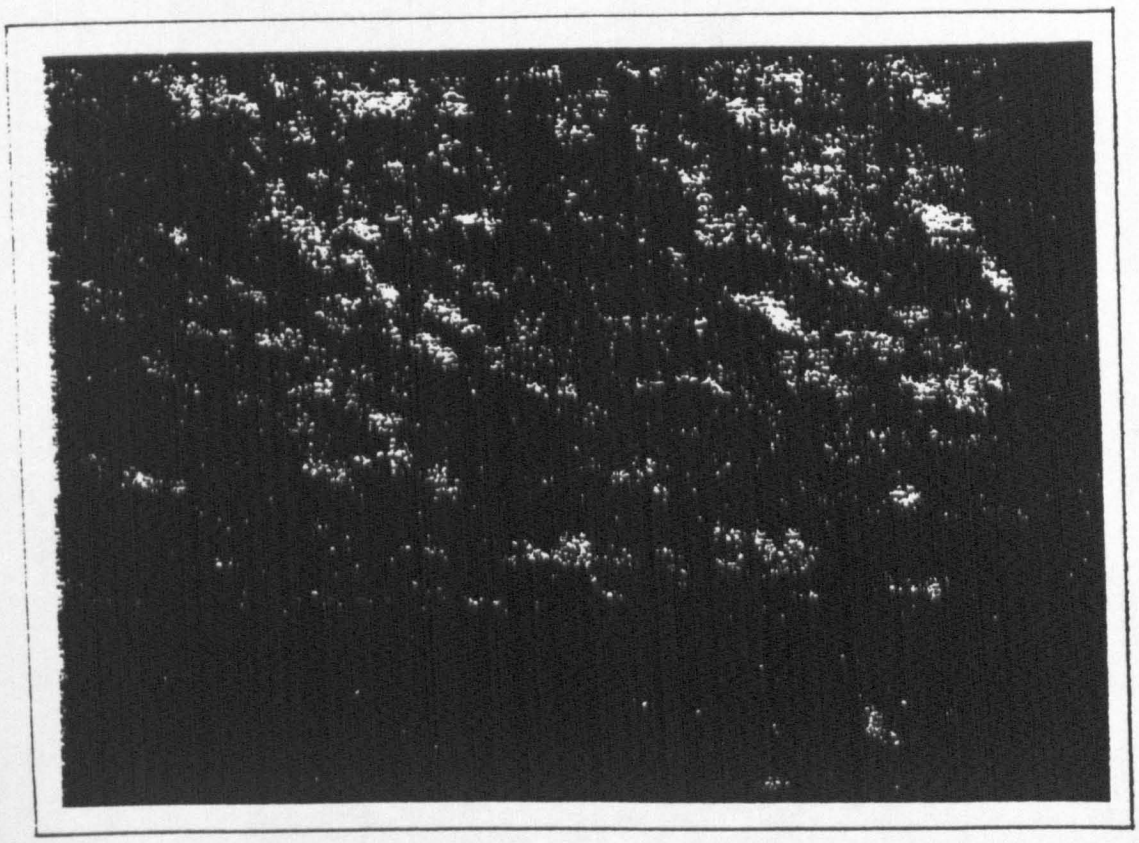

2.8 Electron micrograph of CuPc film. Longer edge of plate is 23 micron.

2.9 Tentative energy band diagram for NiPc inn vacuo [Abdel-Malik, Cox]

2.10 Voltage-time transients for H2Pc [Westgate and Warfield 1967]

2.11 Trapping states for β-ZnPc [Abdel-Malik *et al*, 1982]

2.12 Short circuit photocurrent and open circuit photovoltage in asymetrically substituted CuPc [Yoneyama *et al* 1986]

2.13 Current-temperature thermogram for copper phthalocyanine [Das, Tripathi and Srivastava, 1983]

2.14. Spectra for various α and β phthalocyanines [Lucia, Verderame 1968]

2.15. Response of Au-CuPc-Au sensor to NH_3 [Wilson and Collins 1987]

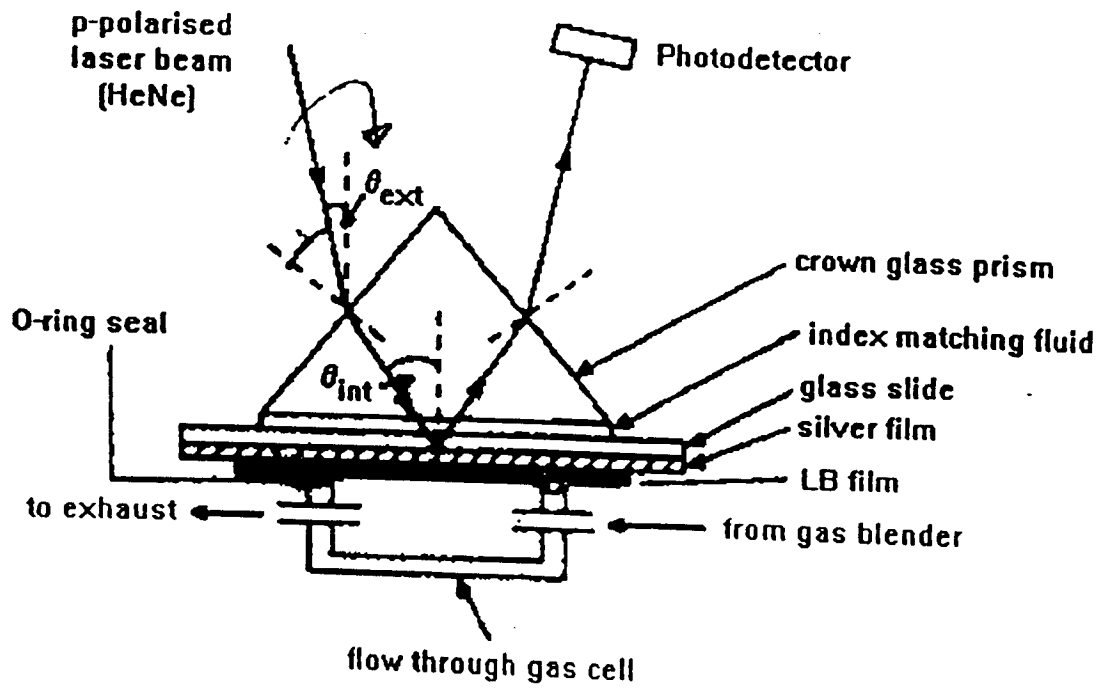

2.16. Surface Plasmon Resonance : experimental arrangement

2.17 Effect of gas adsorption on surface plasmon resonance (Lloyd et. al. 1988)

Chapter 3.

Theoretical Information

3.1 DC property analysis

3.1.1 Introduction

Some background knowledge of the steady state transport properties of organic semiconductors is necessary in order to achieve understanding of their macroscopic dc properties. In organic semiconductors such as phthalocyanines prepared as high resistivity solids, these steady state transport properties are largely controlled by the amount and energy distribution of trapping sites for charge carriers. (Studies on CuPc using blocking contacts have shown that, not unexpectedly for an organic material, the current is predominantly carried by holes.)

The density of holes in thermal equilibrium is established by

$$\overline{p} = N_v \exp(F_0 kT) \qquad (6)$$

with F_0 the distance of the equilibrium Fermi level from the valence band edge.

3.1.2 Types of metal Contact applicable to thin phthalocyanine films

Three main types of metal contact may be made to a thin semiconducting film;

(a) neutral,

(b) ohmic and

(c) blocking (known also as Schottky or rectifying).

The relative work functions of the film and metal decide what the contact type will be. The work function of a material, ϕ, is the energy difference between the Fermi level and the lowest energy level of an electron *in vacuo*.

If the work function of the metal is less than that of the semiconductor, $\phi_m < \phi_s$, then flow of electrons from the metal to the conduction or valence band of the

semiconductor is impeded, and a depletion layer" occurs at the interface. This is a *rectifying* contact.

If the work functions of metal and semiconductor are equal, $\phi_m = \phi_s$, this forms a *neutral* contact.

If the work function of the metal is greater than that of the semiconductor, $\phi_m > \phi_s$, then the junction impedance to the carrier flow is negligible and an *ohmic* contact results.

3.1.3 dc Conduction Regimes

Some phthalocyanines exhibit both ohmic and space charge limited conduction, the conduction being ohmic at low voltages and space-charge-limited at higher ones, as follows.

3.1.3(a) Ohmic Conduction

In the case of ohmic conduction, the current density : voltage relationship is seen to follow Ohm's law, where I∝V. Carriers participating in this type of conduction are of the thermally excited variety only; ie. the number normally present in the material in the absence of applied electric field.

3.1.3(b) Space-Charge Limited Conduction

Space charge limited conduction occurs when the situation arises that carrier injection takes place at an ohmic contact to the material. (more formally, when the carrier injection from the contacts becomes comparable with the carrier density in the material at thermal equilibrium) An ohmic contact, in microscopic terms, is one which promotes an excess of free carriers (or "space charge") in the material in the region of the contact.

Hence the current in the "interior" of the material is limited by the space charge and is independent of the amount of excess carriers at the boundary.

For space charge limited conduction [Gould 1982] there is a power law dependence of the current density J on voltage V such that $J \propto V^n$ with n<=2. The value of n will presently be shown to be a useful indication of the trapping centre energies involved in the conduction process; exact square law dependence is characteristic of traps occurring at a single energy level above the valence band edge. In the event of n≠2, there is postulated to be some manner of distribution of the energies above the valence band edge of the traps.

For the situation where an exponential distribution of traps characterised by [Hamann 1968, Gould 1986, 1990] as

$$P(E) = P_0 \exp(-E / kT_t) \qquad (7)$$

is present, Lampert [1964] proposed the following relation for the current-density/ voltage characteristic:

$$J = e\mu N_v \left[\frac{\varepsilon}{eP_0 kT_t} \right]^l \frac{V^{l+1}}{d^{2l+1}} \qquad (8)$$

where $l=T_t/T$, and total trap concentration $Nt(e)=P_0kT_t$. T_t is a temperature constant characteristic of the trap distribution.

In a sample of thickness L with applied voltage V, the conduction parameters for the two regimes are:

$$J_\Omega = ne\mu \frac{V}{L} \qquad (9)$$

and

$$J_{SCL} = \frac{9}{8} \varepsilon\mu \frac{V^2}{L^3} \theta \qquad (10)$$

where n is the free carrier density, e the electronic charge, the microscopic carrier mobility and the permittivity. is called the trapping factor and is the fraction of all the charge carriers which are free; the ratio of free to trapped charge. It is given by

$$\theta = N_v / N_{t(s)} \exp(-E_t / kT) \qquad (11)$$

with Nv the effective density of states in the valence band, Nt(s) the concentration of traps situated at energy Et above valence band, K Boltzmann's constant and T the lattice temperature. Hassan and Gould (1989) suggested that the observed properties of CuPc in air, ie. a low-density, single-level trapping process, suggested that the presence of absorbed oxygen was a source of extrinsic conductivity.

Equation(11) is valid for the injection of one type of charge carrier only, with a single discrete trap level.

As the electric field in a suitable material is increased under these conditions, there will be observed a sharp increase in conduction, owing to complete trap filling. There is an applied voltage at which complete trap filling is postulated to occur (Lampert, 1956)

$$V_{TFL} = \frac{eN_t L^2}{2\varepsilon} \qquad (12)$$

For voltages in excess of V_{TFL}, the JV^2 dependence is recovered.

Both conduction processes are thermally activated, as may be seen from the terms relating to the charge carriers, n and , in the above Equations. It may also be noted that by the preparation of a plot of log J, or log of conductivity , against reciprocal temperature, one or more straight line segments should be seen, allowing the derivation of one or more activation energy values for the processes.

However, phthalocyanines generally have bandgaps in excess of 1eV, which introduces certain difficulties to the matter of unambiguous interpretation of their activation energies (Schmidlin and Roberts 1974). Measurement of activation energies for both ohmic and SCL conduction are necessary for correct analysis. There is a partition function for electrons and holes, the largest term only of which should be of

importance if an exact activation energy is to be seen; for a particular temperature there should be only one dominant energy level responsible.

The drift mobilities μ of carriers in phthalocyanines with respect to temperature are of considerable interest in the elucidation of charge transfer mechanisms under applied electric fields. They may be determined by means of optically inducing space-charge-limited current. As a result of a pulse of light strongly absorbed by the material, an initial current density

$$J = \frac{e\mu V^2}{2L^3} \qquad (13)$$

may be obtained. The decay of this with respect to time is the measurand, and by analysis of the transient measured on a fast storage oscilloscope, a determination of the drift mobilities of electrons or holes in the bulk may be made.

As far as SCLC is concerned, it has been noted that the index n has under certain conditions been observed greater than 2. This is attributed to there being such a proliferation of carriers that all the traps in the material are filled; the onset of a trap-filled conductivity limit is postulated to be the reason for this.

3.1.4 Van der Pauw resistivity measurements

The van der Pauw method of resistivity determination [van der Pauw, 1958] is a most useful tool in determination of the resistivity of a flat sample, such as a thin phthalocyanine film, since it renders the size and shape of the sample irrelevant to the calculation. Only the thickness need be known, and should be homogeneous.. Four arbitrary contacts are required to be placed at the circumference of the sample, these should be as small as possible; preferably point contacts.

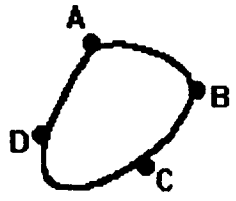

We can define the resistance RAB,CD as the potential difference VD-VC between contacts D and C per unit current through A and B. The resistance RBC,DA is defined similarly. For specific resistance ρ and thickness d for the sample, it follows that

$$\exp(-\pi R_{AB,CD}\frac{d}{\rho}) + \exp(-\pi R_{BC,DA}\frac{d}{\rho}) = 1 \qquad (14).$$

This equation is valid for all sample shape.

For the solution of σ from equation (11) we re-write it thus:

$$\rho = \frac{\pi d}{\ln 2}\frac{(R_{AB,CD} + R_{BC,DA})}{2} f\frac{R_{AB,CD}}{R_{BC,DA}} \qquad (15)$$

f is a function of the two resistances RAB,CD and RBC,DA and satisfies the relation

$$\left(\frac{R_{AB,CD} - R_{BC,DA}}{R_{AB,CD} + R_{BC,DA}}\right) = f\,\text{arcosh}\left\{\frac{\exp(\ln 2/f)}{2}\right\} \qquad (16)$$

f may, when the two measured resistances are almost equal, be approximated by :

$$f \approx 1 - \left(\frac{R_{AB,CD} - R_{BC,DA}}{R_{AB,CD} + R_{BC,DA}}\right)^2 \frac{\ln 2}{2} - \left(\frac{R_{AB,CD} - R_{BC,DA}}{R_{AB,CD} + R_{BC,DA}}\right)^4 \left\{\frac{(\ln 2)^2}{4} - \frac{(\ln 2)^3}{12}\right\} \qquad (17)$$

although recently Ramadan, Gould and Ashour [1994] tabulated values of the correction factor f obtained by a combination of experiment on thin films of copper and aluminium and numerical solution of the condition shown by equation (14), so as to avoid inaccurate estimation from the previously popular graphical presentation and save intensive calculation. .

Hence the resistivity of any film sample may be established so long as the conditions outlined regarding electrode size and placement are satisfied.

3.2 AC property analysis

3.2.1. Impedance spectroscopy - basic definitions

Impedance spectroscopy is the term given to the analysis of the dielectric properties of a material with respect to frequency, and reflects the response of polarisation centres in the material to an applied electric field. The variety of differing polarisation mechanisms, and their relative prevalence, gives rise to a unique frequency dispersion of dielectric properties.

The "relaxation time" for any one of these polarisation processes is a function which describes the decay of polarisation with time subsequent to removal of the polarising field. [Debye,] Analysis of the complex dielectric constant

$$\varepsilon^* = \varepsilon' - j\varepsilon'' \tag{18}$$

is paramount in order to gain an understanding of the distribution parameters. The ac conductivity of a dielectric material is expressible as a complex quantity which may be postulated in terms of the complex dielectric constant, thus:

$$\sigma'(\omega) = \sigma_{ac}(\omega) = \varepsilon_0 \omega \varepsilon''(\omega) \tag{19}$$

$$\sigma''(\omega) = \varepsilon_0 \omega \varepsilon''(\omega) \tag{20}$$

Hence it is possible to establish values for ε'' by use of the conductivity:frequency data. By direct measurement of the loss tangent $\tan\delta = \frac{\varepsilon''}{\varepsilon'}$ it is therefore possible to obtain absolute values for both the real and imaginary parts of the dielectric constant over the range of frequencies and temperatures prescribed by the measurement routines.

G is a quantity related to σ by the sample geometry.

$$C = \frac{\varepsilon A}{d} \tag{21}$$

where C=measured capacitance

$$C(\omega) = C'(\omega) - jC''(\omega) = (\frac{A}{d})\{\varepsilon'(\omega) - j\varepsilon''(\omega)\} \tag{22}$$

c' =ordinary capacitance

c" = dielectric loss component

$$\tan\delta = \frac{c'(\omega)}{c''(\omega)} = \frac{\varepsilon'(\omega)}{\varepsilon''(\omega)} \tag{23}$$

The frequency dependence of tan δ is the same as that for ε", though naturally the absolute values differ.

Knowing C(ω), with A, d and G(ω) we can calculate ε(ω) thus:

$$C''(\omega) = \frac{G(\omega)}{2\pi f} \quad \text{and} \quad \varepsilon''(\omega) = \frac{\sigma(\omega)}{\omega} \tag{24, 25}$$

A loss peak in C or D indicates a region of ω^2 dependence followed by a saturated value of G.

The relationship of capacitance parameters to the dielectric properties is constant, the factor being $C = \frac{\varepsilon A}{d}$ with A the plate area of the model capacitor, and d the interplate distance giving the volume of dielectric -material in use; hence the Cole-Cole model may be used equally well with data for either complex C or ε.

3.2.2. The Kramers-Krönig Relations

Before carrying out analysis of complex dielectric properties in the appropriate manner, it is necessary to pause for a moment in order to examine the mathematical relations governing the relationship between the real and imaginary parts of a complex number, the parts of which in this case provide information about the amplitude and the phase angle of the polarisation. [Kramers 1927, Kronig 1926]

Because, as has been seen, both ε' and ε" are generated by the same function, i.e. the applied frequency, it should be possible in practice to mathematically eliminate this generating function and isolate the relationship between the two resulting parameters.

This situation is applicable in this work also to complex refractive index (N=n-ik) where n is the propagation constant and k the extinction coefficient.

Let us consider a unit step function D(t) where $D(t) = \lim_{s\to 0}[\exp(st)]$ when t<0, and 0 when t>=0. (22)

this Fourier transforms to:

$$\tilde{D}(\omega) = \lim_{s\to 0}(s - i\omega)^{-1} \tag{26}$$

It is apparent that in the time domain, $Q_I(t)$ and D(t) are mutually exclusive, so we can say

$$Q_I(t)D(t) = 0 \tag{27}$$

By Fourier transformation,

$$\tilde{Q}(\omega)\tilde{D}(\omega) = 0 = \lim_{s\to 0}\int_{-\infty}^{\infty}\frac{\tilde{Q}(\omega')}{s - i(\omega - \omega')}d\omega' \tag{28}$$

By integrating the real and imaginary parts separately, we get two integral relationships between the real and imaginary parts of the initiating function. The real and imaginary components may be regarded as the cosine and sine transforms of f(t).

$$\varepsilon'(\omega) = \int_0^{\infty} f(t)\cos(\omega t)dt \tag{29}$$

$$\varepsilon''(\omega) = \int_0^{\infty} f(t)\sin(\omega t)dt \tag{30}$$

It may be seen that the real part is an even function of frequency, and the imaginary part odd. The transform we require is

$$\int_{-\infty}^{\infty}\frac{\sin xt}{x-\omega}dx=\cos\omega t\int_{-\infty}^{\infty}\frac{\sin(x-\omega)t}{(x-\omega)t}d[(x-\omega)t]+\sin\omega t\int_{-\infty}^{\infty}\frac{\cos(x-\omega)t}{(x-\omega)t}d[(x-\omega)t] \qquad (31)$$

The integrals are the Cauchy principal value; the meaning of this is that the imaginary contributions arising from the condition (x=ω) are ignored. The first integral then is equal to π and the second disappears, so that we are left with

$$\left(\frac{1}{\pi}\right)\int_{-\infty}^{\infty}\frac{\sin xt}{x-\omega}dx=\cos\omega t \qquad (32)$$

This integral is known as the Hilbert transform [Berne and Harp 1970] of the function sin(xt).By substituting this into the equations (4.2.2.1) and (4.2.2.2) and changing the range of integration, possible owing to the respective even and odd character of the functions, we obtain

$$\varepsilon'(\omega)=\left(\frac{2}{\pi}\right)\int_{0}^{\infty}\frac{x\varepsilon''(x)}{x^2-\omega^2}dx \qquad (33)$$

$$\varepsilon''(\omega)=-\frac{2\omega}{\pi}\int_{0}^{\infty}\frac{x\varepsilon'(\omega)}{x^2-\omega^2}dx \qquad (34)$$

These formulae enable us to ascertain either parameter of a complex function obeying causality (simply a situation where it may not be assumed that the effect of a causal factor may under any circumstances precede it!) from the other. They have been adapted for the analysis of other complex quantities encountered in the work.

3.2.3. Relaxation Processes

A polar molecule is defined as that which possesses a permanent separation of positive and negative charge centres (a "dipole moment"), this was first postulated by Debye as a

means of explaining the electrical properties of certain asymmetric molecules. This molecule, imagined for the purpose of the model as a sphere, may be aligned in the direction of an applied electric field, but is subject to being disorientated from this position as a result of collision with other molecules owing to thermal motion.

Correlation of dipole moment with molecular structure (Smyth, Pauling et al.) has been attempted by assigning moments to particular bonds in simple molecules, and applying vector algebra to resolve the sum and direction of the moment. This however assumes no interaction between bonds, and so the calculated values are usually higher than the measured ones; this is because in "real life" the inductive effects asserted by a particular bond (ie. sharing of electrons) upon a neighbouring one will prevent each bond attaining its full moment. Eyring *et al.* have however developed an approximate correction for this effect.

At high temperature and low field strength, the thermal energy kT (k is Boltzmann's constant and T in Kelvin) considerably outweighs the applied electrical energy, so that very few of the molecules are able to remain aligned with the field.

We can estimate the net dipole moment by statistical means :

$$P = \frac{4\pi}{3} N\left(\alpha + \frac{\mu^2}{3kT}\right) \qquad (35)$$

where μ is the permanent dipole moment per molecule, and N Avogadro's constant. α is called the polarisability and represents the induced dipole moment per molecule. It is for non-polar molecules the only contribution, corresponding to the optical polarisability as derived from the refractive index.

Molar polarisation is related to the dielectric constant by the Clausius and Mosotti approximation ()

$$\frac{\varepsilon - 1}{\varepsilon + 2}\frac{M}{d} = P \qquad (36)$$

with M the molecular weight and d the density.

Hence, we may establish the permanent dipole moment from the temperature variation of the dielectric constant. This is, however, valid only at low frequencies; if the frequency is increased beyond certain limits below which the molecules are able to follow the oscillations of the applied field, then an out-of-phase component of the dielectric constant develops; this is observed as conductivity or dielectric loss (a dissipation of the exciting energy as heat.) It is found to be the imaginary component of what now becomes a complex dielectric constant:

$$\varepsilon = \varepsilon' - j\varepsilon''$$

$$\varepsilon' - \varepsilon'_\infty = \frac{(\varepsilon'_0 - \varepsilon'_\infty)}{1+\omega^2\tau^2} \qquad (37, 38, 39)$$

$$\varepsilon'' = \frac{(\varepsilon'_0 - \varepsilon'_\infty)\omega\tau}{1+\omega^2\tau^2}$$

Cole and Cole [1941] showed that for the case of a single relaxation time a plot of ε' vs. ε" gives a semicircle centred upon the ε' axis. In real situations, there is however, usually a distribution of relaxation times rather than a single one. This is a statistical parameter applying to the relaxation and can occur, for example, in a solid state material where the structure impedes the free movement of the molecules. The model must therefore be modified for this case, and a variety of such treatments will now be discussed.

3.2.4. Debye Relaxation Model for Condensed Matter

The relation

$$\varepsilon^* = \varepsilon_\infty + \frac{\varepsilon_s - \varepsilon_\infty}{1+jx} \qquad (40)$$

describes the ideal frequency response for oscillation in condensed matter [Debye]

The function x is equivalent to $\omega\tau$, where τ is the Debye relaxation time, ε_∞ the high frequency or optical dielectric constant (calculable, as will be described later in the work, from the optical absorption properties of the material) and ε_S the static or low frequency

dielectric constant. Functions of these latter two parameters are defined; the expression $\varepsilon_s - \varepsilon_\infty$ being referred to as the dielectric relaxation strength, and the ratio $\varepsilon_s/\varepsilon_\infty$ as the relaxation ratio r, of the static to the optical dielectric constant.

The Debye relaxation may be described in terms of the loss tangent tan δ. This parameter is best described by visualising a vector diagram of the ratio of loss current to charging current for a capacitor :

with the angle δ being the angle between loss and charging currents.

$$\tan\delta = \frac{r-1}{r+x^2}x \qquad (41)$$

tan δ indicates the ratio of energy dissipated in the dielectric to energy stored at the polarisation peak.. It is dissociated from the sample geometry, being a ratio of two parameters containing the same factor of geometry.

Further, the complex impedance can be described by :

$$Z^* = \frac{R}{1+jx/r} - j\frac{R}{(r-1)x/r} \qquad (42)$$

For single relaxation, the dielectric constant describes a semicircle in the complex plane; the complex impedance diagram becomes more approximate to a semicircle with increasing relaxation ratio r. r has to be fairly large for this condition to be satisfied. This effect

The relaxation times are calculated as follows;

$$\tau_{\tan\delta} = \frac{\tau}{\sqrt{r}}$$

and (43, 44)

$$\tau_m = \frac{\tau}{r}$$

3.2.5. Cole-Cole relaxation model

The Cole-Cole model [Cole and Cole 1941] is an amendment or addition to the Debye equations, which proposes that the deviation from the single relaxation model which may be readily observed from experimental data is an effect of there being not a single relaxation time, but a distribution thereof, characterised by a *distribution parameter* α. The descriptive equation is

$$\varepsilon^* = \varepsilon_\infty + \frac{\Delta\varepsilon}{1+(jx)^{1-\alpha}} 0 \le \alpha < \tag{45}$$

It is readily observed that for the case α=0 this equation corresponds to the Debye equation (4.2.1). The value of α for "real" materials tends to fall between 0.2 and 0.5. The distribution coefficient α may be ascertained from the plot of ε" vs. ε', where the familiar depressed semicircle may be observed. The depression angle is πα/2 rad.

As a consequence, the peak predicted by the Cole-Cole theory is broader and less pronounced than that from Debye theory. An expression for the full width half maximum (FWHM) value is given by :

$$FWHM = 2\log\left[2+\sin\frac{\pi}{2}\alpha+\sqrt{\left(2+\sin\frac{\pi}{2}\alpha\right)^2-1}\right] \tag{46}$$

The distribution function is given as

$$F(U) = \frac{1}{2\pi}\frac{\sin(\alpha\pi)}{\cosh(1-\alpha)U-\cos(\alpha\pi)} \tag{47}$$

Having established the function for ε*, the formulae for other dielectric functions may be adapted also...

$$\tan\delta = \frac{(r-1)x^{1-\alpha}\cos\pi/2\alpha}{r+(r+1)x^{1-\alpha}\sin\pi/2\alpha+x^{2(1-\alpha)}} \tag{48}$$

and

$$Z^* = \frac{R_t}{1 + jx_t} - j\frac{R_t}{(r-1)(x_t - \tan \pi/2\alpha)}$$

where

$$x_t = \tan \pi/2\alpha + \frac{x^{1-\alpha}}{r \cos \pi/2\alpha}$$

$$R_t = \frac{R}{x^{\alpha} \cos \pi/2\alpha}$$

(49, 50, 51)

A generalised formula to establish the relaxation time distribution in dielectrics has been postulated by Al-Refaie [1991]. This involves analysis of the complex dielectric plot for multiple arc distributions. For example, for the double arc relation the condition $\varepsilon'' = \varepsilon_1'' + \varepsilon_2''$ holds, which indicates the presence of two distinct relaxation processes with differing frequency properties. This analysis also offers the possibility of being extended to any number of arcs, m, as may be present in the plot; there are as many terms in F(U) as there are arcs, each of the form of Equation (4.2.8) but preceded by a weighting factor of the general form

$$\frac{(\varepsilon_{sn} - \varepsilon_{\infty n})}{\sum_{n=1}^{m} (\varepsilon_{sn} - \varepsilon_{\infty n})} \qquad (52)$$

The complete expression for the RTD then takes the form

$$F(U) = C\sum_{n-1}^{m} \frac{(\varepsilon_{sn} - \varepsilon_{\infty n})\sin(\alpha_n \pi)}{\cosh(1-\alpha_n)(U+\beta_n) - \cos(\alpha_n \pi)}$$

where

$$C = \frac{1}{2\pi}\sum_{n=1}^{m}(\varepsilon_{sn} - \varepsilon_{\infty n})$$

$$\beta_n = \ln\left(\frac{\tau_{01}}{\tau_{0n}}\right)$$

$$U = \ln\left(\frac{\tau}{\tau_{01}}\right)$$

(53, 54, 55, 56)

n designates any particular arc specified by the above parameters.

3.2.6. ac Conductance

At low temperatures, the frequency dependence of ac conductivity in phthalocyanine may be expressed as

$$\sigma(\omega) = A\,\omega^{s} \qquad (57)$$

A is a complex proportionality constant. The index s requires further discussion, since there appears from the literature to be some disagreement as to its temperature dependence, though it decreases with increasing frequency. The exponent s is defined as

$$s = \frac{d\ln\sigma(\omega)}{d\ln\omega} \qquad (58)$$

For the correlated barrier hopping model postulated to be occurring in our materials, the following model for s applies:

$$s(f) = \frac{p^2 N^2 e}{24}\left(\frac{8e_r^{\,2}}{eW_m}\right)^{6}\frac{(2pf)^{s}}{t_0^{\,1-s}} \qquad (59)$$

with W the maximum height of the barrier, t_0 a characteristic relaxation time, e the effective dielectric constant and n the spatial density of defect states.

The exponent s is given as

$$s = 1 - \frac{6kT}{W_m} \tag{60}$$

3.2.7. Capacitance

Various equivalent circuit models have been postulated to describe the effects of frequency and temperature upon the capacitance of a thin film device. The capacitance is again a complex quantity; tan δ is equivalent to $C''(\omega)/C'(\omega)$.

If we define the geometrical capacitance as that capacitance which would be obtained were the dielectric material in our device replaced by free space, we have a useful method of determining the relative permittivity of the medium :

$$\varepsilon_r(\omega) = \frac{C(\omega)}{C_0} = \frac{\varepsilon(\omega)}{\varepsilon_0} \tag{61}$$

There are some observations worth making concerning the relationship between C" and G; a loss peak in the capacitance or dielectric constant often corresponds to a square law conduction:frequency regime followed by a saturated value for conduction; and if C" remains proportional to reciprocal ω whilst remaining independent of frequency, this corresponds to dc conduction.

The consideration of a variety of circuit models [Jonscher 1983] is necessary in order to properly establish the correct parameters for a particular device. Some suitable models are:

(a) R-C series;

(b) R-C Parallel;

(c) Series R-C in parallel with C;

(d) two parallel R-C circuits in Series.

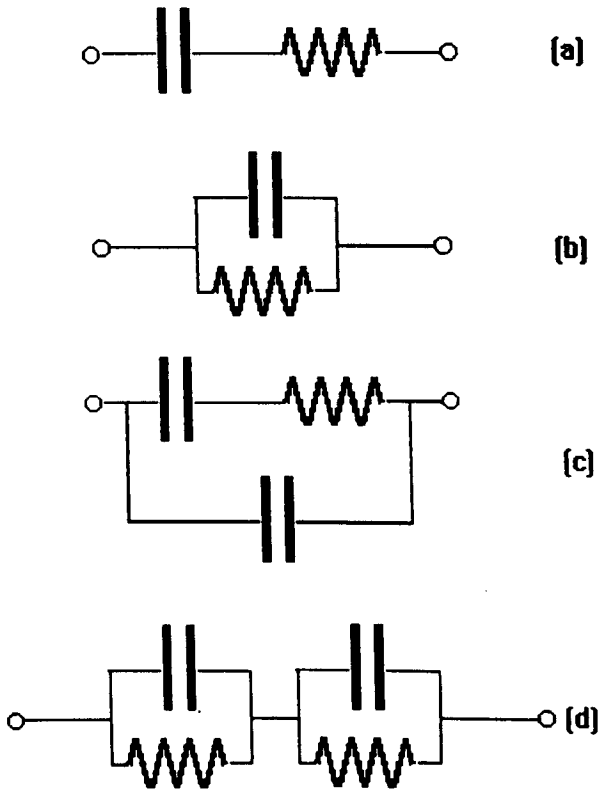

As is the practice in ac theory, the current responses of these circuits will be discussed in vector form; this system has already seen mention in the earlier discussion of dielectric loss. The ratio of current to voltage when discussing ac . is known as the admittance, analogous to conductance in dc theory.

In this case the presence of a frequency and temperature independent capacitance element **C** is assumed, a resistance element **R** in parallel with the capacitance (the film) and a further series resistance **r** present in the leads of the measurement apparatus. The model for impedance of this circuit is given by :

$$Z = \frac{R}{1 + j\omega CR} + r = \frac{R + r(1 + \omega^2 R^2 C^2)}{1 + \omega^2 R^2 C^2} - \frac{j\omega CR^2}{1 + \omega^2 R^2 C^2} \qquad (62)$$

There is a further, more complicated model which requires consideration, as it is used in the modelling of a capacitative device one or both of the electrodes of which have high sheet resistance; the uniform distributed R-C line:

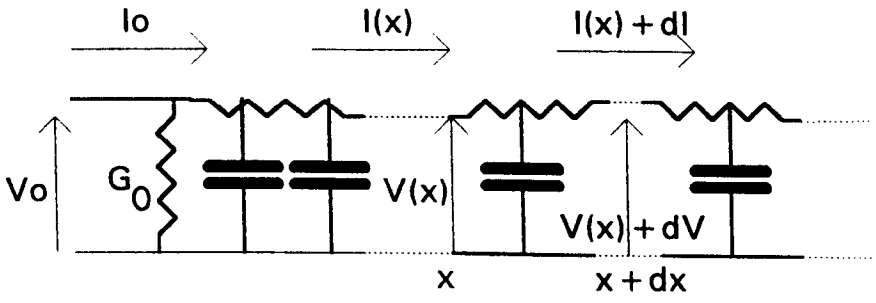

The model parameters are the following: The X direction is the distance from the external contact into the material. The resistance per unit length in this direction is assumed to be constant r. The capacitance per unit length is c.

If

$$A = (1+i)(rc/2)^{0.5}\omega^{0.5} \tag{63}$$

then

$$\frac{d^2V}{dx^2} = A^2V(x) \tag{64}$$

the solution of which gives

$$(x) = V_0(\cosh Ax - B\sinh Ax)$$

and (65, 66)

$$I(x) = -\left(\frac{1}{r}\right)\frac{dV}{dx} = -\left(\frac{V_0A}{r}\right)(\sinh Ax - B\cosh Ax)$$

where Vo is the input voltage to the line and B a constant related to the boundary conditions at the far end. (B=1 for line of infinite length.) The complex permittivity of the system is

$$\varepsilon(\omega) \propto (i\omega)^{0.5} \qquad (67)$$

Remarkably, the real and imaginary parts are equal and increase indefinitely toward low frequency.

3.3 Absorption of Light; Processes and Effects; Theory of Dispersion

Radiation at optical frequencies may be absorbed by a medium according to the energy of the incident wave and the free carrier density in the medium; the dielectric constant at such frequencies is a parameter in the process.

Let us begin by considering the response of the system to an impulse in the form of a very brief electric field; we can then predict the response of the system to an alternating applied electric field.

The effect of applying any electric field will be to cause partial alignment of dipoles in the material. By applying a short pulse, we can promote an alignment process which cannot be fully completed during the duration of the pulse. The partially induced alignment will then decay back to zero, by means of one or a number of processes; for the case of the single oscillator model we shall assume this decay to be exponential. If we call the polarisation at time t $Q_I(t)$ then for a pulse at t=0:

$$Q_I(t) = 0 (t < 0)$$
$$Q_I(t) = Q_0 \exp(-t/\tau) (t \geq 0) \qquad (68,69)$$

τ is as usual the time constant of the decay process.

An electric field, $E_0 \exp(i\omega t)$ may be represented as a series of impulses at intervals dt and magnitude $E_0 \exp(i\omega t)dt$. For linear response to a series of such impulses, the total response P(t) is obtained by the combination of all the individual responses.

$$\begin{aligned} P(t) &= \int E_0 \exp(i\omega t') Q_I(t-t')dt' \\ &= E_0 \tilde{Q}(\omega) \exp(i\omega t) \\ \tilde{Q}(\omega) &= FT(Q(t)) \end{aligned} \tag{70}$$

The dielectric constant is related to the two parameters P(t) and E_0 thus:

$$\varepsilon(\omega)\varepsilon_0 E_0 \exp(i\omega t) = \varepsilon_0 E_0 \exp(i\omega t) + P(t) \tag{71}$$

so it follows that

$$\begin{aligned} &\varepsilon_0\{\varepsilon(\omega)-1\} = \tilde{Q}(\omega) \\ &\textit{where} \\ &\tilde{Q}(\omega) = Q_0(i\omega + 1/\tau)^{-1} \end{aligned} \tag{72}$$

By solution for the real and imaginary parts we obtain

$$\begin{aligned} \varepsilon_1(\omega) - 1 &= \{\varepsilon(0)-1\}/(1+\omega^2\tau^2) \\ \varepsilon_2(\omega) &= -\{\varepsilon(0)-1\}\omega\tau/(1+\omega^2\tau^2) \end{aligned} \tag{73, 74}$$

The high frequency limits of the preceding pair of equations are significant; $\varepsilon_1(\omega) \rightarrow 1$ from above this value, and $\varepsilon_2(\omega) \rightarrow 0$.

In this type of system, $Q_I(t)$ must be zero at $t<0$. This is the mathematical condition of causality which was touched upon during the discussion of Kramers-Kronig relations. Naturally, any appropriate functional form may be written for $Q_I(t)$ and its Fourier transform, so as to account for the exact relaxation processes prevailing in the particular medium considered.

3.4 Photoconductivity

3.4.1 Introduction

Photoconductivity is simply defined as that property possessed by a material whose conductivity increases under illumination. It can arise from one of two cases, (a) an increase in the number of free carriers, or (b) an increase in their mobility. The possible mechanisms which may cause either of these states of affairs will presently be discussed.

In simplest terms, for the case of one type of carrier present only:

$$\sigma_{ph} = \Delta\sigma = \Delta n e \mu + \Delta \mu e n \tag{75}$$

e is the unit charge, n the free carrier density and μ the mobility.

In empirical terms, if we consider that the illumination of a photoconductor causes formation of x carriers per unit volume per second then $\Delta n = x\tau$ where τ is the carrier lifetime. x is the product $\eta\alpha\Phi_0$ with η the quantum efficiency of photogeneration, α the absorption coefficient and Φ_0 the incident photon flux. If we consider the case of a solid bounded by ohmic contacts, we can write

$$i_{ph} = \sigma_{ph} F = \eta\Phi\tau e\mu F / L \tag{76}$$

This equation, when the condition is applied that the carrier mobility is unaffected by the incident light, represents the photocurrent. F is the electric field strength, and Φ the total absorbed light radiation per unit surface area per second. l is the thickness of the film/sample.

3.4.2 Processes of Photocarrier generation

There are broadly two types of processes which may occur in molecular solids; however, the sum total of these processes may be divided in two distinct ways as shown in the succeeding table.

Table 1

Category of Process	Involves Dissociation	Does Not Involve Dissociation
Intrinsic	Autoionisation	Band to Band Transitions
Extrinsic	Dissociation at E/S Boundaries Trapped Carrier/Exciton Interaction Interactions of Excitons and Impurities	Trapped Carrier Excitation into Conduction or Valence Bands

Firstly : those which involve exciton (hole/electron) dissociation and those which do not.. In the former category are dissociation at electrode/semiconductor boundaries, interaction of trapped carriers with excitons, autoionisation and interaction of excitons and impurities.

In the latter category: trapped carrier excitation into conduction or valence bands, and band to band transitions.

However (secondly) autoionisation and band to band transitions are characteristic of intrinsic photoconduction; the other mentioned processes extrinsic and more likely to occur at longer wavelengths.

Approximate free carrier lifetime in metal-free Pc crystals has been found to be about 10^{-8} sec. (Trapping time for electrons) The trapping time for holes is estimated to be at least this long. The drift-mobility in CuPc thin films is reported as 10^{-3}-$10^{-4}cm^2Vs$ (Simon and Andre 1985)

In order to make a more efficient photogeneration device utilising CuPc, a multilayer structure has been proposed by Takada, Awaji, Koshioka, Nakajima and Nevin (1992). The efficiency may be increased by a reduction of the probability of hole/electron recombination and has been achieved in this manner : TiO(x≈2) which has a higher electron affinity than CuPc and little or no photoconductive ability, is used for charge transport. Photoconduction is initiated in the CuPc, but the electrons are transferred to the TiO(x2) whilst the holes remain in the CuPc. This renders recombination far less

likely than for the situation of both types of carriers being present in the same material. More efficient charge separation, coupled with a greater mobility in the TiO(x~2) led to an increase in efficiency of between one and two orders of magnitude.

3.4.3 Effects of ambient parameters on photocurrent.

The relationship elucidated by Rose [1951] governing the relationship between incident light intensity, temperature, photocurrent and trap distribution is:

$$p^* = (f/kT_cP_0vS) \exp (T_c/(T+T_c) * N_v \exp (T/T+T_c)` \quad (77)$$

where :-

p^* is density of photoexcited holes,

T_c is a parameter relating to how fast the defects fall off with the energy E in the exponential model of levels.

F is the steady state Fermi level

P_0 is the density of defects at the edge of the valence band, per unit energy.

The trapping states, kT wide at the Fermi level, exercise control over the space charge limited conduction.

Variation of the ratio free carrier density to total carrier density determines the i-V characteristic in the SCLC region. The limiting gradient value for the SCLC I/V curve is $(T_c+T)/T$.

Having obtained the characteristic temperature T_c, it is then possible to determine the density of states from data for the thermal variation of photoconductivity. This is achieved by plotting log (photocurrent-dark current) against $(T_c+T)/T$, where a linear plot with slope Nv should be obtained.

The following models the I-V relation for exponential distribution of trapping states.

$$j = p\mu\varepsilon_0[(V+V_x)/V_x]^{T_c/T}V/d \qquad (78)$$

(T = temperature, T_C is characteristic temperature of the trap distribution.) valid for TcT >= 1.1 for the current-voltage relationship :

$$j = \rho\mu\varepsilon_0 V/d = \rho\mu\varepsilon_0 \exp[(F-F_0)/kT]V/d \qquad (79)$$

The activation energy value obtained from the plot of log J vs. 1/t for dark conductivity is suggested to be a good measure of F_0.

3.5.1 Absorption and Reflection Spectrophotometry and Associated Calculations

Measurement of the absorption and reflection data for a thin film in the visible and UV region provides valuable information about electronic processes in the material at those wavelengths.

Absorbed, transmitted and reflected radiation are linked by the equation

$$R+T+A=1 \qquad (80)$$

where absorption A and the transmittance T are given in terms of I_0 and I_t, the input and output optical intensities, respectively.

The absorption coefficient α for a film of thickness t is defined by the condition that the energy in the wave falls to a value of exp(−1) in a distance α^{-1}.

The complex index of refraction N is defined by the following terms:

$$N = n - ik \qquad (81)$$

where n is the "real refractive index" or propagation constant, and k the extinction coefficient, equivalent to

$$k = \frac{\alpha\lambda}{4\pi} \qquad (82)$$

Calculation of n from measured values of R and k is performed using quadratic solution of the relationship

$$R = \frac{(n-1)^2 + k^2}{(n+1)^2 + k^2} \tag{83}$$

Also, the complex dielectric constant

$$\varepsilon^* = \varepsilon_1 - j\varepsilon_2 \tag{84}$$

is related to n and k by the following:

$$\varepsilon_1 = n^2 - k^2 \tag{85}$$

and

$$\varepsilon_2 = 2nk \tag{86}$$

Hence from absorption and reflection spectra only, it is possible to obtain a great deal of information about the dielectric properties of the material under test.

From the absorbance spectrum alone, having calculated α from the absorbance and film thickness, we are able to ascertain the density of localised states (from the Urbach relation) and the optical band gap, in terms of the one-electron theory for molecular solids. The Urbach relation is

$$\alpha(\nu) = \alpha_0 \exp[(\frac{h\nu}{\Delta}) - b] \tag{87}$$

where α_0 and b are temperature-dependent constants and Δ band tail distribution.
By plotting ln (α) versus hν, the linear variation of ln (α) in the low energy side of the Q band peak may be used to calculate Δ. This quantity has been postulated to represent the widths of band tails for some materials, but this explanation does not suffice for phthalocyanines, the variation being too small to fit the model of band-tail distribution. It is thought that van der Waals' forces give rise to the observed distribution of random fields.

In the region of direct band to band transition, the absorption coefficient is given in the form

$$\alpha(\nu) = (\frac{B}{h\nu})[h\nu - E_0]^x \qquad (88)$$

where E_0 is the optical gap. The index x takes the value 0.5 for allowed transitions. Plotting $(\alpha h\nu)^2$ against photon energy allows examination of the relevant region, for our phthalocyanines around 2.7-3.5eV, where straight line fitting will allow elucidation of the optical gap E_0.

The intrinsic bandgap in phthalocyanines is believed to be in the region of 2eV, varying subject to the type of central substituent present.

The surface roughness of the films may be ascertained by measurement of the reflectance of both front and rear of the film-substrate interface (provided the substrate is transparent in the region to be measured!)

This quantity is given in terms of the exponential dependence of irregularity height σ on the incident wavelength λ:

$$R \propto R_0 \exp\left[-\frac{4\pi\sigma}{\lambda}\right]^2 \qquad (89)$$

where R_0 is the reflection obtained from a smooth surface. The angle of acceptance of the instrument must be small for this to apply (Gupta, Maiti et. al .1995) which is the case here. Plotting $\log(R/R_0)$ against $1/\lambda^2$ allows σ to be determined from the slope.

4.1 Introduction

The experimental work for this project consisted of the following procedures :-

(a) purification of powdered phthalocyanines by entrainer sublimation;

(b) vacuum evaporation of metals and Pc materials to form devices for testing;

(c) post-deposition treatments of sample devices by voltage-cycling and annealing;

(d) determination of film thicknesses by surfometry;

(e) optical characterisation of sample films by transmission spectrophotometry;

(f) electrical characterisation of device properties over a range of temperatures.

The materials studied were:

(i) Heavy-fraction bisphthalocyanine HF (pc)(pc*). This is a diphthalocyanine with a number of rare earth elements present at the central substitution site.

(ii) Gadolinium bisphthalocyanine Gd(pc)(pc*).

(iii) Thulium bisphthalocyanine Tm(pc)(pc*)

(iv) Lutetium bisphthalocyanine Lu(pc)(pc*)

(v) Fluorochromium phthalocyanine FCrPc.

4.2 Entrainer Sublimation

Some phthalocyanines used in the project may be readily obtained from commercial suppliers. These are supplied as powders, as what is termed "analytical grade". These materials are not particularly pure, and contain greater or lesser proportions of solvents and unreacted materials used in their synthesis. The process of entrainer sublimation allows the separation of the phthalocyanine and contaminants without resorting to any form of chemical treatment. The apparatus used for this purpose is illustrated in Fig. 4.1.

The principle of operation is to place a amount of powder into one end of a glass tube about one metre in length, which has a constriction near this end. A light plug of glass wool is placed in the constriction. Dry nitrogen, pre-treated by passing it over heated copper turnings to remove residual oxygen, is passed through the tube at a rate of approx.100ml/minute. A temperature gradient is applied to the tube, about 550C at the point where the Pc is, and decreasing toward the far end of the tube. The phthalocyanine and associated impurities sublime, and are carried along the tube by the nitrogen flow. According to the molecular weights of the components and their temperature, the various components are deposited at different points along the tube. After a few hours the tube is cooled, and the pure phthalocyanine identified by its monoclinic needle-like crystals. The tube is cut open at this point and the pure material recovered. The purpose of the bubbler at the end of the nitrogen flow line is to remove volatile materials before the spent nitrogen is vented to atmosphere.

4.3 Vacuum Evaporation for Film and Device Preparation

The method of physically preparing a Pc film for use as an experimental sample requires great care and dexterity of implementation to prevent any damage occurring. If *vacuum evaporation* is employed as the means of film deposition, it must be borne in mind that most of the operational parameters of a vacuum deposition system have some effect upon the film structure or quality; background pressure, material purity and substrate temperature (in addition to the film thickness) are important factors in the themselves onto any cold surface (substrate, bell-jar and chamber fittings). The thickness of the deposited layer may be measured using a quartz crystal oscillator. This is a quartz wafer which is caused to oscillate at its natural frequency. The frequency of oscillation decreases as material is deposited on it, and this change may be translated to a thickness so long as the density and acoustic impedance of the material are known.

When the required thickness of layer has been formed, the power is switched off and the chamber allowed to cool, since allowing air to enter whilst the material is still hot might promote undesirable oxidation effects. After an hour or so has elapsed, the chamber is pressurised and the sample recovered.

This process would have to be repeated at least twice with different materials to make a sample for electrical testing.

The requirements for deposition of electrodes on samples held on ITO glass are more rigorous than those for non-conductive glass; the evaporation must be maintained at a very slow rate, and it is necessary to cool the substrate. This is because any resublimation of the film material as a result of failure to observe these conditions may result in a physical contact being formed between the metal and glass, rendering the sample useless. The same phenomenon can occur as a result of the film evaporation

process; vacuum-sublimed layers are often markedly non-uniform, and pinholes can be present in thin (<1m) layers prepared by this method. Filling of the pinholes with the metal is the problem in this case. This phenomenon is not, however, an exclusive prerogative of films on ITO glass; film resublimation may also cause failure of contact between metal and Pc on planar structures, although pinholing of the sample material is not so appreciable a problem with this type of structure.

The type of electrode material(s) used in the manufacture of devices for testing is an important parameter, as the electronic behaviour of the film/metal interfaces present in a device has some considerable bearing upon its overall properties. The reasons for this are outlined in Chapter 3.

4.4 Post-Deposition Treatments

The procedures for post deposition treatment are as follows :

(a) Untreated : no post-deposition process is employed.

(b) Annealed : simply involves baking the material at a predetermined temperature in a furnace for a certain time. The effect is usually to promote a partial phase change in the material crystalline structure. (Lucia and Verderame, 1968)

(c) Voltage cycled to blue :

and

(d) Voltage cycled to red : This procedure is applicable to materials such as HF (pc)(pc*) which are *electrochromic.* This means that they can exhibit a colour change when the film is subject to a potential gradient between its opposing faces, which promotes an oxidation or reduction process in the material.

Voltage cycling is performed by setting up a cell consisting of a small beaker containing a 5-10% w/v solution of KCl in water. The sample is used as one of the electrodes, and a sinusoidally varying voltage is applied to the cell. The "direction" of voltage cycling, whether to red or blue, is determined by the applied dc bias to the signal. A change of colour may be readily observed, but unfortunately bleaching can occur to certain compounds as a result of repeated voltage cycling. See Fig. 4.4.

4.5. Determination of film thickness by surfometry

It can be useful to double-check the film thicknesses, as the value is critical for calculation of resistivity and optical constants. The surfometer is a device for mechanically measuring film thickness. It operates by tracking a stylus connected to an optical lever over the border of the film on the glass, and provides a direct reading of the step height thus observed. Fig. 4.5 illustrates the apparatus and its principle of operation.

4.6 Transmission Spectrophotometry

Some samples were optically characterised by means of a Phillips PU8720 UV/Visible single beam spectrophotometer before addition of the electrodes was carried out. (Exley, Ray, Ahmet and Silver, 1994) It is necessary to employ a "blank" (an

uncoated substrate) of the same type as that on which the film is coated. This must be placed in the beam and calibration data stored for the base line and zero settings throughout the wavelength range in use. This procedure is distinct from a double-beam device which effects continuous comparison between the reference and sample. The wavelength range used in this case was 300nm < < 900nm. The coated substrate is then substituted, and data for absorption and transmission are recorded as a sequence of 750 data points, corresponding to a wavelength step of *ca.* 0.8nm. As the machine is interfaced to an IBM-PC which may log the spectral data, these results were saved to floppy-disk in readiness for their processing on another computer. From these data, there have been calculated the extinction coefficient k, the propagation constant or "real refractive index" n, and the real and imaginary parts of the dielectric constant at optical frequencies, ε_1 and ε_2. n was derived from the absorption spectrum of the materials by means of an integral method (Jonscher 1983, Kramers and Kronig,)

4.7 Electrical Characterisation of devices

4.7.1. Installation of Measurement System

Having established that a large amount of the work required for elucidation of the properties of Pc compounds would involve measurement of their electrical and photoelectric properties at a range of temperatures, it was decided that the most convenient method of collecting data in the quantities necessary would be to install a system of measuring equipment capable of being interrogated and controlled by a computer. As a result of this, the first steps in the production of experimental data for this thesis were to obtain, interface and program a suitable system of instrumentation to carry out all these tasks.

4.7.2. Measurement System Hardware

The finished system consists of an Oxford Instruments liquid nitrogen cryostat (Fig. 4.6), of a type incorporating its own liquid nitrogen reservoir. This model is economical on cryogen compared to its continuous-flow counterparts, and the temperature of its sample space is measured and governed by an Oxford ITC4 intelligent temperature controller. This controller operates on the proportional/integral/derivative (PID) control system, although proportional/integral (PI) temperature control has proven entirely adequate without the use of any derivative term in the loop. The controller is driven from the serial communications port of the IBM-PC computer, and is

capable of regulating and measuring sample temperatures from 77K to 300K. Above 300K, an automatic thermal trip isolates the heater from its supply so as to prevent damage to the cryostat by overheating.

The temperature probe supplied with the cryostat is a thermocouple located in the sample heat exchanger; this is effectively somewhat distant from the sample itself, and raised questions concerning the possibility of a temperature gradient existing between the heat exchanger and the sample. This was investigated by use of a second thermocouple on the sample head itself, and using nitrogen as an exchange gas in the sample chamber (not the most ideal exchange gas; helium is preferable) it was observed that the worst-case temperature discrepancy between the sample head and heat exchanger was 1K at steady state.

The cryostat incorporates a quartz window adjacent to the sample head, and an aperture in the sample mount itself, permitting the impingement of light of considerable wavelength range onto either surface of the sample device. Rotation of the sample in the cryostat is possible without the necessity of breaking the vacuum in the sample chamber.

For electrical property measurement, there are present a Hewlett-Packard 4284A Precision LCR meter, used to indicate AC capacitance, conductance and dielectric loss factor of a sample at frequencies between 20Hz and 1MHz. The peak-to-peak voltage of the applied signal may be preset to any value not exceeding 20V, and the possibility exists of applying a dc bias to the material.

In addition to this, a second instrument (a Hewlett-Packard 4191A RF impedance analyser) is available, allowing measurement of the aforementioned

parameters to be extended to the frequency range 1MHz - 1GHz in steps of 100 kHz. For both these bridges, it was necessary to internally compensate the leads and connections against parasitic inductance, capacitance and impedance before use. This is achieved by an on-board calibration function of the instrument.

A Keighley 617 digital electrometer is employed in the collection of DC I/V conduction data. This incorporates a voltage source which can provide a dc level of 130V to -130V, in conjunction with a picoammeter. This is also used in conjunction with a Solartron Schlumberger 7150 digital multimeter to obtain resistivity data by the van der Pauw 4-point probe method. (q.v.)

A Farnell SW1B IEEE-488 switching unit is employed to allow appropriate connection of the sample to these instruments by the computer. This is simply an array of 32 two-way latching relays under IEEE control.

The complete system schematic is shown in Fig. 4.7. and device types tested are illustrated in Fig. 4.8.

4.7.3 Measurement And Data Logging Software

With the aforementioned exception of the temperature controller, all the apparatus is controlled from a National Instruments "GPIB-PC" IEEE GPIB interface card present in the PC. The software which addresses the instruments and collects the data was developed by the author in Microsoft QBasic and allows the operator to pre-select a range of temperature steps, the default being 77K-152K in 5K steps, and 152K-292K in 10K steps, and the following types of measurement :

(a) I/V characteristics - three measurement sequences are selectable, offering easy setting of minimum and maximum voltages for the sweep, along with the step size. It is therefore possible, for example, to test a sample in the range -20V to +20V with steps of 1V from -20V to -3V and 3V to 20V, and 0.05V steps from -3V to +3V.

(b) Dielectric loss D, a.c. conductance G and capacitance C may be automatically measured at forty eight semi-logarithmic preset steps in the range 20Hz - 1MHz.

(c) van der Pauw resistivity measurements may be performed over any suitable voltage range and step increment, as for I/V measurements in (a) above. Switching of the sample contacts is performed automatically by the Farnell switching unit.

(d) Any combination of the above may be performed over a range of selected temperature values falling between 77K and 300K. Once the sequence has been initiated, no further attention is needed other than to periodically maintain the supply of liquid nitrogen in the cryostat. A time delay may also be introduced between the recording of individual data points for a particular temperature; this is for the purpose of negating the effects of polarisation of the sample. (in real terms, this means that at a fixed applied voltage, there may well be observed a current-time profile; after a certain length of time the current will stabilise and the measurement may then confidently be taken. For the reasoning behind the polarisation processes, see "Theory".

The data are saved to disk in the form of ASCII (text) columns of number values delimited by a space; the file name is selected automatically; the main part indicates the temperature at which the measurement was performed ("T_77", "T_292" and so on) and the three-letter extension the type of measurement, as follows.

Table 2. File Extensions for Data Acquisition Software

File Extension	Measurand (X,Y)	Description
.IVM	V(V), I(A)	I : V, resistance
.IAB	I(A), V(V)	Van der Pauw 1
.IAD	I(A), V(V)	Van der Pauw 2
.CAP	F(Hz), C(F)	Capacitance C vs F
.CON	F(Hz), G(S)	Conductance G vs F
.DIL	F(Hz), D	Dielectric loss D vs F

The sample material name, or a convenient abbreviation thereof, is usually selected as the name of the directory on the PC hard disk to which the results are saved, enabling all the data obtained from a particular sample to be accessed from the same source. These data may be read by the Microsoft "Excel" spreadsheet package, wherein appropriate calculations may be performed. The results can be presented in graphical form using the "Easyplot" program.

A subroutine to computer-drive a Spex monochromator for photoelectric measurements was later developed independently due to the kind assistance of a colleague, who carried out the work as a BSc. project. This was subsequently incorporated into the main controller program by the author, and used in gathering photoelectrical data for fluorochromium phthalocyanine samples.

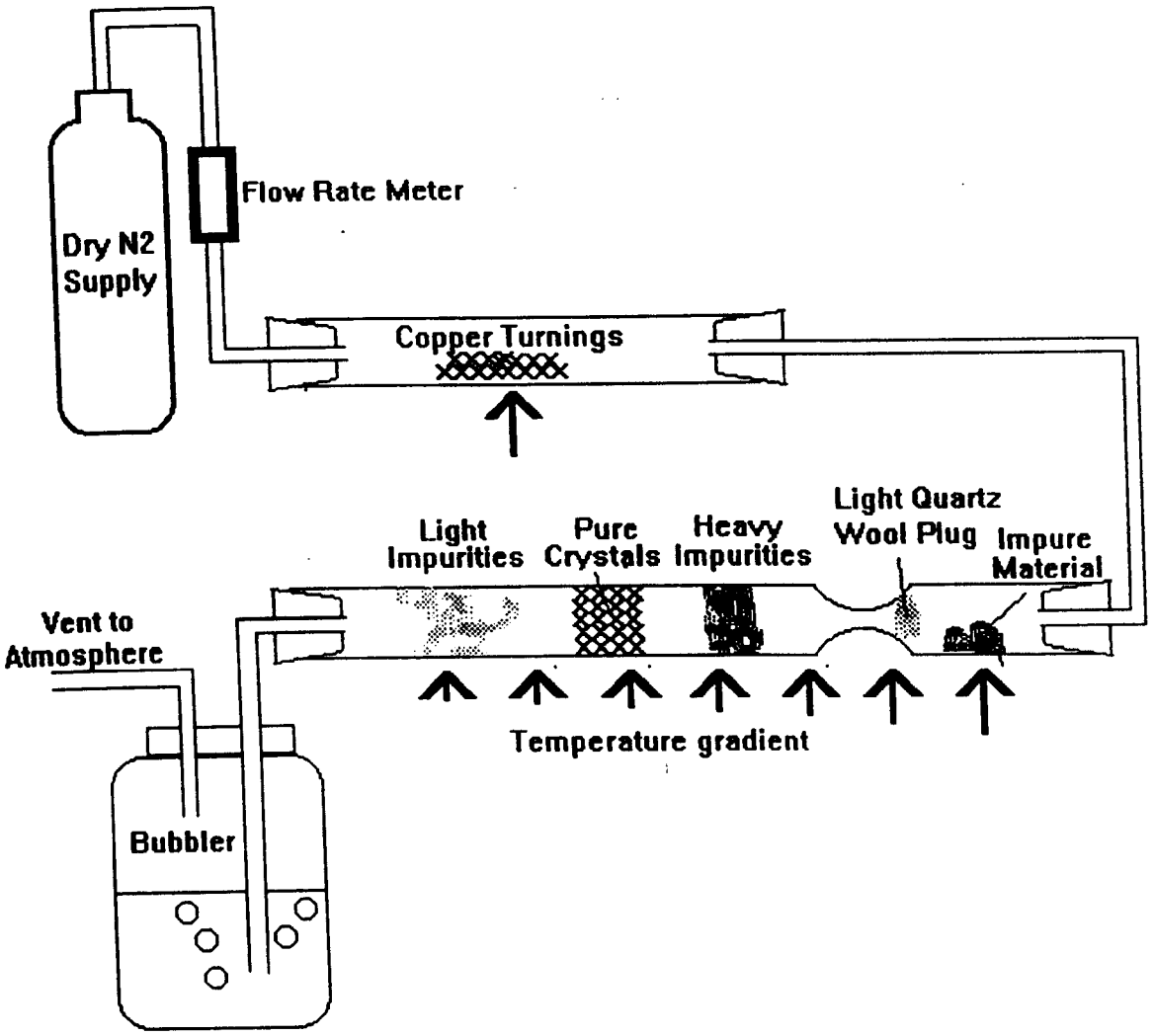

4.1 Schematic of Entrainer Sublimation process apparatus.

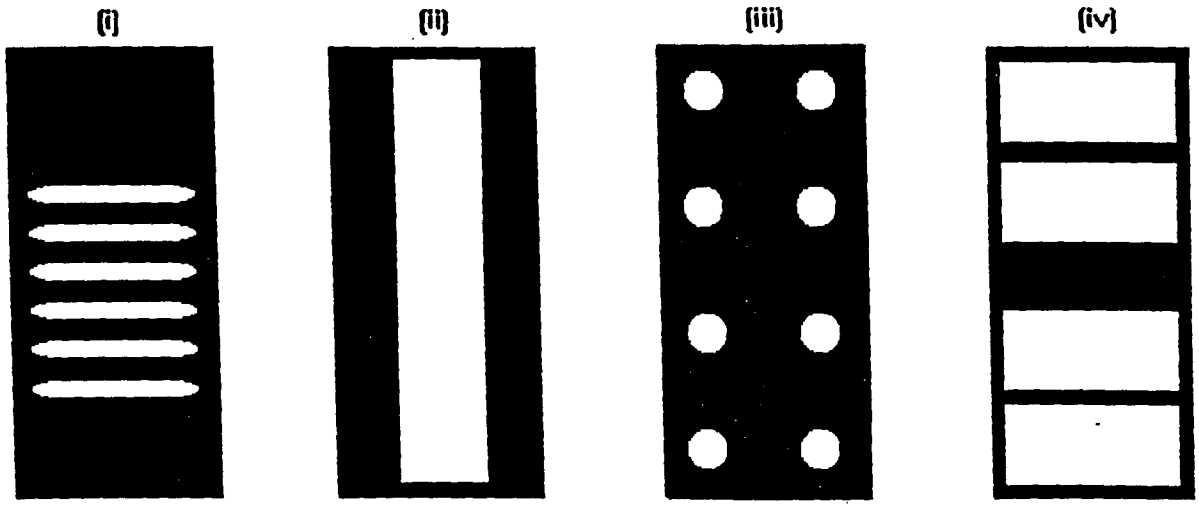

(i) base electrode for sandwich structure
(ii) top electrode " " "
(iii) electrodes for van der Pauw measurement
(iv) electrodes for planar measurement

4.2 Illustrations of the various electrode configurations employed in our investigations

(a) apparatus for evaporation of metal electrodes

(a)

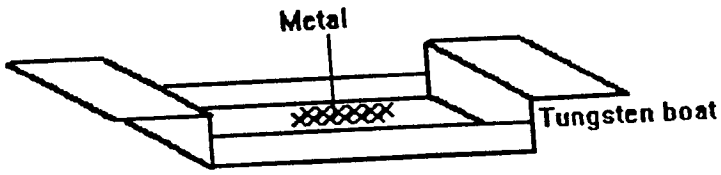

(b) apparatus for evaporating phthalocyanine

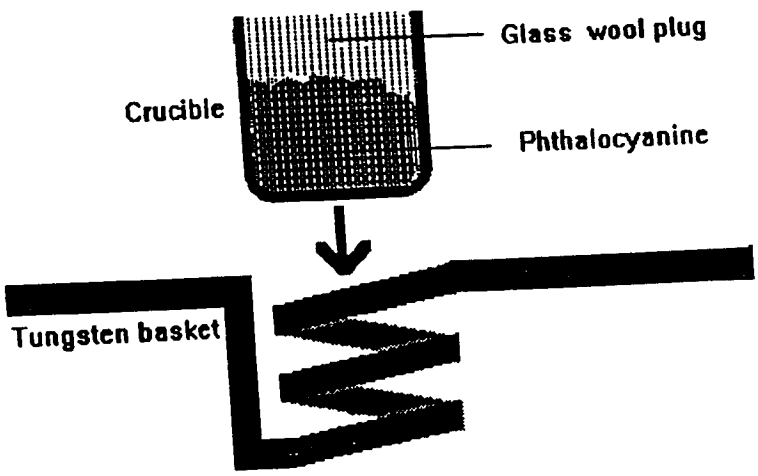

4.3 (a) detail of holder for phthalocyanine vacuum deposition;
(b) detail of boat for metal deposition;

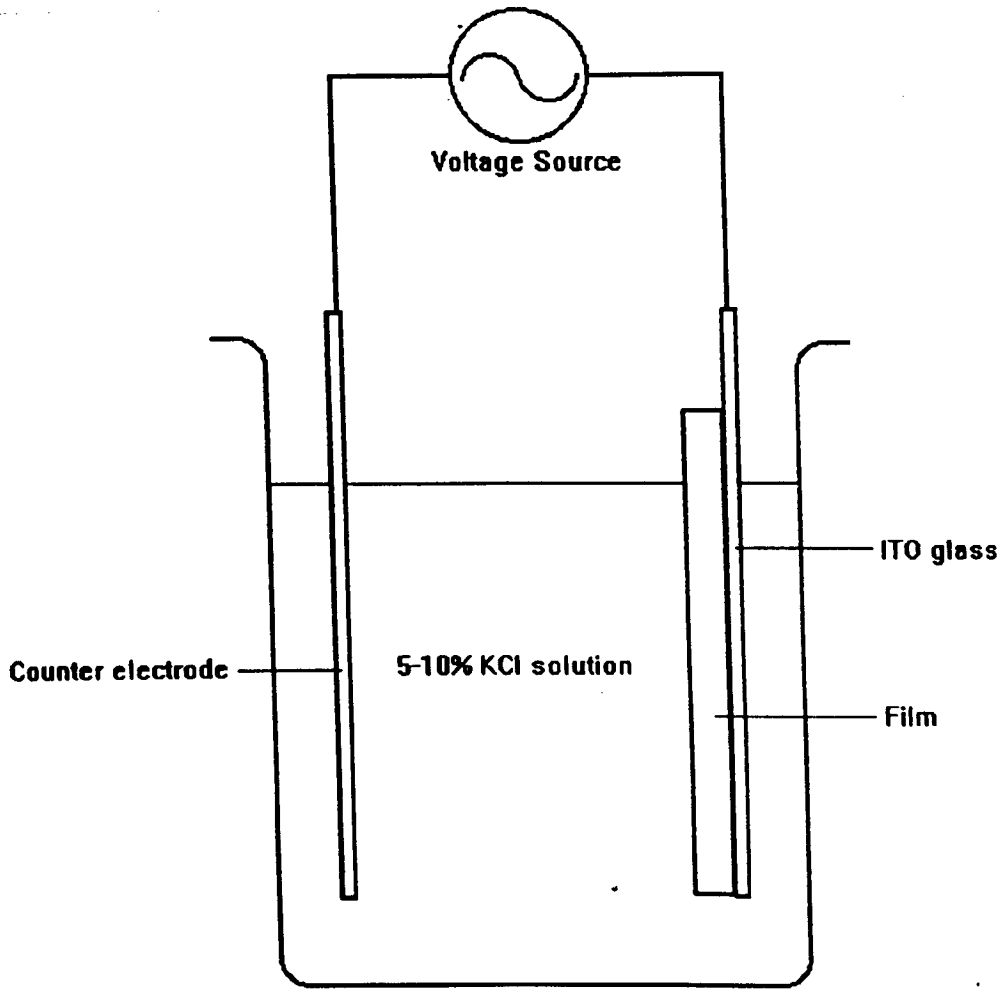

4.4 Voltage cycling cell suitable for bisphthalocyanines.

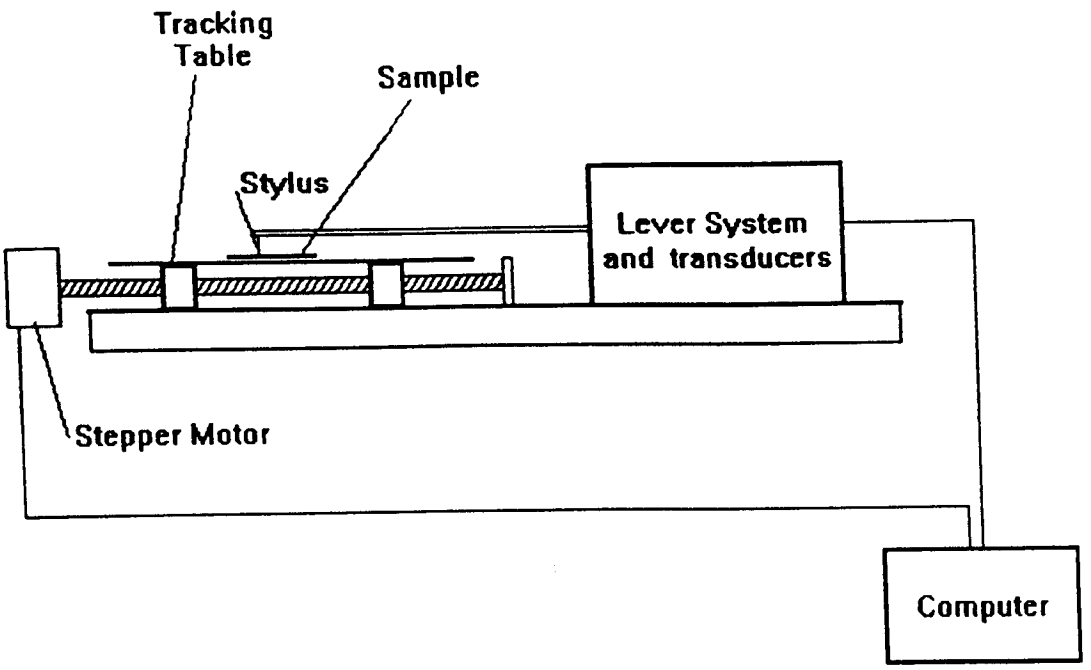

4.5 Taylor Hobson Form Talysurf surfometer; schematic

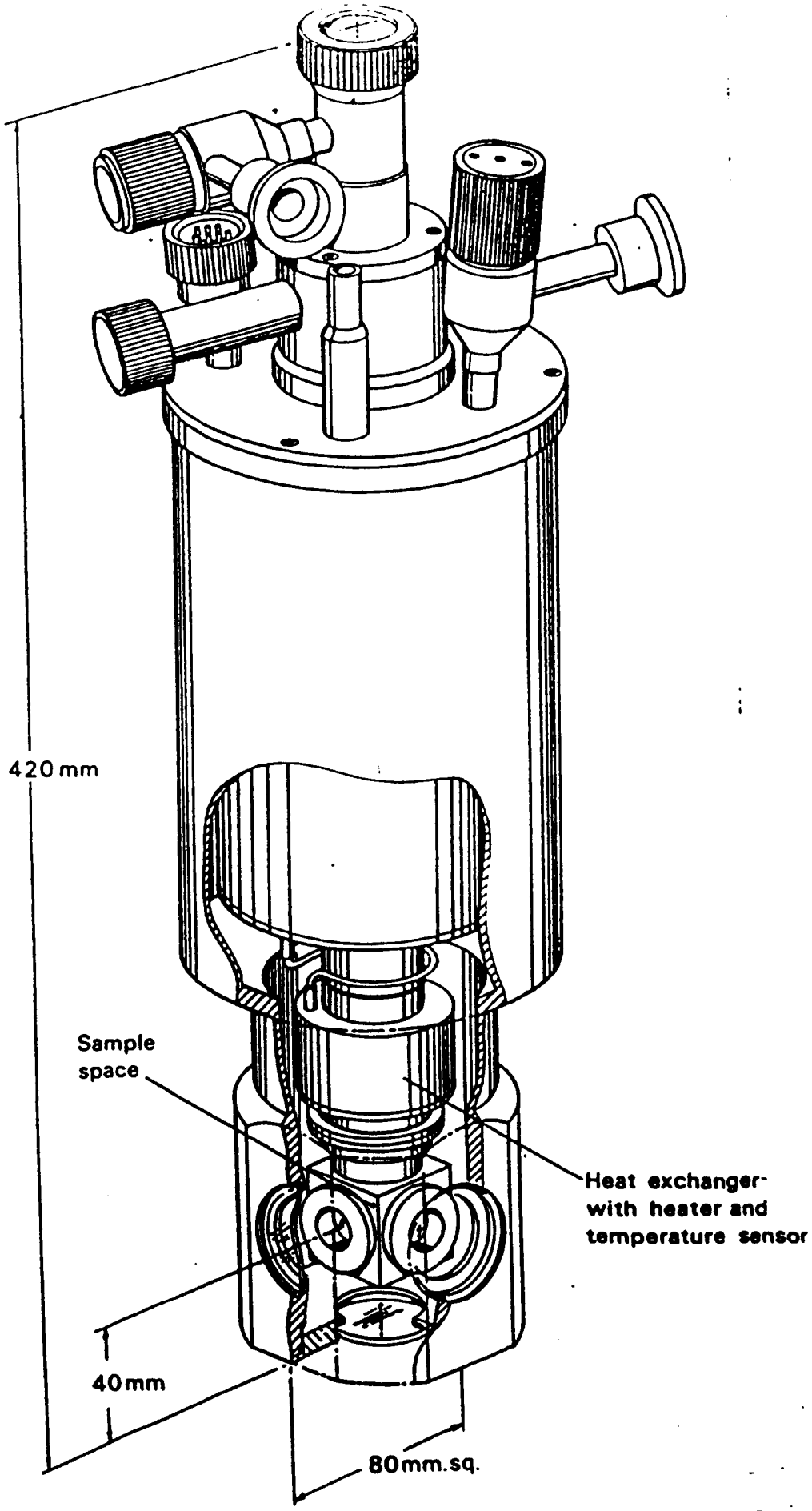

4.6 Schematic of liquid nitrogen cryostat employed for low-temperature measurements

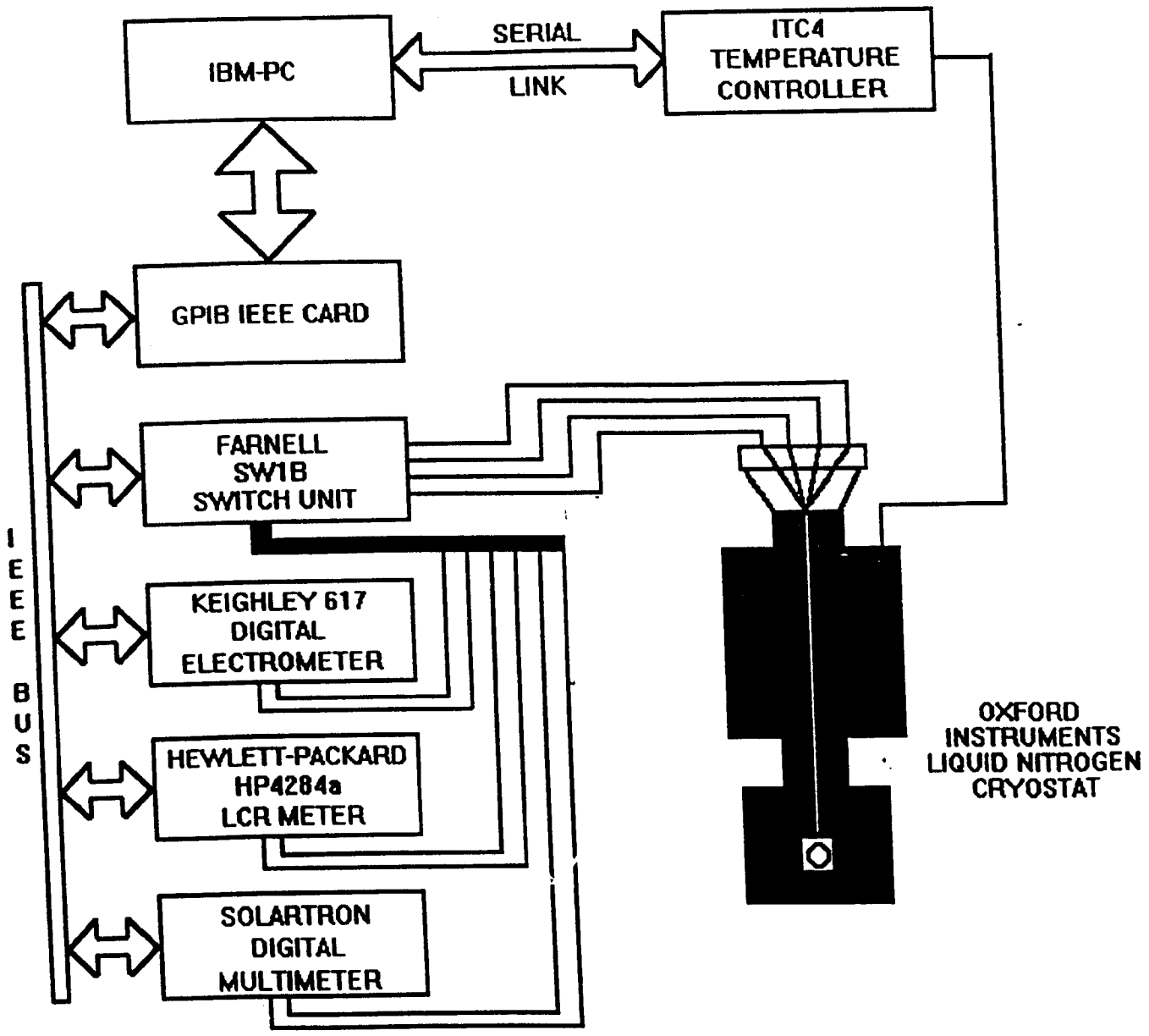

4.7 schematic of custom-built electrical measurement system.

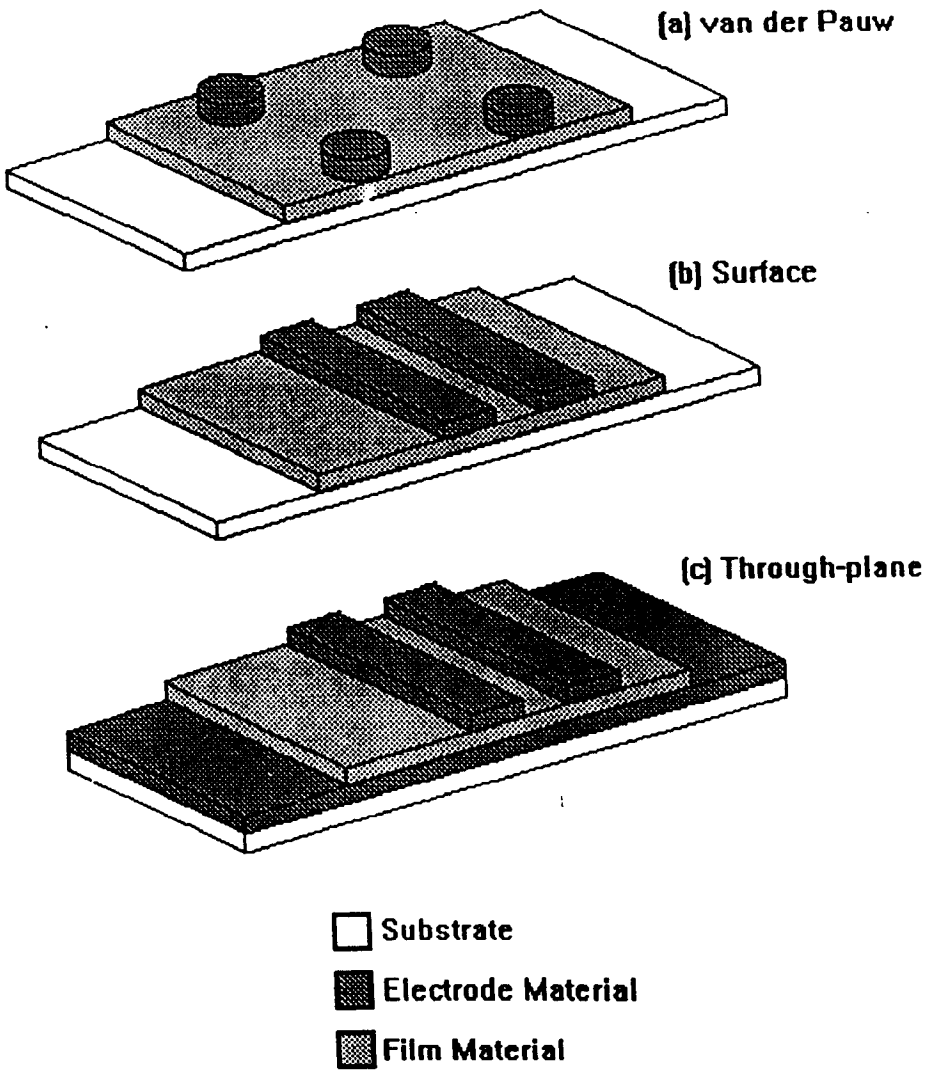

4.8 Impression of finished device types tested.

Chapter 5.

Experimental Results and Analysis

Table 3. Summary of Experiments Performed

Material	Annealed	Voltage cycled	Optical Absorption	DC	AC	Photoresponse
HF(pc)(pc*)	●	●	●	●	●	
Gd(pc)(pc*)	●	●	●			
Tm(pc)(pc*)	●	●	●			
LuPc	●	●	●	●		
FCrPc			●	●	●	●

5.1 Optical

Attention to the optical absorption and reflection spectra is here used to obtain information concerning structure and electronic properties, namely characterising intermolecular effects which cause variation in the energy distribution of band gaps participating in the absorption process, and the band-tail widths and central values of the distribution of energies at which optical transitions are seen to occur.

Further, the reflection data are employed in tandem with the absorption, to calculate values of n and k the propagation constant and extinction coefficient, and thus both components of the complex dielectric constant for the materials.

5.1.1 Optical Absorption

Optical absorption (Figures 5.1 to 5.12) and reflection measurements (Figures 5.13 to 5.24) are used to elicit information concerning the band structure of our phthalocyanine compounds, as well as to ascertain the complex dielectric constant, propagation constant and extinction coefficient in the range $1.2eV<h\nu<3.5eV$. Information as to the distribution of localised states, and the optical band gap are presented also. The effect of annealing and voltage cycling upon the absorption properties of the samples is used to offer an explanation as to the outcome of such treatments upon the film structure.

Here are tabulated the photon energies of observed absorption maxima in the absorbance spectra of all the materials tested in this manner, together with calculated values of optical band-gap E_0 and band-tail width Δ.

Table 4. Summary of Parameters of Optical Absorption in the four compounds studied in this manner

Material		B Band		X Band		Q Band		Optical constants	
	Condition	Energy (eV)	Abs.	Energy (eV)	Abs.	Energy (eV)	Abs.	E_0 (eV)	Δ (eV)
[HF(pc)(pc*)]	Untreated	3.9	0.55	2.4	0.14	1.9	0.29	2.3	0.10
	Annealed	3.8	0.71	2.6	0.21	1.9	0.51	2.11	0.08
	Voltage cycled (Blue)	3.8	0.50	2.6	0.14	1.9	0.40	2.08	0.08
	Voltage cycled (Red)	3.9	0.51	2.5	0.16	1.9	0.27	2.19	0.09
[Gd(pc)(pc*)]	Untreated	3.6	0.67	2.7	0.41	1.9	0.84	2.54	0.12
	Annealed	3.8	0.83	2.6	0.32	1.9	0.78	1.80	0.10
	Voltage cycled (Blue)	3.7	0.88	2.7	0.38	1.9	0.99	1.82	0.06
	Voltage cycled (Red)	3.9	0.92	2.6	0.35	1.9	0.75	1.95	0.06
[Tm(pc)(pc*)]	Untreated	3.3	0.30	2.4	0.21	1.9	0.28	1.16	0.11
	Annealed	3.3	0.25	2.5	0.17	1.9	0.26	0.77	0.12
	Voltage cycled (Blue)	3.3	0.18	2.4	0.16	1.9	0.21	1.12	0.10
	Voltage cycled (Red)	3.3	0.27	2.4	0.19	1.9	0.28	1.15	0.05
[Lu(pc)(pc*)]	Untreated	>3.0	unk	2.61	0.45	1.92	≈1	2.8	0.06

5.1.2 Calculation of Optical Band Gap

The increase in values of absorption α in the range of incident photon energies between 1.66eV and 1.9eV is found to be exponential in the form of the Urbach relation for all the samples. (Figs 5.49 to 5.60). This allows calculation of the optical band gap E_0 in the materials, from Equation (87). We see that for all the samples, apart from [Tm(pc)(pc*)], the values taken on are in the order of 2eV. This corresponds with previously reported values. All post-deposition treatments are seen to promote a decrease in this parameter from those values seen in the untreated material.

The tail-width Δ of localised states in the band-gap is also established (Figs. 5.61 to 5.72), and the values tabulated above.

Optical absorption for the range of $2.84eV \leq h\nu \leq 3.4eV$ is attributed to the allowed band-to-band transitions. This means that strongest absorption occurs when the optical energy is exactly sufficient to cause electronic excitation without phonon generation, and enables an estimation of the average band gap energy present in each material.

5.1.3 Effects of post-deposition Treatments on absorption spectra

Table 4 summarises the main points of our observations which include the positions in the energy domain for the B, X and Q bands, together with their peak intensity absorbance values. The relative heights of the Q and X band peaks are modified as a result of the post-deposition treatments.

Figures 5.13 to 5.24 shows the spectrum of optical reflectivity ***R*** for the same batch of samples. The sharp changes in reflectances correspond to an electronic transition. It is

observed on close examination that the Soret band $a_{2u} \rightarrow e_g$ and Q-band $a_{1u} \rightarrow e_g$ transitions take place at 2.76eV and 1.94eV, respectively.

The variations of extinction coefficient κ follow a similar pattern to those for absorbance, as expected from the relationship between the two parameters (vide Equation (82)) Similar behaviour is observed for monophthalocyanines.

Figures 5.1 to 5.4 display four sets of absorption spectra for heavy fraction rare-earth bisphthalocyanine [HF(pc)(pc*)] sublimed films within the visible optical frequency range, one set for a particular type of treatment. As reported previously [Collins, Krier, Abass 1993], the Q band peak shown for the [HF(pc)(pc*)] untreated sample is not sharp probably due to the interaction of molecules in the solid phase. The different post-deposition treatments produce different effects on the intensity of absorption but, irrespective of the post-deposition treatment, the intensity of the Q-band absorption remains always higher than the X-band absorption. Upon annealing, the intensity of absorption increases approximately by a factor of two and at the same time the peak becomes narrower. On voltage cycling to blue, there is a noticeable broadening of the Q band with a shoulder and the peak intensity is increased by a factor of about 1.5 over that for the untreated sample. For the voltage cycling to red, the opposite effect is observed in terms of diminished Q-band peak. The treatment which has introduced pronounced effect on the Q-band has the least effect on the X-band in terms of relative peak heights; for example, the greatest absorption takes place for the annealed sample while the X-band is only slightly observable on the voltage cycling to red. It may be inferred that the effect of voltage cycling on this material is to cause a change in the

oxidation states of the material, giving the derivative $[M(pc)_2]^-$ for reduction to blue, and oxidation or voltage cycling to red giving $[M(pc^*)_2]^+$.

Figures 5.9 to 5.12 give the similar plots of optical absorption spectra for thulium [Tm(pc)(Pc*)] phthalocyanine compounds. There are two interesting features in the spectrum: (i) a shoulder to the Q band at 2.1eV and (ii) a pronounced absorption edge at 1.5eV. Both these energy values quoted here are correct to two significant figures. The blue shoulder is attributed to the Q (1-0) vibronic band, generally more clearly resolved at lower temperatures. Like the other sample compounds, the tail towards red is due to smearing of many hot bands. Annealing of the sample does not appear to cause any noticeable shift of the Q band peak along the energy scale, but the overall absorption is decreased. For 1.2V voltage cycling to blue five times, the overall absorption increases and there is a very slight blue shift in the Q band. The intensity of absorption decreases slightly on voltage cycling to red and there is a pronounced effect on the shape of the shoulder at about 2.1eV. For the sample which has been voltage-cycled to red, a significant increase in absorption between the peak at 2.6eV and the Q band is observed.

As shown in Figure 5.5, the Q and B bands in the spectra for the untreated gadolinium [Gd(pc)(Pc*)] phthalocyanine film are of approximately equal strength, in addition to the extra band in the energy window centred at around 2.6eV. The 5×1.2V voltage cycling to blue causes a decrease in the absorption at the Q band and X bands but the Q-band occurs at an increased energy. Cycling at the same voltage to red induces a shift in the energy of the Q band and a decrease in the peak absorption thereof; the X band is less significantly decreased than for the voltage-cycled to blue. The annealing has pronounced effect on Gd(pc)(pc*) spectra:

(i) an increase in the energy at which the Q band occurs in the spectrum,

(ii) a decrease in the peak absorption and

(iii) the broadening of the Q band.

This suggests that the effect of the annealing process has been to promote a change in the structure of the film, possibly, a phase change in the film material. This is similar to previously published data for the transformation of α-FePc to the β form. [Lucia, Verderame 1967]

Using t = 50nm, values of the absorption coefficient α are calculated for all three untreated samples from values of $[I_t/I_0]$ obtained from the absorption spectrum.

5.1.4 Complex index of refraction from absorption and reflection

Values of the reflectivity R at a given incident energy hν are obtained by means of a transmission spectrophotometer equipped with an integrating sphere. With the knowledge of values of the absorption coefficient α, the extinction co-efficient, κ, which is the imaginary part of the complex refractive index *N* is evaluated from Equation (78). The variations of extinction coefficient κ follow a similar pattern to those for absorbance, as expected from the relationship between the two parameters. A similar behaviour is observed for monophthalocyanines. Equation (83) is reduced to a set of quadratic equations in n, when values of R and κ are substituted. The physically meaningful root of these equations gives the value of n, the real part of the complex refractive index, or propagation constant. The dispersion behaviour of n is shown for all three samples and all treatments in Figures 5.25 to 5.36. For each of the samples, the variation of n takes the following patterns. n takes a value between 1.3 and 4 throughout the energy range.

For all three compounds, a strong peak in n occurs at approximately the same energy as is observed for the Q band in the absorption spectrum. The second peak may be seen at a position corresponding to the X band. Calculations have been performed for the samples which have undergone post-deposition treatments. The relative heights of the Q and X band peaks do not correspond to the variations seen in the absorption spectra as a result of the post-deposition treatments, and, in fact, the peaks in n observed at approximately 2eV are diminished by all the post-deposition treatments. For the X band absorption in [HF(pc)(pc*)], the effect of annealing increases the propagation constant n slightly, but both forms of voltage cycling cause a decrease. The observed dispersive behaviour does not follow any polynomial of low order for the function n(hν) where hν is the photon energy, and therefore the Cauchy relation is not expected to hold over the entire photon energy range. This anomalous behaviour is in keeping with the Debye theory.

5.1.5 Optical complex dielectric constant

Once values of n and are κ known, values of both real and imaginary parts ε_1, ε_2 of the complex dielectric constant ε^* are determined for all samples, fresh and treated, from Equation (4) as functions of incident photon energy hν. Resulting dependences of ε_1, ε_2 on hν are presented respectively in figures 5.37 to 5.48.

For [HF(pc)(pc*)] and [Tm(pc)(pc*)] films, the variation of the real part broadly follows the same pattern as the imaginary part, obvious peaks being seen at about 2eV, the values falling between 0.2 and 3.7 over the photon energy range considered; but the value of the real part is appreciably higher. ($2.5 < \varepsilon_2 < 12$). For

[Gd(pc)(pc*)] films, the imaginary part of the dielectric constant broadly follows the transmission spectrum in shape.

μ takes a value between 2 and 3 throughout the energy range for [HF(pc)(pc*)] and [Tm(pc)(pc*)], and for [Gd(pc)(pc*)], a little higher, approaching 4.1 at the maximum. The observed dispersive behaviour does not follow any polynomial of low order for the function $\mu(h\nu)$ where $h\nu$ is the photon energy, and therefore the Cauchy relation is not expected to hold over the entire photon energy range. This anomalous behaviour is in keeping with the Debye theory. The real and imaginary parts ε_1, ε_2, respectively of the dielectric constant ε^* are related to μ and κ through Equations (85) and (86).

For all films, the variation of the real part broadly follows the same pattern as the imaginary part, both of which resemble the envelope of the absorption spectrum, obvious peaks being seen at about 2eV, but values of the real part are appreciably higher.

Calculations have been performed for the samples which have undergone post-deposition treatments, the results being presented for n (Figs. 5.24 to 5.36) and ε_1 and ε_2 in Figs. 5.37 to 5.46. The effects of the post-deposition treatments are apparent in the values of the propagation constant in all cases. The energy shifts in the peaks of the propagation constants observed in the calculated spectra after treatments are marked for the X band; additionally the intensities of the two peaks for [HF(pc)(pc*)] are approximately reversed, indicating the phase change induced by the annealing process. The upper and lower limits of the propagation constant, however, remain reasonably constant throughout the treatments. The effects broadly follow the absorption spectra.

Our surface roughness data produced values of 18.5nm for HF(pc)(pc*), 26nm for Gd(pc)(pc*) and 12.1nm for Tm(pc)(pc*) in their untreated states. These values are very high relative to the film thickness, although for a thin, vacuum-evaporated layer which, in

these cases, is visibly inhomogeneous, this result is of a reasonable magnitude. This value is hypothesised to be also a factor of the roughness of the relatively thick ITO film between the Pc and the glass substrate; the thin phthalocyanine film follows the contours of this.

The effects of the various post-deposition treatments upon the optical frequency dielectric properties of these three materials have been examined. For phthalocyanines, electronic transitions occur notably in the 600-800nm visible region (the Q band) and 300-400nm (the B or Soret band), both being due to π-π^* transitions. The Q band is highly localised on the phthalocyanine ring, and is reported for many phthalocyanines to be highly susceptible to a number of macrostructural factors, particularly to the geometry of nearest neighbour molecules in the structure. (Lucia, Verderame 1968). This in the light of the results appears to hold true for the three compounds investigated, and signals that the phase changes are promoted by annealing. This also suggests that no structural damage to the phthalocyanine rings has occurred during treatment.

The effect of annealing upon the Q band intensity is different for [HF(pc)(pc*)] to the other two compounds, there being an increase in absorption for the former, and a decrease for the latter. This effect must be related to differences in the structure of [HF(pc)(pc*)] compared to the other materials; [(Lu(pc)(pc*)] is reported to form liquid crystals, so the annealing process causes closer ordering in this material than is noticeable in the raw state. Annealing [HF(pc)(pc*)] shows a narrowing of the Q band and an increase in its intensity; this may be due to a reordering of molecules in the structure, leading to a more highly ordered phase. The reverse effect on the other two compounds indicates a more random ordering illustrated by the peak broadening.

The reversible redox processes resulting from voltage cycling are reduction or voltage cycling to blue giving the derivative $[M(pc)_2]^-$, and oxidation or voltage cycling to red giving $[M(pc^*)_2]^+$.

5.2 dc Electrical properties

In this Section the conduction and activation energy parameters for three of the materials, heavy fraction bisphthalocyanine, fluorochromium phthalocyanine and lutetium bisphthalocyanine, are ascertained. All these samples are untreated subsequent to deposition. Two conduction regimes are recorded in each case, their dominance being controlled by the temperature of the material.

5.2.1 Conduction regimes from the two-point probe method

The circulating current I was measured for [HF(pc)(pc*)] films as the applied bias potential V was varied up to 100V, both in forward and reverse directions. Figure 5.73 displays a family of curves showing the variation of current as a function of the applied dc voltage at five different temperatures from 77K to 297K. The I(V) characteristics are reproducible and symmetrical in both forward and reverse directions. This implies that the field due to the applied potential is symmetrically distributed in the bulk of the film. This conduction is not strictly ohmic, but at a given temperature T, the current is found to obey a power law dependence upon the potential V in the form of $I = \rho V^s$,

where the coefficient ρ and index s are both temperature-dependent quantities. The value of s varies from 0.7 at 77K to 1.1 at room temperature. ρ, on the other hand, takes on the values of $7.2k\Omega^{-1}V^{0.3}$ and $21\Omega^{-1}V^{-0.1}$ at corresponding temperatures. The temperature of transition from the dependence with $s < 1$ to that with $s > 1$ is believed to be 162K, over which region the I(V) characteristic is found to obey Ohm's law. As expected, the conduction generally increases with the rise of temperature, but the rate of the rise in conductivity is not as large at the temperatures below 127K as at those temperatures above 127K.

For fluorochromium phthalocyanine, measured current-voltage data (Fig. 5.75) show that in the region $-50V < V < 50V$, there is proportionality of s to v over the entire region measured. This pattern is symmetrical about 0V indicating no rectifying effect at the metal-film contacts. It is postulated that the increase of carrier injection at the electrodes with increasing current density promotes progressive filling of traps so that that the visible conductivity increases with applied voltage.

At the voltages measured, we see no trap-filling limit being reached, although it would be expected that the J-V characteristic would achieve linear dependence at higher values still of V.

Conversely, for lutetium bisphthalocyanine (Fig. 5.74), nearly linear I-V data are observed, in a manner much the same as those for heavy fraction bisphthalocyanine.

Having used similar configurations for measurement of all three compounds, we are able to propound direct comparison of the properties of the three, all other factors being equal with the exception of control of the film thickness. In terms of the physical and electronic structure of these materials, we see that there is a similarity in behaviour

between the two bisphthalocyanines we have investigated, with space-charge-limited conduction, if any, becoming prevalent only at higher applied voltages.

However, the non-linear dependence of I upon V in FCrPc, which follows $I \propto V^n$ is thought to be a product of space-charge-limited carrier injection, again with trap filling occurring progressively as V is increased, increasing the macroscopic conductivity of the film.

5.2.2 Activation energies for dc conduction processes

Nearly linear I(V) characteristics were obtained for our samples of bisphthalocyanine complexes in planar configurations with aluminium or gold electrodes. The excitation to a singlet state below the conduction edge is associated with the conduction process at high temperatures while carrier transport between localised states is a dominant mechanism at a low temperature range.

The calculated activation energies are summarised in Table 5, and agree with previously available data for phthalocyanines.

Table 5. DC activation energies for the three materials tested.

Material	Transition Temperature	E_A (Low Temperature) (eV)	E_A (High Temperature) (eV)
[HF(pc)(pc*)]	162K	7×10^{-3}	0.18
[Lu(pc)(pc*)]	160K	6.8×10^{-3}	0.20
FCrPc	150K	8.1×10^{-3}	0.15

A tentative band diagram for electronic transport has been given for phthalocyanines (Fig. 2.9) . The intrinsic band gap is normally believed to be 2.0eV. This value is likely to vary depending upon the nature of the central metal atom, and this observation is

borne out by our differing results across the range of compounds tested. The pairs of values obtained for E_0 are considered too small for the excitation of carriers from the valence band to the conduction band. Singlet states S_1 which lie in the energy band gap of a phthalocyanine film, are believed to be involved with the conduction at high temperatures, since the activation energies seen in this temperature regime compare well with the value of 0.21eV for the approximate distance of the singlet state from the conduction band edge. The low temperature activation energy, on the other hand, is thought to be associated with hopping of carriers between localised states close to the Fermi level. The existence of these states is consistent with the non-crystalline nature of sublimed films and the associated distribution effects of the electronic parameters.

5.2.3 Conductance as a function of time

For some materials in vacuum ambient, it has been observed that due to slow polarisation processes occurring in the devices, there can be a decrease in circulating current for a fixed voltage with respect to time. In order to attain accurate results with our measurements, several minutes were left between successive readings to allow a standard period of stabilisation of the material. Allowing completion of these polarisation effects would have necessitated a factor of hours or days between readings, and this was therefore deemed impracticable. However, if a device is run continuously at fixed applied voltage, it is possible to overlook this matter in practice.

5.3 AC and Dielectric Properties

Measurements of conductance, capacitance and loss tangent have been carried out on samples of HF(pc)(pc*) and FCrPc. The results and associated analysis of these are summarised in Sections 5.3.1 to 5.3.5.

5.3.1 ac Conductance

Information obtained as to the frequency and temperature dependence of ac conductivity is now employed to determine relative effects and parameters of hopping and band-model conduction. Band-model conductivity is frequency independent, and the temperature dependences differ for each regime. One of the two mechanisms predominates according to the experimental conditions; mainly band-type at high temperatures and low frequencies, and hopping at low temperature and high frequency.

Figures 5.77 and 5.89 illustrate plots of ac conductance G versus applied frequency on a log scale for heavy fraction bisphthalocyanine and fluorochromium phthalocyanine measured as planar sample structure, for ambient temperatures varying between 77K and room temperature. The conduction in each case follows the relation $()=A^{s}$ (similar, it will be noted, to the controlling equation for dc conduction) with A as a complex proportionality constant. s as a function of frequency and temperature is an indicator of conduction type. s is presented here in tabular form for both compounds:

Table 6. Conductance index s in heavy fraction bisphthalocyanine

Temperature (K)	Low frequency s	High frequency s
77	0.709	1.85
102	0.641	1.78
152	0.07	2.04
202	0.05	1.99
252	0.081	1.81
292	0.081	1.61

Table 7. Conductance index s in fluorochromium phthalocyanine

Temperature (K)	Low frequency s	High frequency s
102	1.90	1.97
152	1.45	1.95
202	1.61	1.95
252	0.49	1.93
292	0.18	1.66

The values and behaviour of s help us to postulate a model as to what type of conduction is occurring in the two materials. Two regimes are visible over the measured frequency range, throughout each of which s is effectively independent of frequency. This leads us to believe that the hopping mechanism present is suitable for the correlated barrier hopping model, which is described by Equations (59) and (60). Small polaron hopping is not thought to be occurring here. Although s would be expected to be both frequency- and temperature- independent, an increase in s with temperature would be expected for this model to apply, and in fact the converse applies to our materials.

Values of s greater than unity above a particular frequency threshold are generally indicative of "two-centre" hopping between similar centres, and values approaching 2, comparable to ours, have been observed in MgPc and CuPc by Vidadi.

5.3.2 Activation energies for ac conductance

By plotting log G versus reciprocal of temperature, it has been possible to determine the activation energies for ac conduction in HF(pc)(pc*) and FCrPc. These plots are represented in Fig. 5.82 and 5.101. It is seen that in each case a change in gradient, or transition, is seen for each experimental line, with this transition occurring at a temperature depending on the frequency at which the measurement was taken. This temperature is seen to vary between 111K and 180K. according to the applied frequency. In the succeeding Tables 8 and 9 are presented the values of these activation energies in [HF(pc)(pc*)] and in fluorochromium phthalocyanine for various frequency points:

Table 8. Activation energies for ac conduction in heavy-fraction bisphthalocyanine.

Measurement Frequency	Low temperature E_a (eV)	Transition temperature	High temperature E_a (eV)
100Hz	0.007	106K	0.18
500Hz	0.007	108K	0.182
1kHz	0.008	113K	0.180
5kHz	0.008	138K	0.168
10kHz	0.006	142K	0.125
50kHz	0.003	154K	0.117
100kHz	0.0014	188K	0.112
500kHz	0.0004	204K	0.024
1MHz	0.0001	219K	0.008

Table 9. Activation energies for ac conduction in fluorochromium phthalocyanine.

Measurement Frequency	Low temperature E_a (eV)	Transition temperature	High temperature E_a (eV)
1kHz	0.006	222	0.197
5kHz	0.003	227	0.193
10kHz	0.006	227	0.075
50kHz	0.003	232	0.063
100kHz	0.004	244	0.084
500kHz	0.004	251	0.008
1MHz	unknown	257	0.006

These activation energies demonstrate the temperature and frequency dependence of band-to-band and hopping conduction in the material. We see that the range of prevalence of the low temperature regime extends with increasing frequency, this correlating with the theory.

In each case, the activation energies obtained at lower frequencies are comparable with those values obtained for dc conduction, the values for each visible regime decreasing as the applied frequency increases.

The apparent decrease in activation energy for increased frequency may be explained in terms of the decrease in polarisation effects which occurs in the film as the applied frequency increases, recombination becoming less likely with rising F. Equation (62) which applies to the parallel C-R and series R model illustrates that impedance is reciprocally proportional to applied frequency and in terms of this model the increase in conduction of the capacitance element at increasing frequency is analogous to the frequency-depensent behaviour of a "real capacitor" Measured capacitance values of the material are now examined.

5.3.3 Capacitance

For all the materials, capacitance reaches a steady-state value at higher frequencies after a drop occurring about a centre frequency for which a change in conduction is noted. This agrees with the behaviour predicted by Equation (16) illustrating this relationship between σ and ε'.

The capacitance results will not be discussed here *per se*, as they are put to fuller use in Section 5.3.5 for elucidation of the relaxation properties.

5.3.4 Dielectric Loss

The relationship between dielectric loss peak and capacitance/conductance is discussed in section 3.2, and our data fit well with the theory presented therein. Presentation of these loss peaks occur in Figure 5.81 for [HF(pc)(pc*) and Figure 5.93 for FCrPc; the envelopes of the data are in agreement with values for C" the imaginary part of the complex capacitance when compared with Figures 5.79 and 5.91 respectively.

5.3.5 Analysis of Relaxation Properties

By employing a version of the Cole-Cole analysis technique modified to account for multiple arcs, it has been possible to derive the real and imaginary parts of the complex dielectric constant for the materials at various temperatures. This analysis has been carried out for heavy fraction bisphthalocyanine, and fluorochromium phthalocyanine.

From Fig. 5.80, we see that the effect of temperature upon the ac conductance of [HF(pc)(pc*)] becomes more pronounced with decrease in frequency, with very little temperature dependence upon conductance at 1 MHz, and a pronounced increase in G with temperature at the lowest frequency.

A plot of log(G) vs. log (F) illustrates the temperature independence of the high frequency regime well, as the gradients are seen to match in this region.

Geometric constructions added to the plot enable us to estimate the most probable relaxation time, τ for the material at each temperature. This quantity is seen to increase with decreasing temperature. This dependence is related to the relative dominance of each of the conduction regimes discussed earlier at the particular temperature. The results of these calculations are summarised in Table 10, and the graphical representations over the measured range of temperatures are seen for [HF(pc)(pc*)] in Figures 5.83 to 5.88, and for FCrPc in 5.93 to 5.100. Figure 5.83 is presented complete with constructional lines, and is used by way of example to demonstrate the steps of geometric construction required to solve for the relaxation time data.

Table 10. Relaxation time distributions in heavy-fraction bisphthalocyanine.

Temperature (K)	C' max (F)	C' ($\omega\tau$=1) (F)	C" max (F)	C" ($\omega\tau$=1) (F)	τ(s)
77	not reached	2.89×10^{-10}	not reached	1.01×10^{-11}	2.21×10^{-3}
102	not reached	2.79×10^{-10}	not reached	7.34×10^{-13}	4.09×10^{-4}
152	3.23×10^{-10}	3.26×10^{-10}	4.41×10^{-11}	4.33×10^{-11}	1.33×10^{-3}
202	3.17×10^{-10}	3.27×10^{-10}	4.40×10^{-11}	4.38×10^{-11}	7.96×10^{-4}
262	3.26×10^{-10}	3.24×10^{-10}	4.41×10^{-11}	4.40×10^{-11}	1.94×10^{-4}
292	3.22×10^{-10}	3.30×10^{-10}	4.41×10^{-11}	4.34×10^{-11}	9.04×10^{-5}

Since we know d and A for our sample, these could be readily converted to give values of ε' and ε'' by the simple means of accounting for the geometry of the ideal capacitor formed by the sample.

The progressive decrease in relaxation time with increasing temperature seen in [HF(pc)(pc*)] correlates with the data obtained for conduction regime prevalence; it suggests that the relaxation time for band-to-band excitation is less than that for correlated barrier hopping as the latter becomes dominant. The frequency at which the C" peak occurs is seen to increase with temperature, demonstrating the frequency dependence of this conduction model in practice.

At low temperatures, it has proven impossible with [HF(pc)(pc*)] to observe a peak in capacitance within the frequency range measurable with the available equipment.

Values for fluorochromium phthalocyanine are more difficult to analyse in the frequency range permitted by our measurement instrument. This is because no peak is observed in the Cole-Cole graphs, this peak occurring at a lower angular frequency than was measurable in practice. We can however assert that for these materials, τ>8ms within the temperature range measured.

5.4 Photoconductivity of Fluorochromium Phthalocyanine

Van der Pauw resistivity and standard two-point I-V measurements have been carried out on 400nm thick vacuum-sublimed samples of fluorochromium phthalocyanine with area 6mm square and electrodes at the corners thus formed, both in darkness and under illumination of various wavelengths between 300 and 900 nm. Additionally, by keeping note of the voltages and currents present at both electrode pairs during the van der Pauw process, it has been possible also to determine data for photocurrent/voltage throughout this temperature range.

From these data, we have been able to establish the following parameters for the material: the photoresponse, ie. the effect of incident wavelength upon photogeneration and its correspondence with the absorption spectrum; the effect of temperature upon the generated photocurrent and corresponding dark conductivity. The dark conductivity data obtained from the 4-point process is illustrated in Fig. 5.102.

The envelope of the photoresponse spectrum is seen to broadly follow the generic absorption spectrum for phthalocyanines; as might reasonably be expected, the most strongly absorbed wavelength is that whose energy matches the central region of the optical band gap distribution in the material. This indicates to us that the first step in photocarrier generation in this material is excitation across the band gap of the FCrPc molecule itself.

The photoresponse of the material at six ambient temperatures is illustrated in Figures 5.102 to 5.108.

As it proved impossible to obtain functional through-plane devices of this material, because severe pinholing of the film during deposition ensured that all such devices presented interelectrode shorting, full and accurate characterisation of the photoconduction process in these materials proved to be somewhat difficult. However, we have demonstrated the viabibity of using the van der Pauw method for determination of changes in conductivity occurring as a result of illumination, and would suggest that this has potential as a valuable method of interrogating such a device, seeing that no

absorption of incident light due to semitransparent electrodes covering the entire active surface will occur, thereby allowing possible greater sensitivity and a more natural spectral response for the material itself. Furthermore, we have demonstrated that fluorochromium phthalocyanine shows a very marked photoresponse to light in the region of the optical band gap.

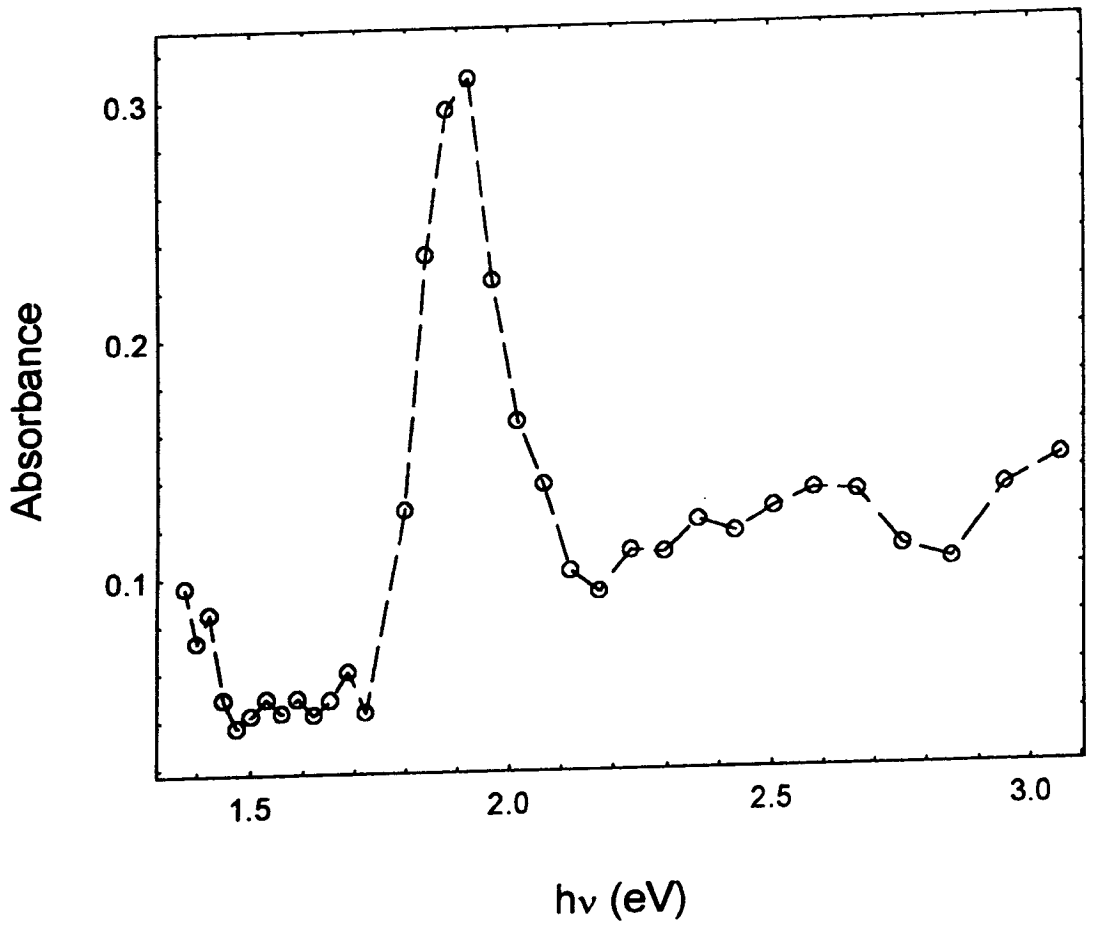

5.1 Absorption spectrum for untreated [HF(pc)(pc*)]

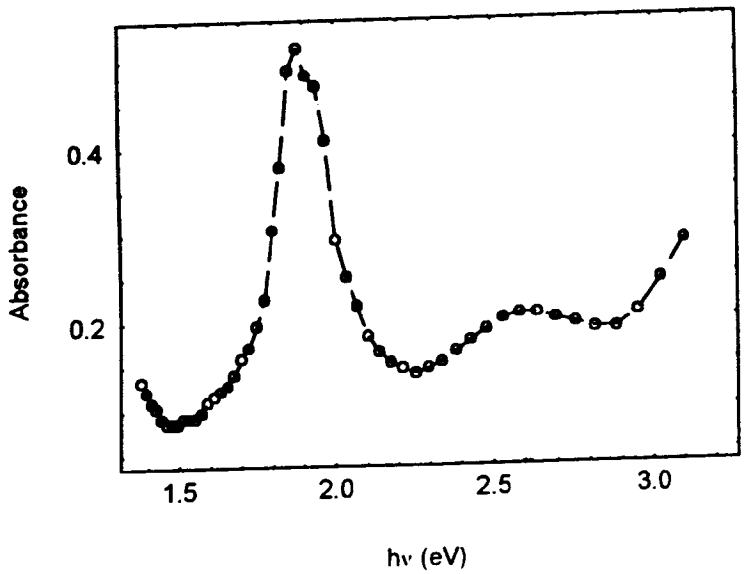

5.2 Absorption spectrum for anncaled [HF(pc)(pc*)]

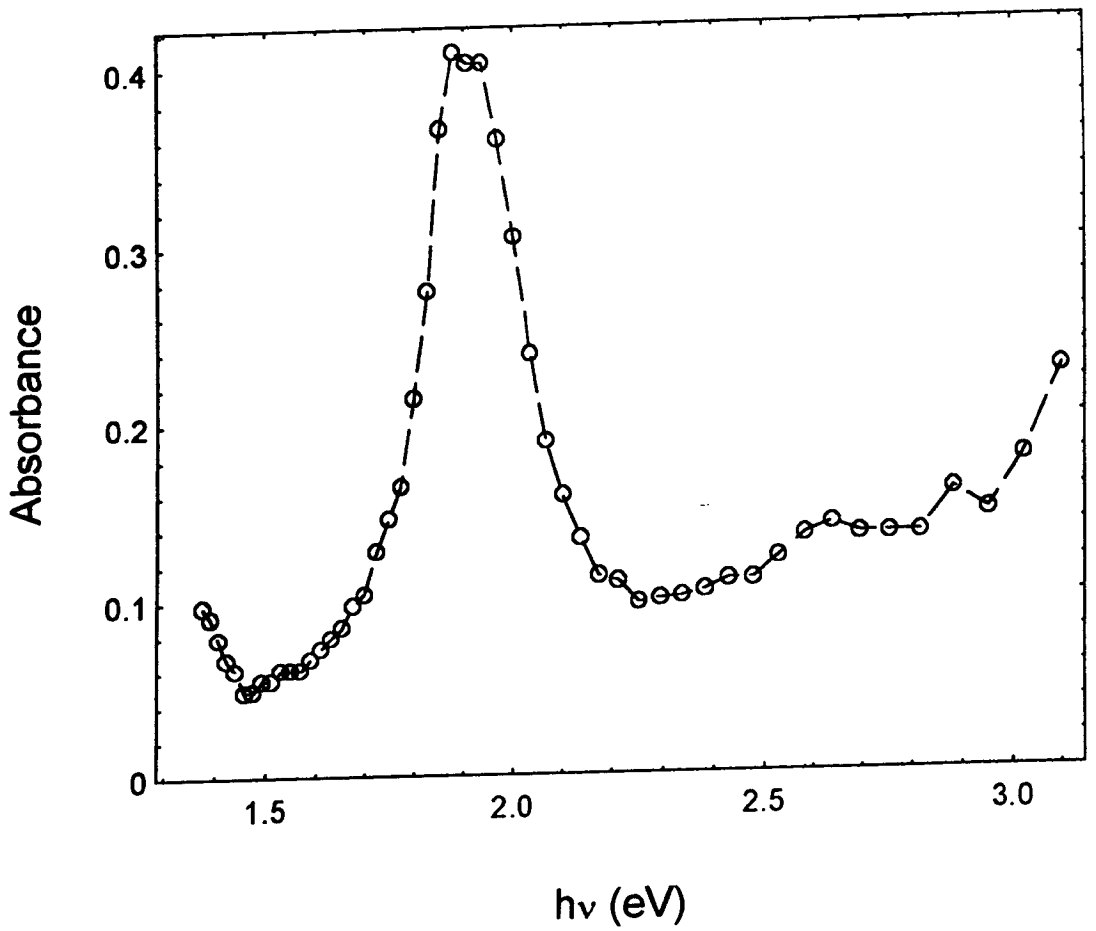

5.3 Absorption spectrum for [HF(pc)(pc*)] voltage cycled to blue

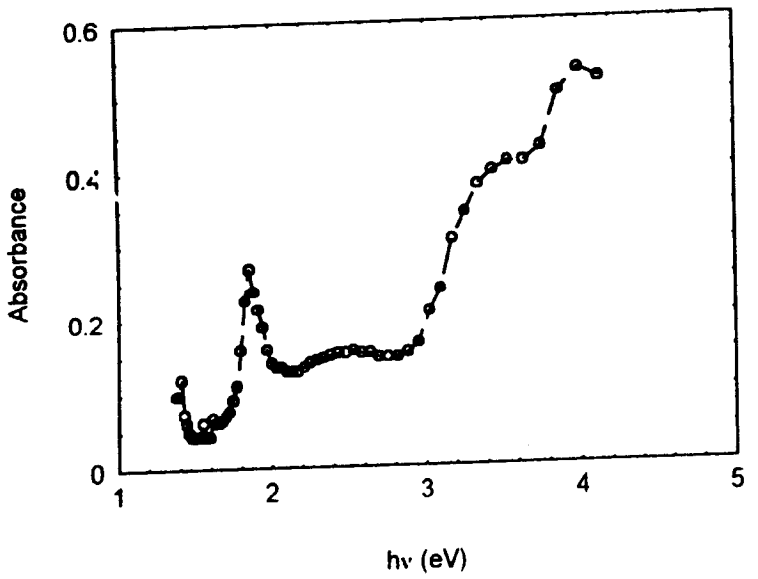

5.4 Absorption spectrum for [HF(pc)(pc*)] voltage cycled to red

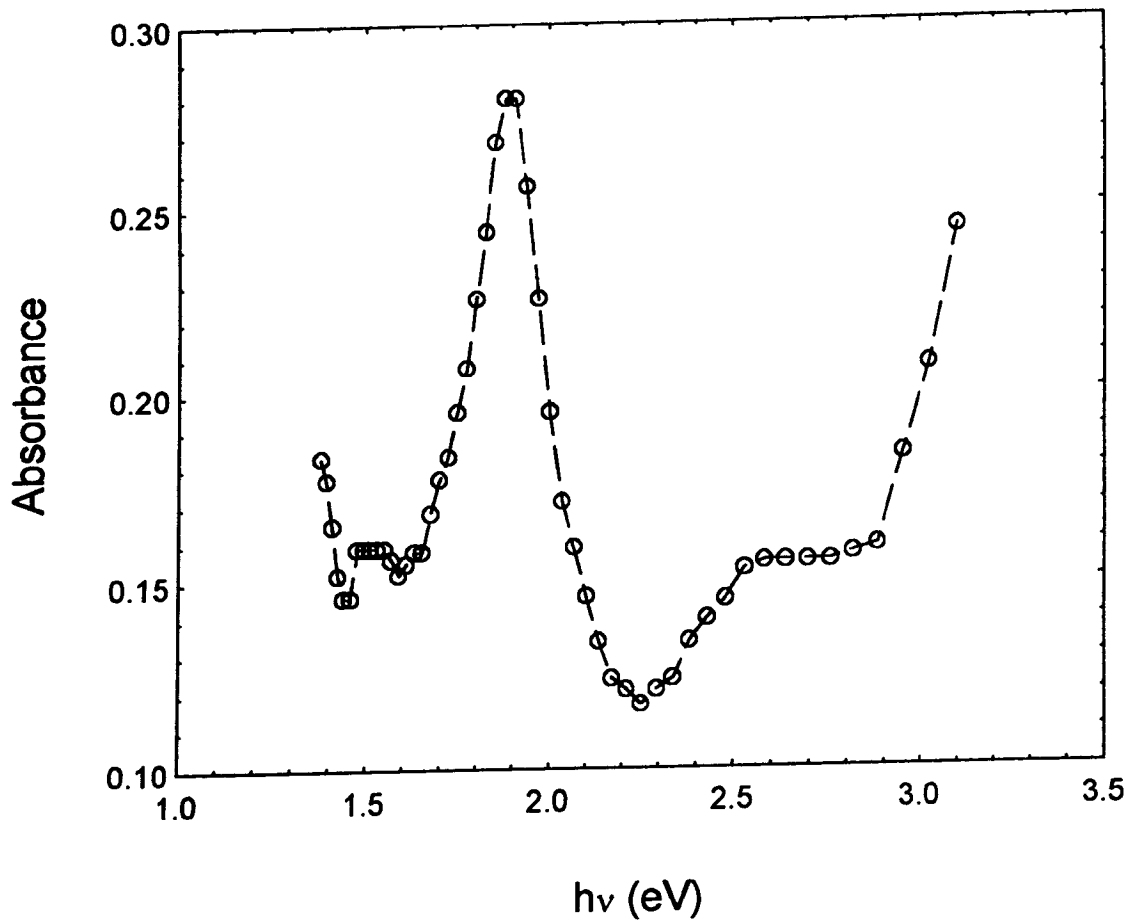

5.5 Absorption spectrum for untreated [Gd(pc)(pc*)]

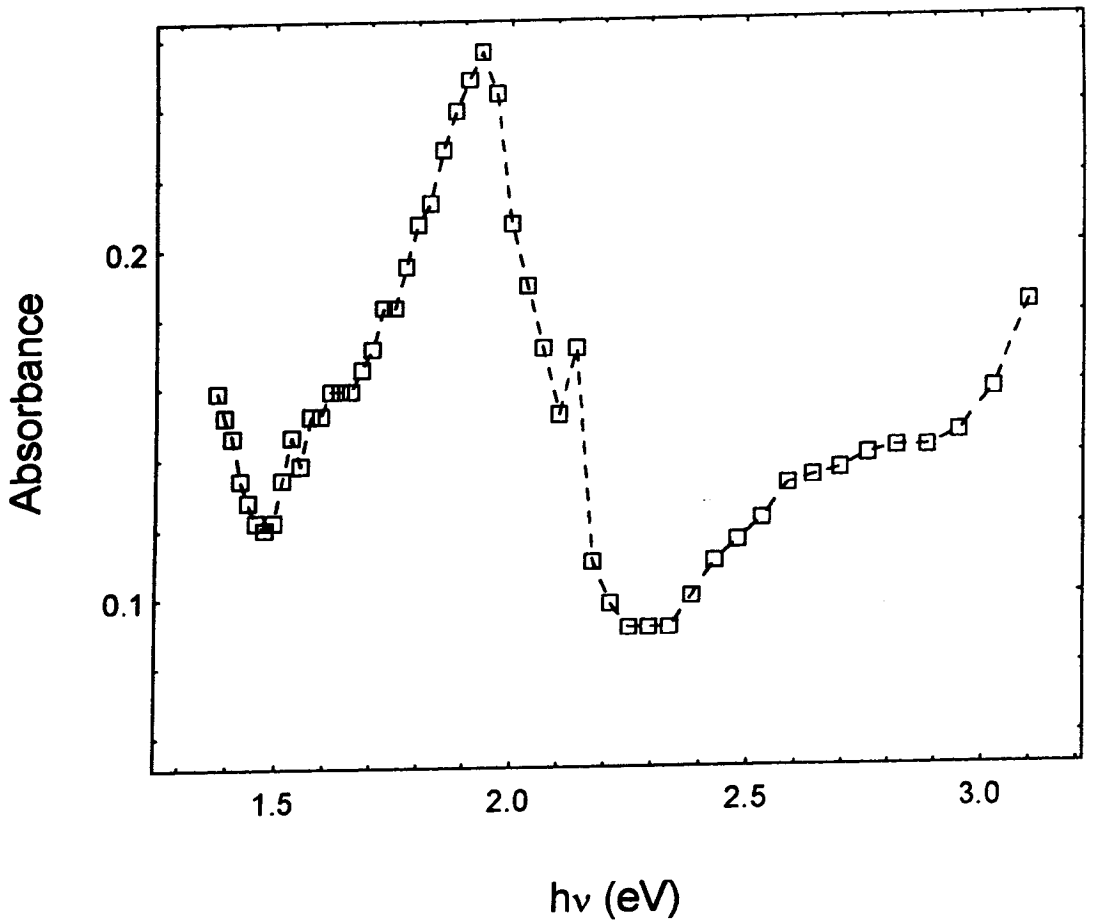

5.6 Absorption spectrum for annealed [Gd(pc)(pc*)]

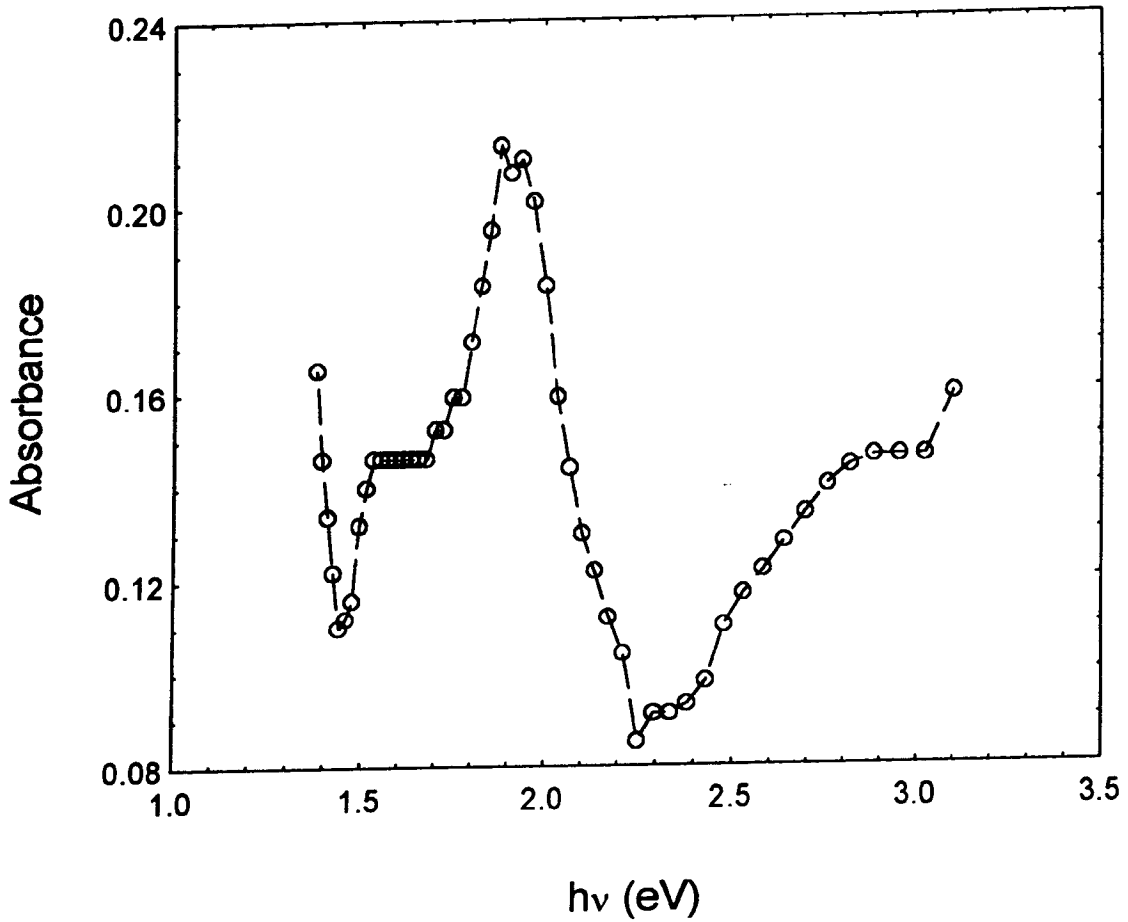

5.7 Absorption spectrum for [Gd(pc)(pc*)] voltage cycled to blue

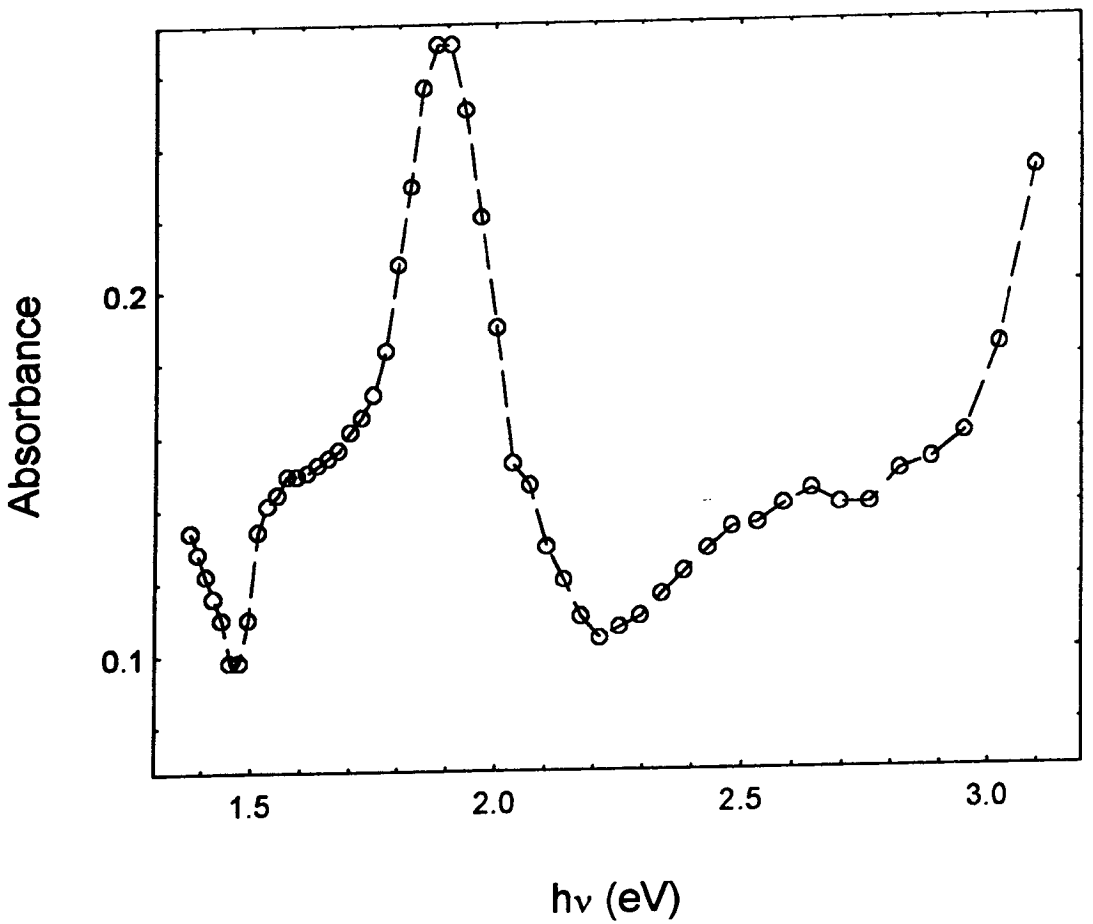

5.8 Absorption spectrum for [Gd(pc)(pc*)] voltage cycled tored

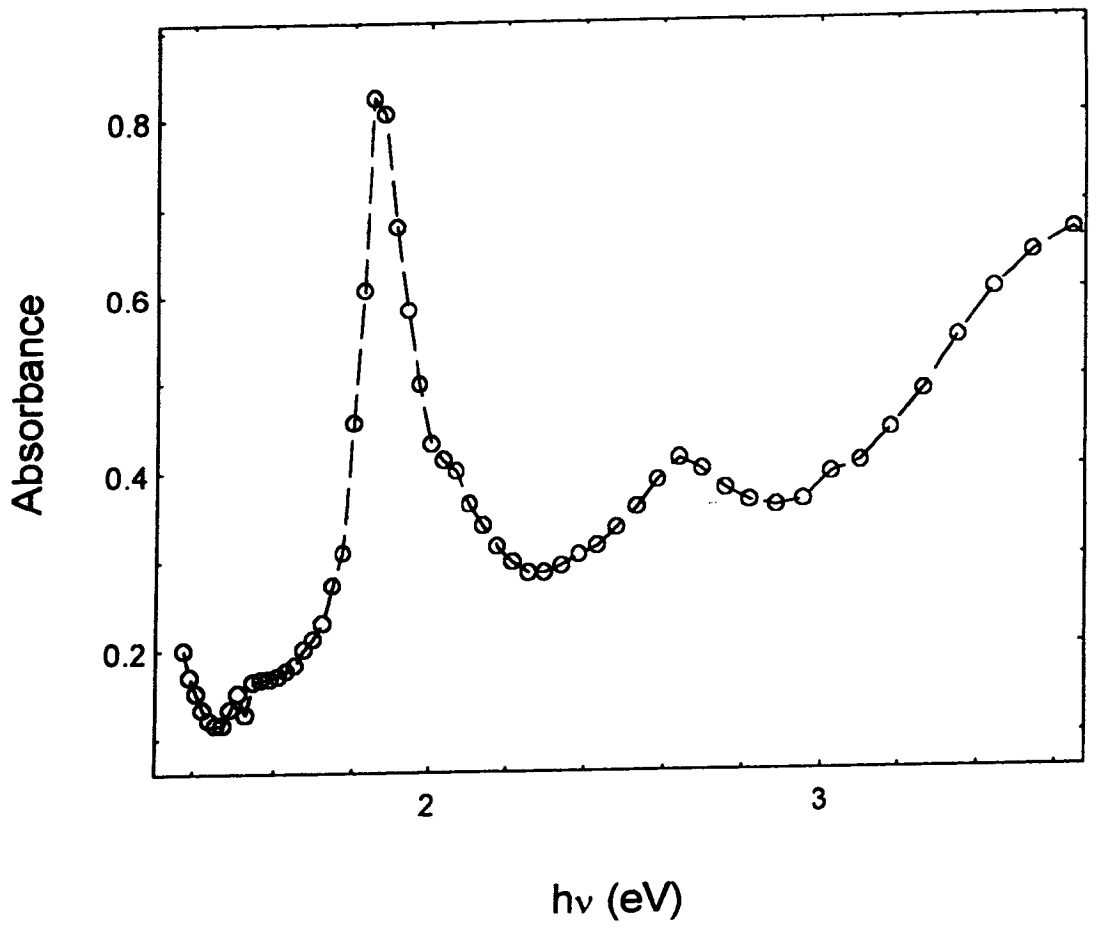

5.9 Absorption spectrum for untreated [Tm(pc)(pc*)]

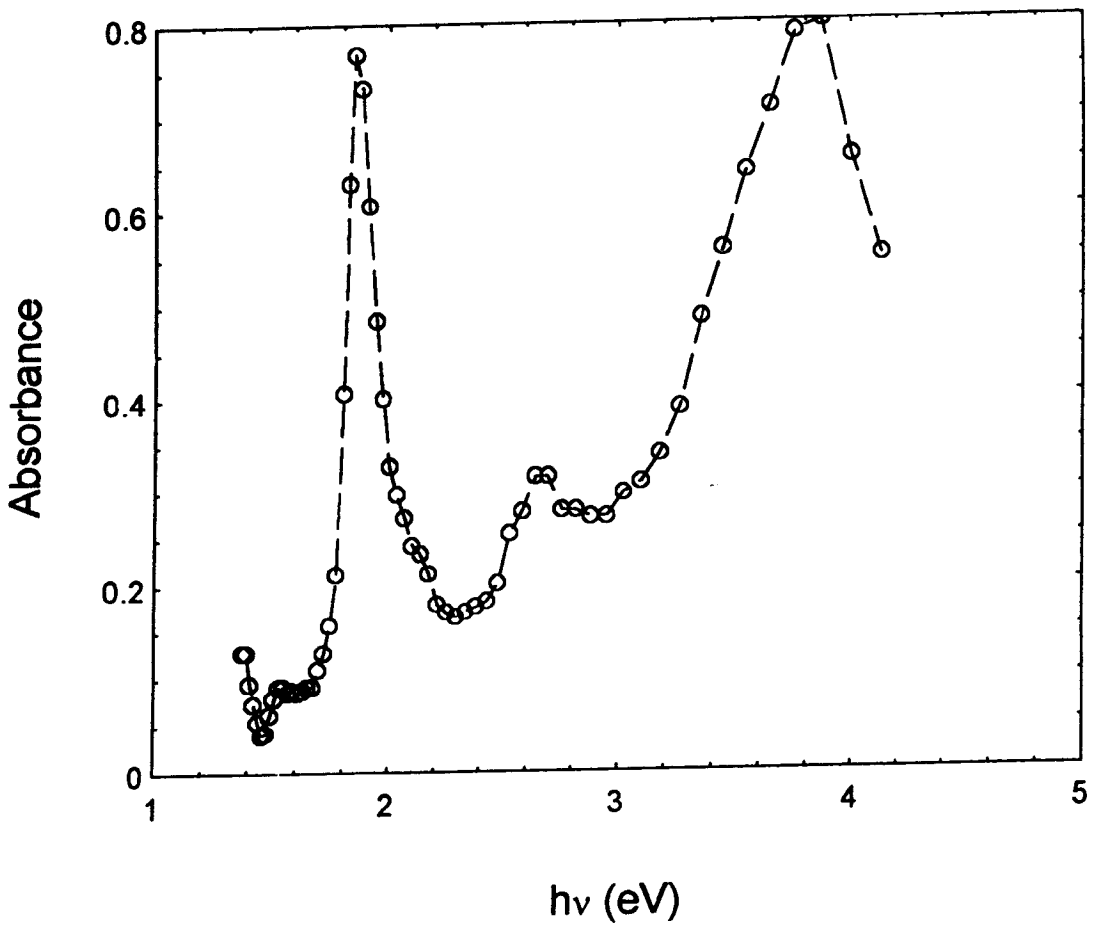

5.10 Absorption spectrum for annealed [Tm(pc)(pc*)]

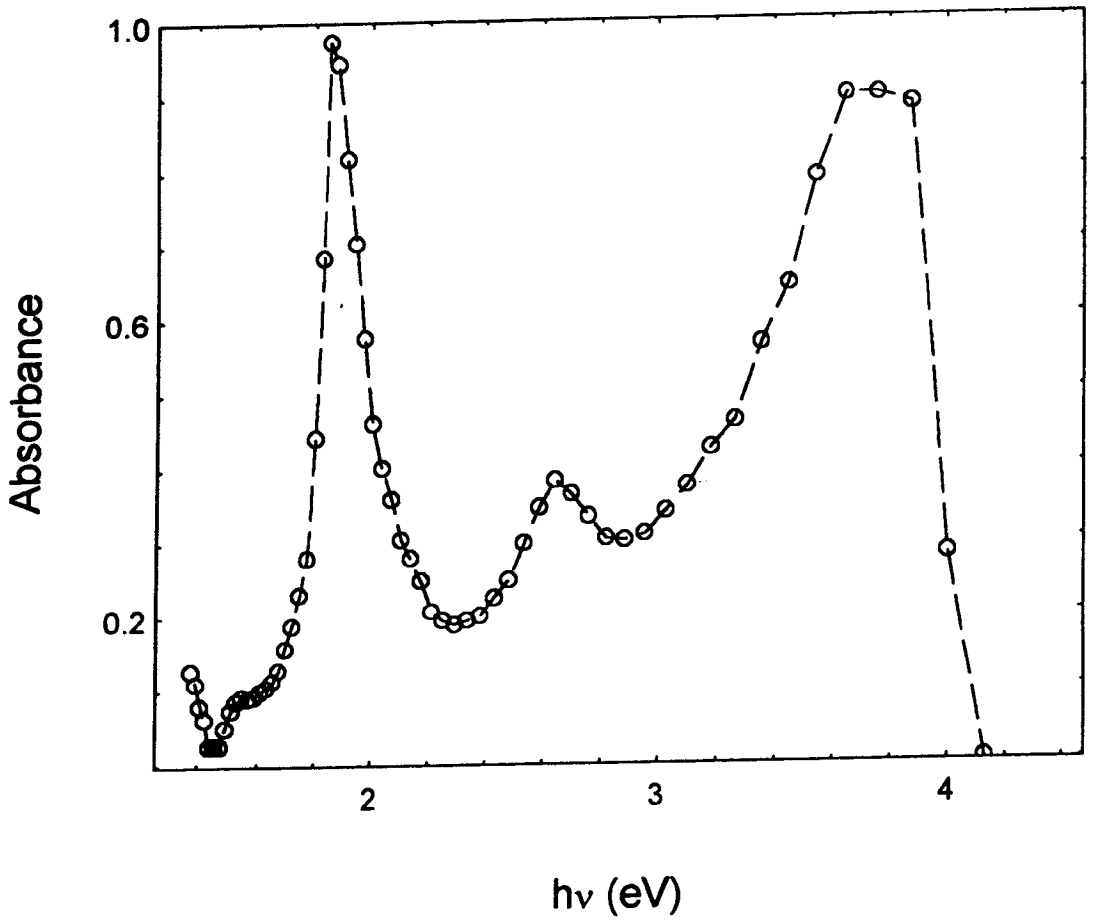

5.11 Absorption spectrum for [Tm(pc)(pc*)] voltage cycled to blue

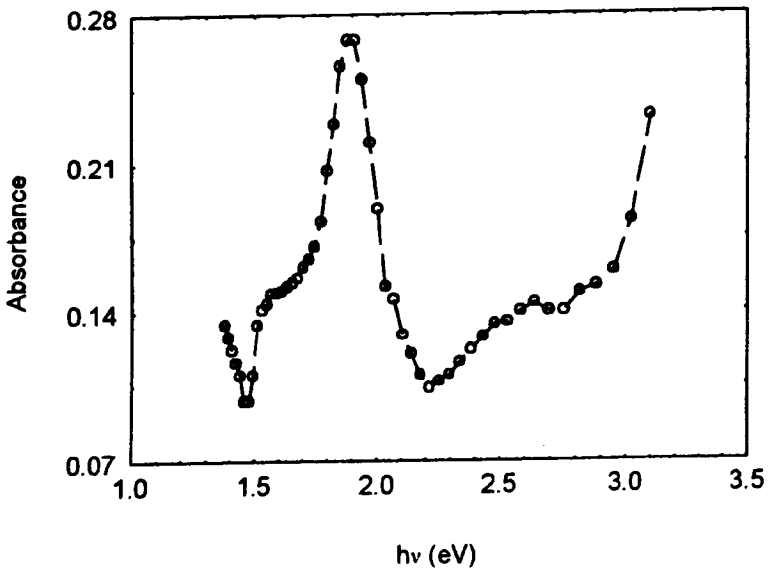

5.12 Absorption spectrum for [Tm(pc)(pc*)] voltage cycled to red

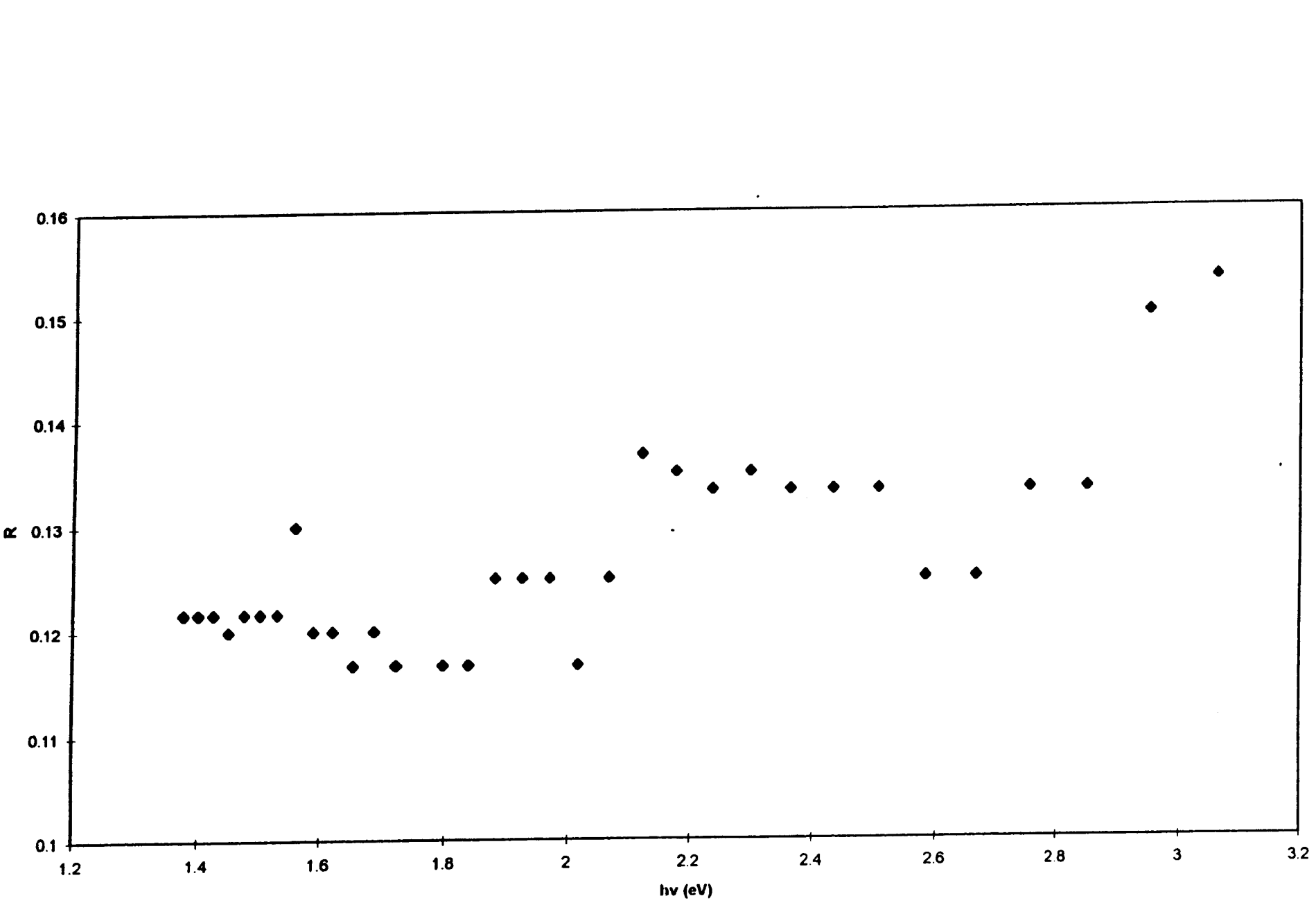

5.13 Reflection spectrum for untreated [HF(pc)(pc*)]

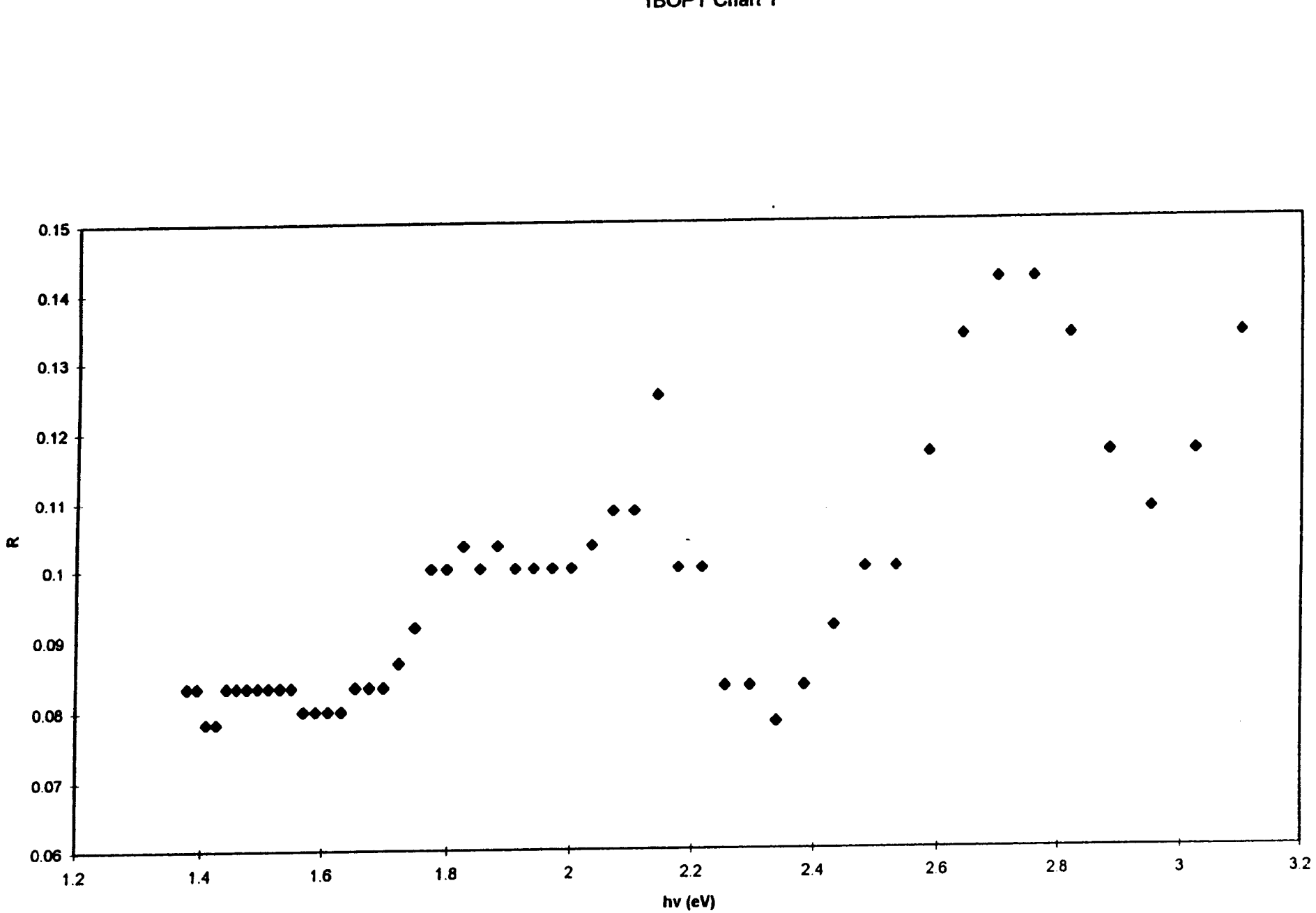

5.14 Reflection spectrum for annealed [HF(pc)(pc*)]

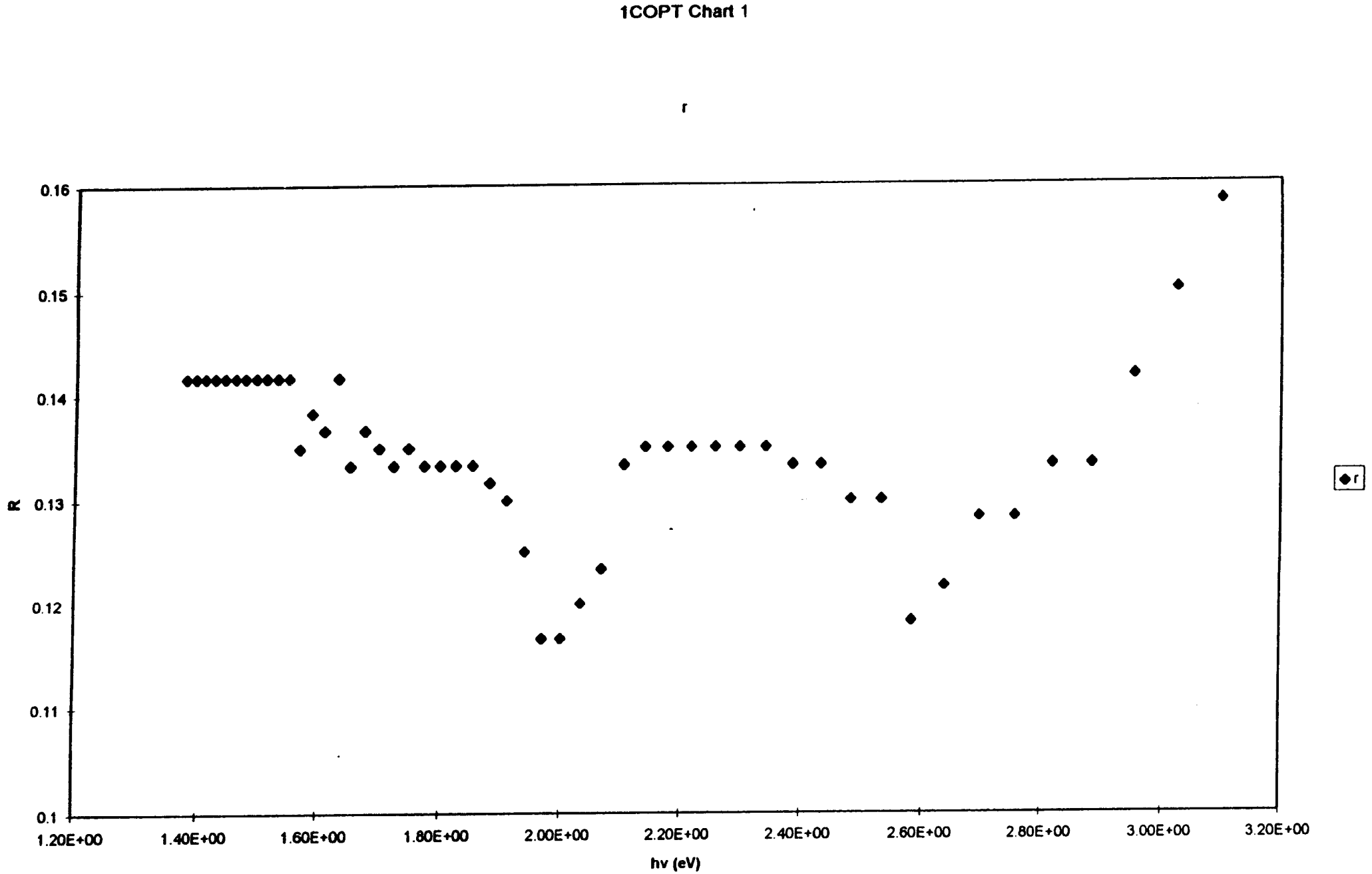

5.15 Reflection spectrum for [HF(pc)(pc*)] voltage cycled to blue

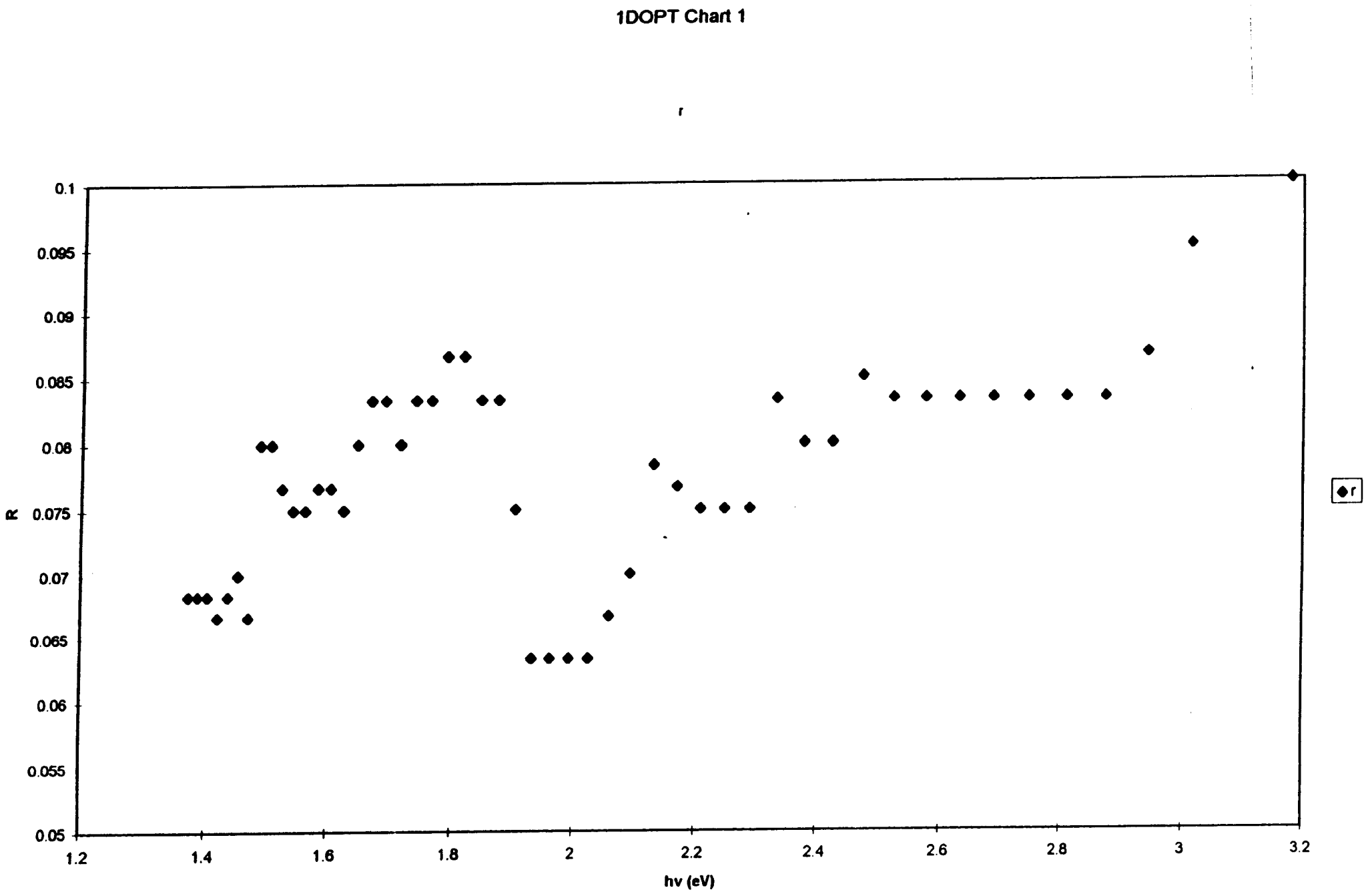

5.16 Reflection spectrum for [HF(pc)(pc*)] voltage cycled to red

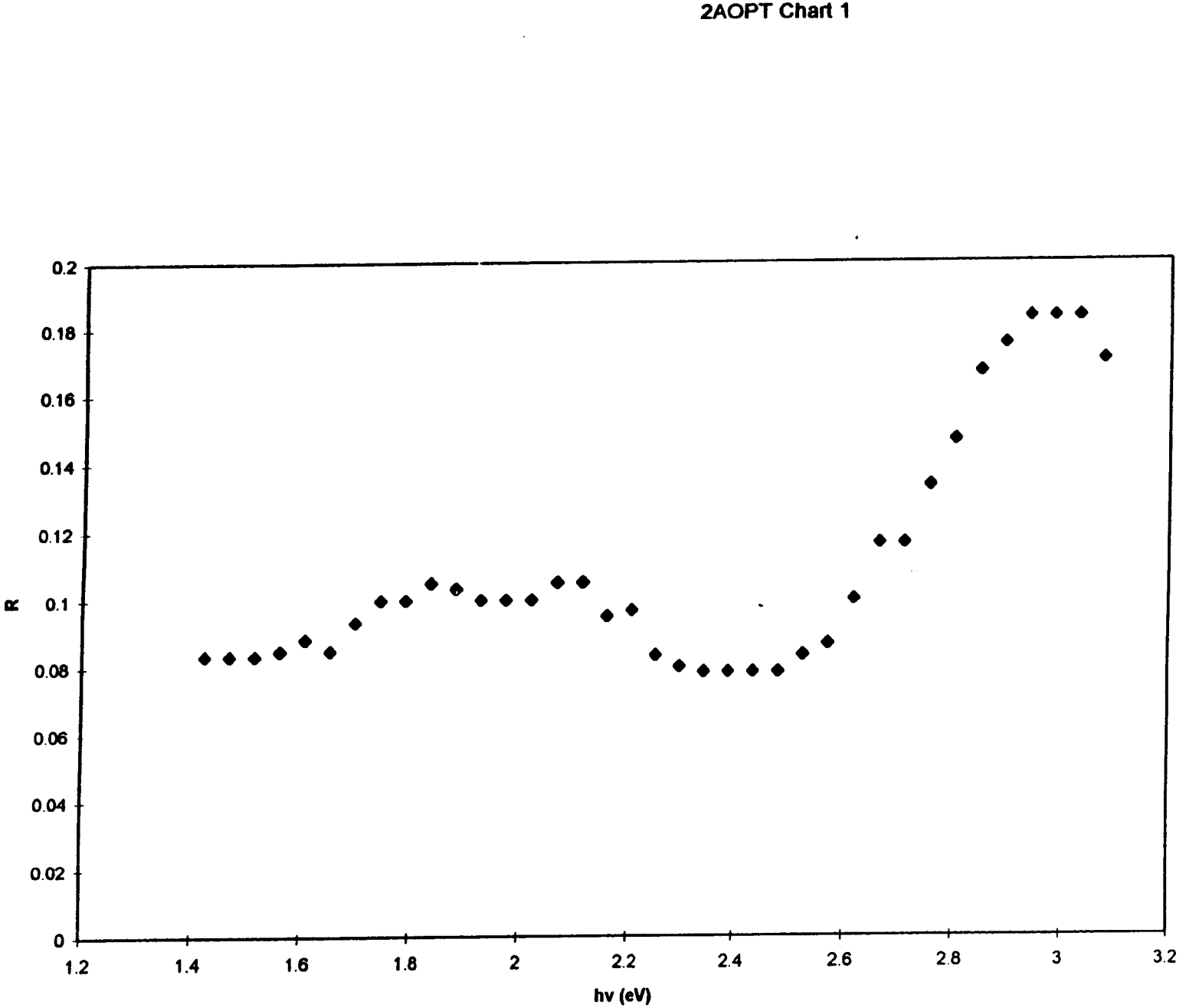

5.17 Reflection spectrum for untreated [Gd(pc)(pc*)]

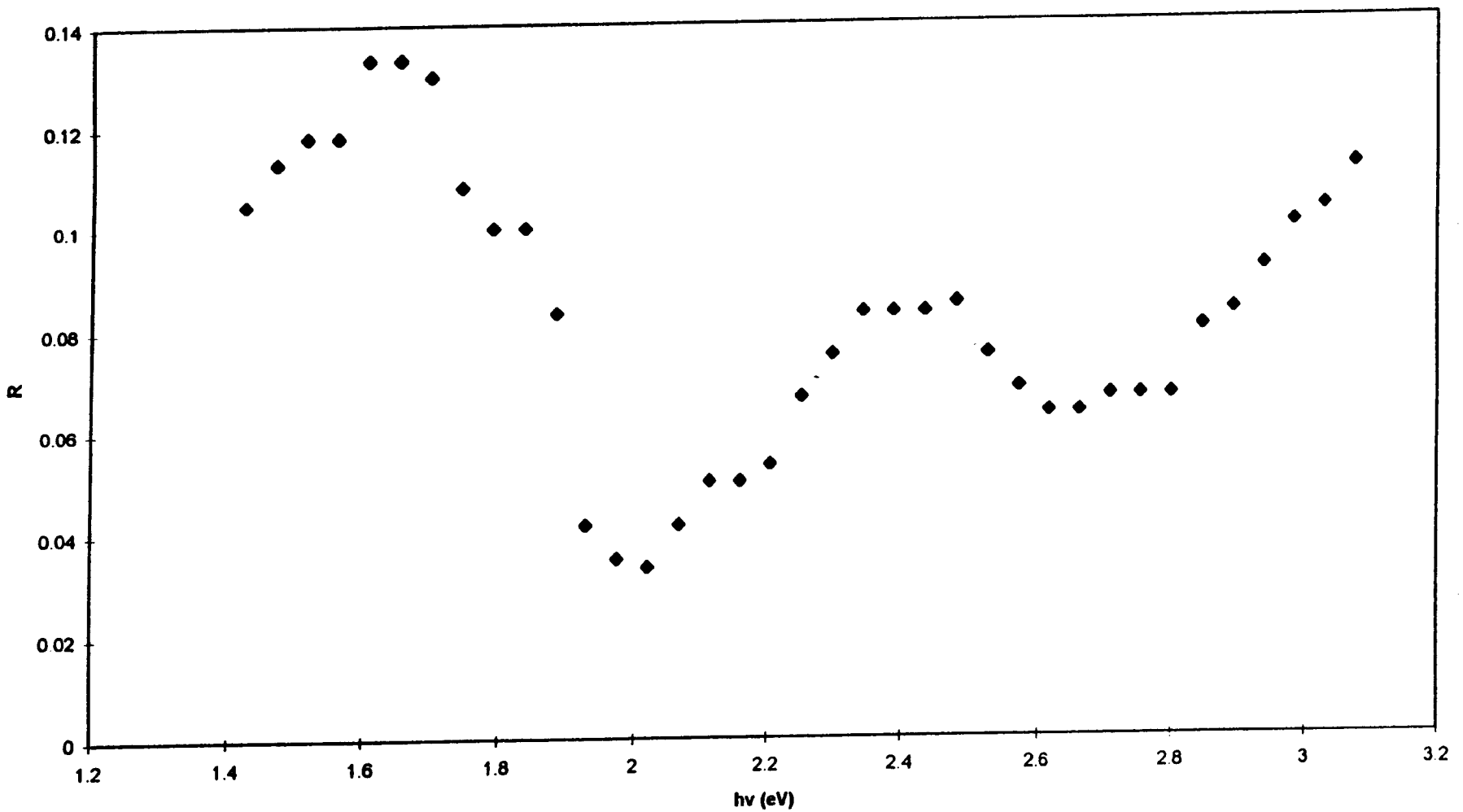

5.18 Reflection spectrum for annealed [Gd(pc)(pc*)]

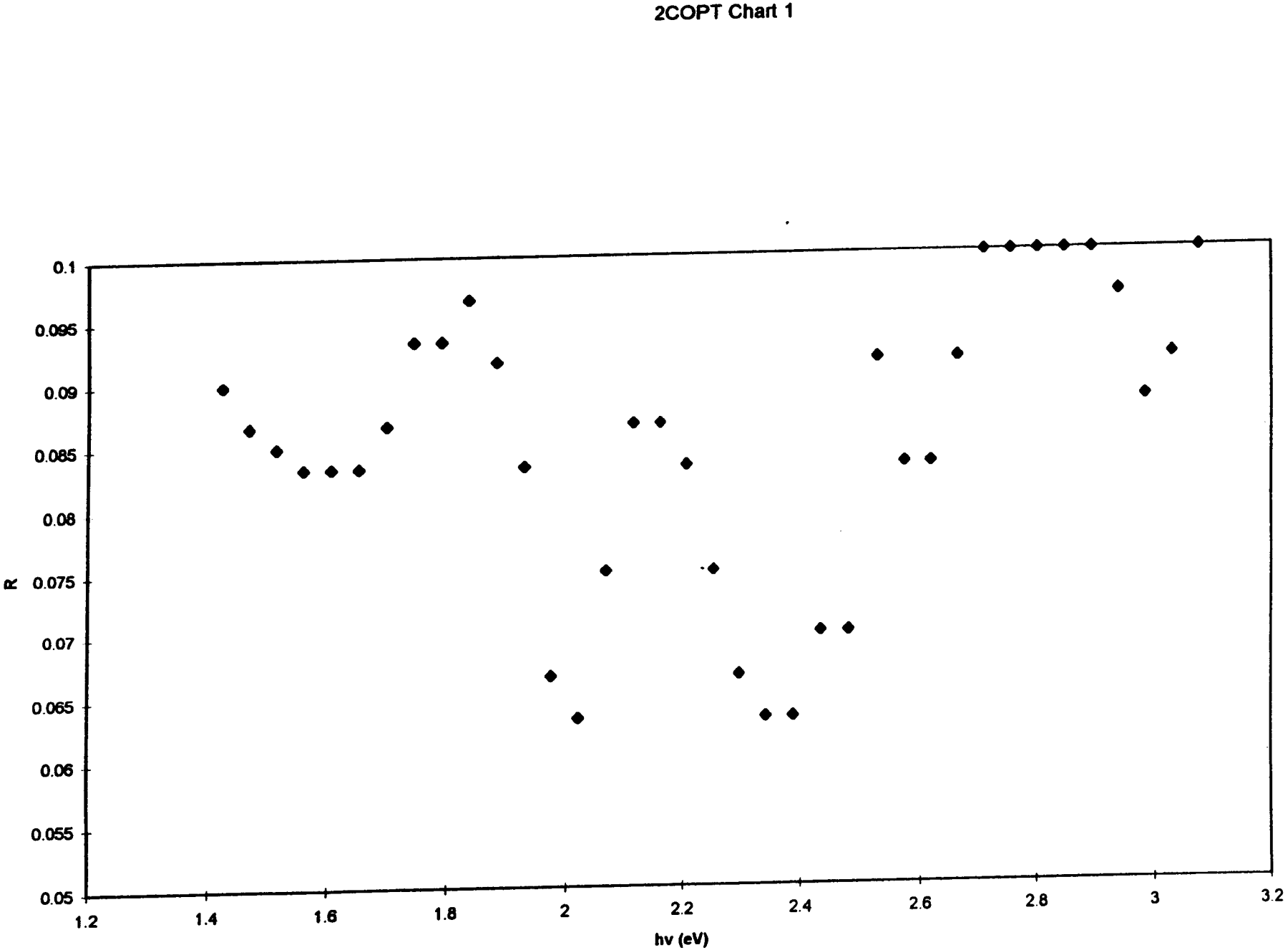

5.19 Reflection spectrum for [Gd(pc)(pc*)] voltage cycled to blue

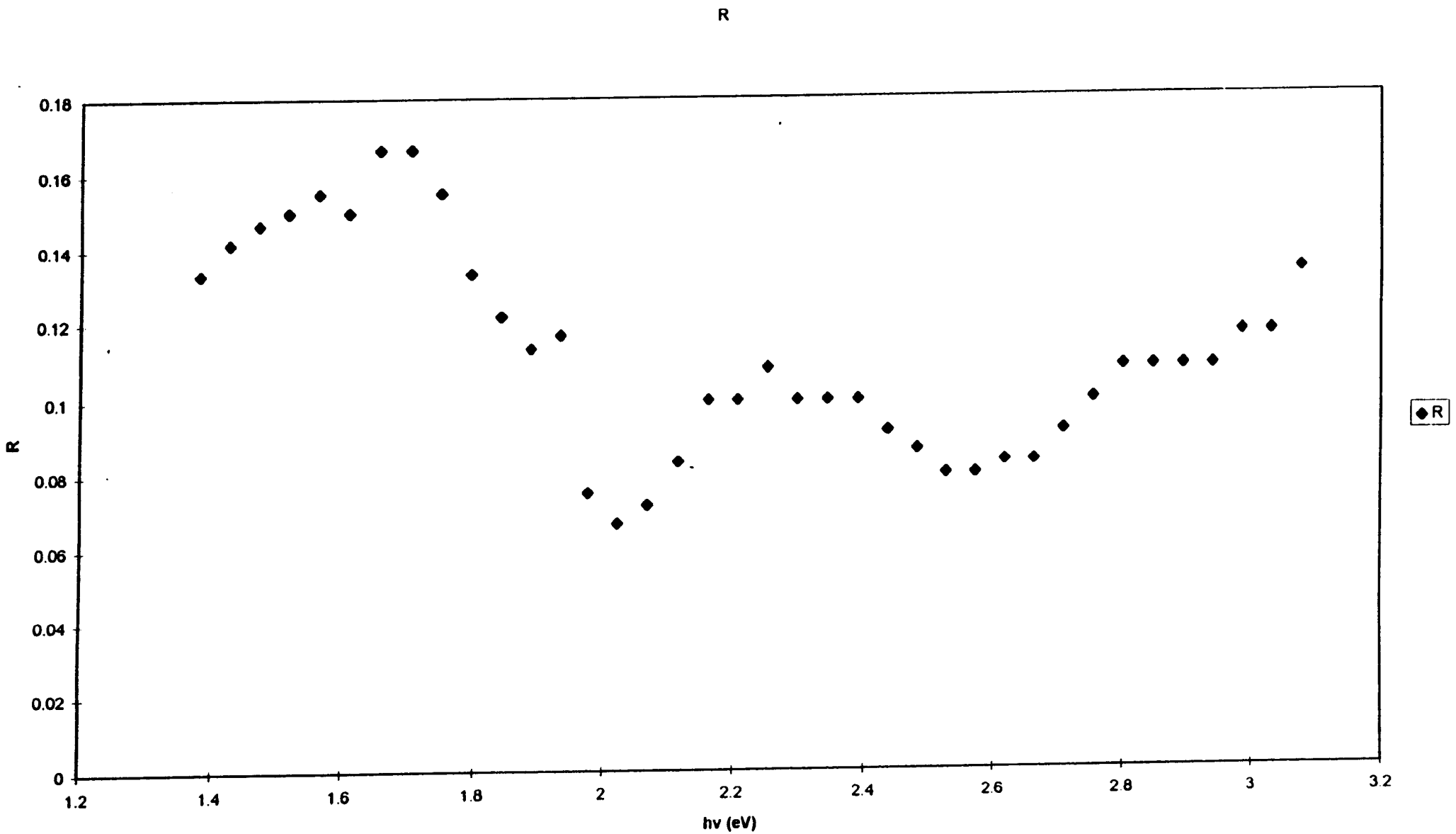

5.20 Reflection spectrum for [Gd(pc)(pc*)] voltage cycled to red

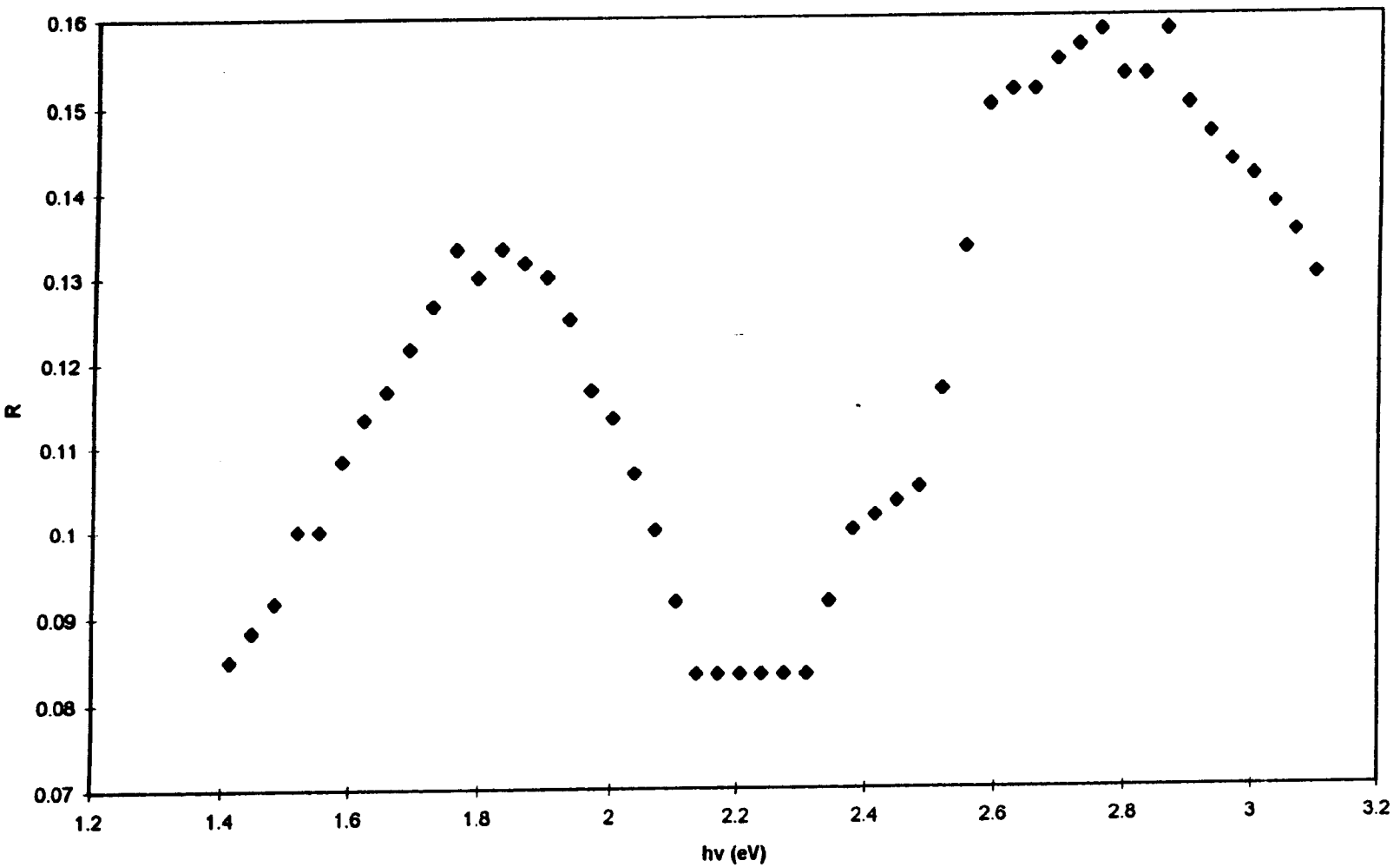

5.21 Reflection spectrum for untreated [Tm(pc)(pc*)]

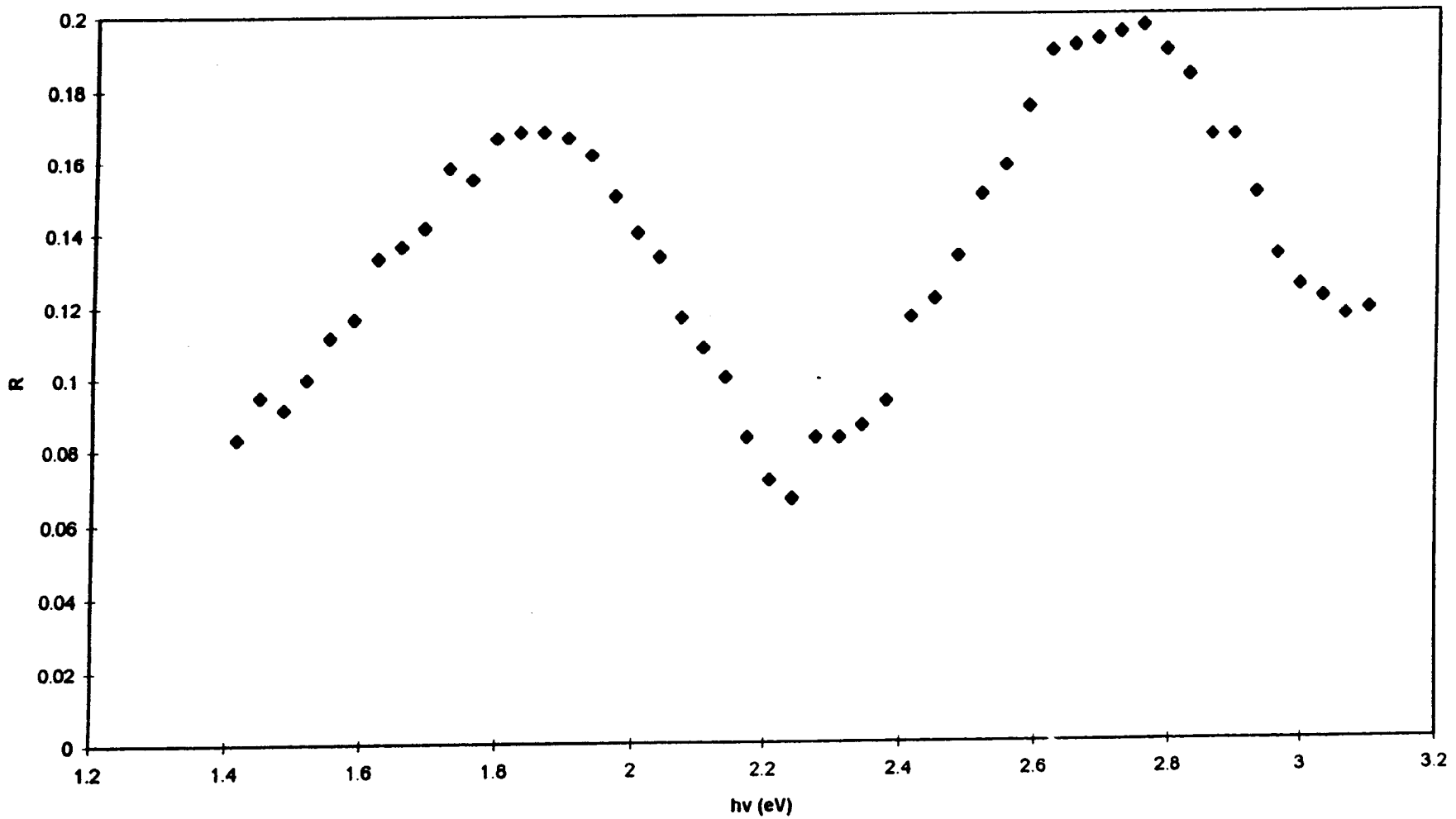

5.22 Reflection spectrum for annealed [Tm(pc)(pc*)]

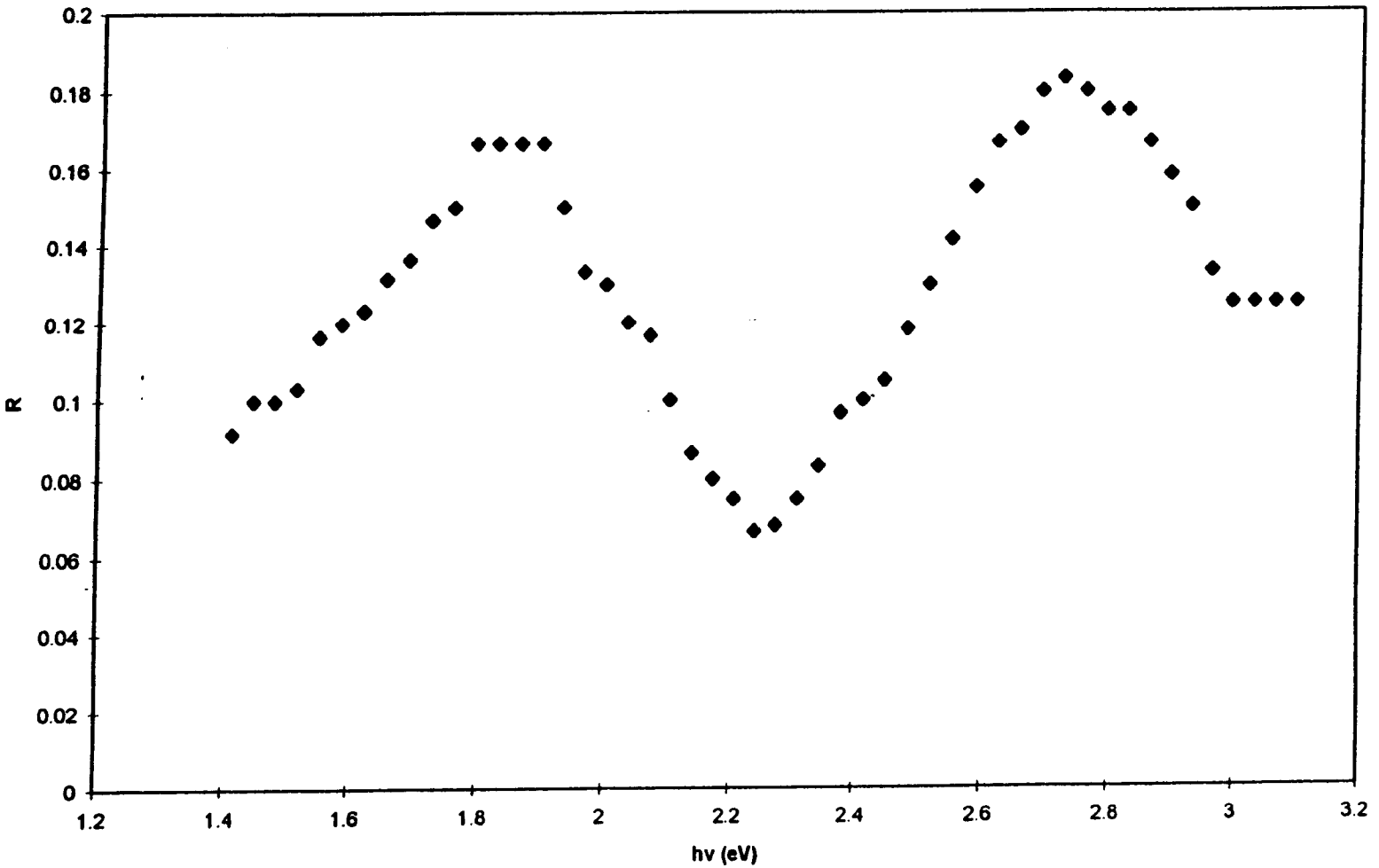

5.23 Reflection spectrum for [Tm(pc)(pc*)] voltage cycled to blue

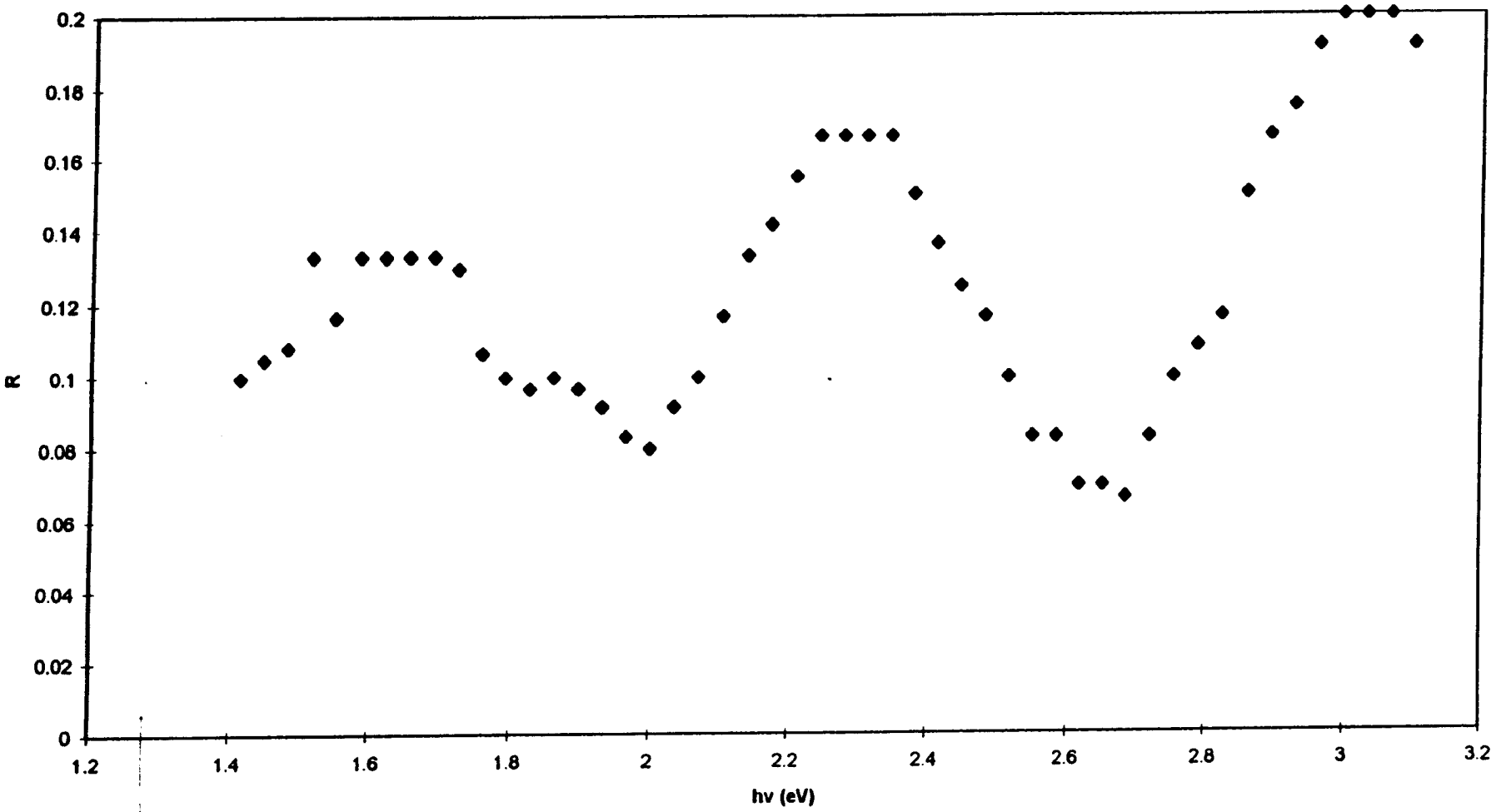

5.24 Reflection spectrum for [Tm(pc)(pc*)] voltage cycled to red

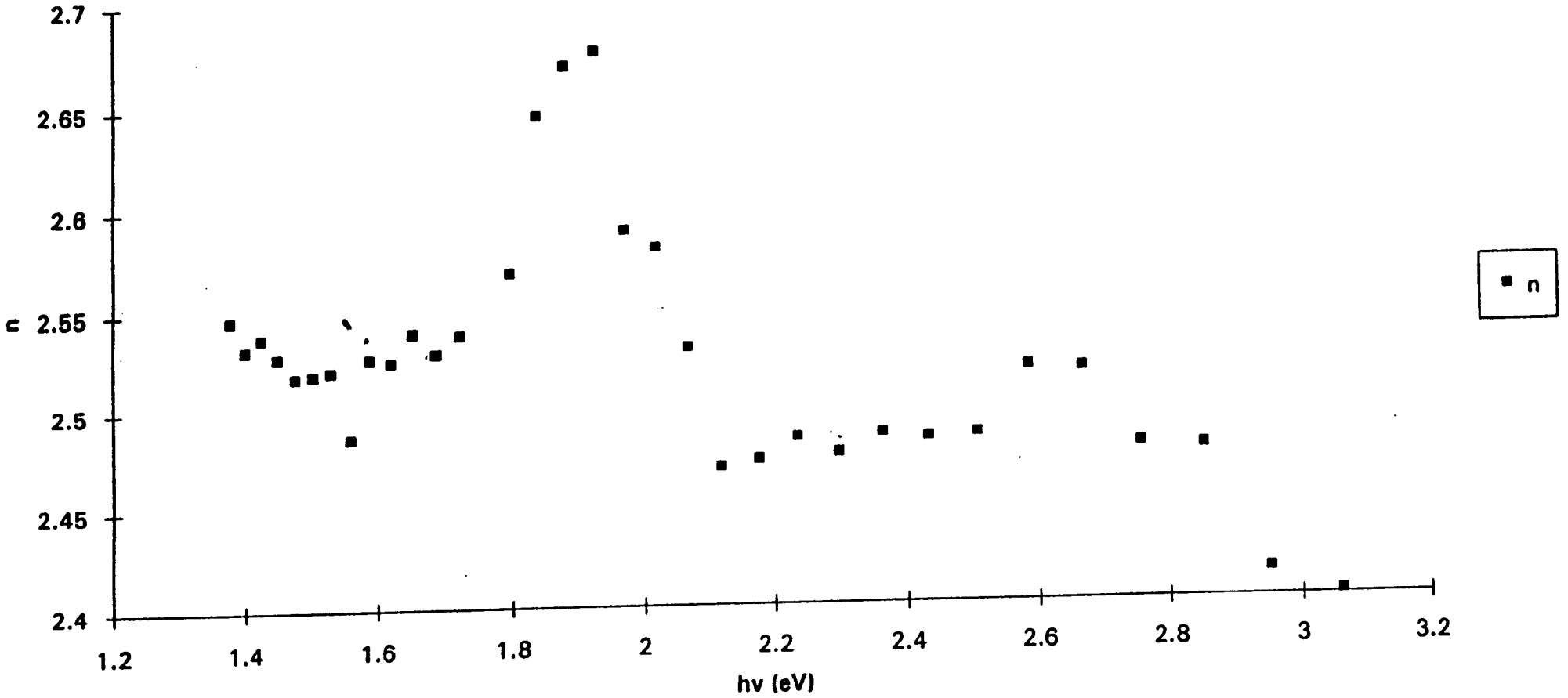

5.25 Propagation constant n for untreated [HΓ(pc)(pc*)]

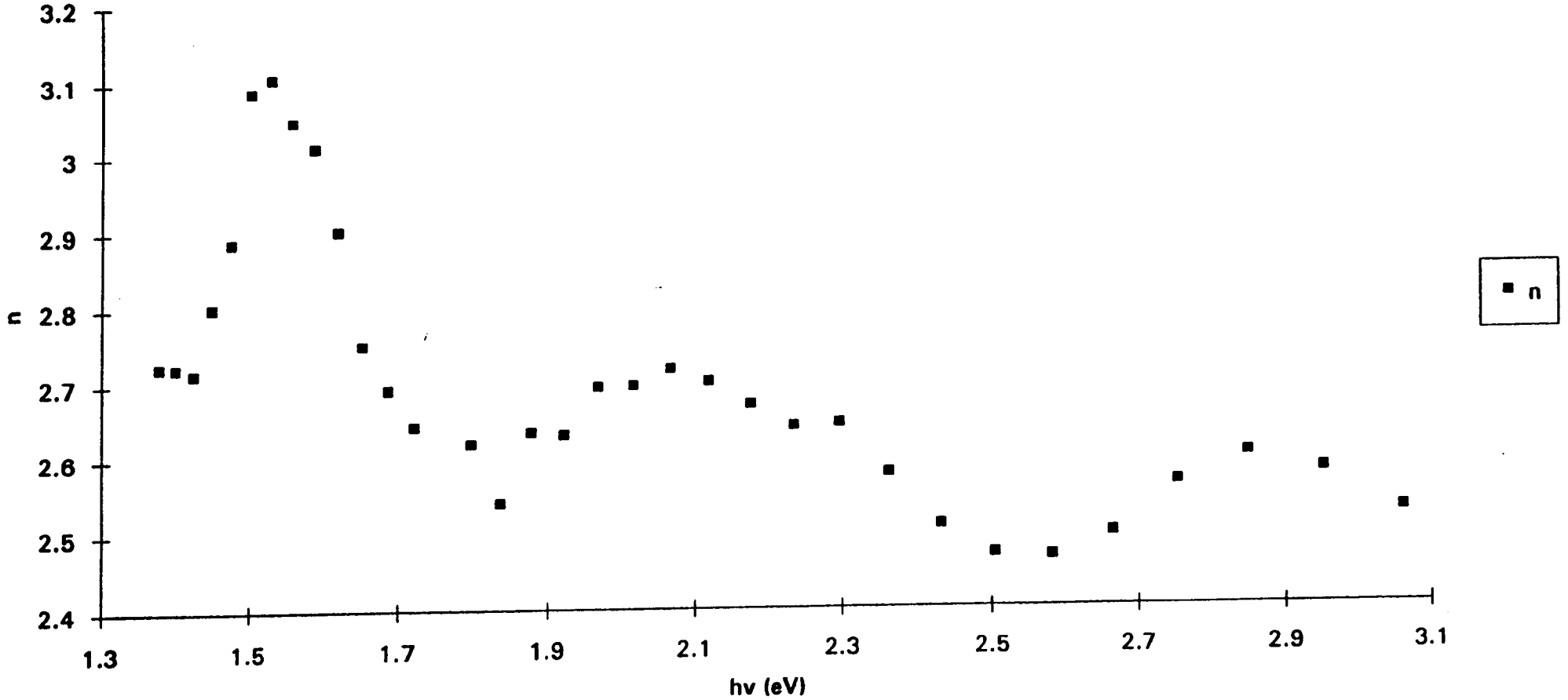

5.26 Propagation constant n for annealed [HF(pc)(pc*)]

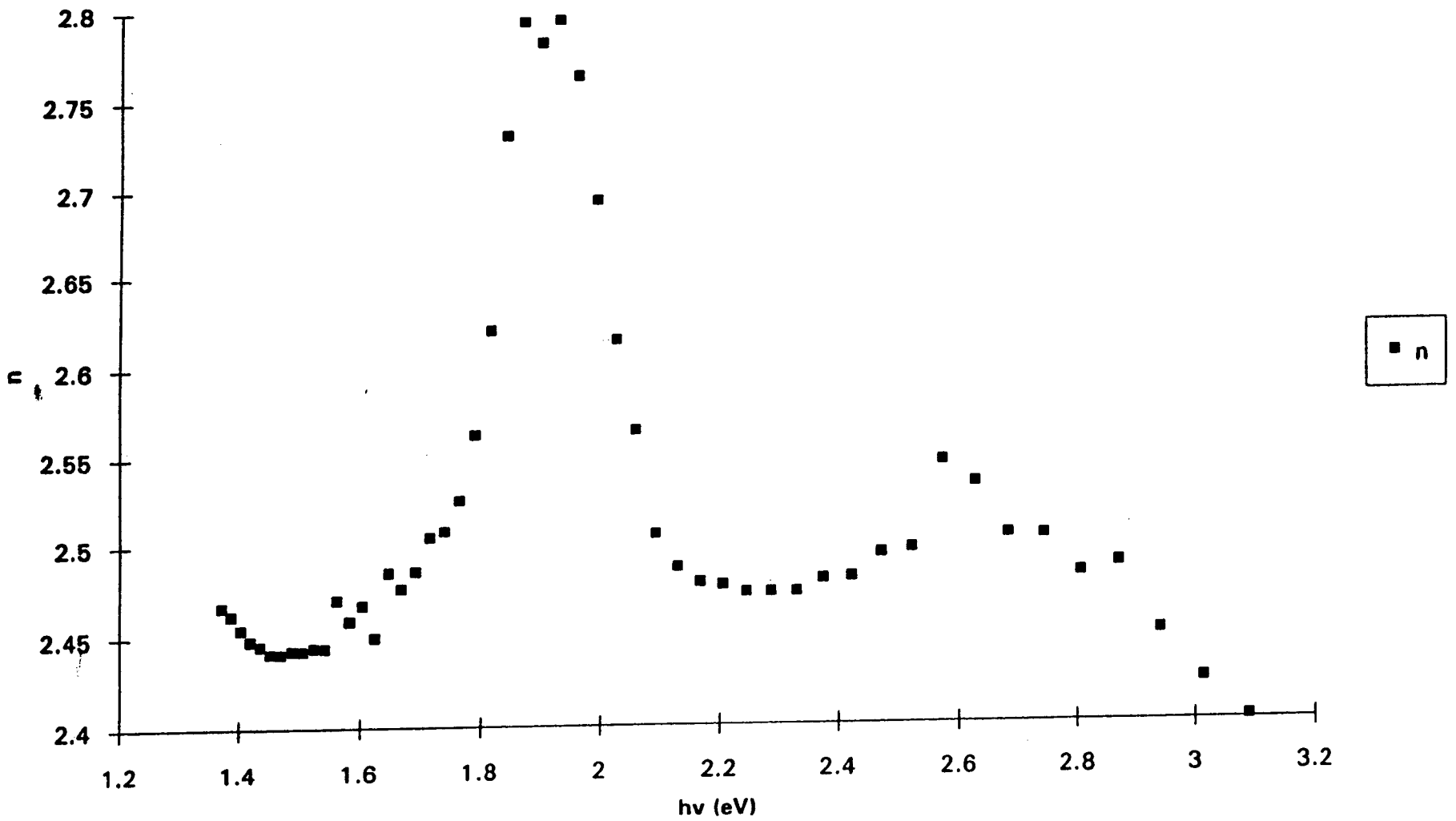

5.27 Propagation constant n for [HF(pc)(pc*)] voltage cycled to blue

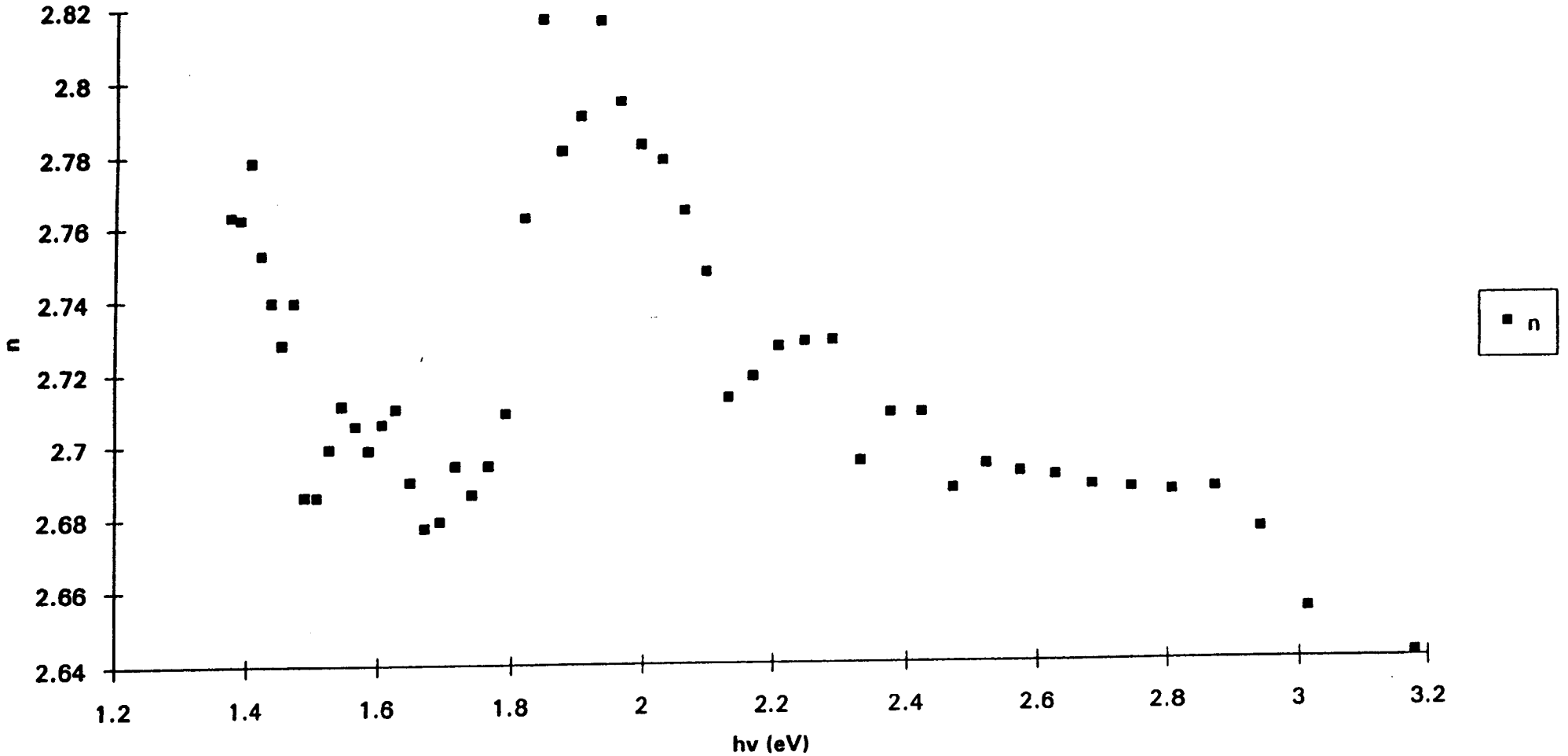

5.28 Propagation constant n for [HF(pc)(pc*)] voltage cycled to red

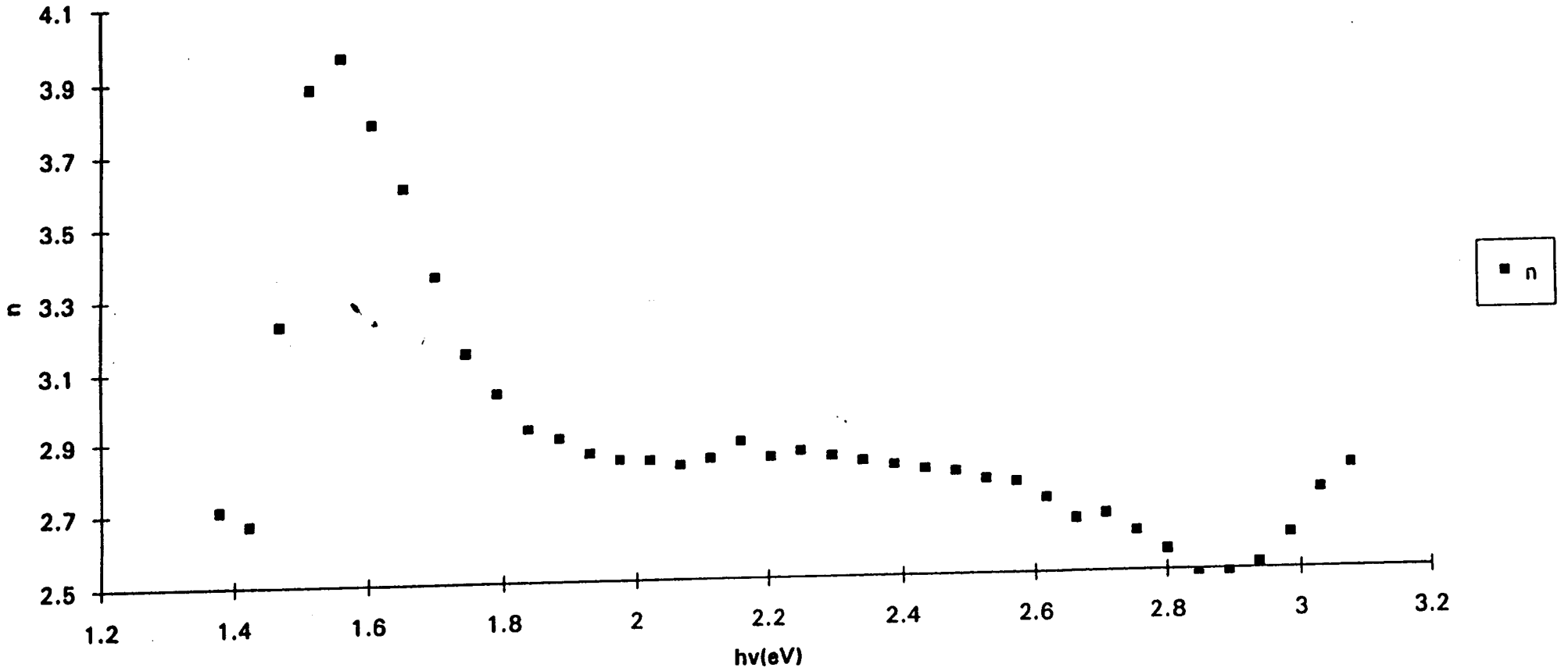

5.29 Propagation constant n for untreated [Gd(pc)(pc*)]

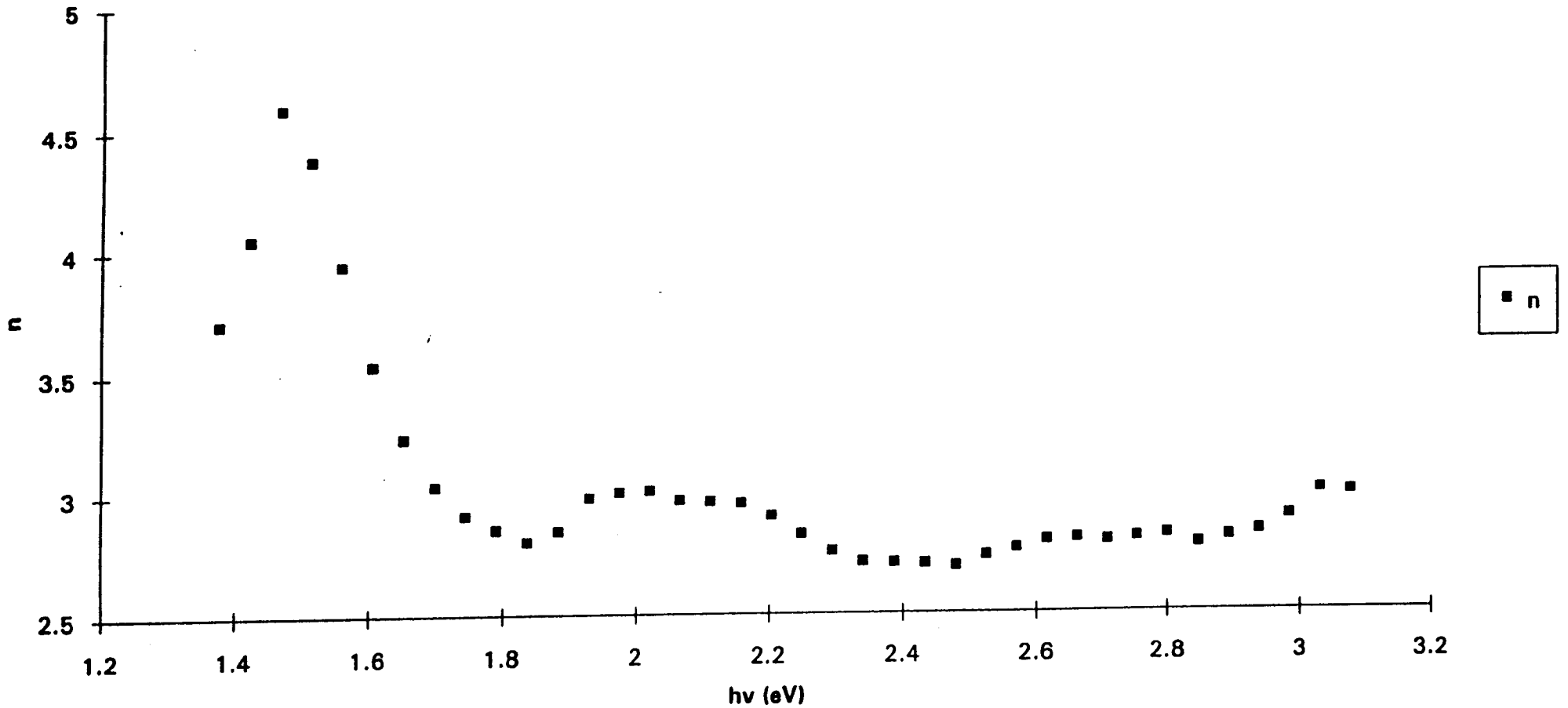

5.30 Propagation constant n for annealed [Gd(pc)(pc*)]

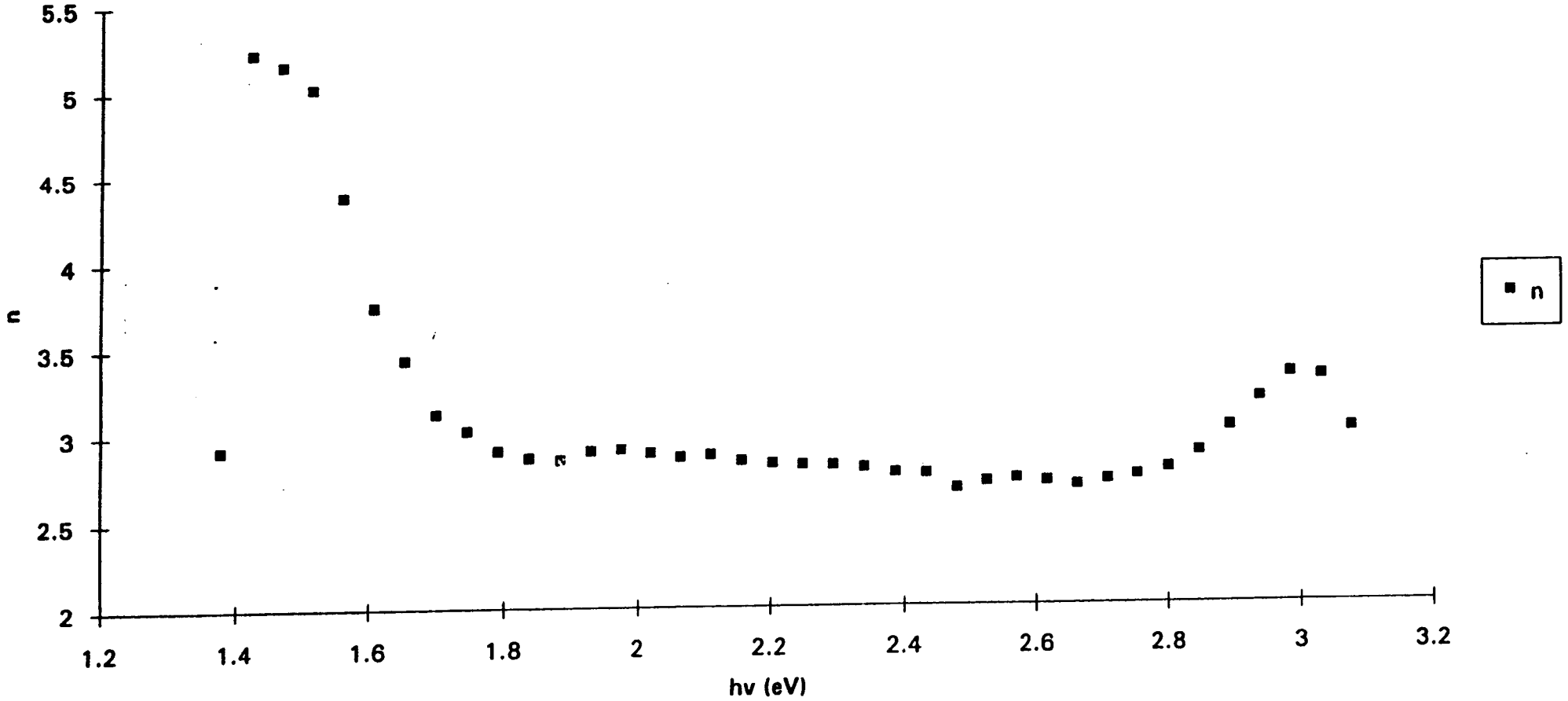

5.31 Propagation constant n for [Gd(pc)(pc*)] voltage cycled to blue

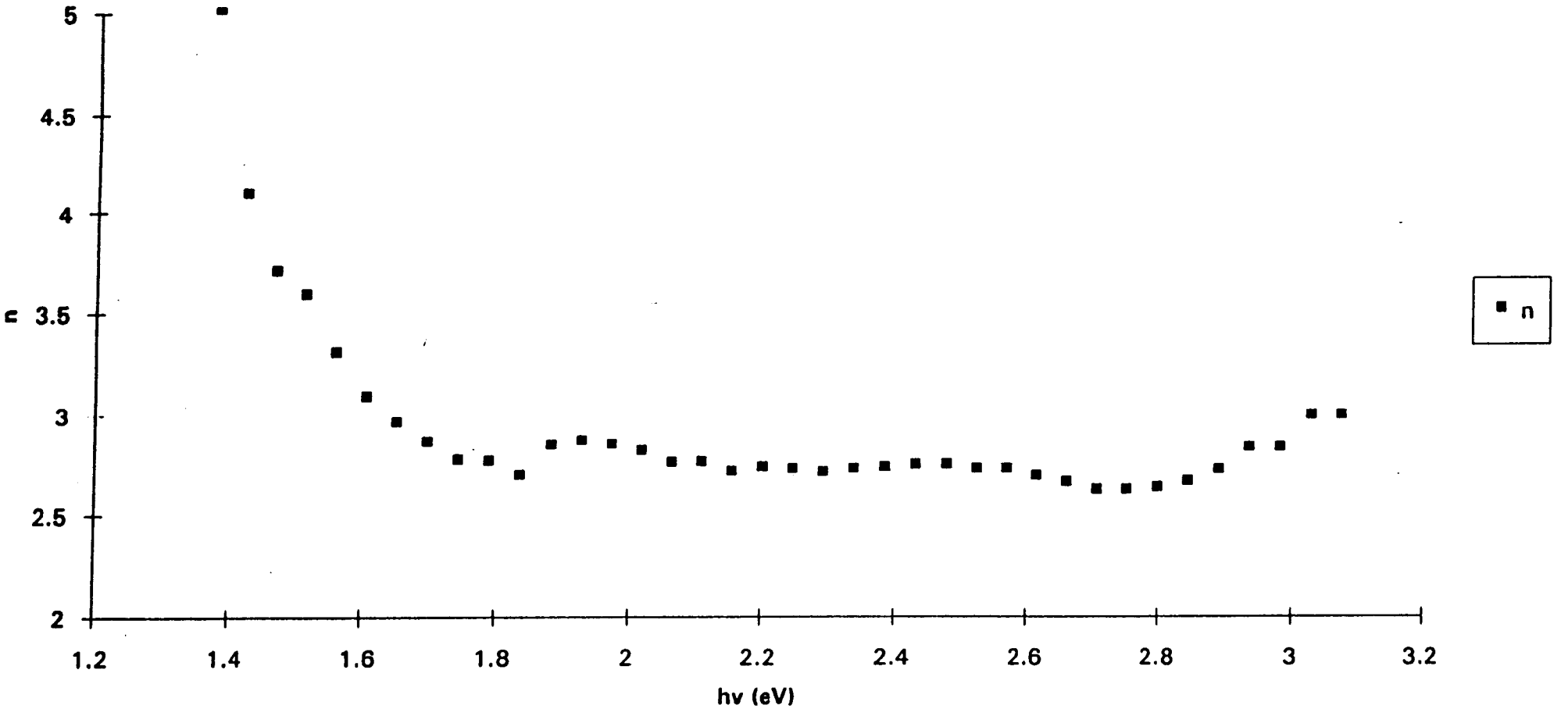

5.32 Propagation constant n for [Gd(pc)(pc*)] voltage cycled to red

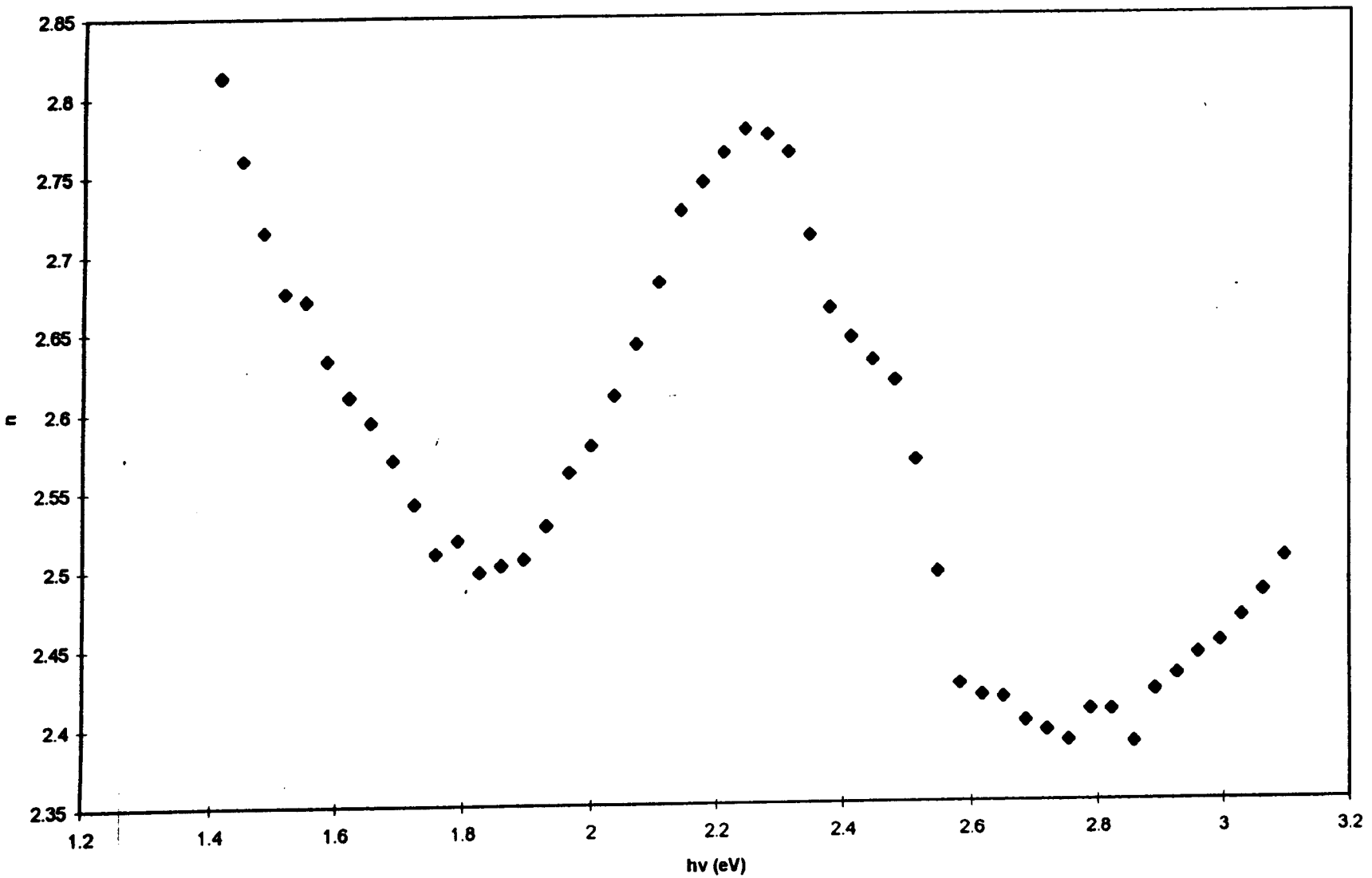

5.33 Propagation constant n for untreated [Tm(pc)(pc*)]

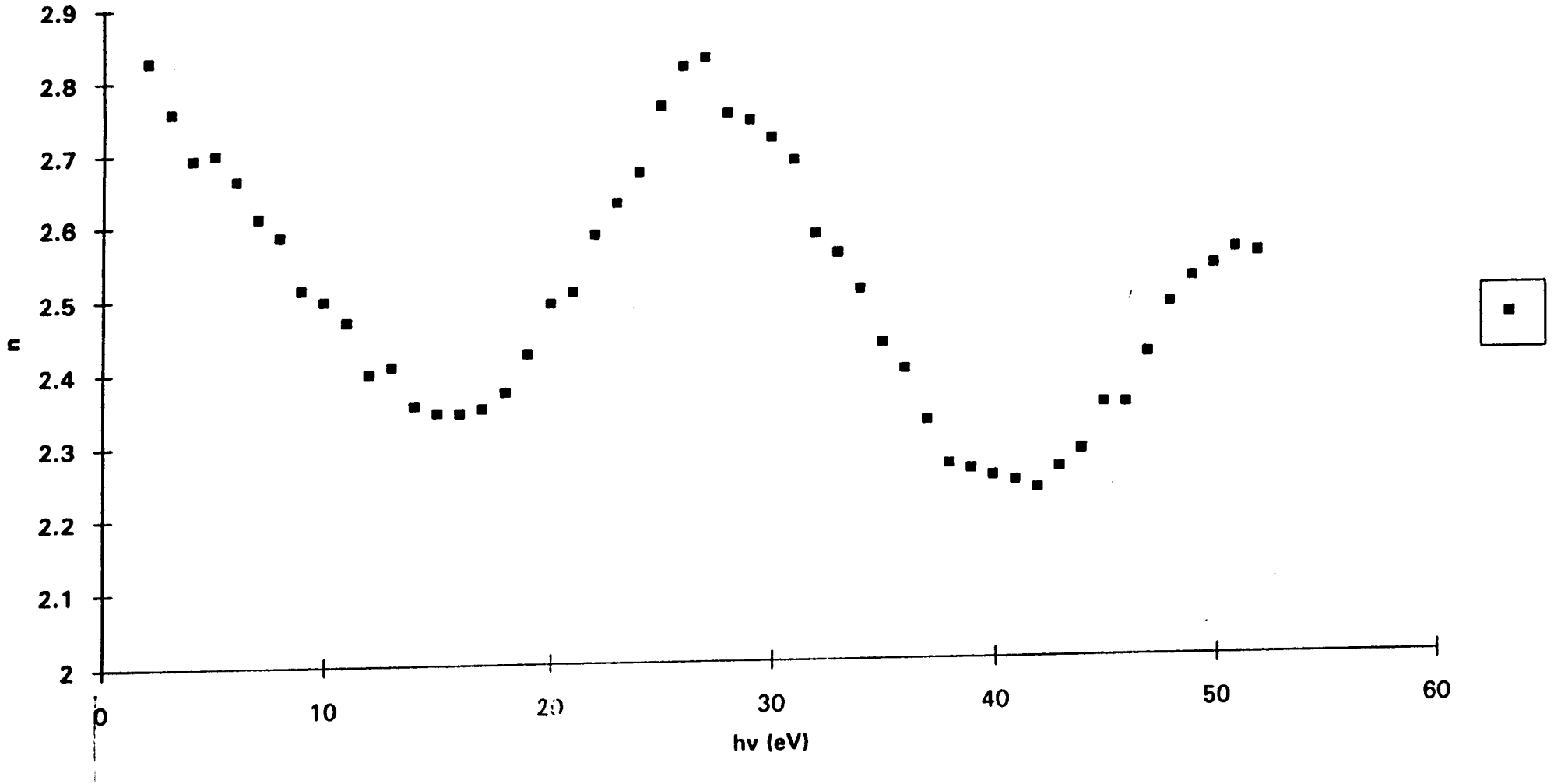

5.34 Propagation constant n for annealed [Tm(pc)(pc*)]

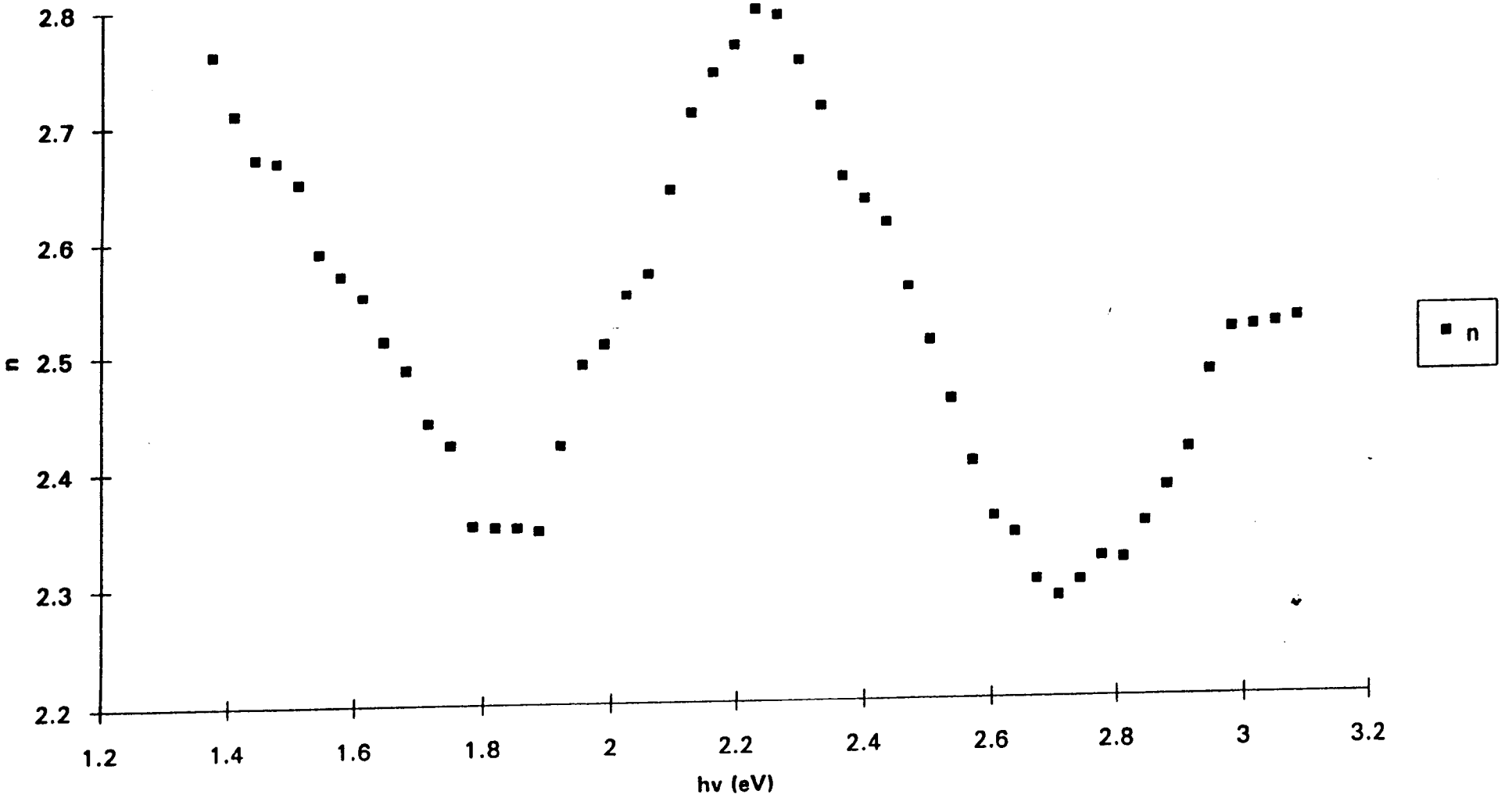

5.35 Propagation constant n for [Tm(pc)(pc*)] voltage cycled to blue

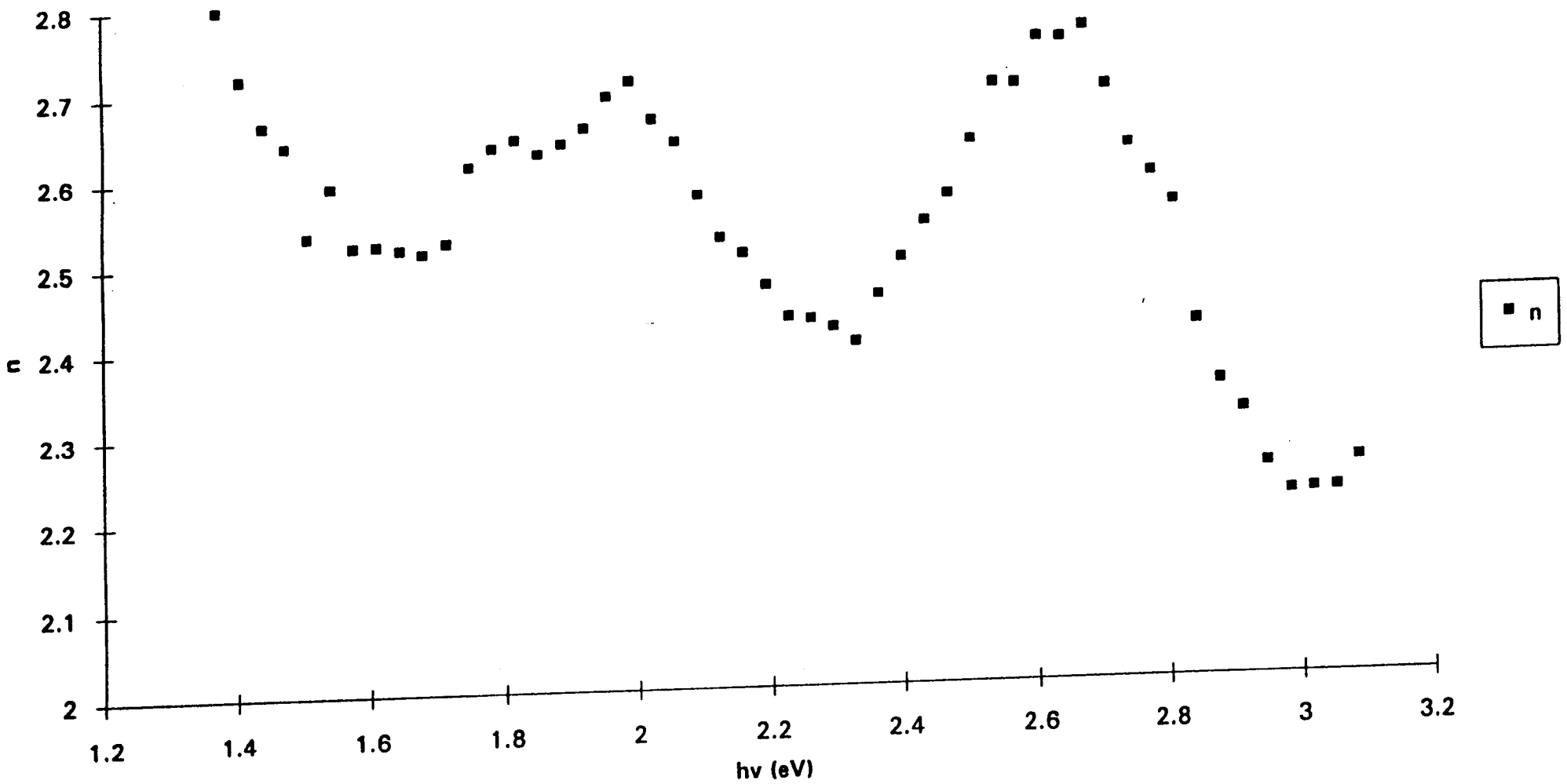

5.36 Propagation constant n for [Tm(pc)(pc*)] voltage cycled to red

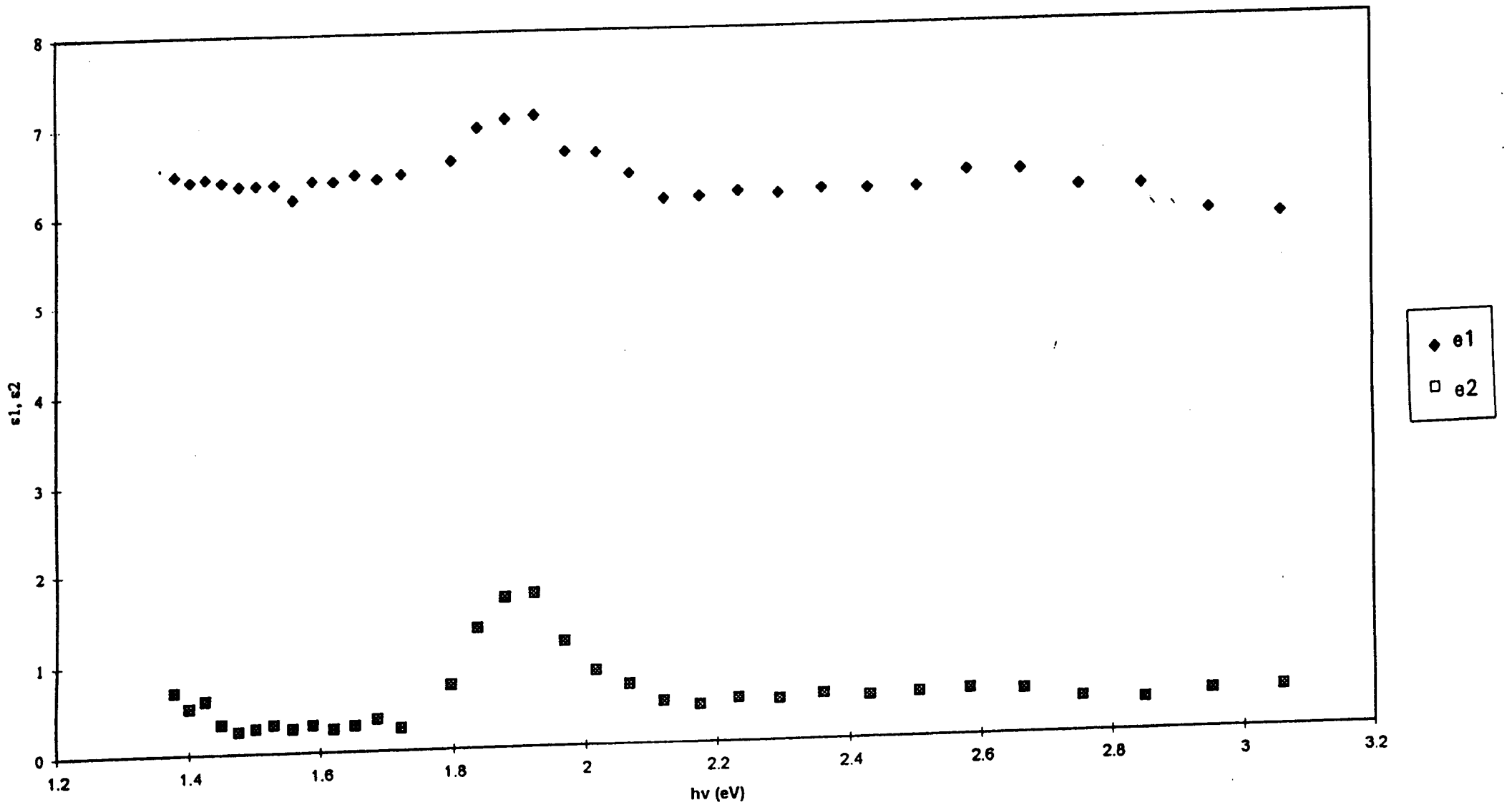

5.37 Real part ε_1 and imaginary part ε_2 of complex dielectric constant for untreated [HF(pc)(pc*)]

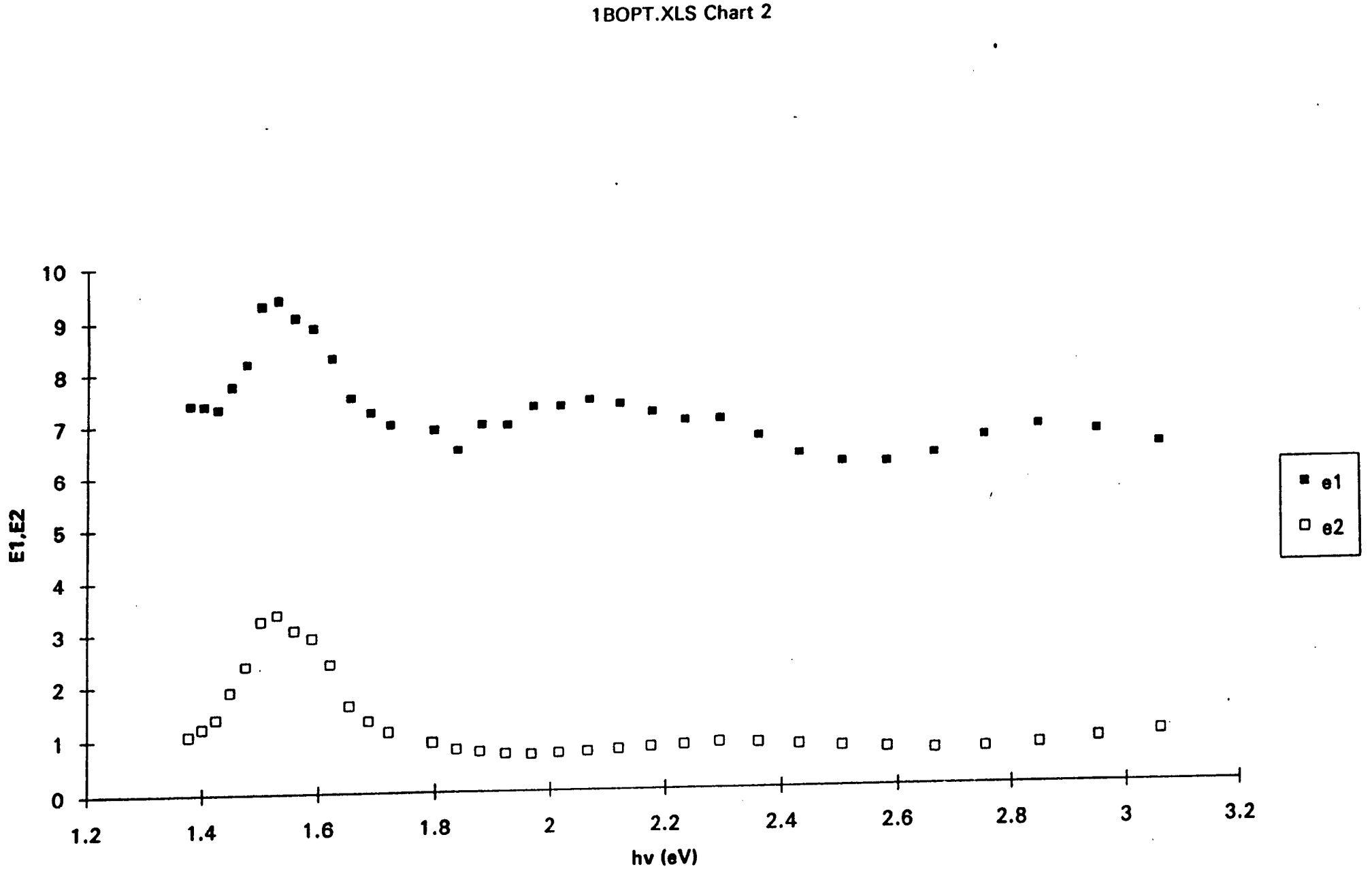

5.38 Real part ε_1 and imaginary part ε_2 of complex dielectric constant for annealed [HF(pc)(pc*)]

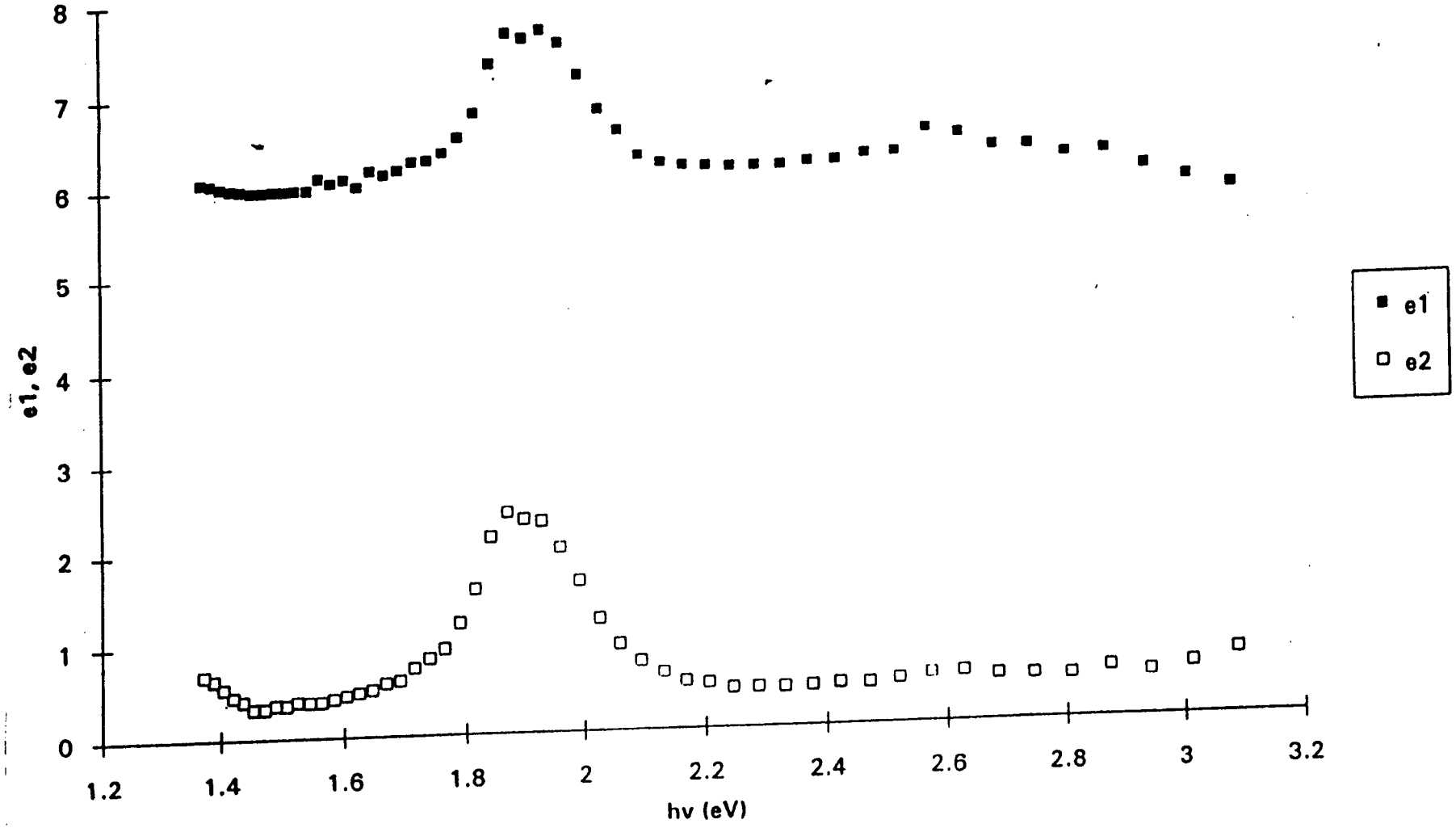

5.39 Real part ε_1 and imaginary part ε_2 of complex dielectric constant for [HF(pc)(pc*)] voltage cycled to blue

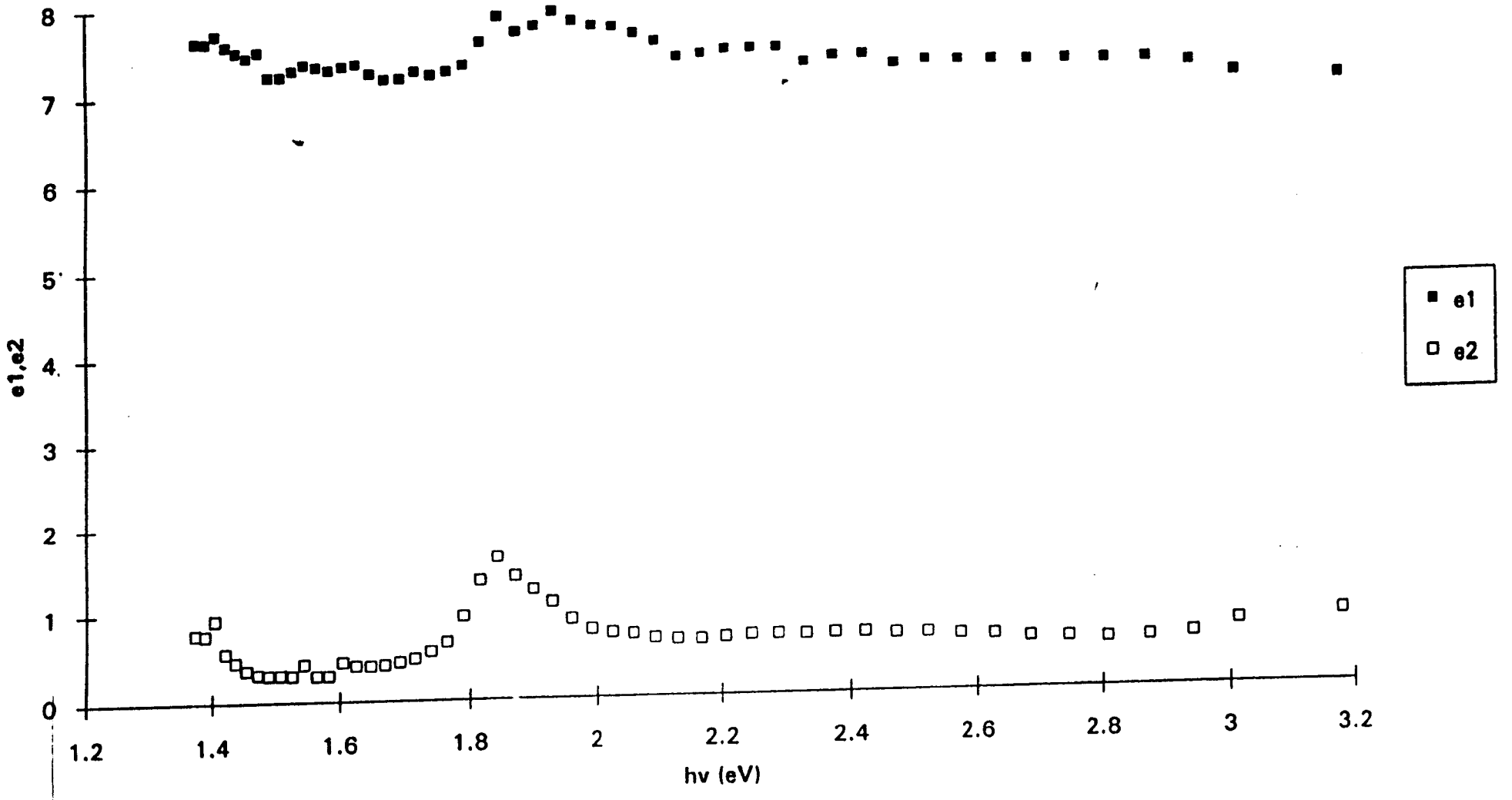

5.40 Real part ε_1 and imaginary part ε_2 of complex dielectric constant for [HF(pc)(pc*)] voltage cycled to red

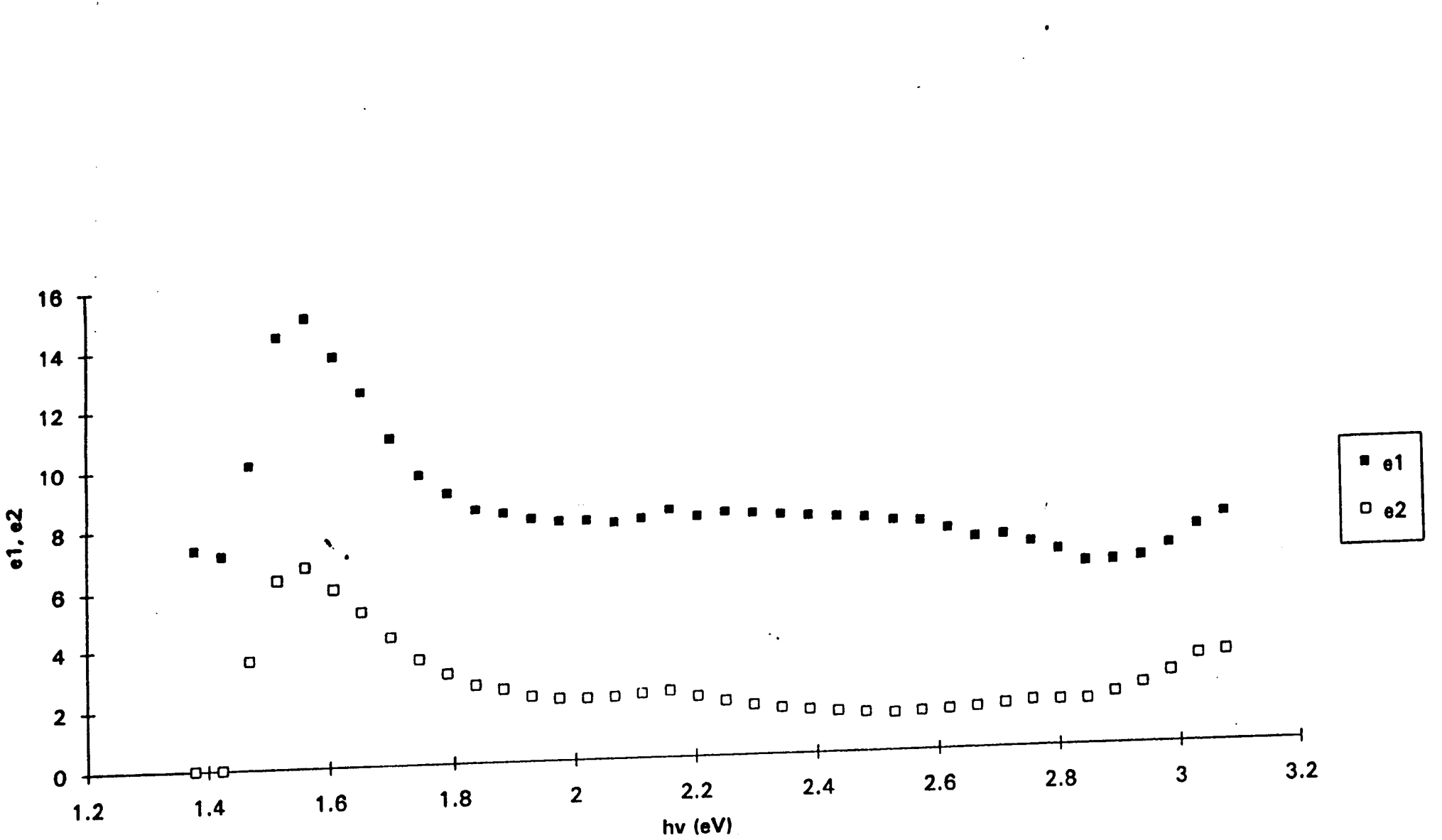

5.41 Real part ε_1 and imaginary part ε_2 of complex dielectric constant for untreated [Gd(pc)(pc*)]

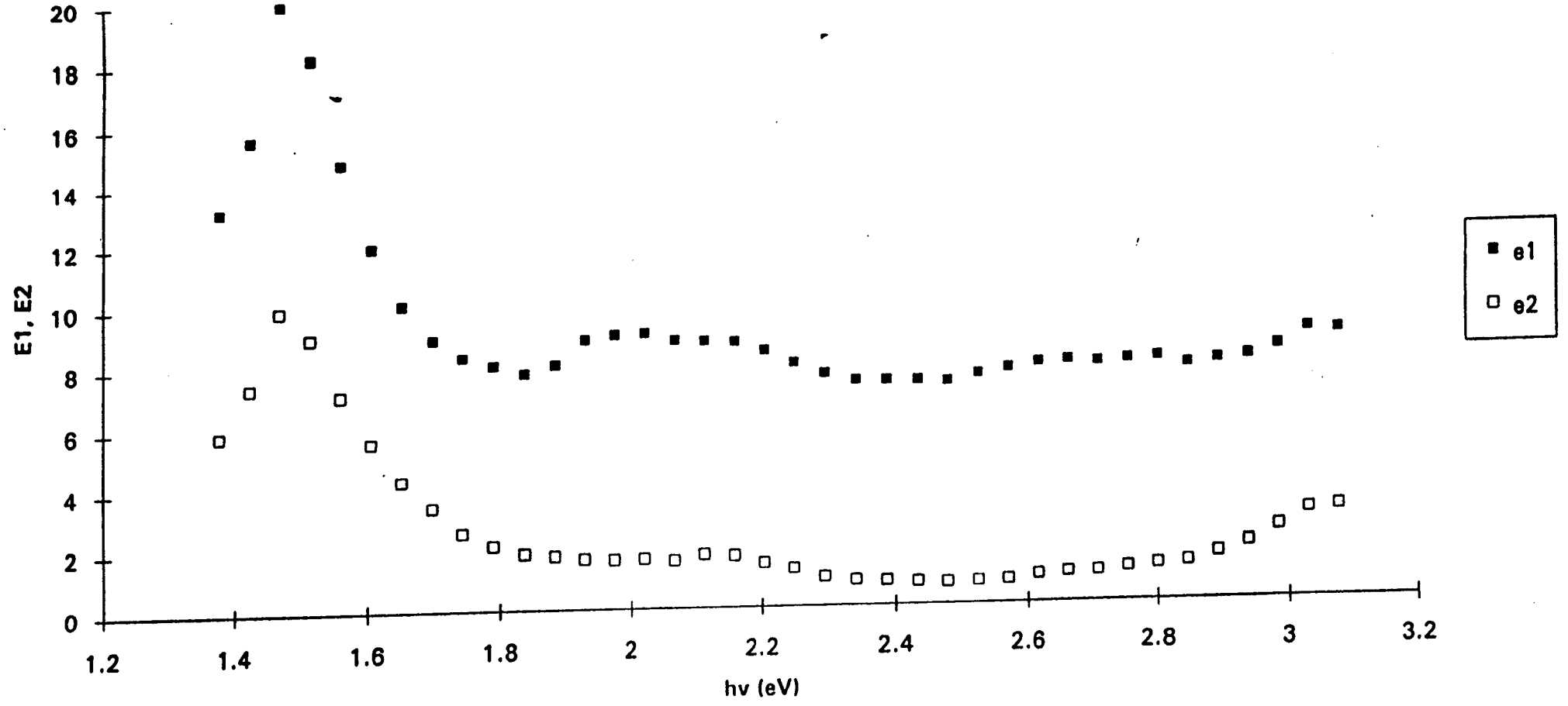

5.42 Real part ε_1 and imaginary part ε_2 of complex dielectric constant for annealed [Gd(pc)(pc*)]

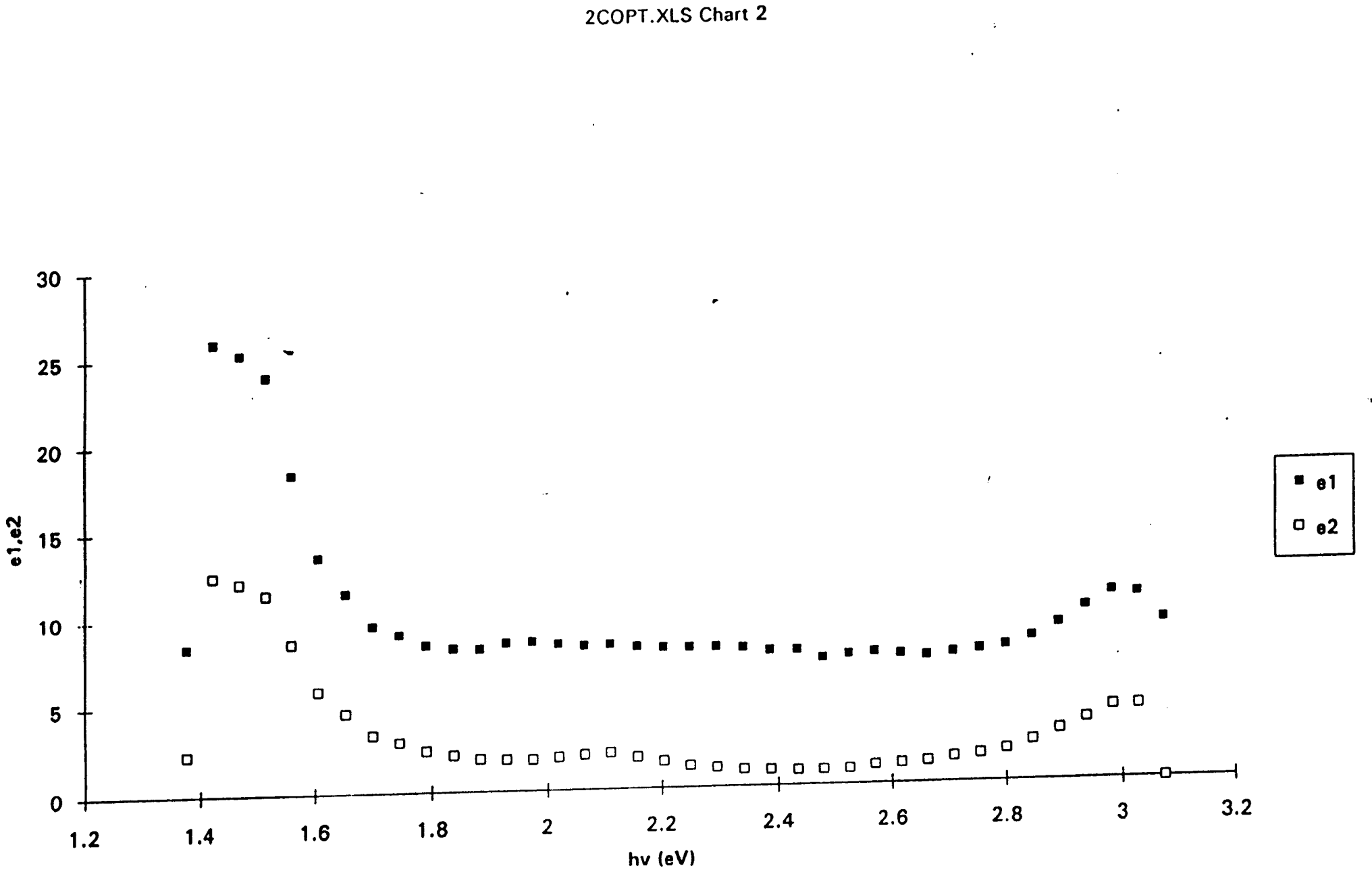

5.43 Real part ε_1 and imaginary part ε_2 of complex dielectric constant for [Gd(pc)(pc*)] voltage cycled to blue

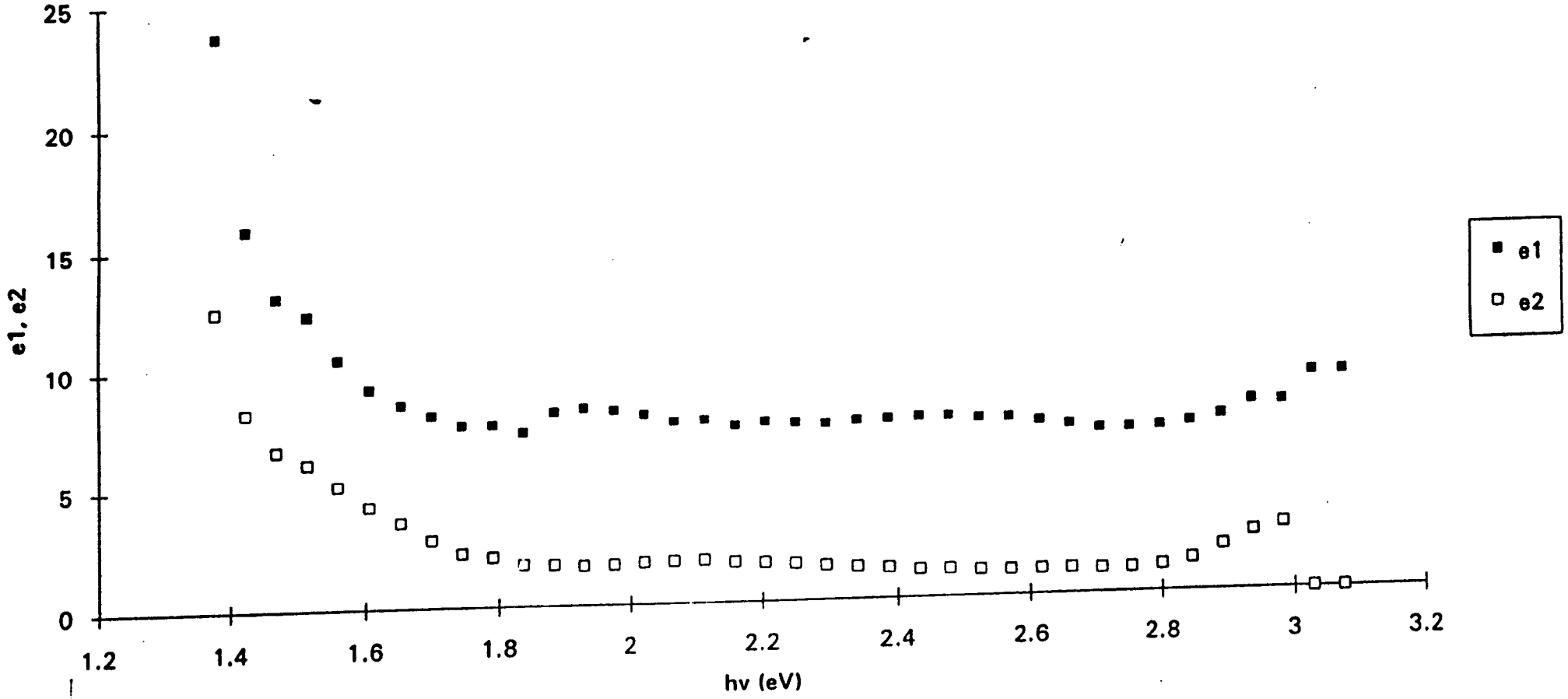

5.44 Real part ε_1 and imaginary part ε_2 of complex dielectric constant for [Gd(pc)(pc*)] voltage cycled to red

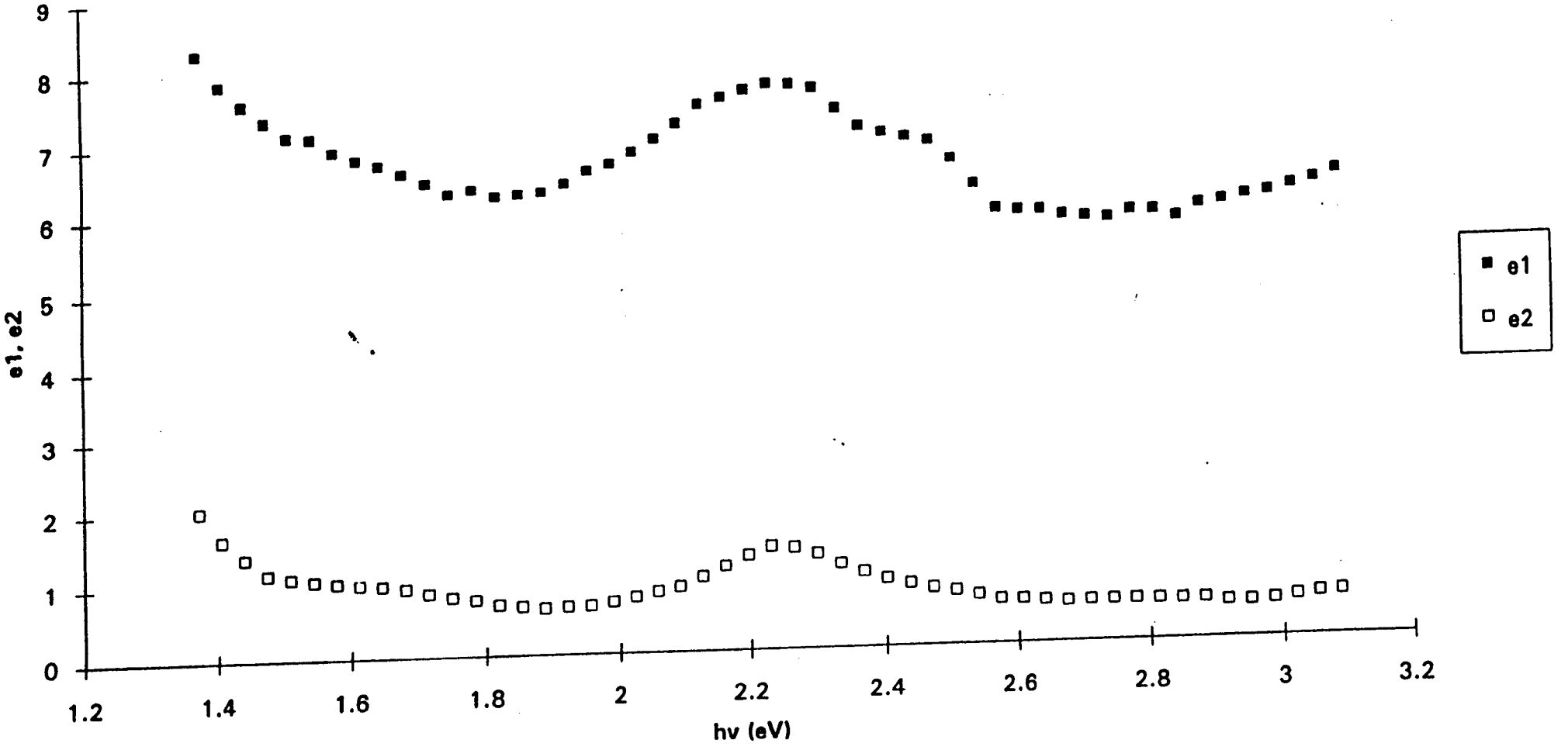

5.45 Real part ε_1 and imaginary part ε_2 of complex dielectric constant for untreated [Tm(pc)(pc*)]

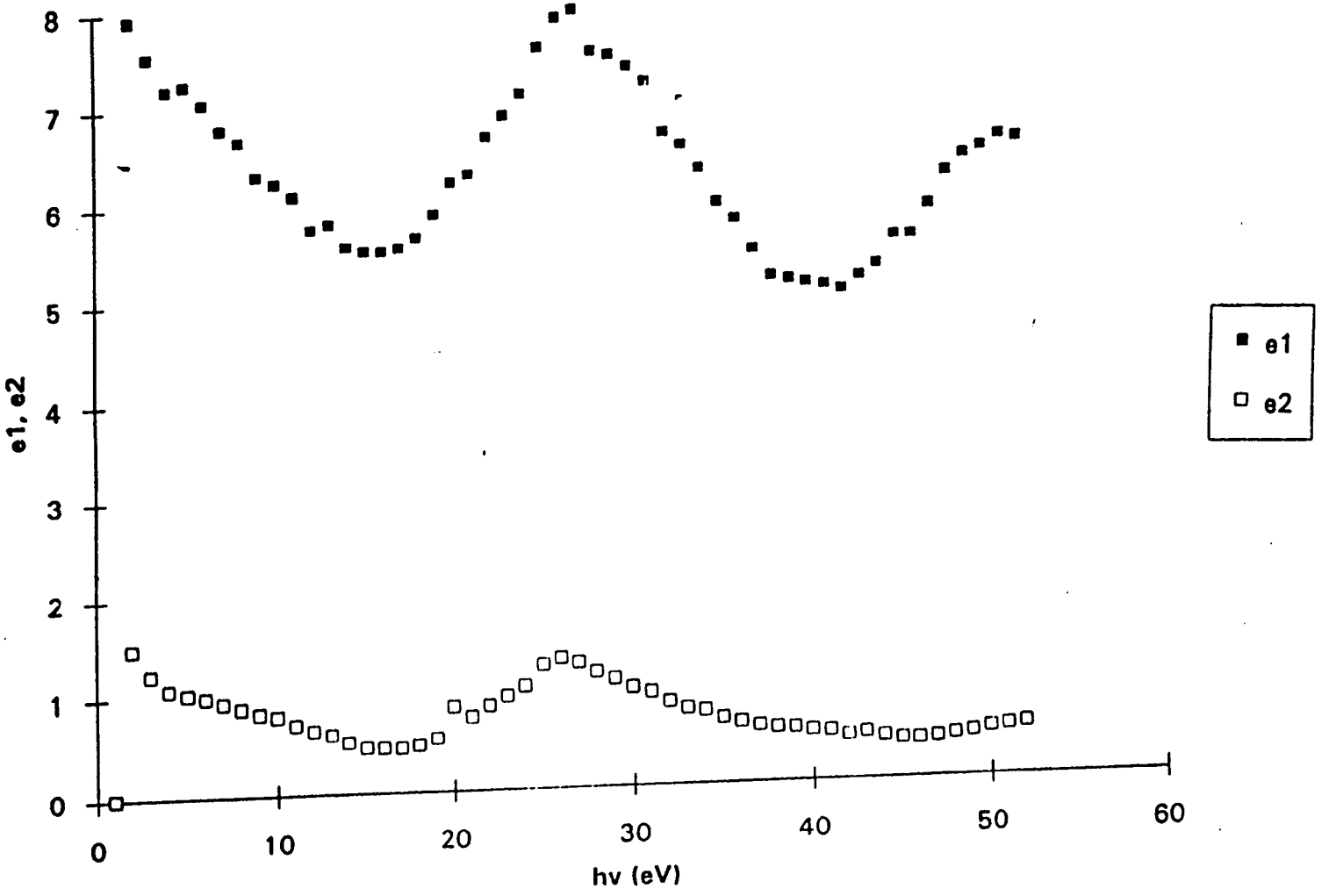

5.46 Real part ε_1 and imaginary part ε_2 of complex dielectric constant for annealed [Tm(pc)(pc*)]

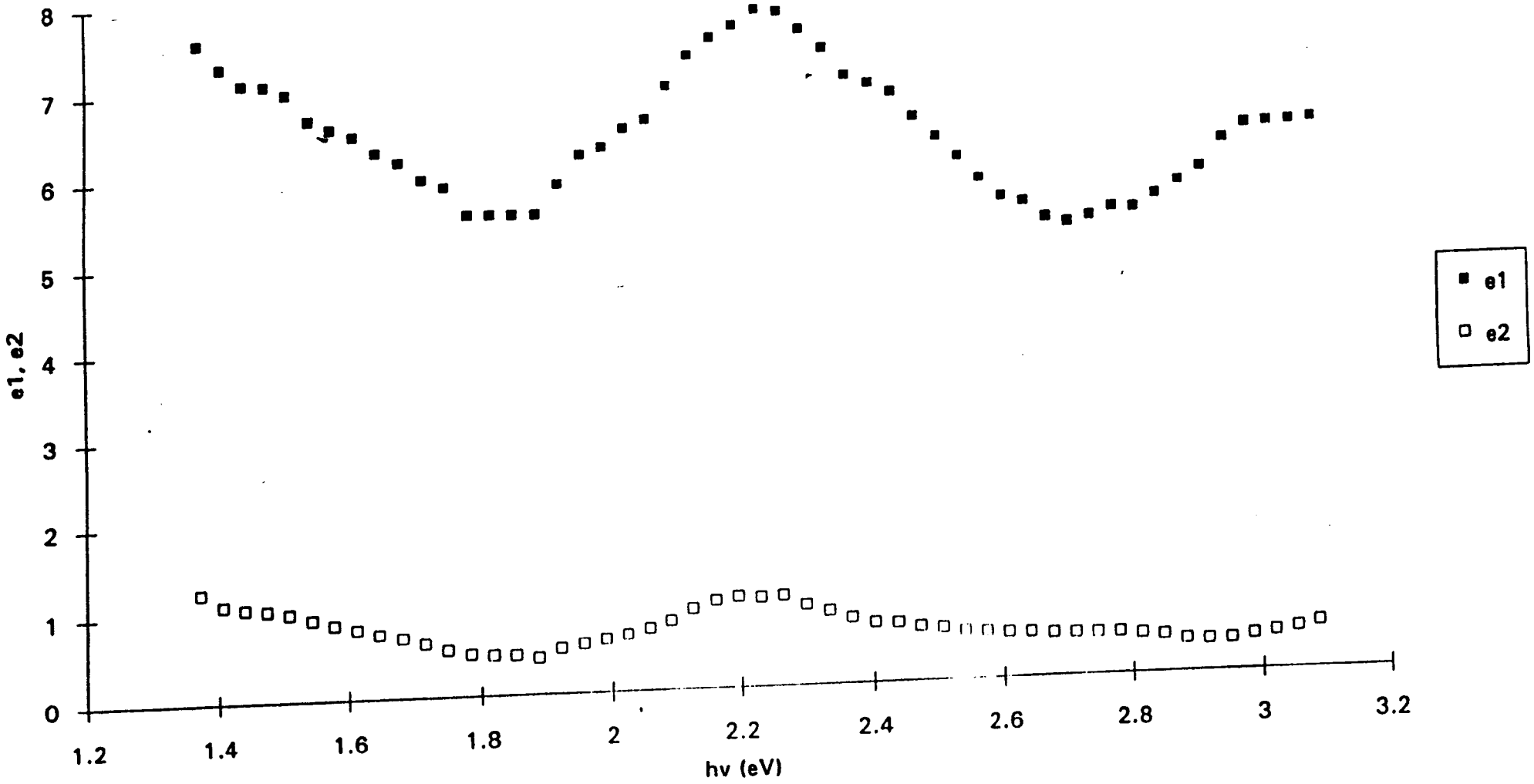

5.47 Real part ε_1 and imaginary part ε_2 of complex dielectric constant for [Tm(pc)(pc*)] voltage cycled to blue

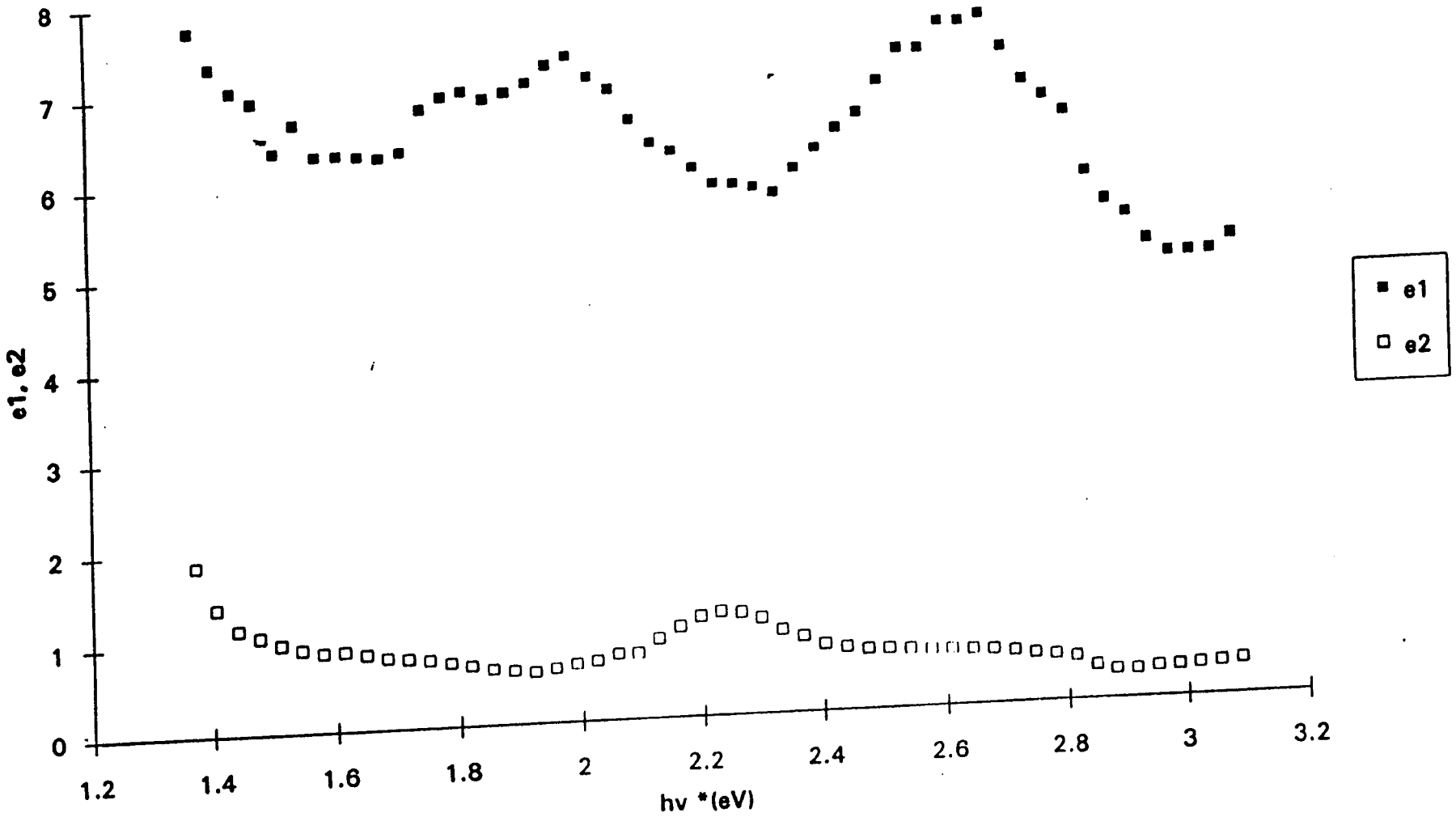

5.48 Real part ε_1 and imaginary part ε_2 of complex dielectric constant for [Tm(pc)(pc*)] voltage cycled to red

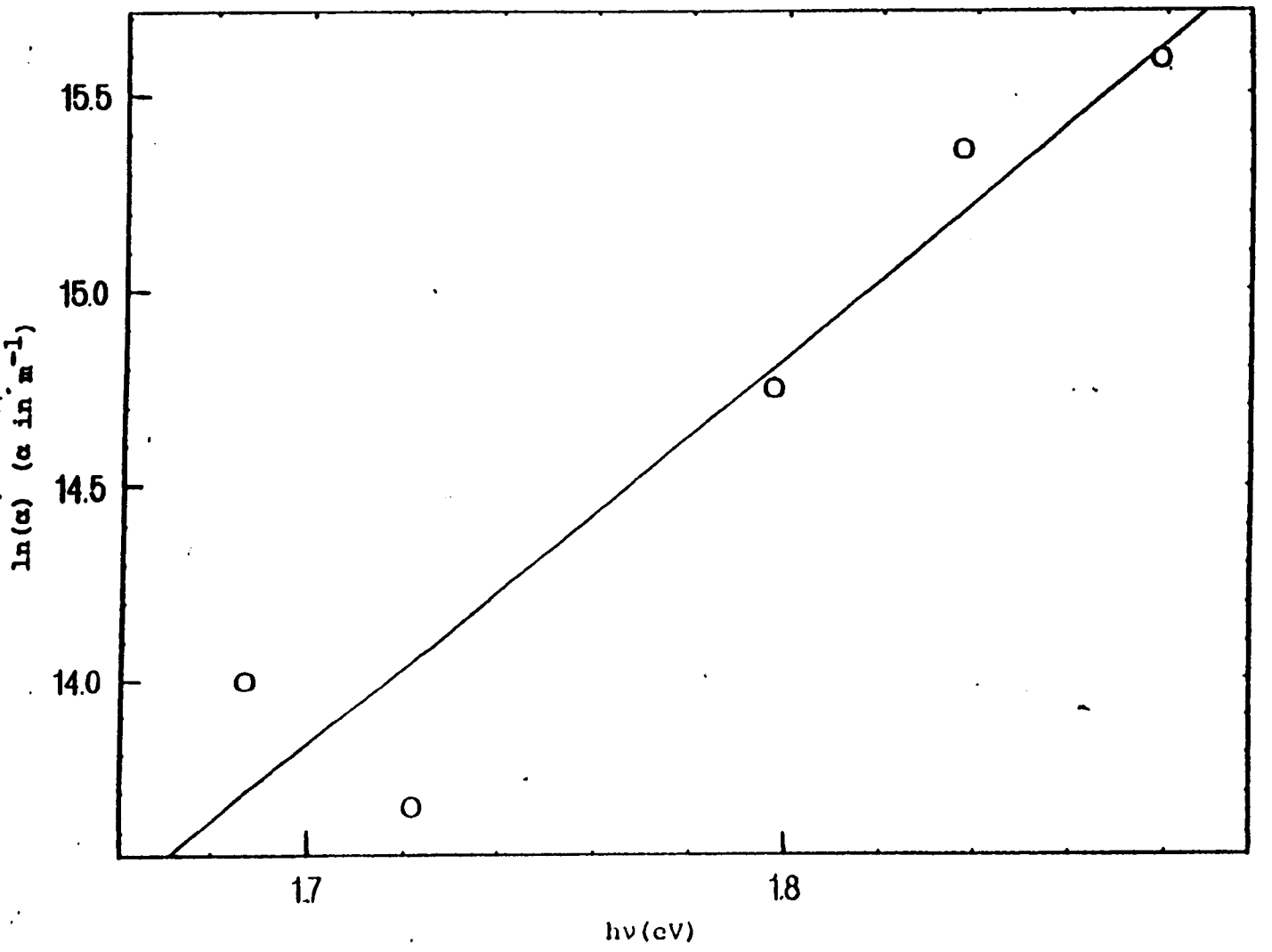

5.49 Ln (a) vs. hv for ur:treated [HF(pc)(pc*)]

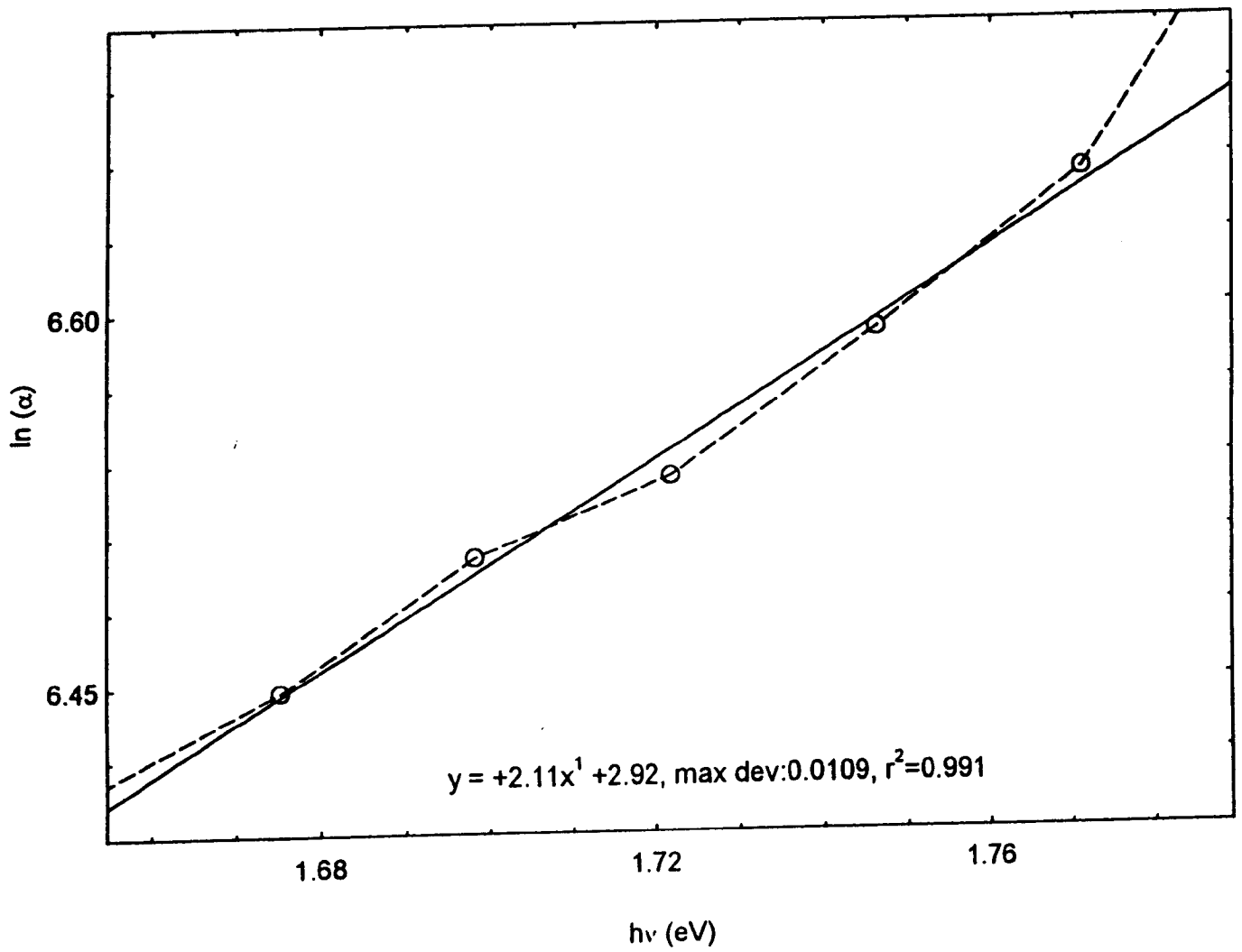

5.50 Ln (a) vs. hv for annealed [HF(pc)(pc*)]

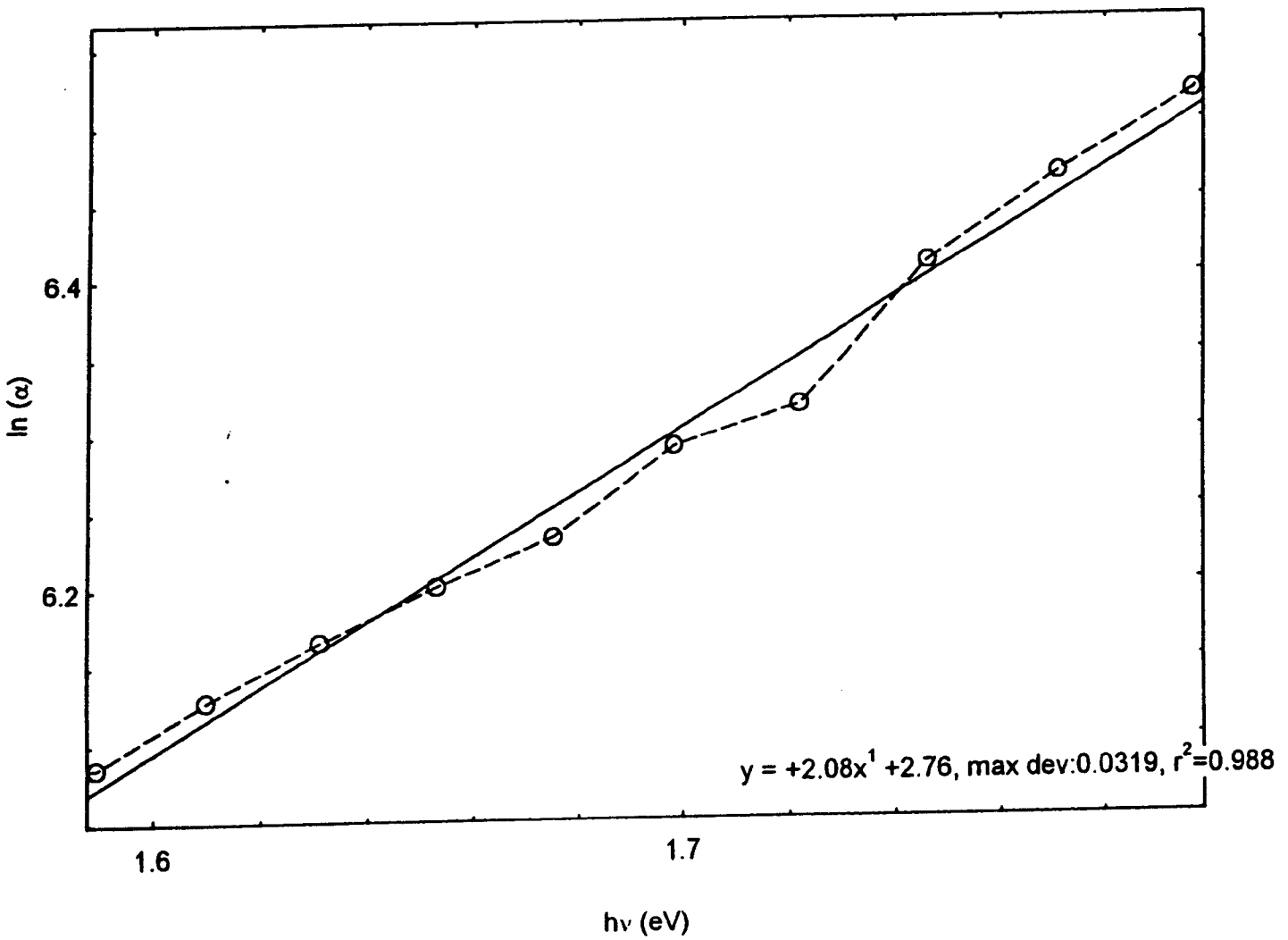

5.51 Ln (a) vs. hv for [HF(pc)(pc*)] voltage cycled to blue

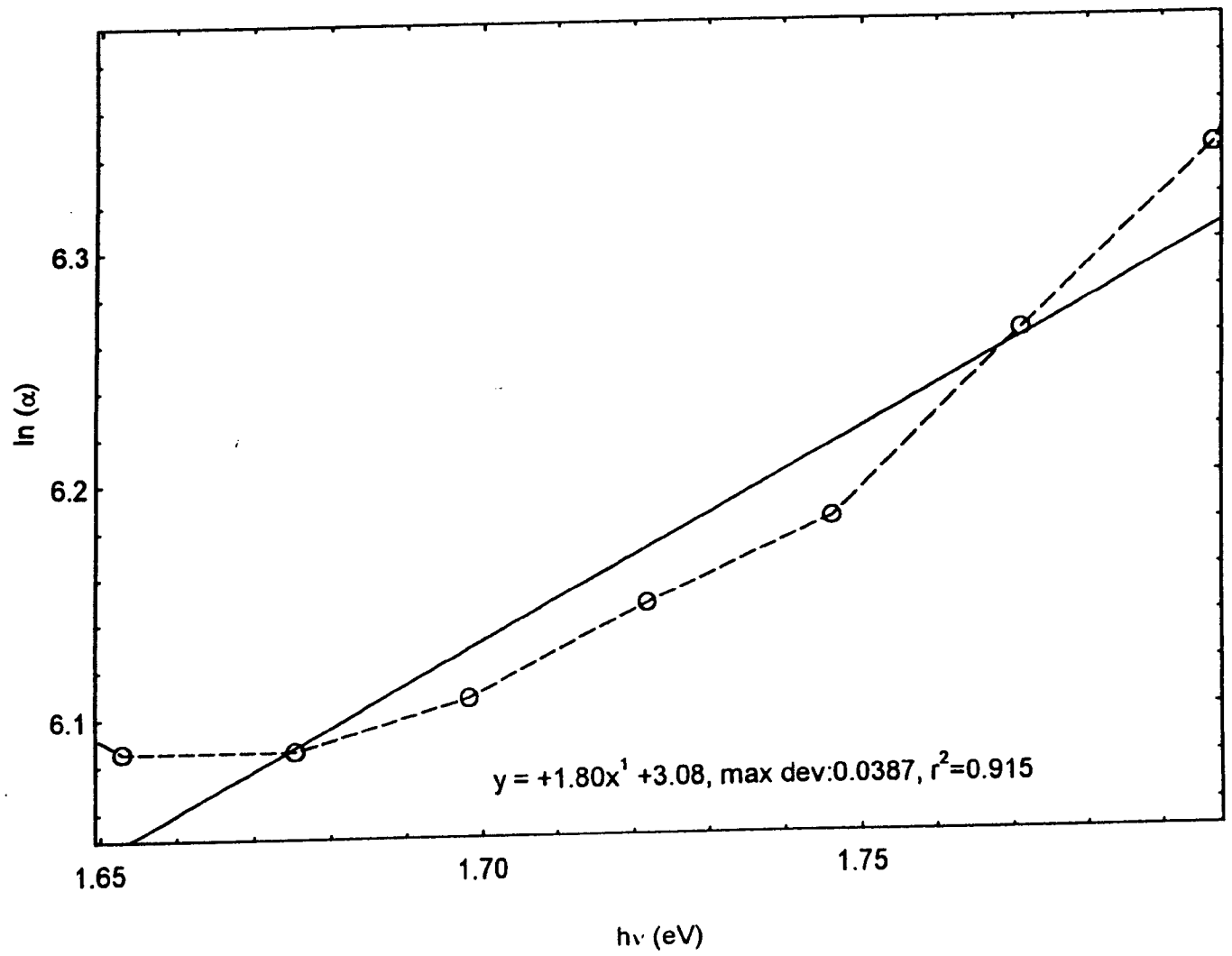

5.52 Ln (a) vs. hv for [HF(pc)(pc*)] voltage cycled to red

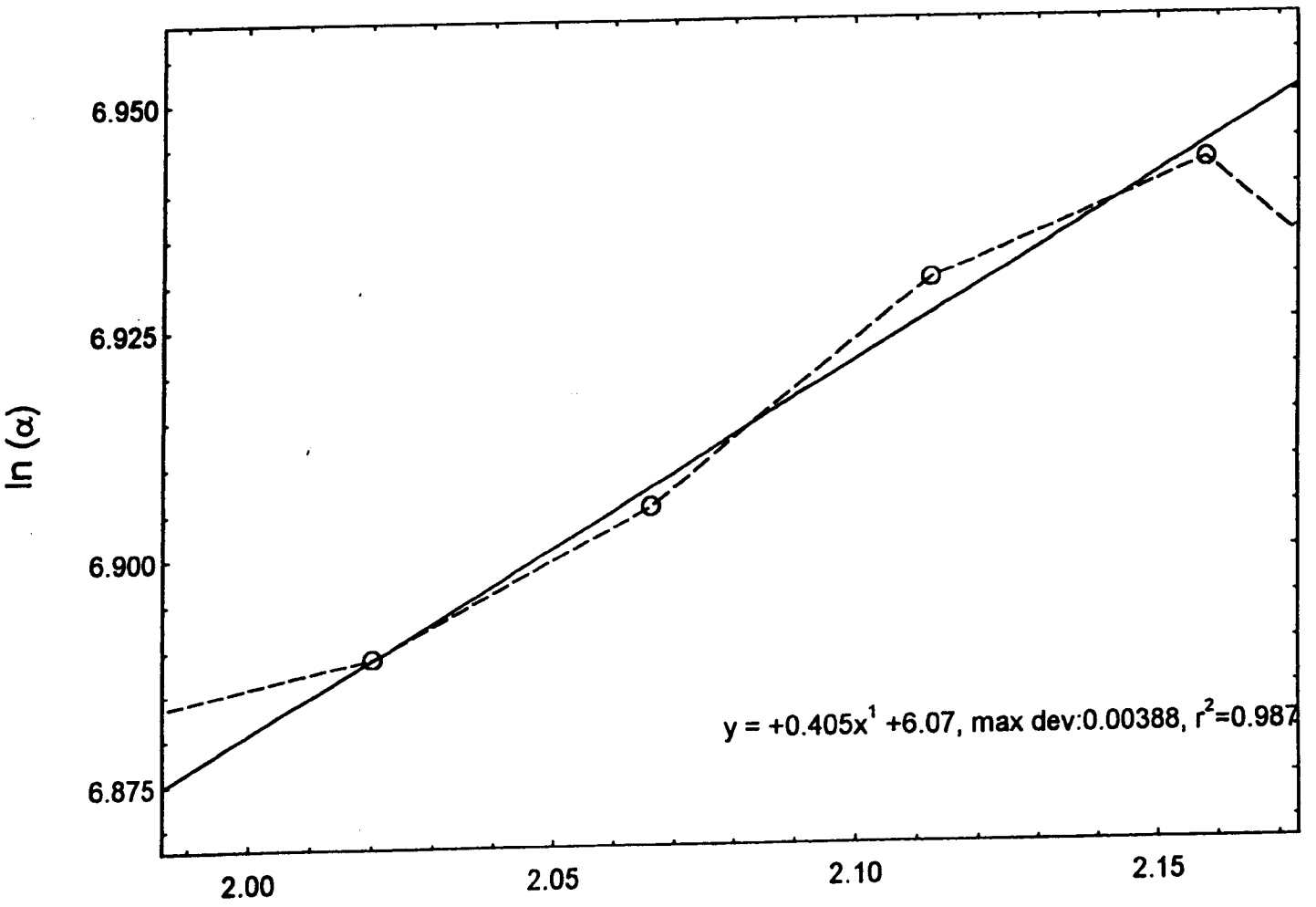

5.53 Ln (a) vs. hv for untreated [Gd(pc)(pc*)]

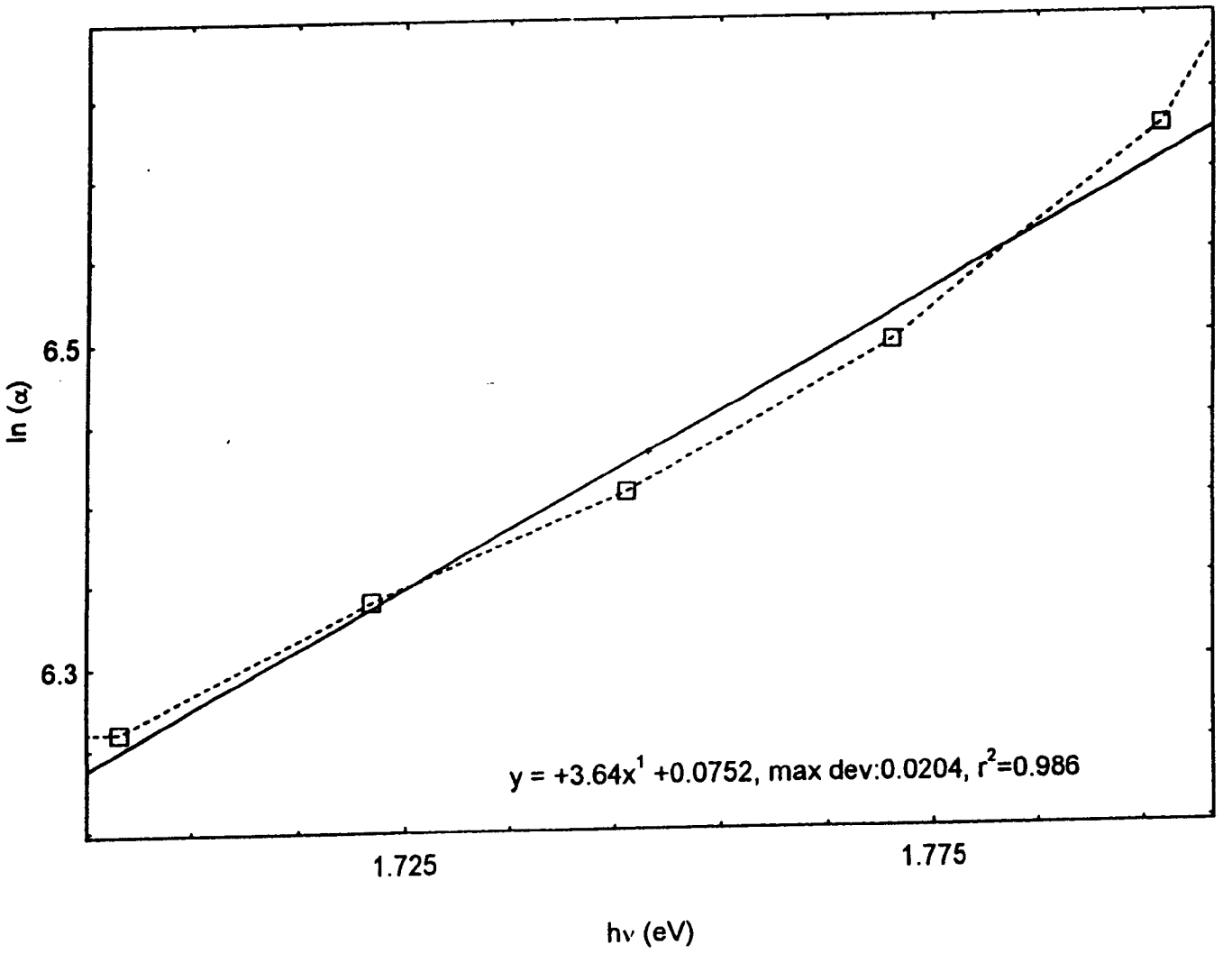

5.54 Ln (a) vs. hv for annealed [Gd(pc)(pc*)]

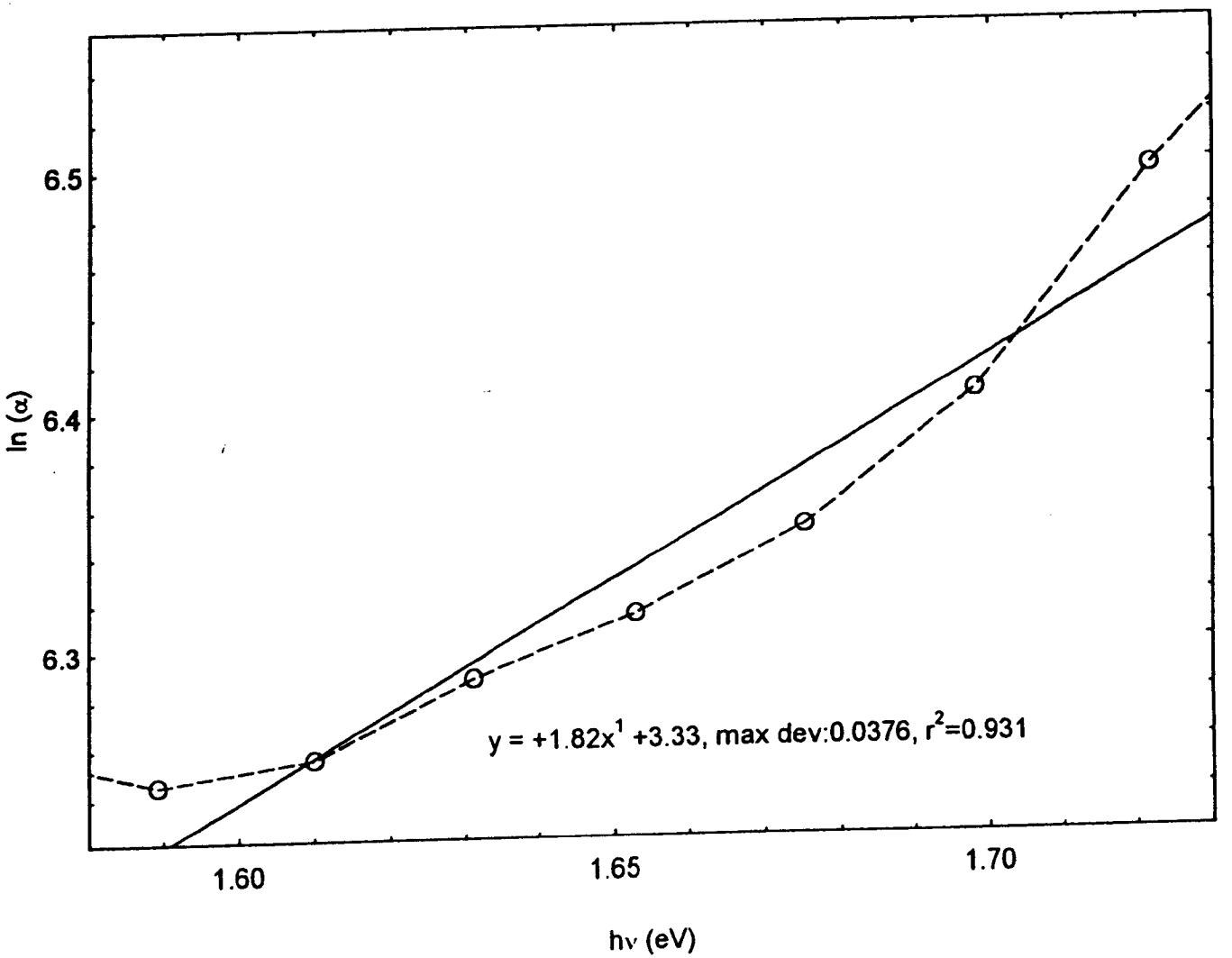

5.55 Ln (a) vs. hv for [Gd(pc)(pc*)] voltage cycled to blue

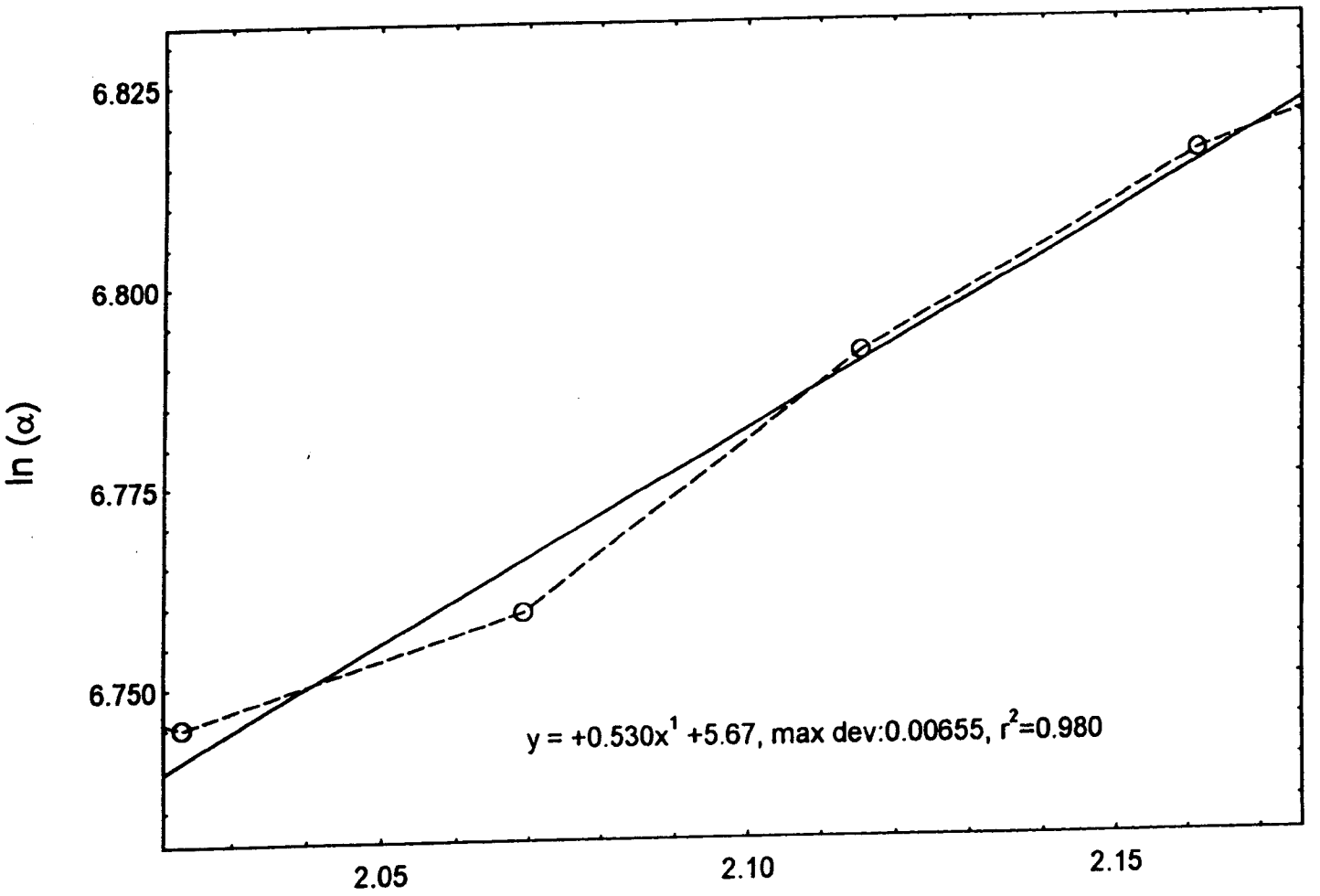

5.56 Ln (a) vs. hv for [Gd(pc)(pc*)] voltage cycled to red

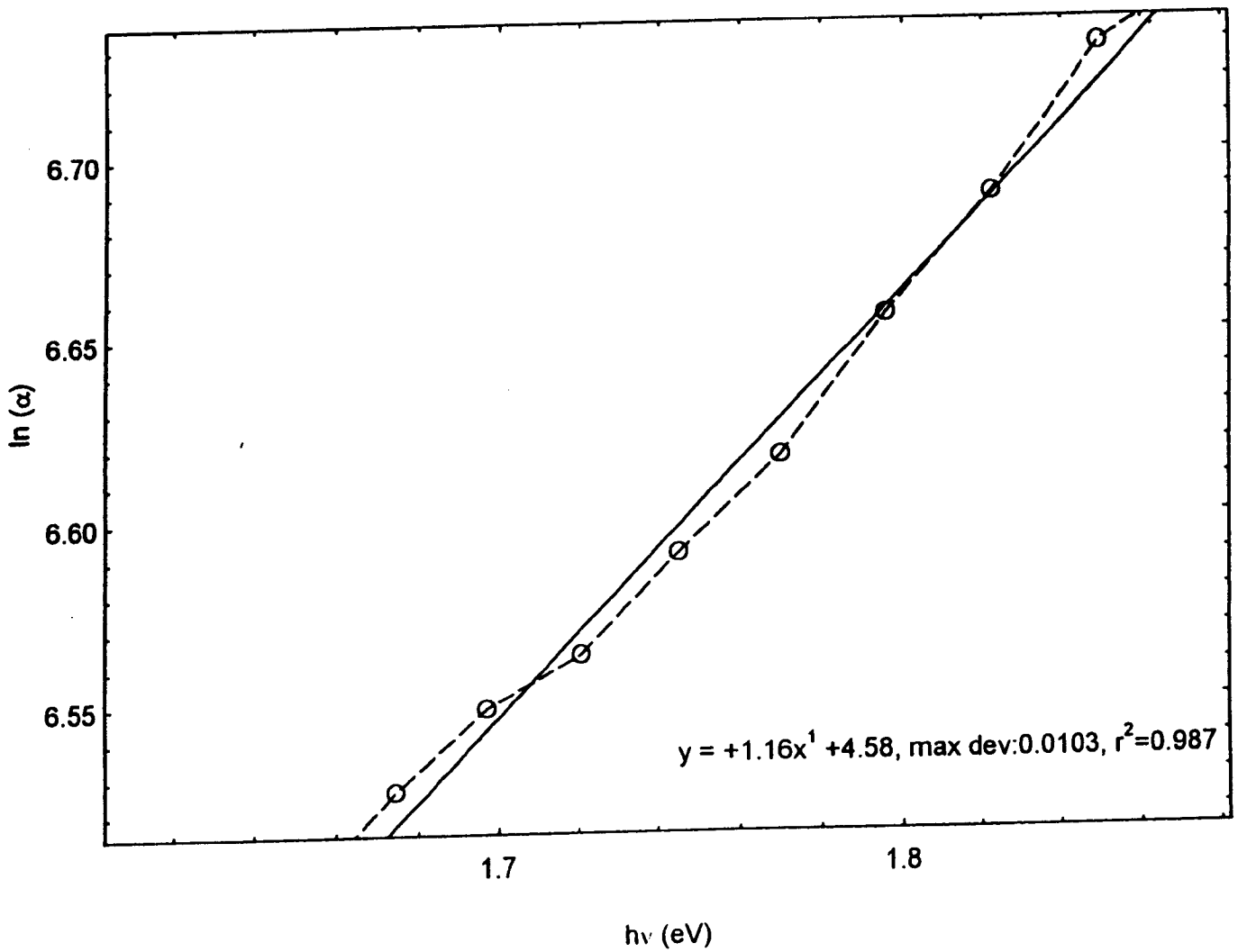

5.57 Ln (a) vs. hv for untreated [Tm(pc)(pc*)]

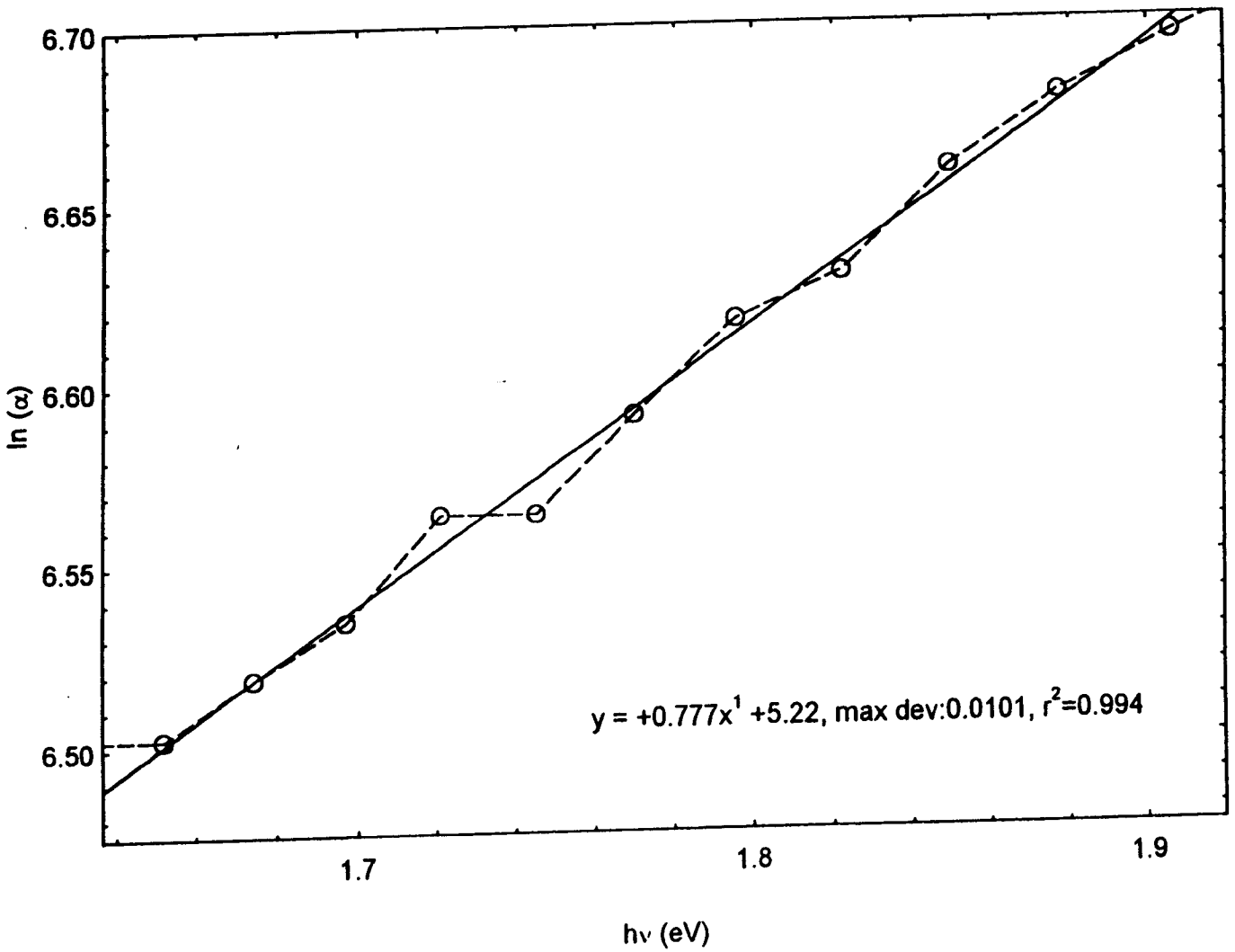

5.58 Ln (a) vs. hv for annealed [Tm(pc)(pc*)]

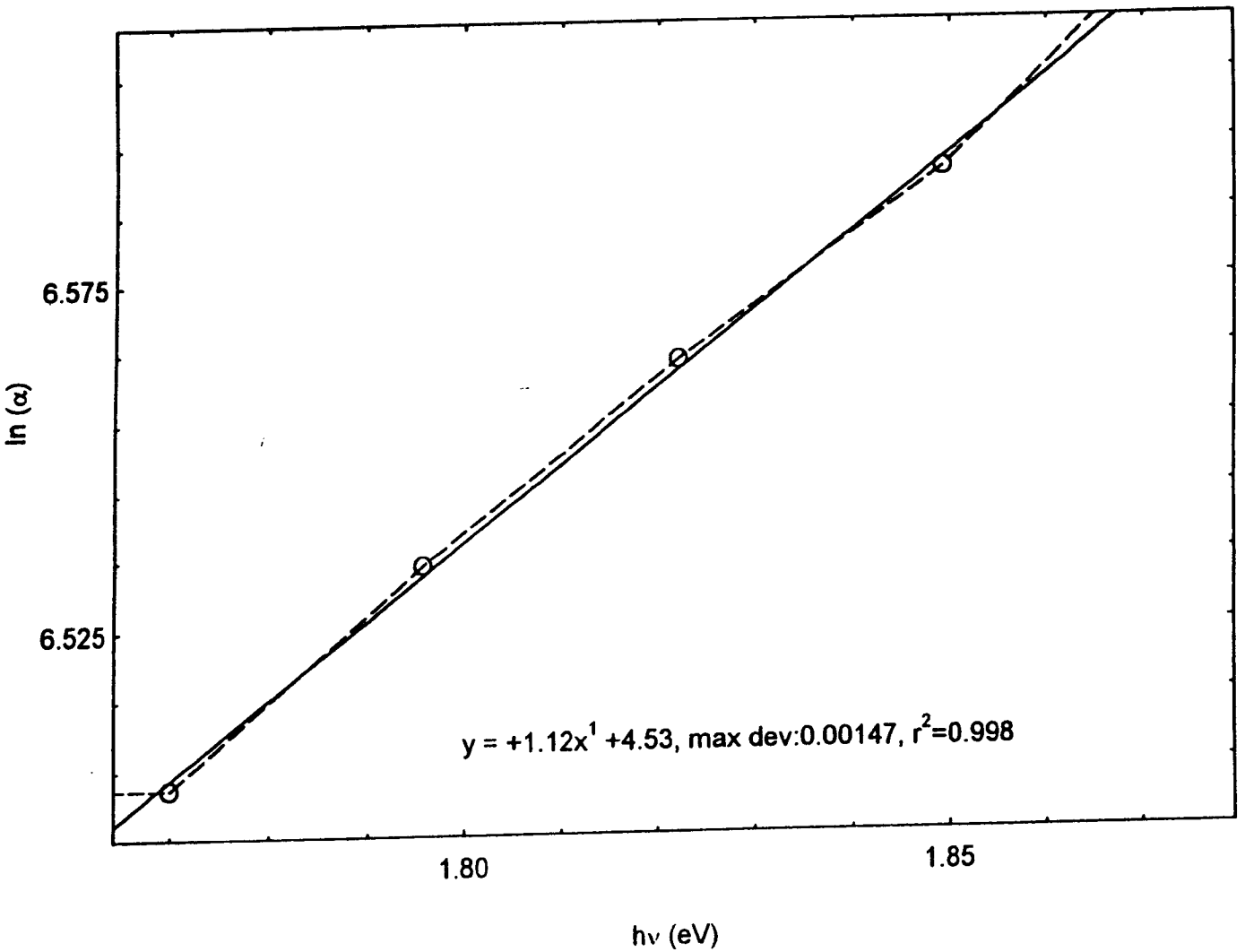

5.59 Ln (a) vs. hv for [Tm(pc)(pc*)] voltage cycled to blue

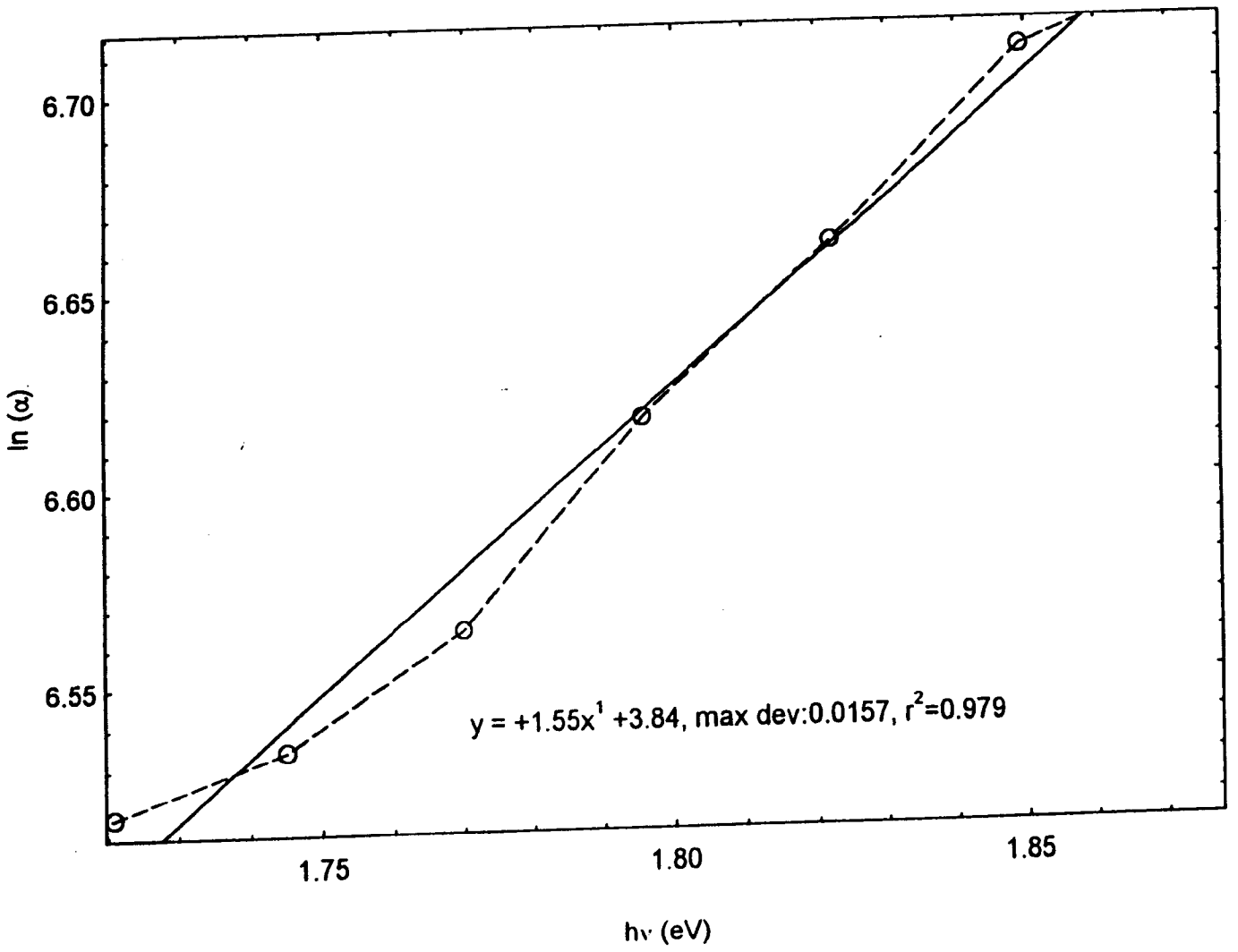

5.60 Ln (a) vs. hv for [Tm(pc)(pc*)] voltage cycled to red

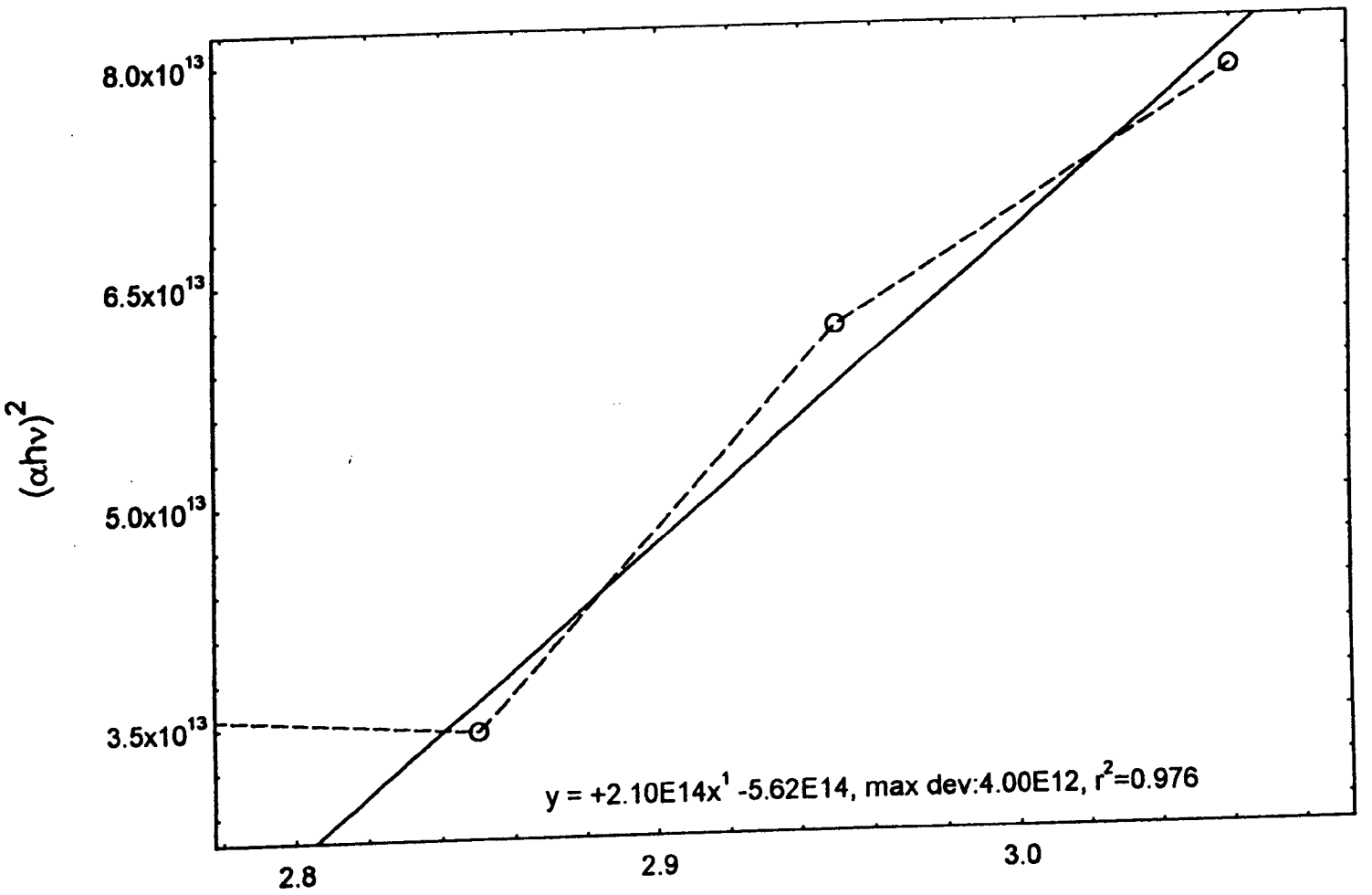

5.61 $(\alpha h\nu)^2$ vs. hv for untreated [HF(pc)(pc*)]

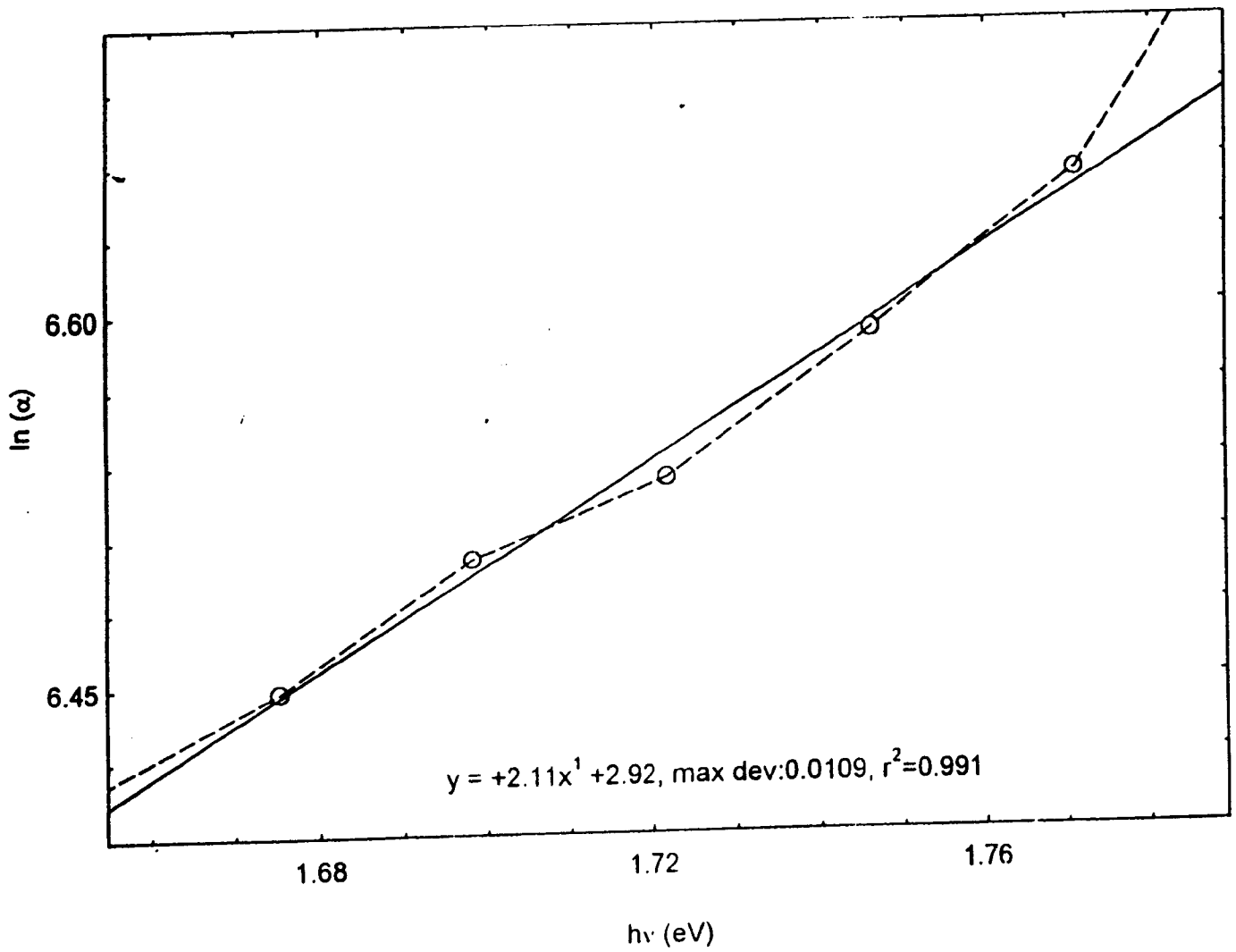

5.62 $(\alpha h\nu)^2$ vs. hν for annealed [HF(pc)(pc*)]

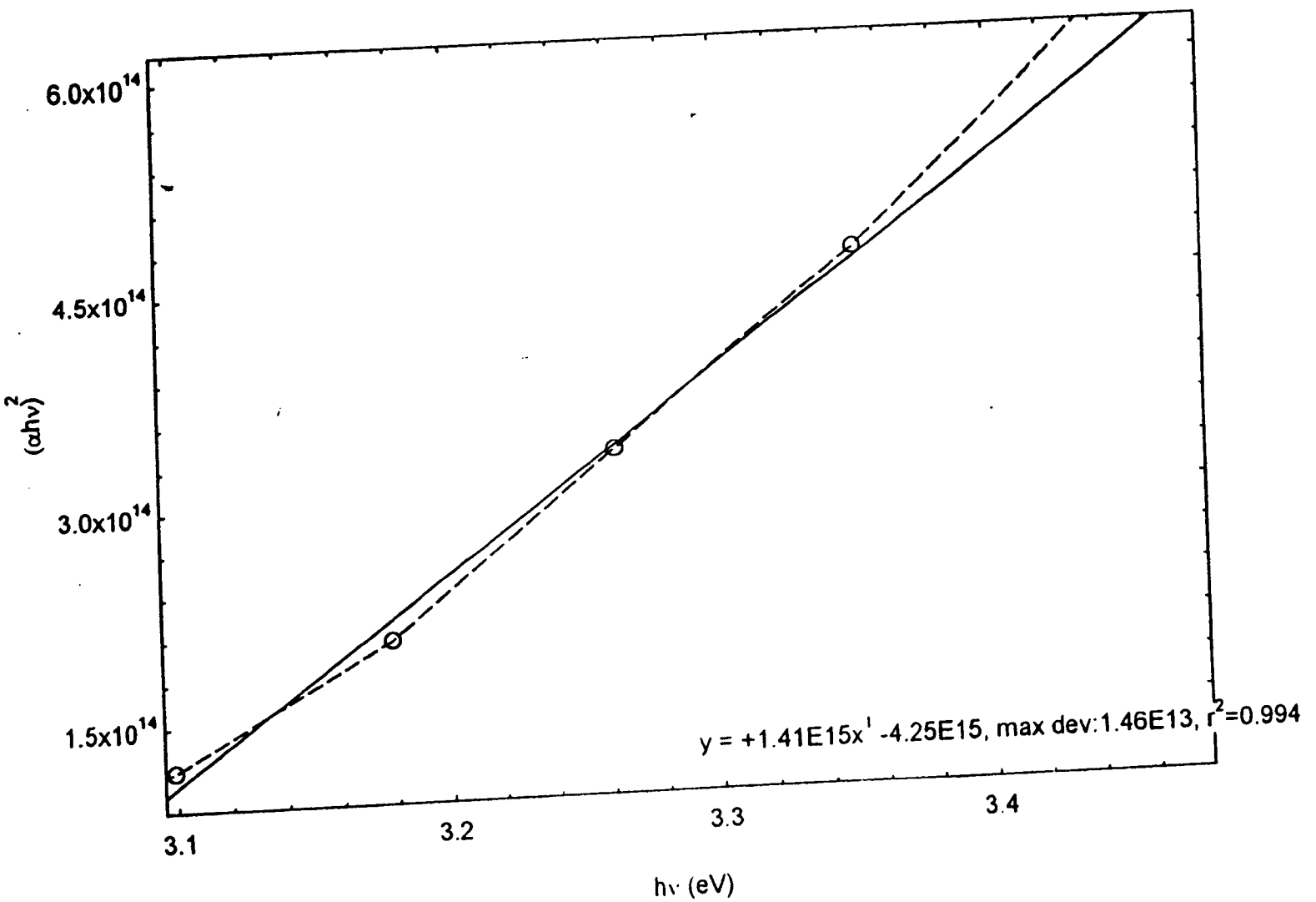

5.63 $(\alpha h\nu)^2$ vs. hv for [HF(pc)(pc*)] voltage cycled to blue

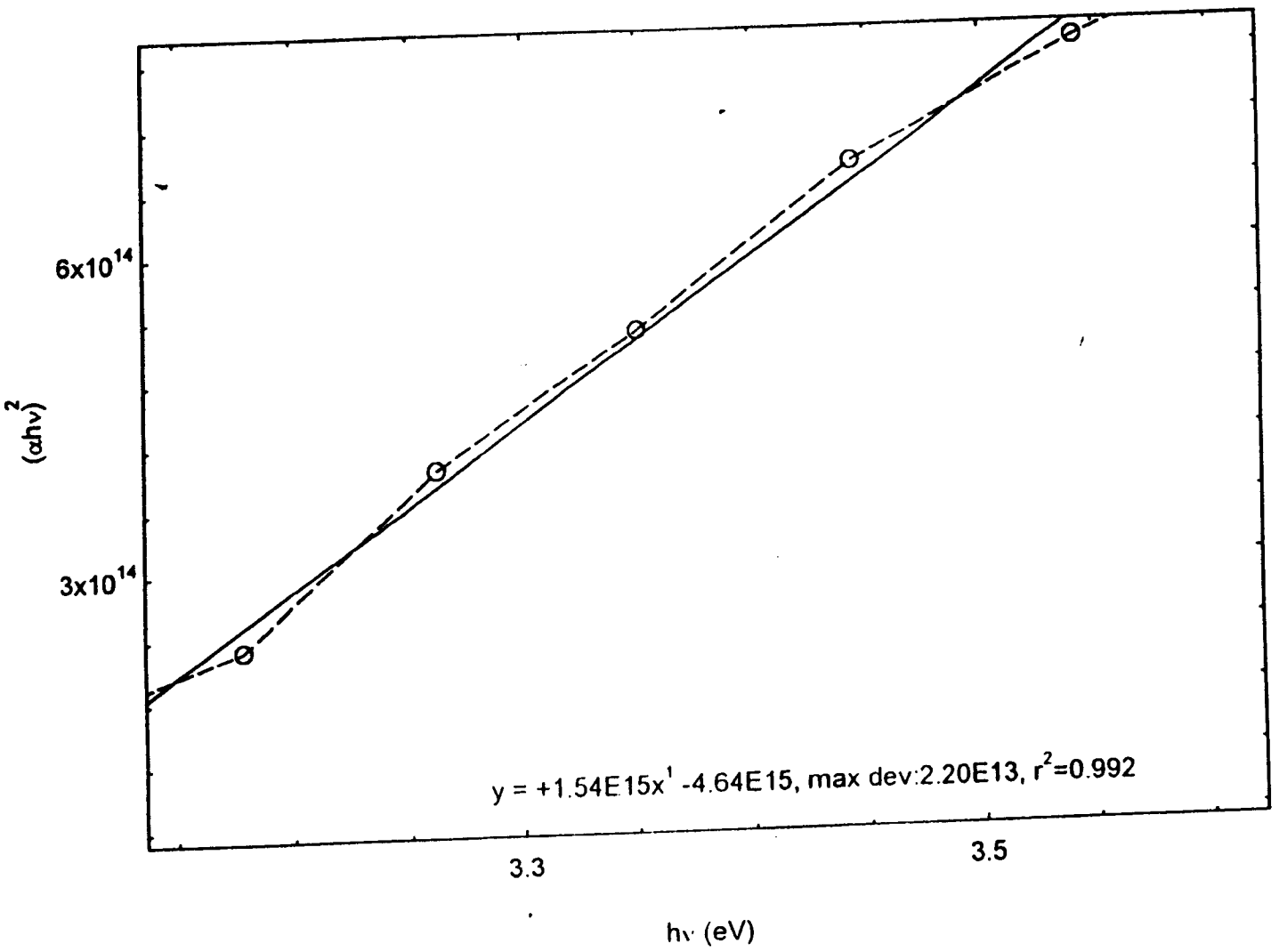

5.64 $(\alpha h\nu)^2$ vs. hv for [HF(pc)(pc*)] voltage cycled to red

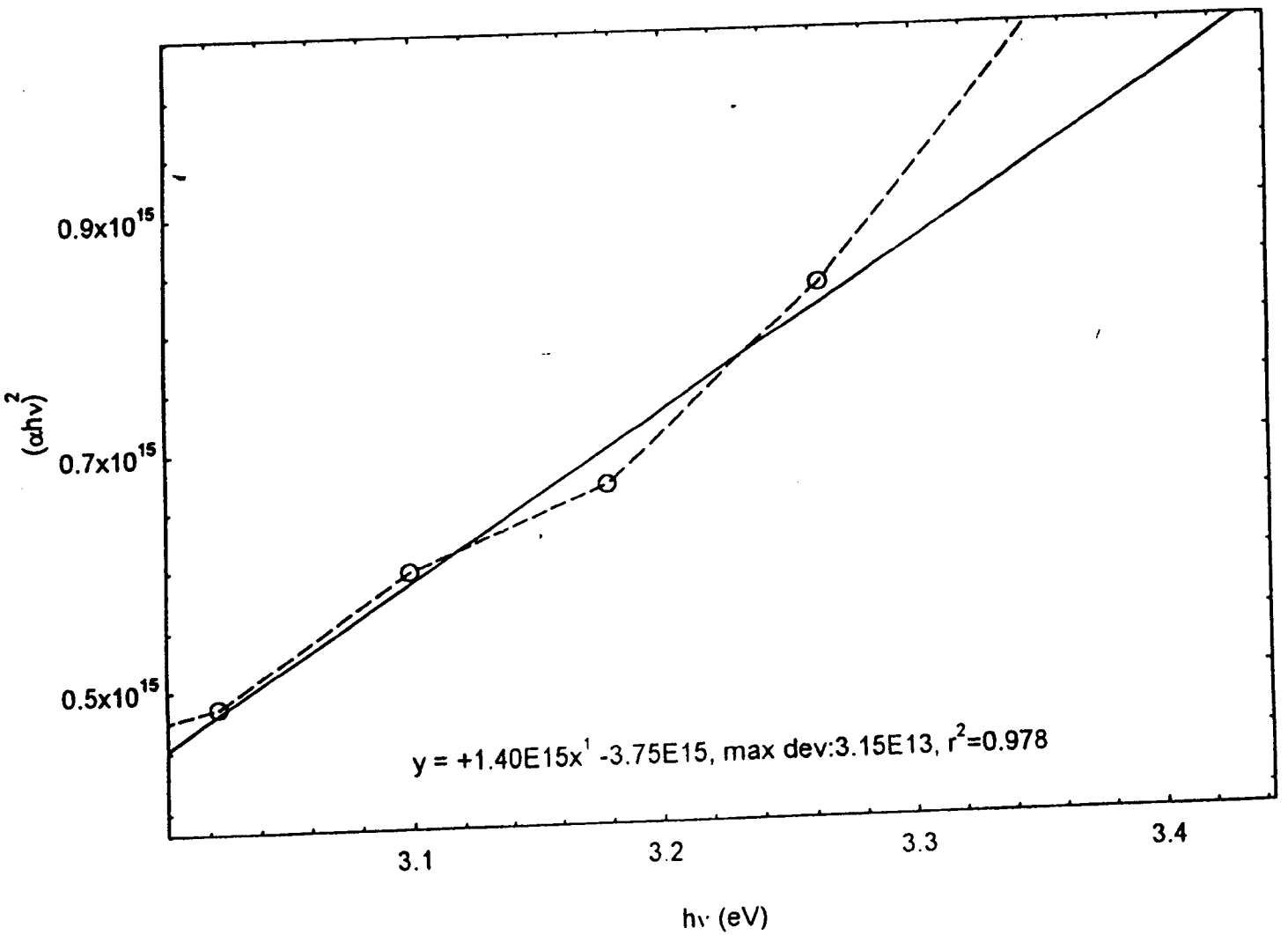

5.65 $(\alpha h\nu)^2$ vs. hν for untreated [Cd(pc)(pc*)]

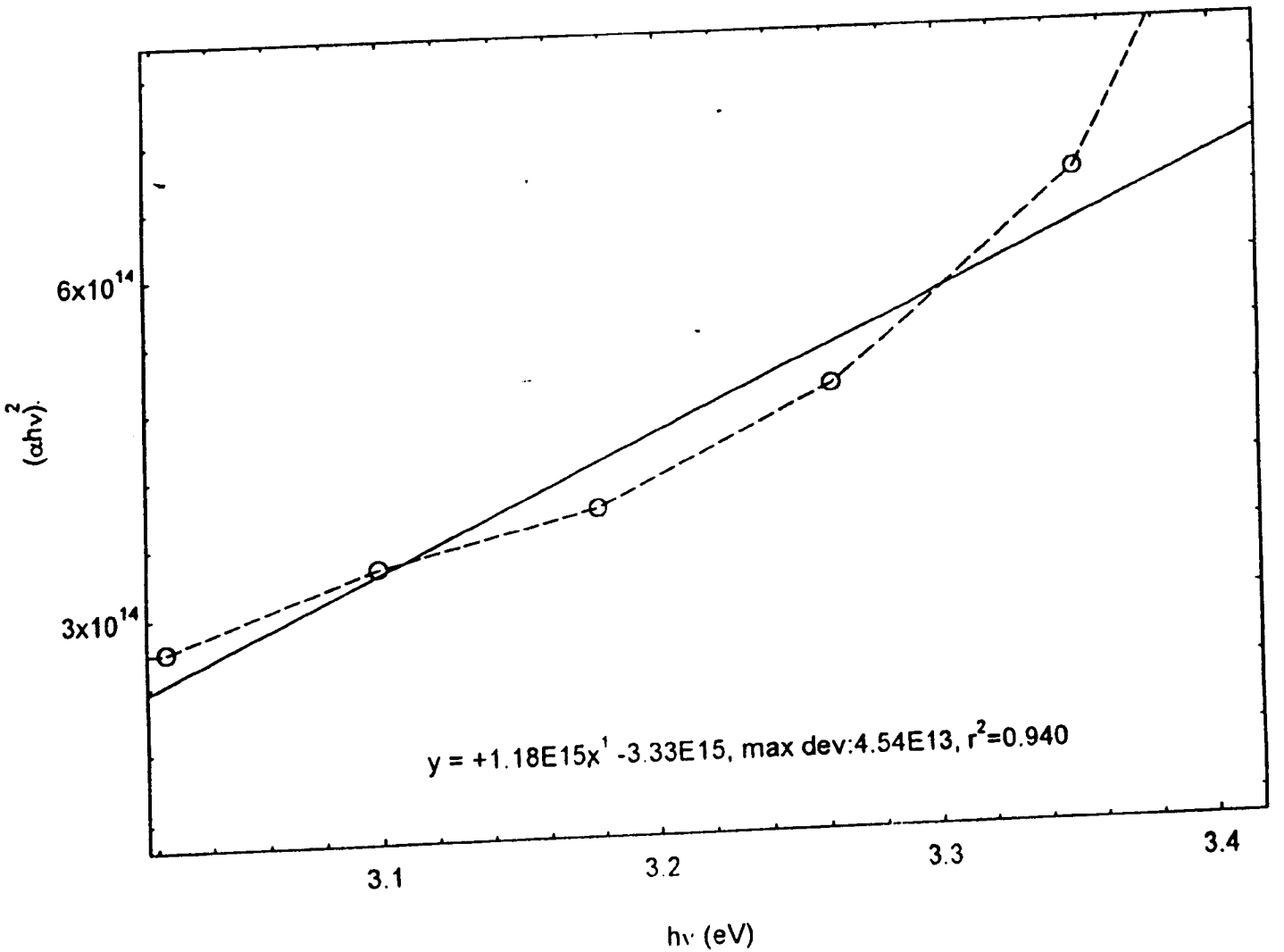

5.66 $(\alpha h\nu)^2$ vs. hv for annealed [Gd(pc)(pc*)]

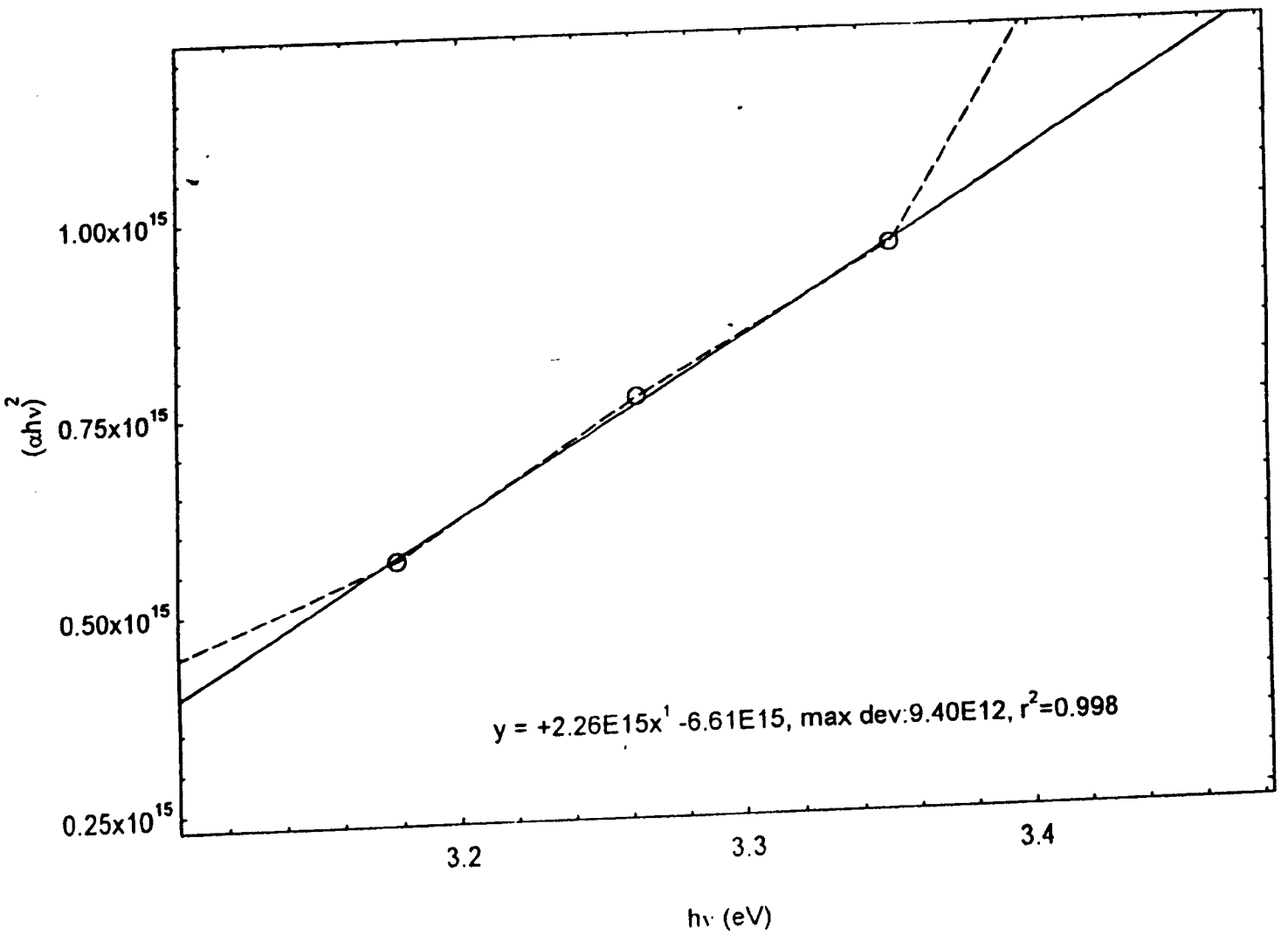

5.67 $(\alpha h\nu)^2$ vs. hv for [Gd(pc)(pc*)] voltage cycled to blue

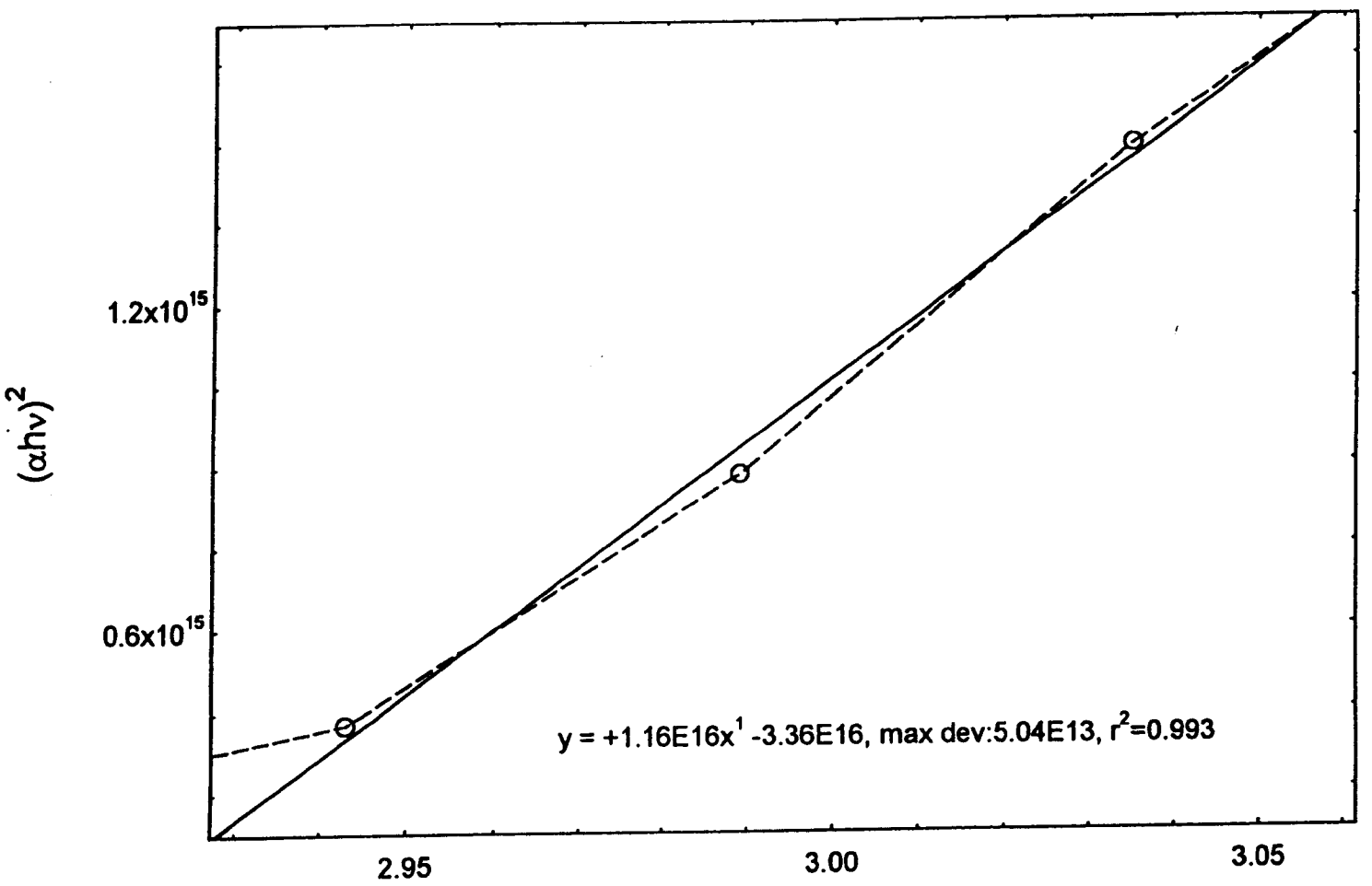

5.68 $(\alpha h\nu)^2$ vs. hv for [Gd(pc)(pc*)] voltage cycled to red

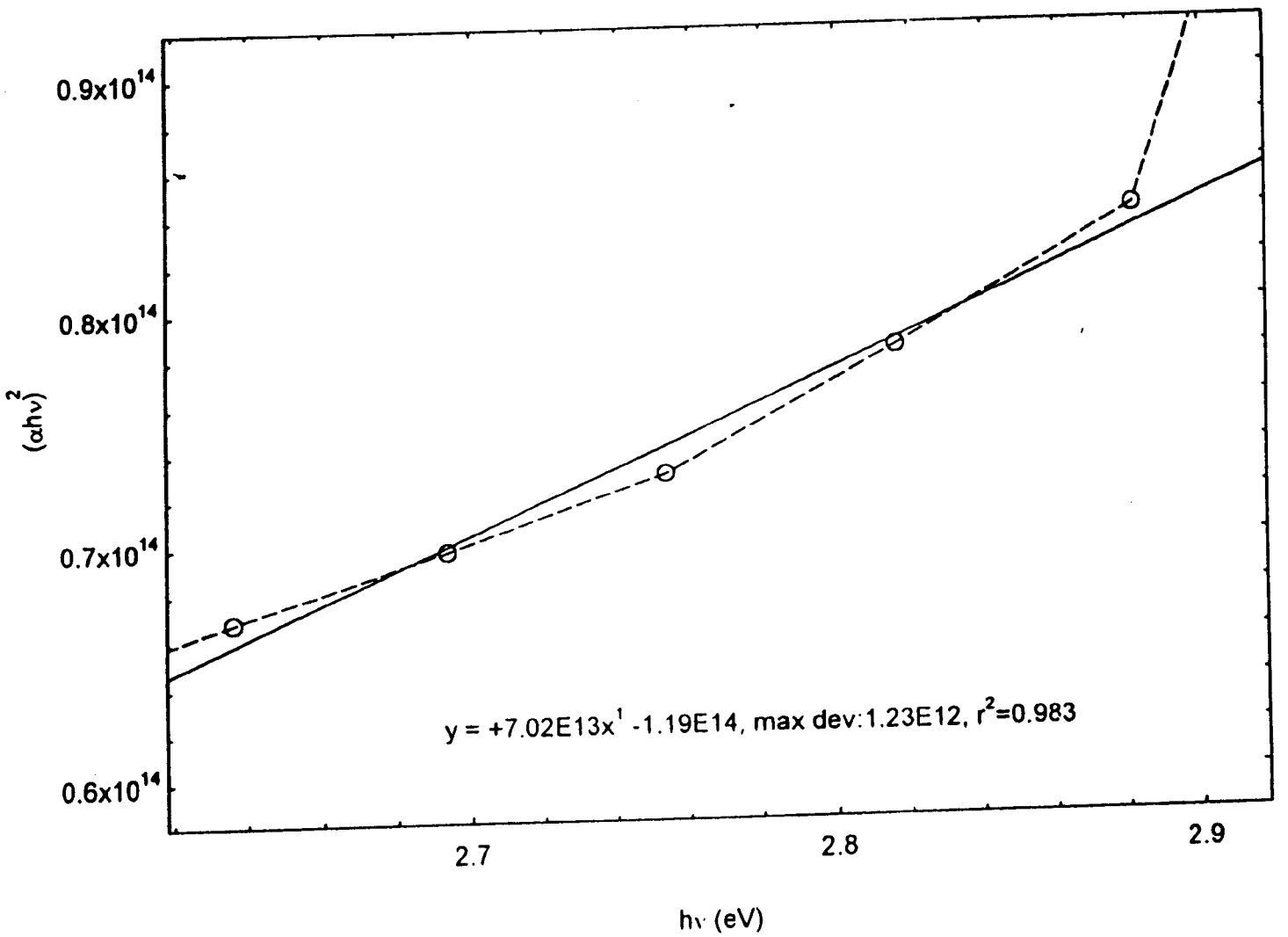

5.69 $(\alpha h\nu)^2$ vs. hv for untreated [Tm(pc)(pc*)]

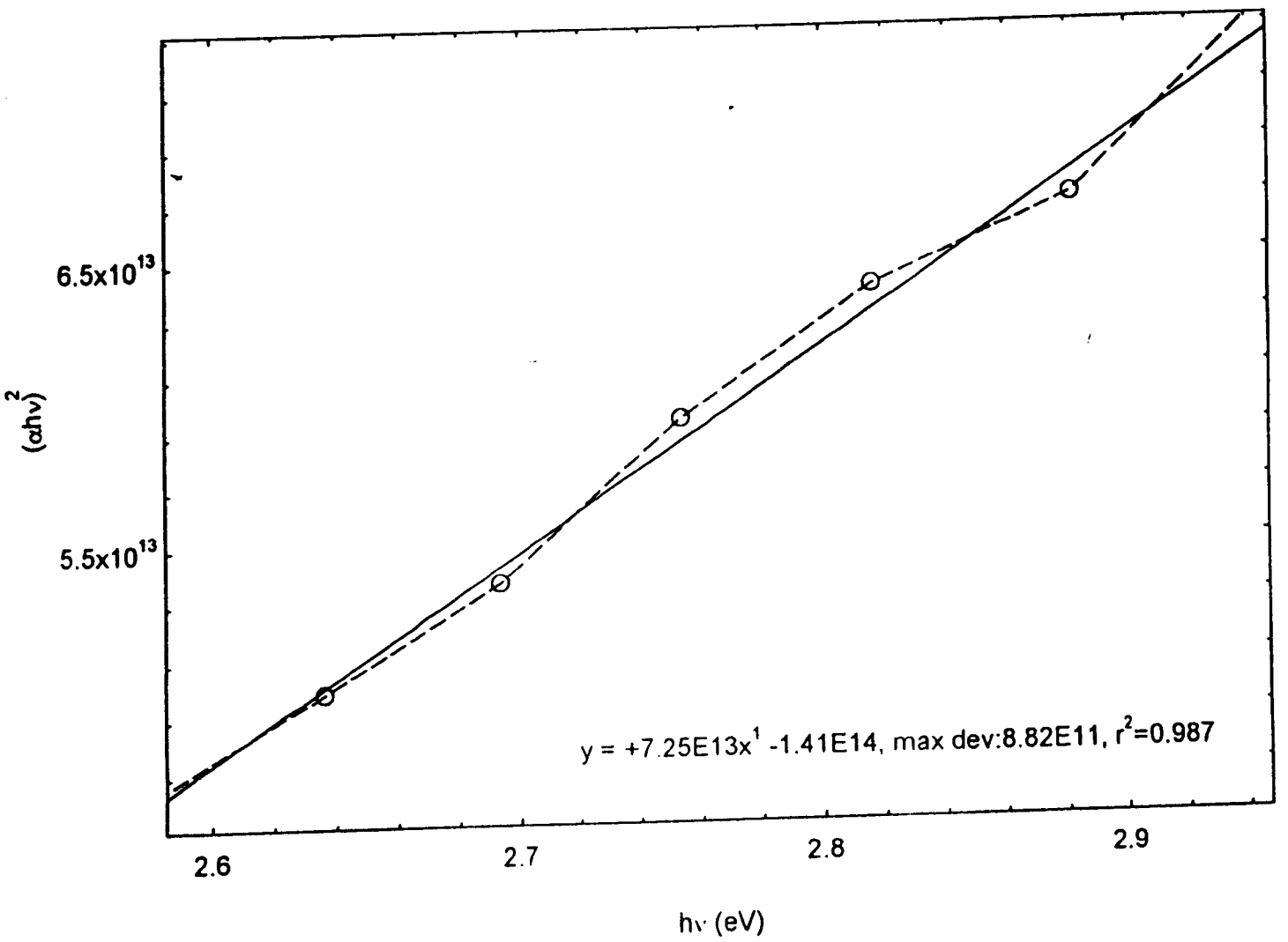

5.70 $(\alpha h\nu)^2$ vs. hν for annealed [Tm(pc)(pc*)]

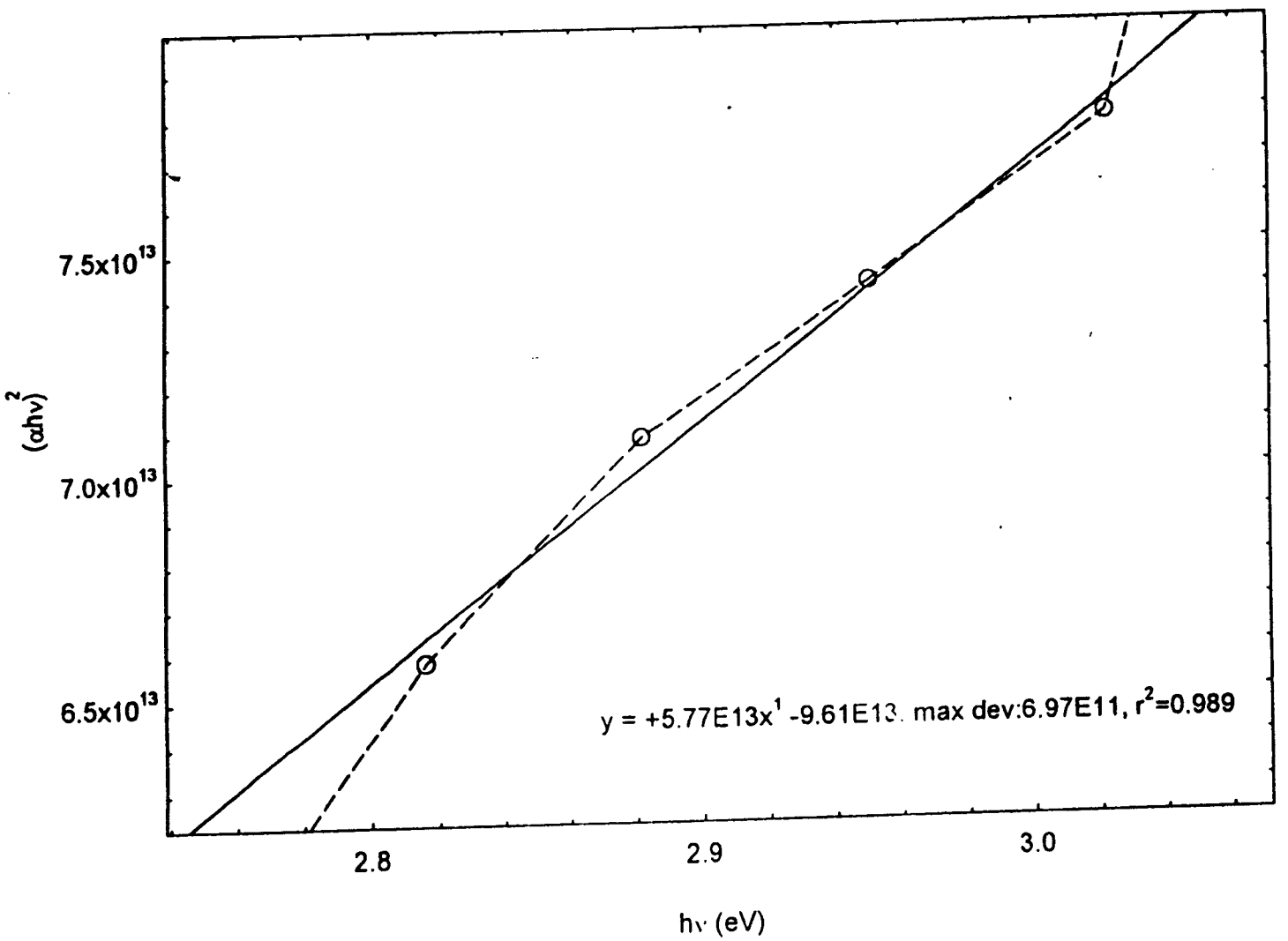

5.71 $(\alpha h\nu)^2$ vs. hv for [Tm(pc)(pc*)] voltage cycled to blue

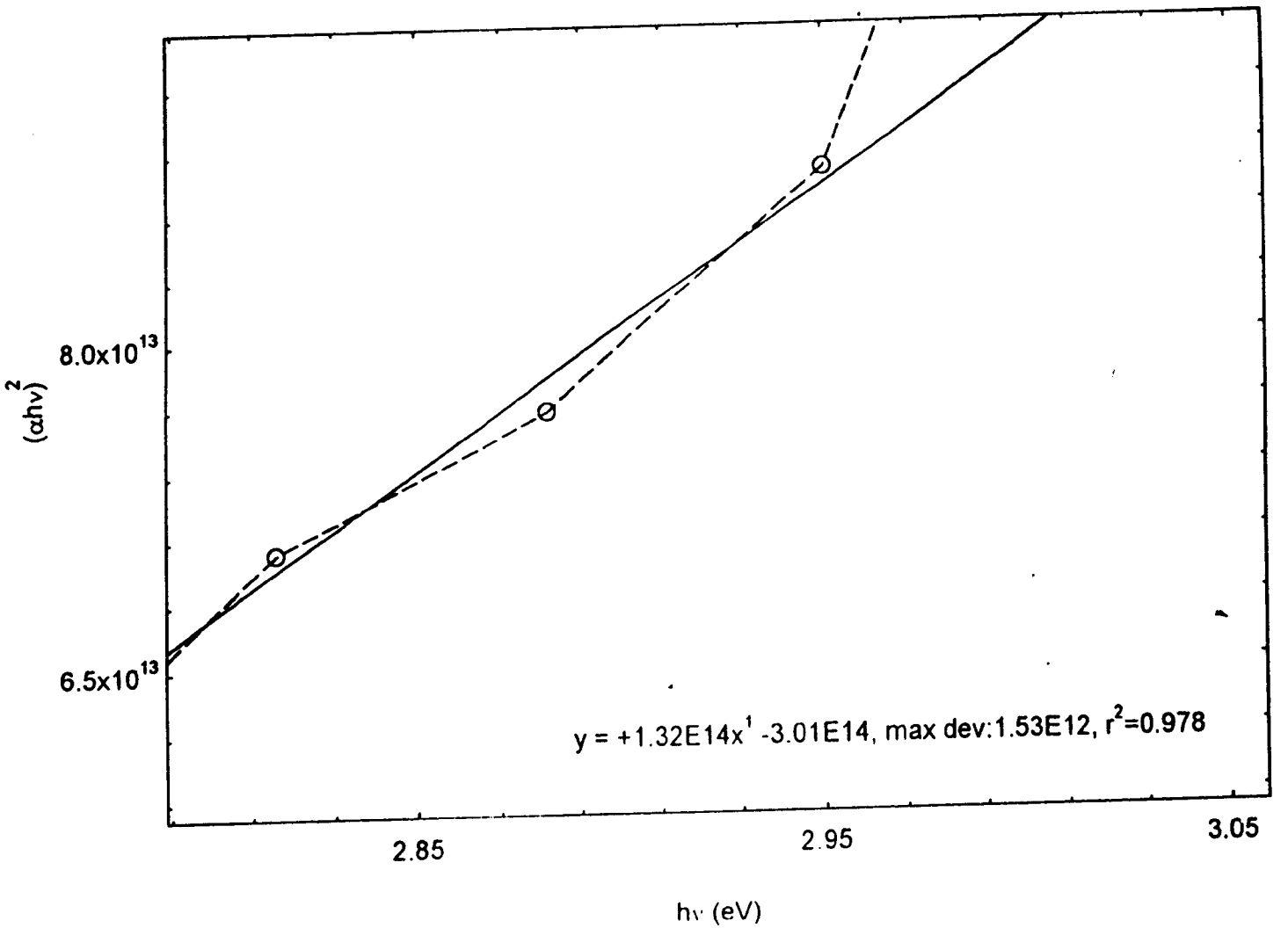

5.72 $(\alpha h\nu)^2$ vs. hν for [Tm(pc)(pc*)] voltage cycled to red

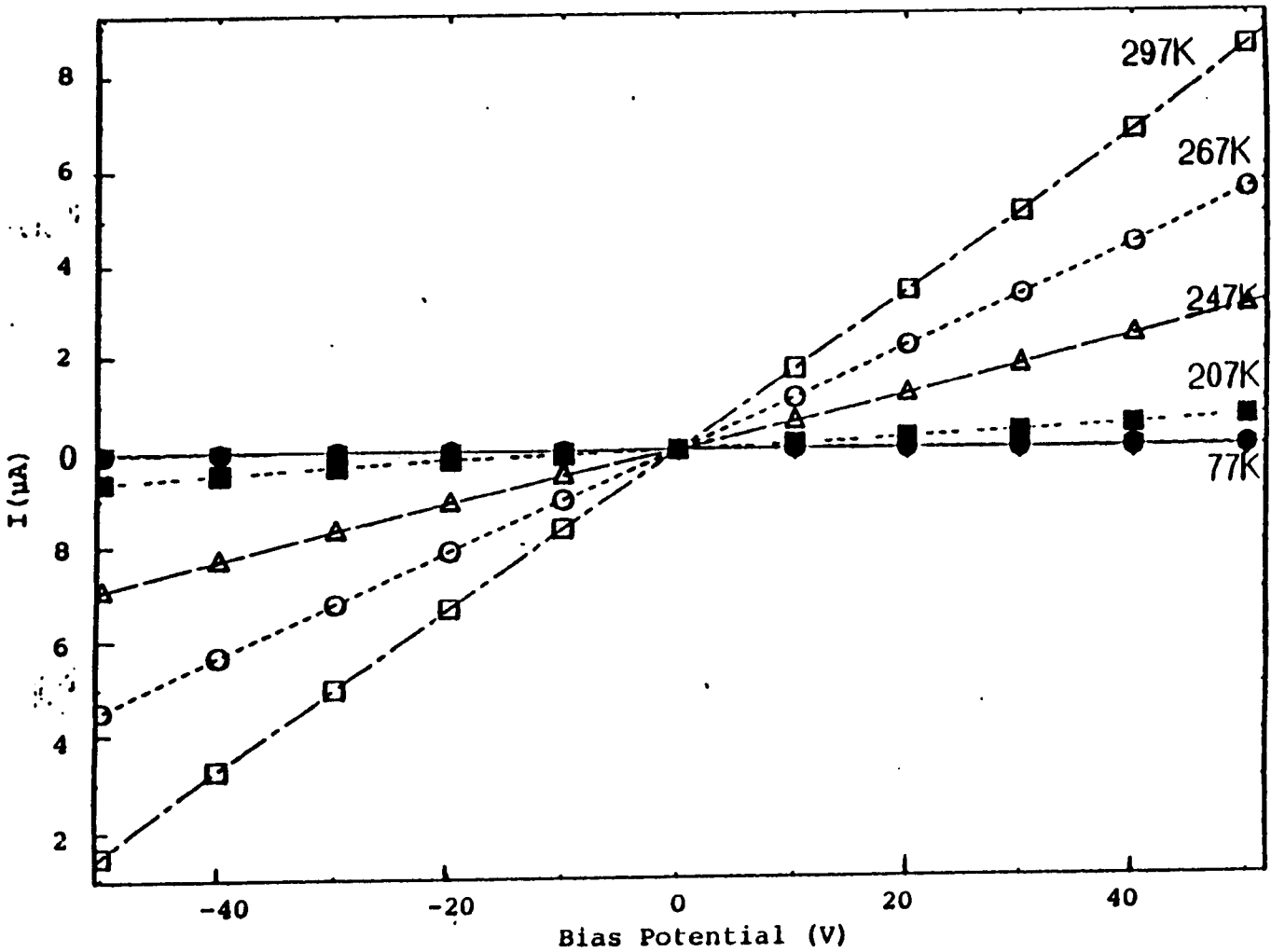

5.73 Plot of circulating current J vs. voltage V for [HF(pc)(pc*)] at varying temperatures.

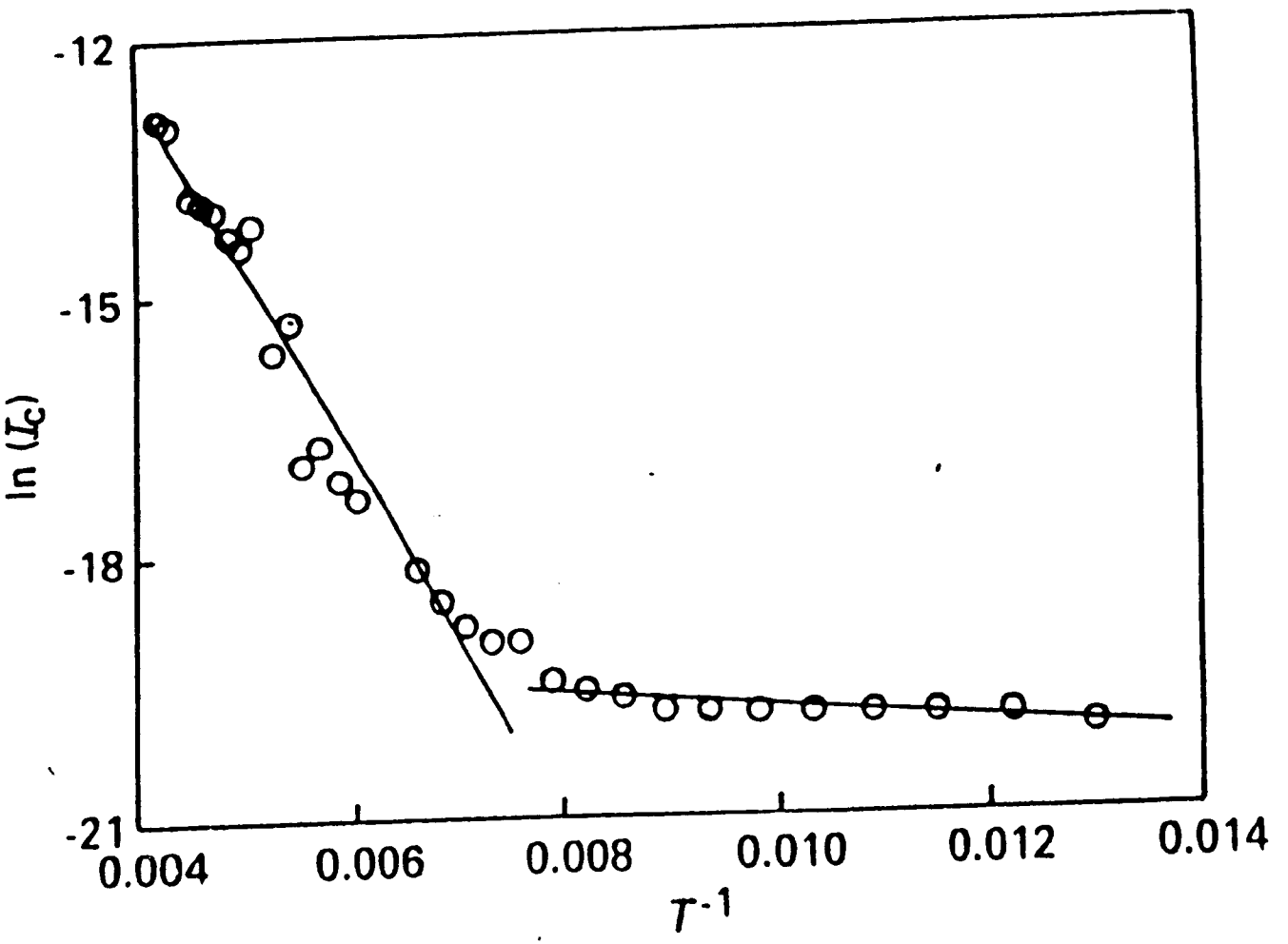

5.74 Arrhenius plot for [HF(pc)(pc*)]

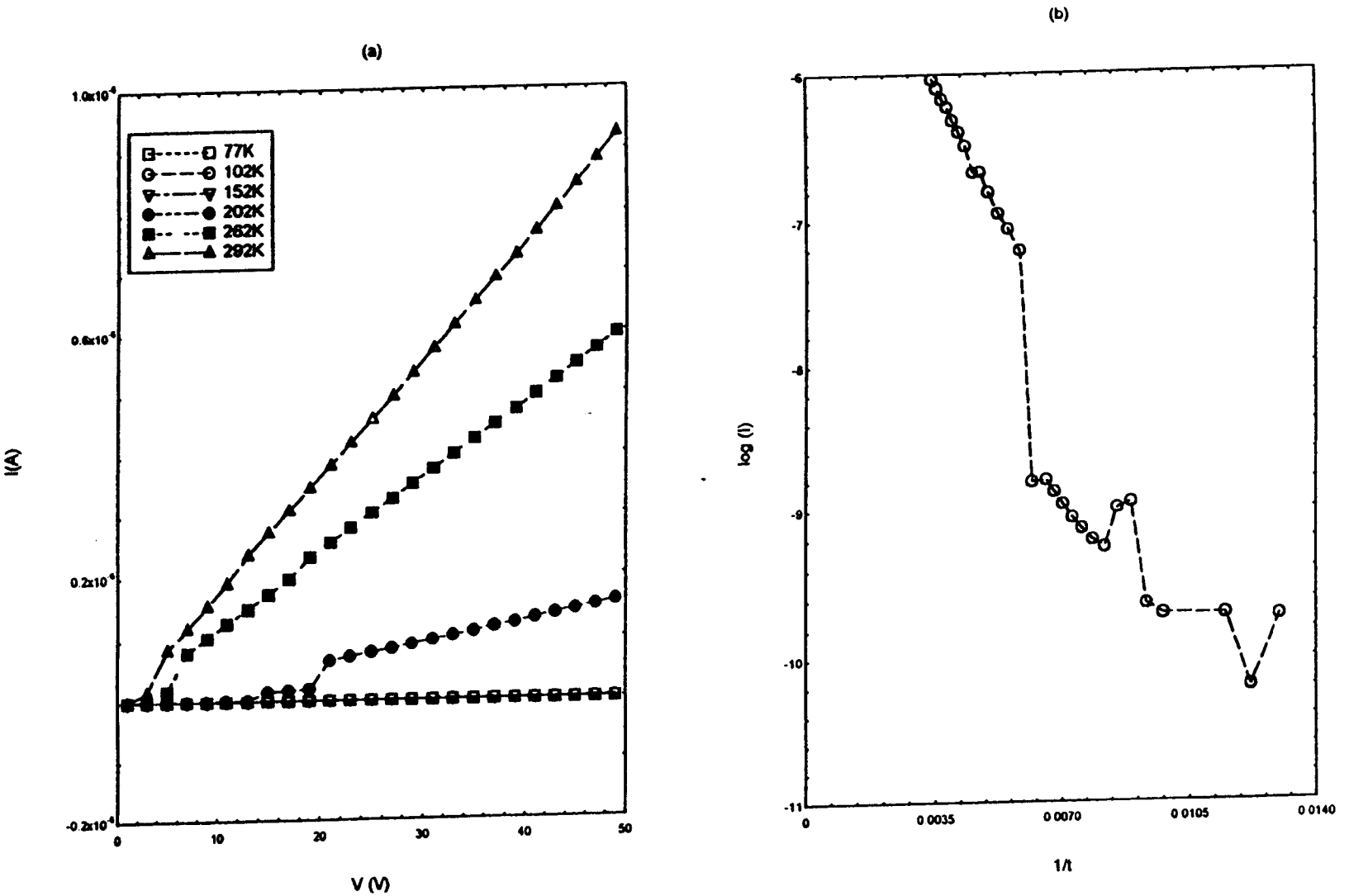

5.75 Plot of circulating current I vs. applied voltage V for FCrPc at varying temperatures, and associated Arrhenius plot

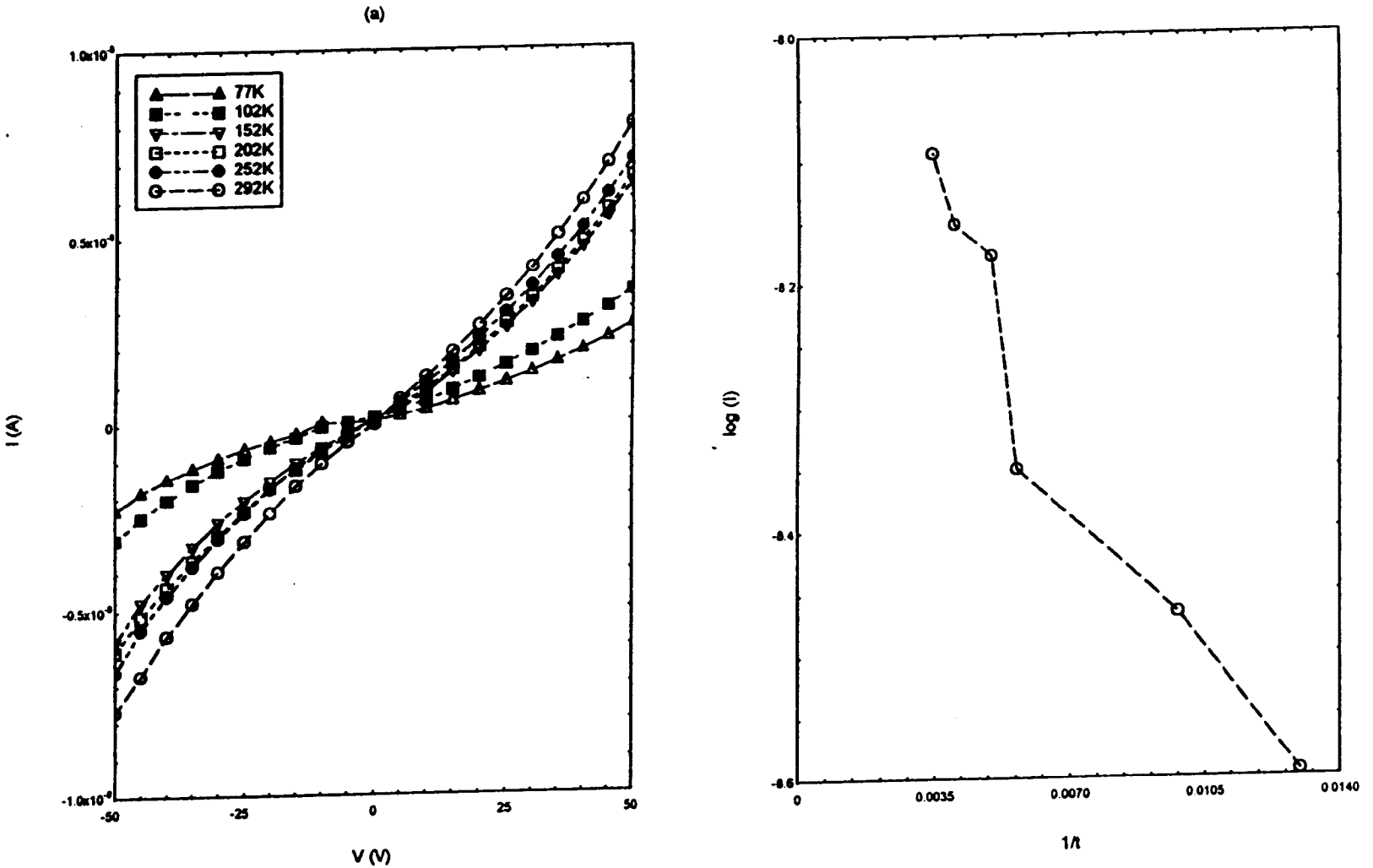

5.76

Plot of circulating current J vs. voltage V for [FCr(pc)(pc*)] at varying temperatures.

Arrhenius plot for [FCr(pc)(pc*)]

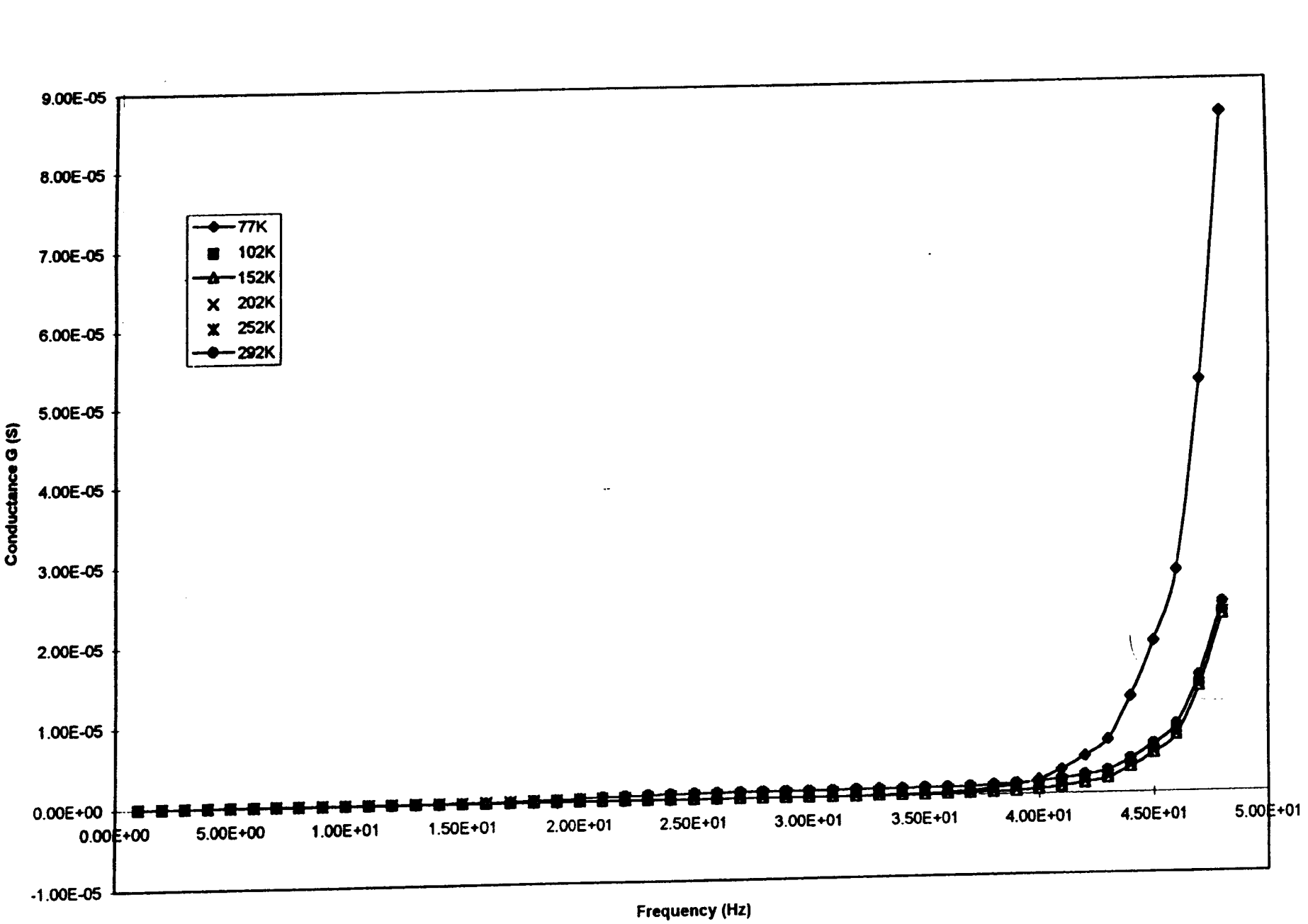

5.77 Plot of G vs. F for [HF(pc)(pc*)] at various temperatures

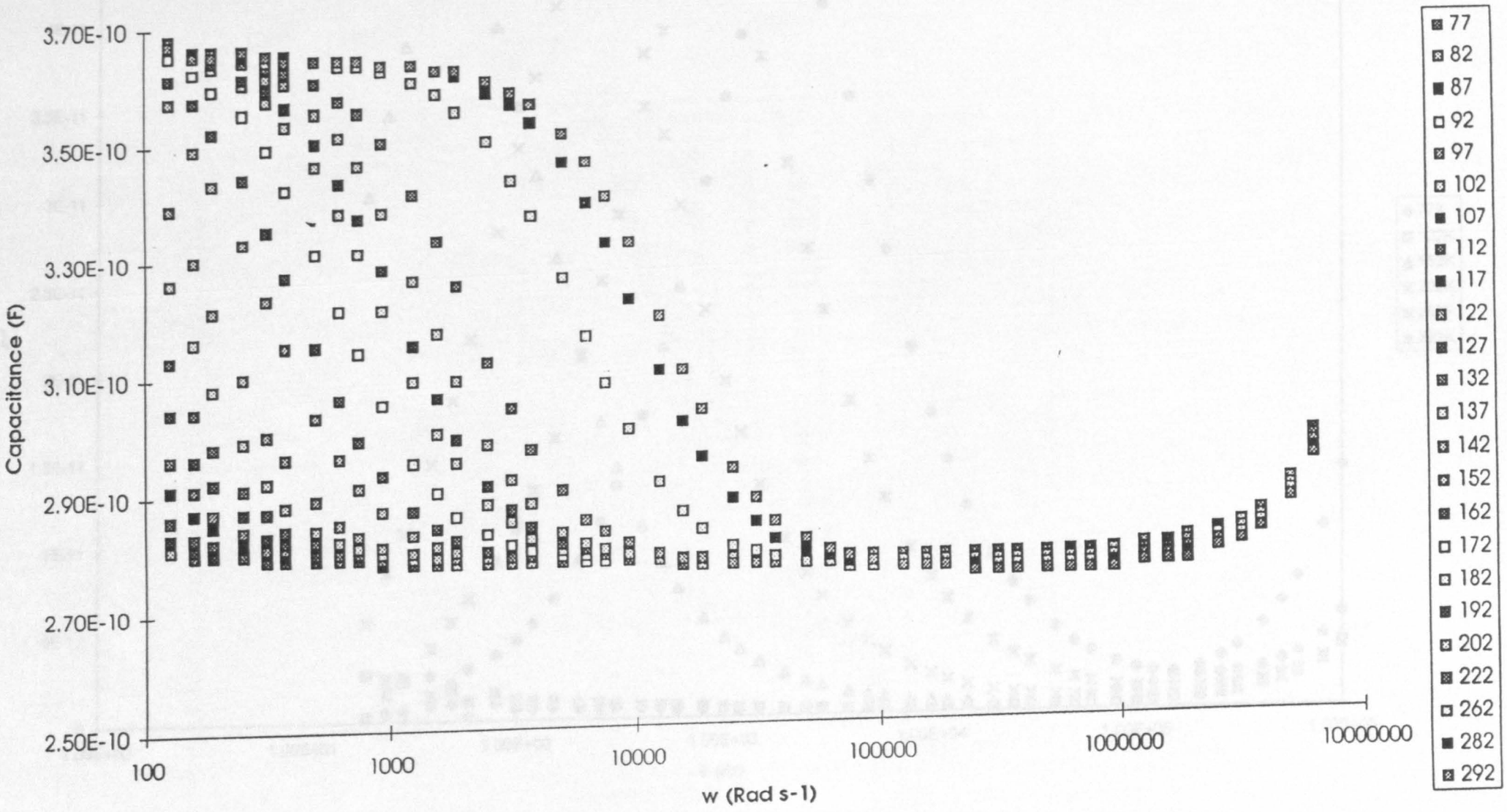

5.78 Plot of C vs. ω for [HF(pc)(pc*)] at varying temperaures

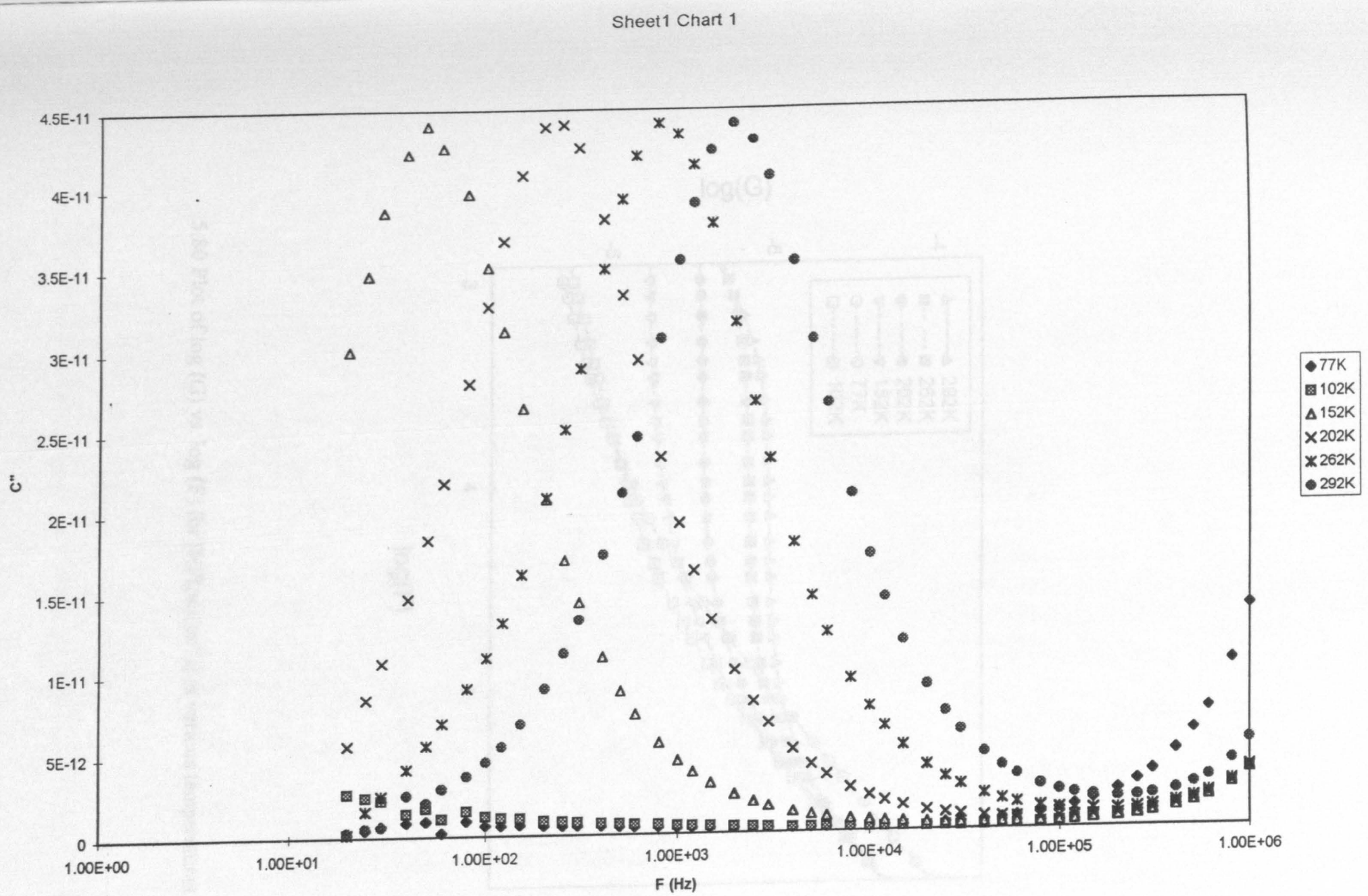

5.79. C" vs. F for [HF(pc)(pc*)]

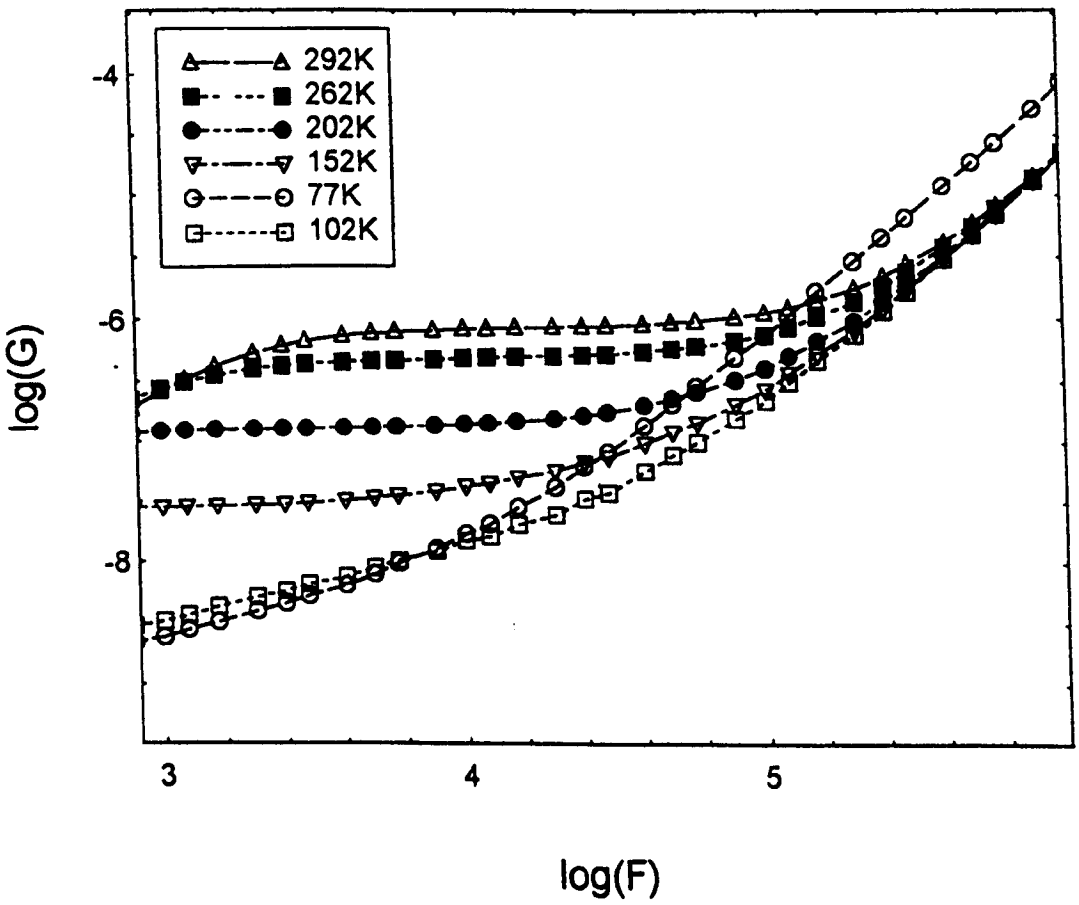

5.80 Plot of log (G) vs. log (F) for [HF(pc)(pc*)] at various temperatures

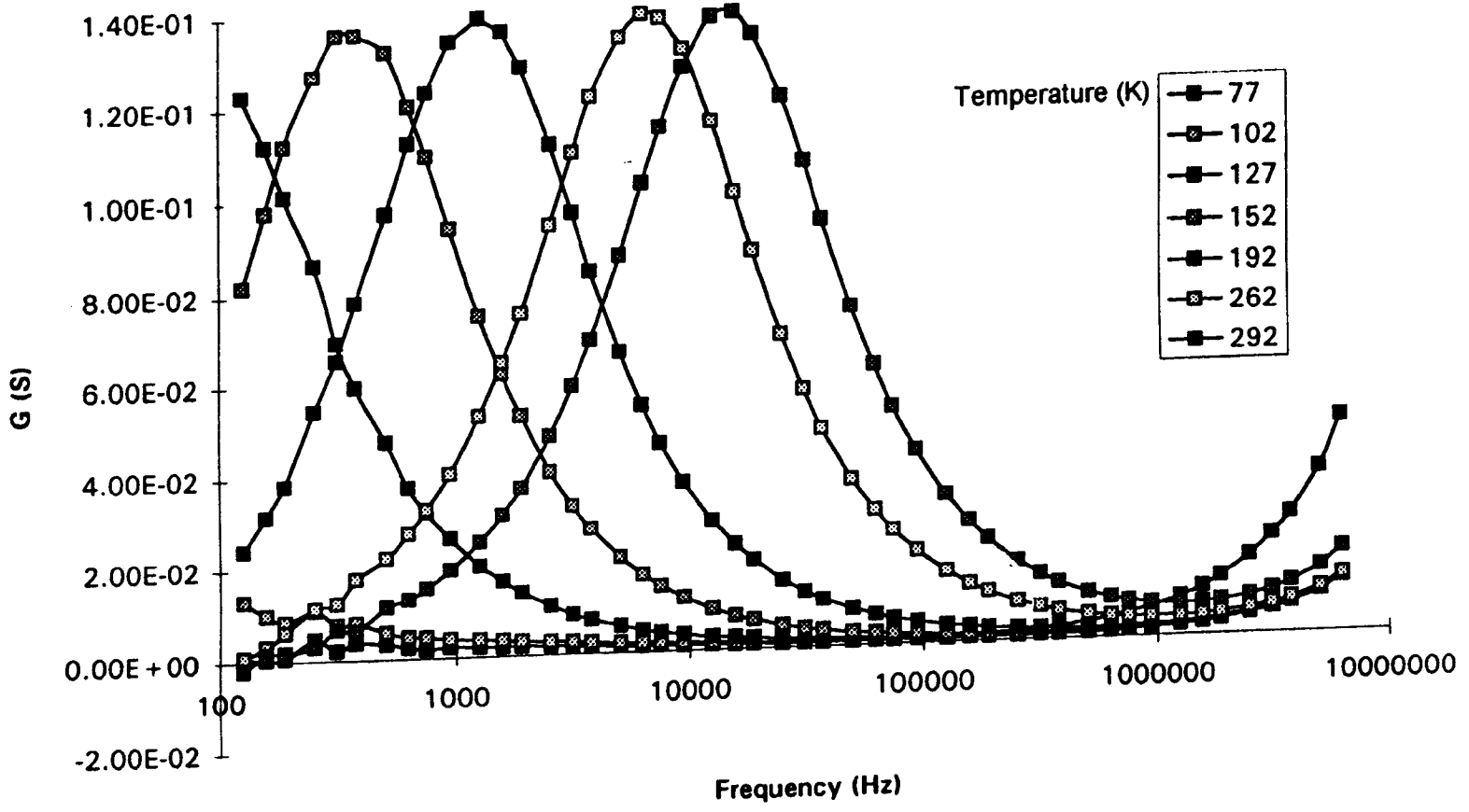

5.24 Plot of D vs. ω for [UE(pc)(pc*)] at varying temperatures

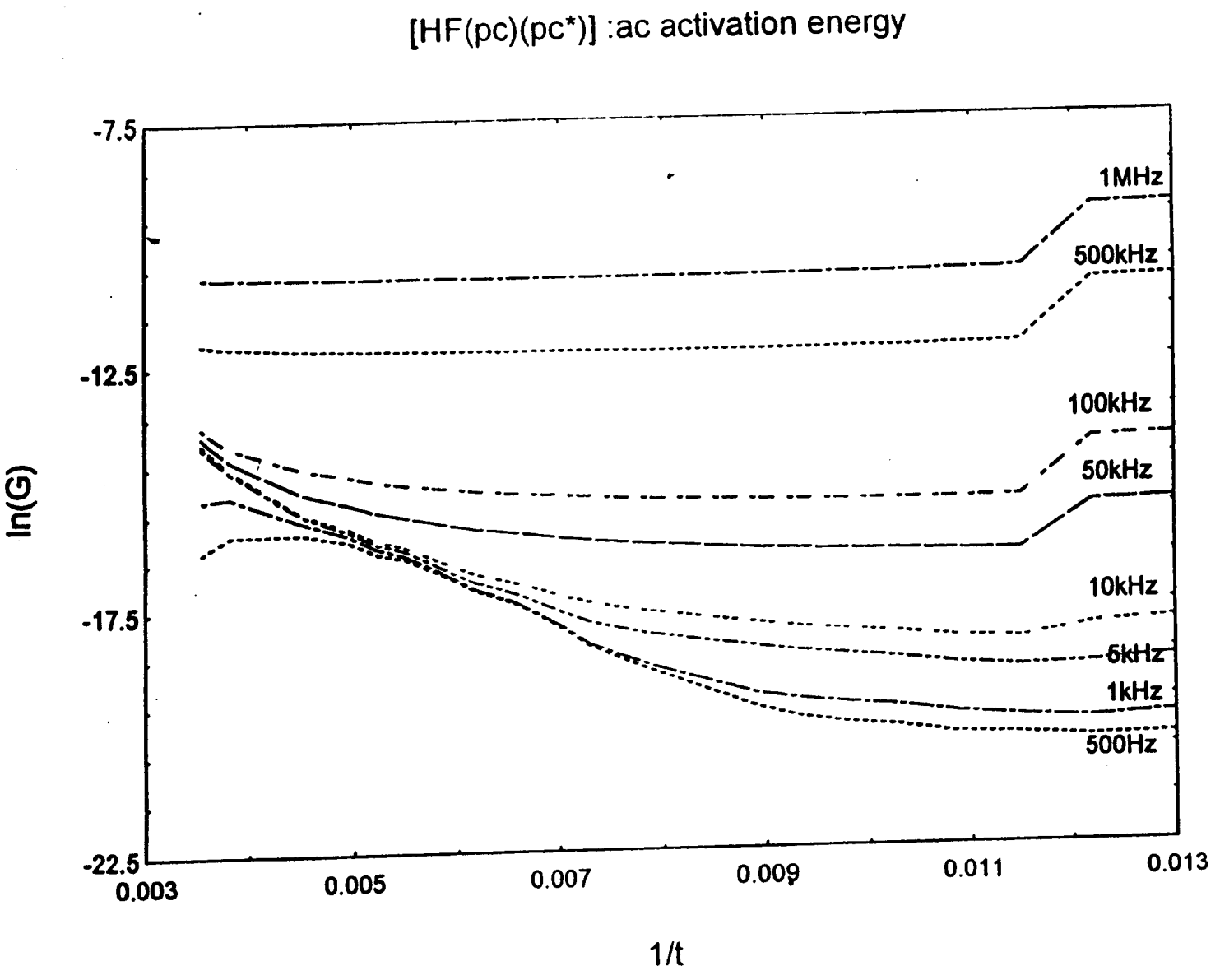

5.82 Activation energy plot for [HF(pc)(pc*)] at various frequencies

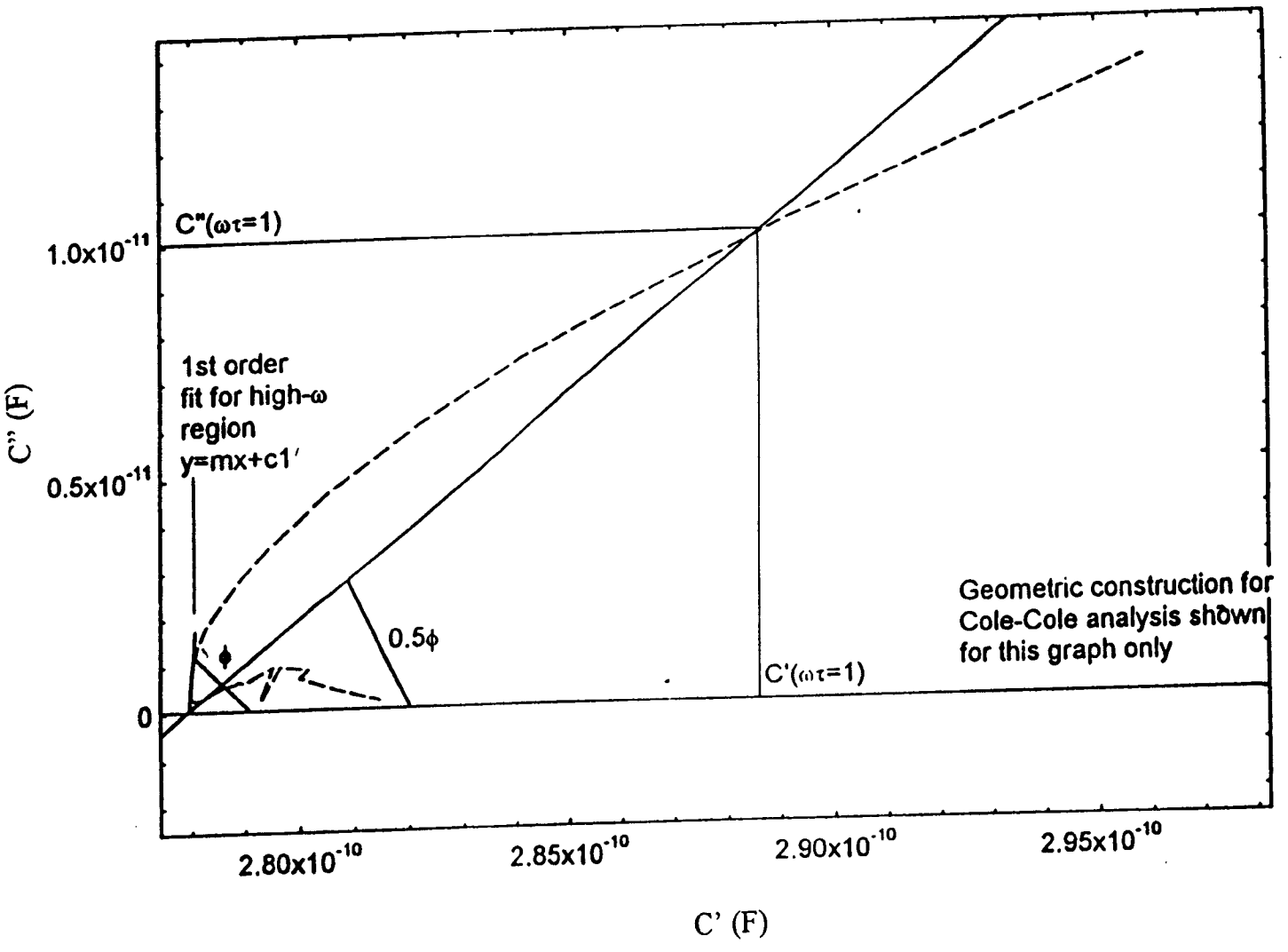

5.83 Cole-Cole plot, with constructional data, for [HF(pc)(pc*)] at 77K.

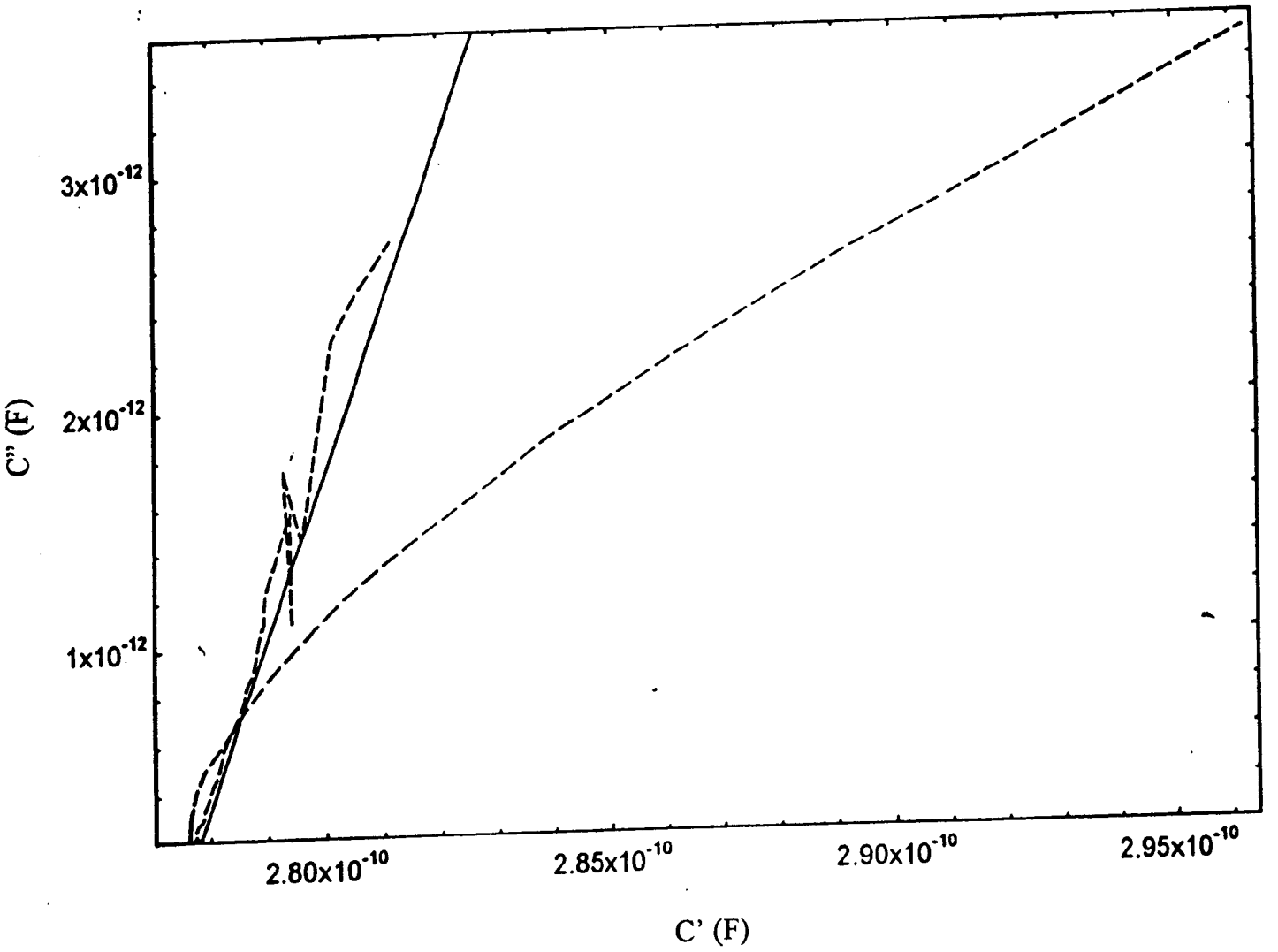

5.84 Cole-Cole plot for [HF(pc)(pc*)] at 102K.

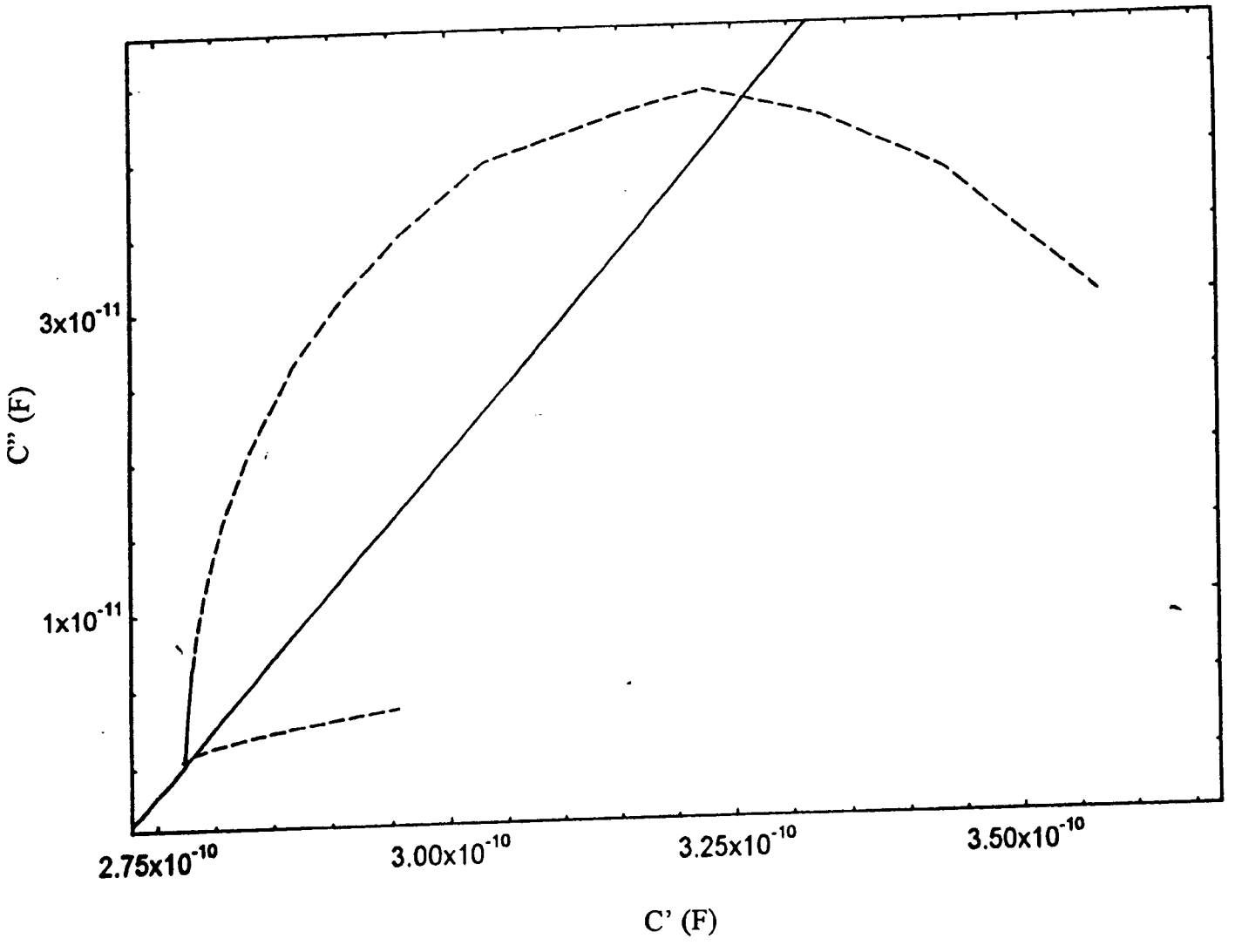

5.85 Cole-Cole plot for [HF(pc)(pc*)] at 152K

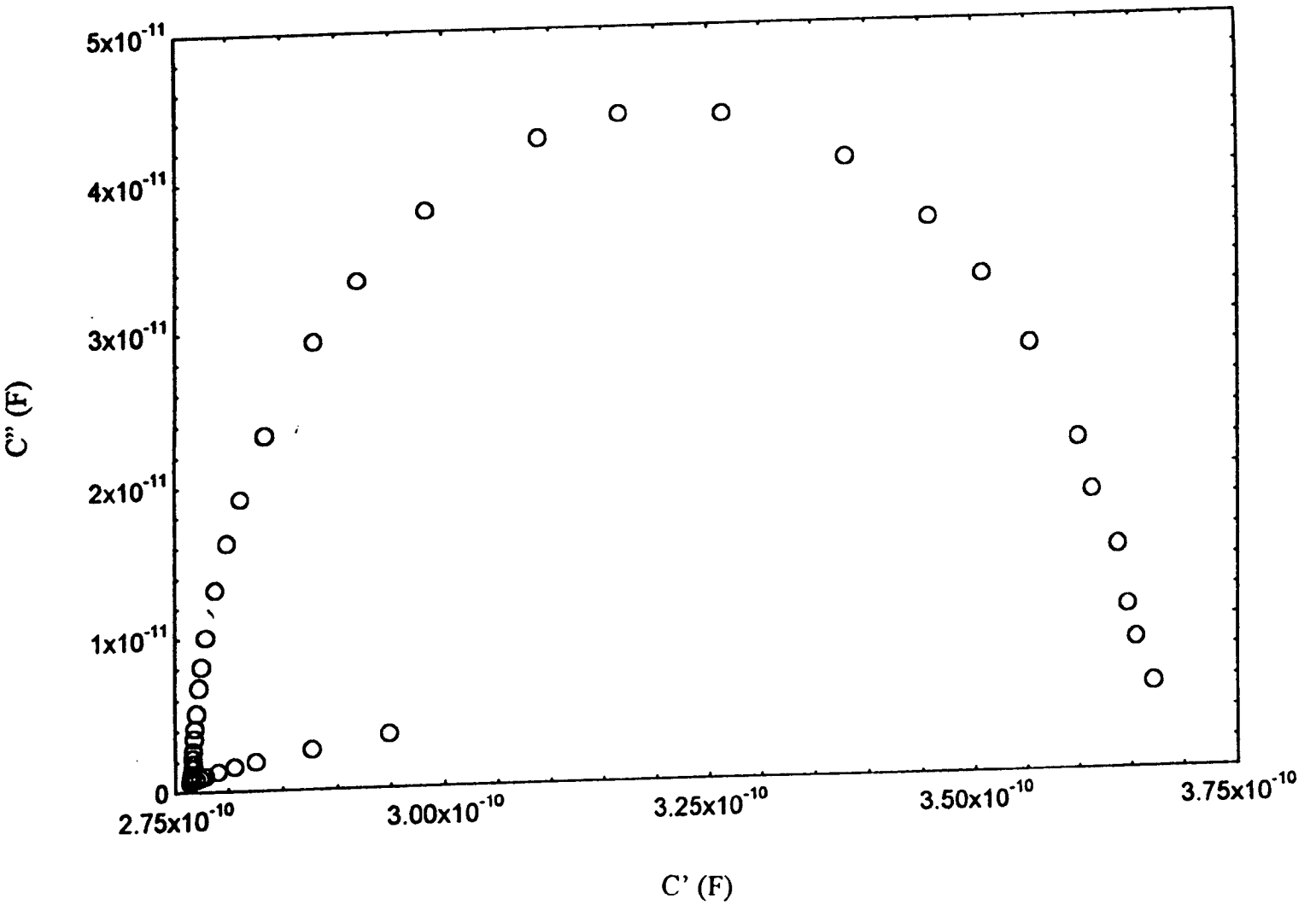

5.86 Cole-Cole plot for [HF(pc)(pc*)] at 202K

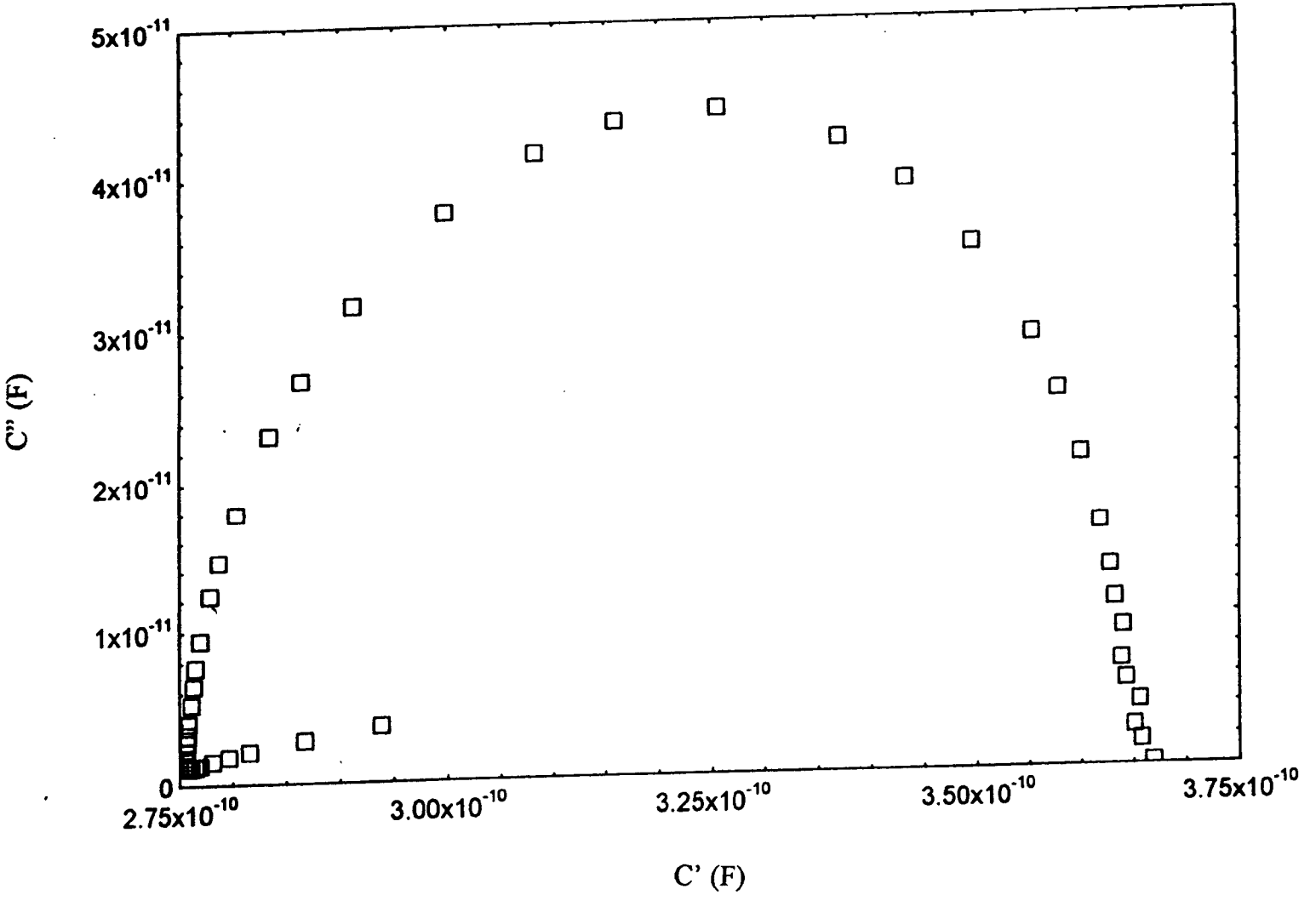

5.87 Cole-Cole plot for [HF(pc)(pc*)] at 262K

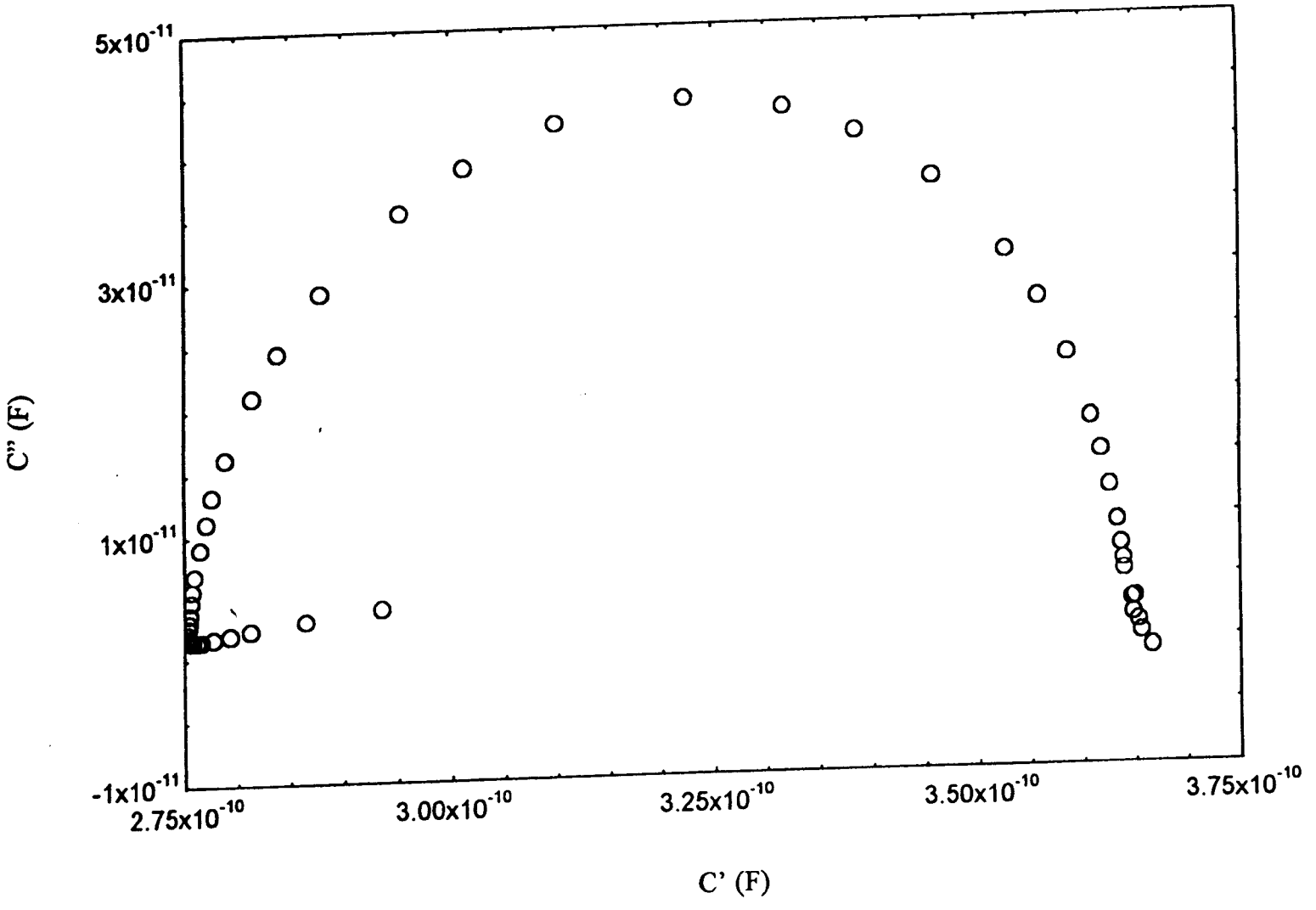

5.88 Cole-Cole plot for [HF(pc)(pc*)] at 292K

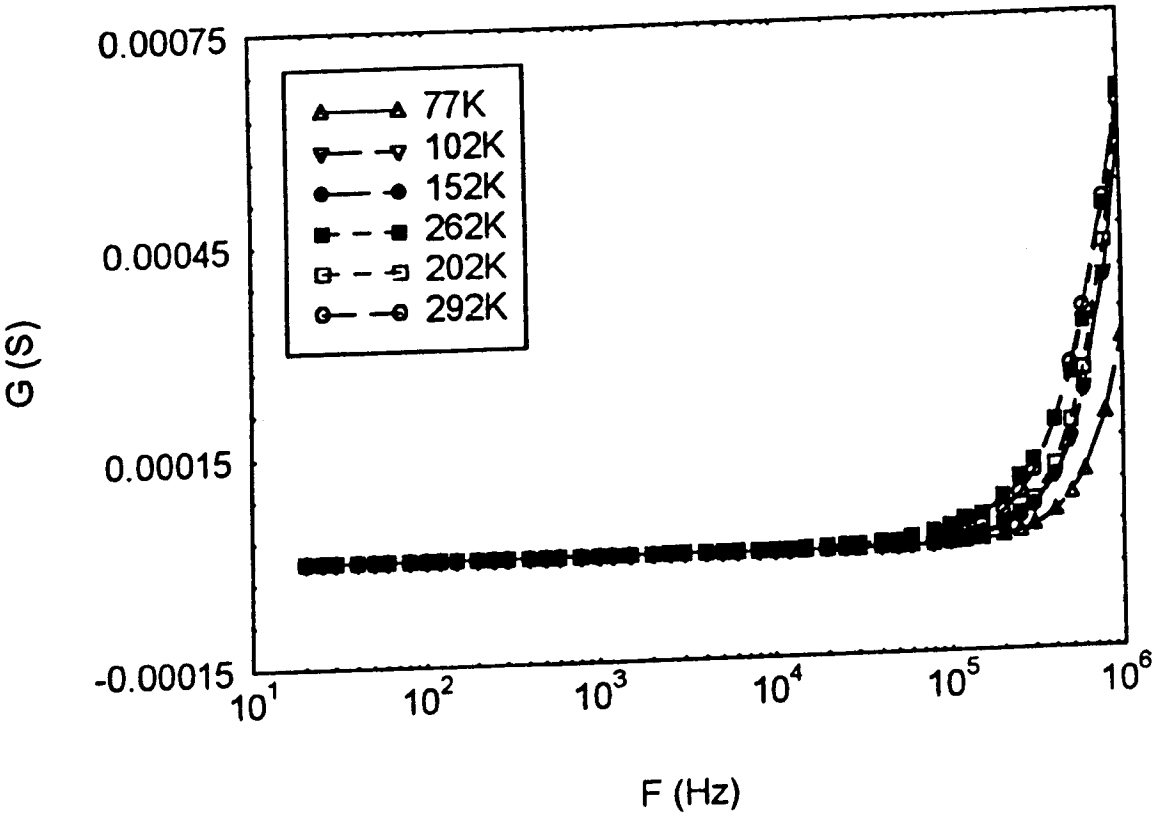

5.89 Plot of G vs. F for FCrPc at various temperatures

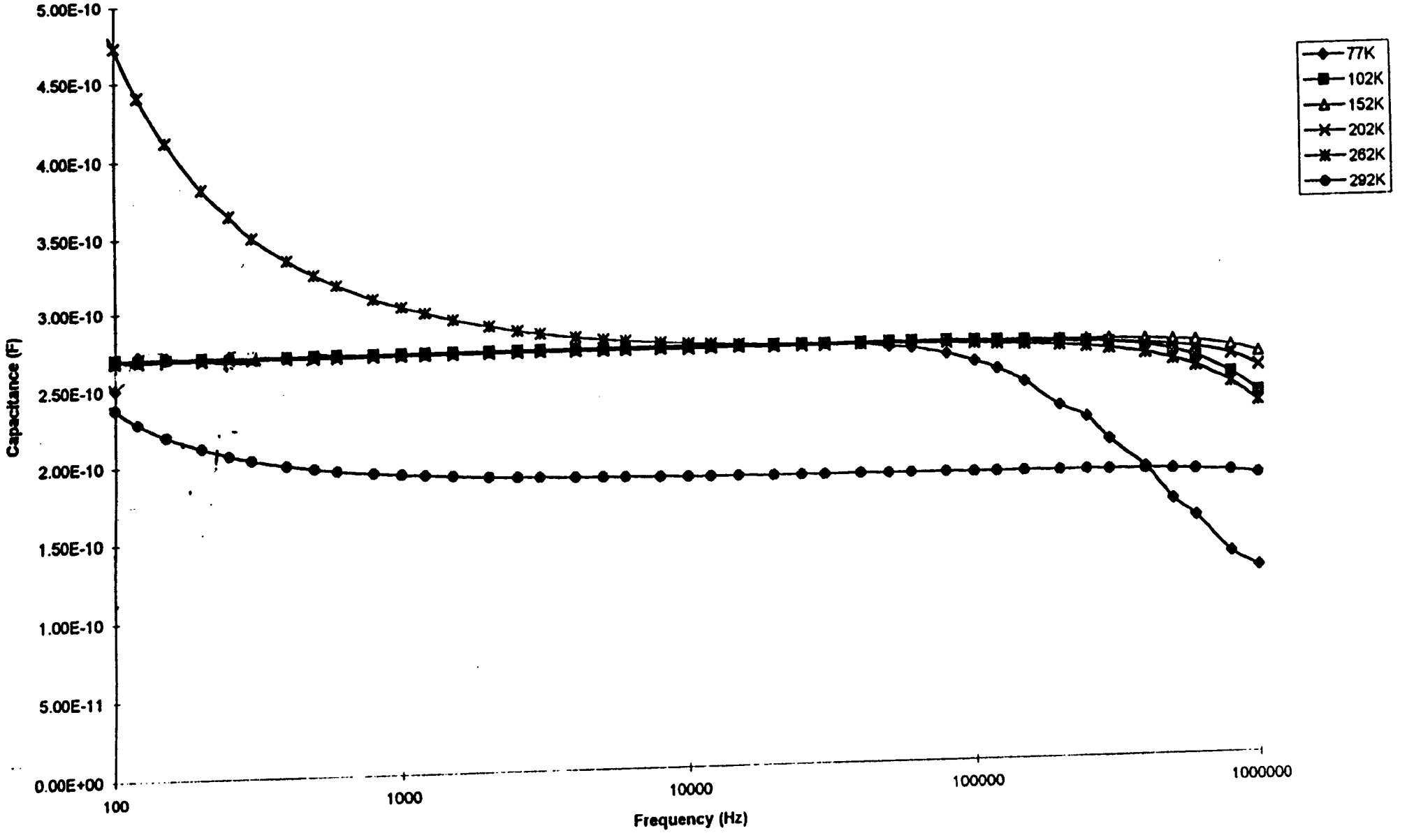

5.90 Plot of C vs. F for FCrPc at various temperatures.

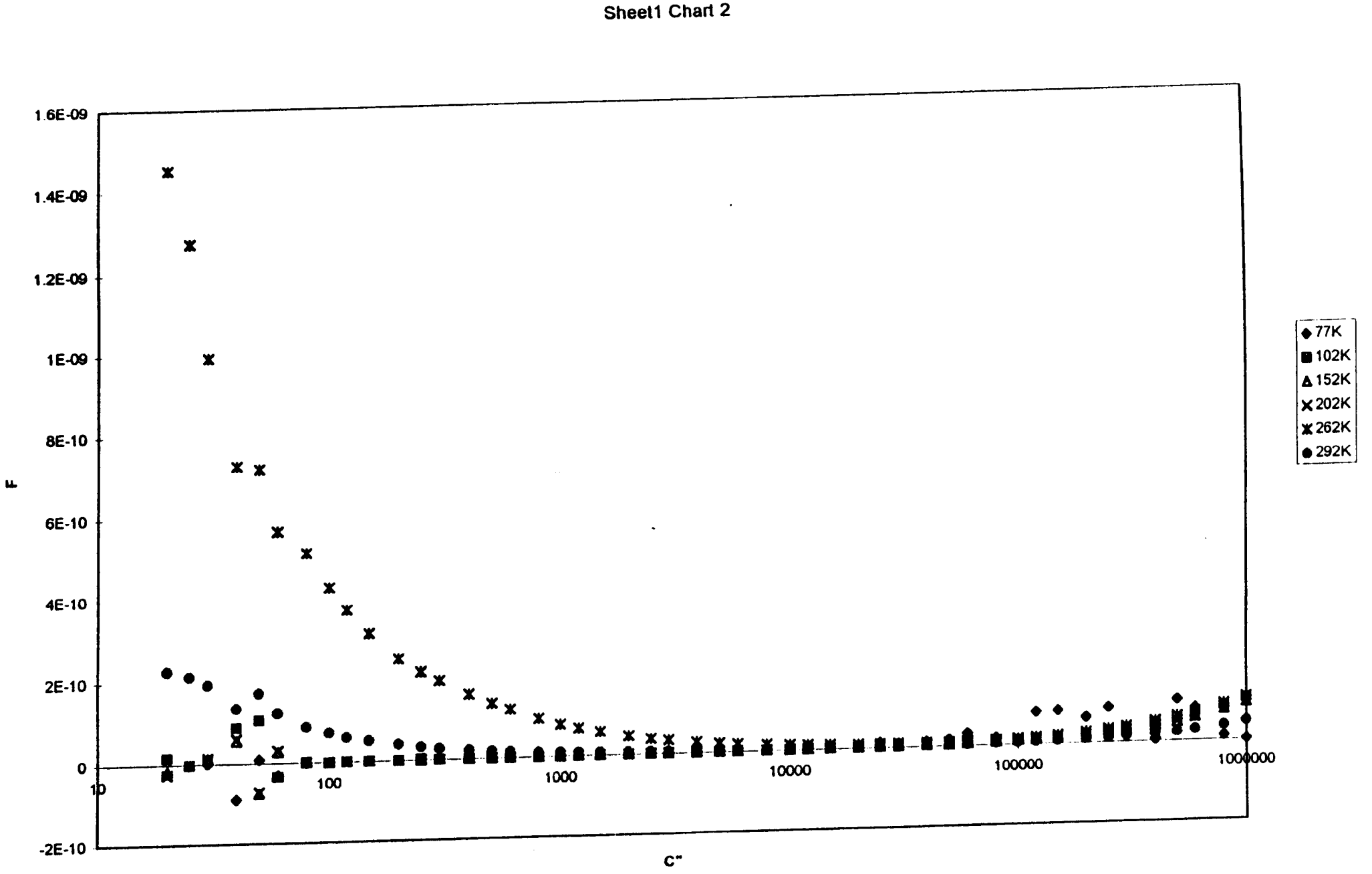

5.91. C" vs. F for FCrPc

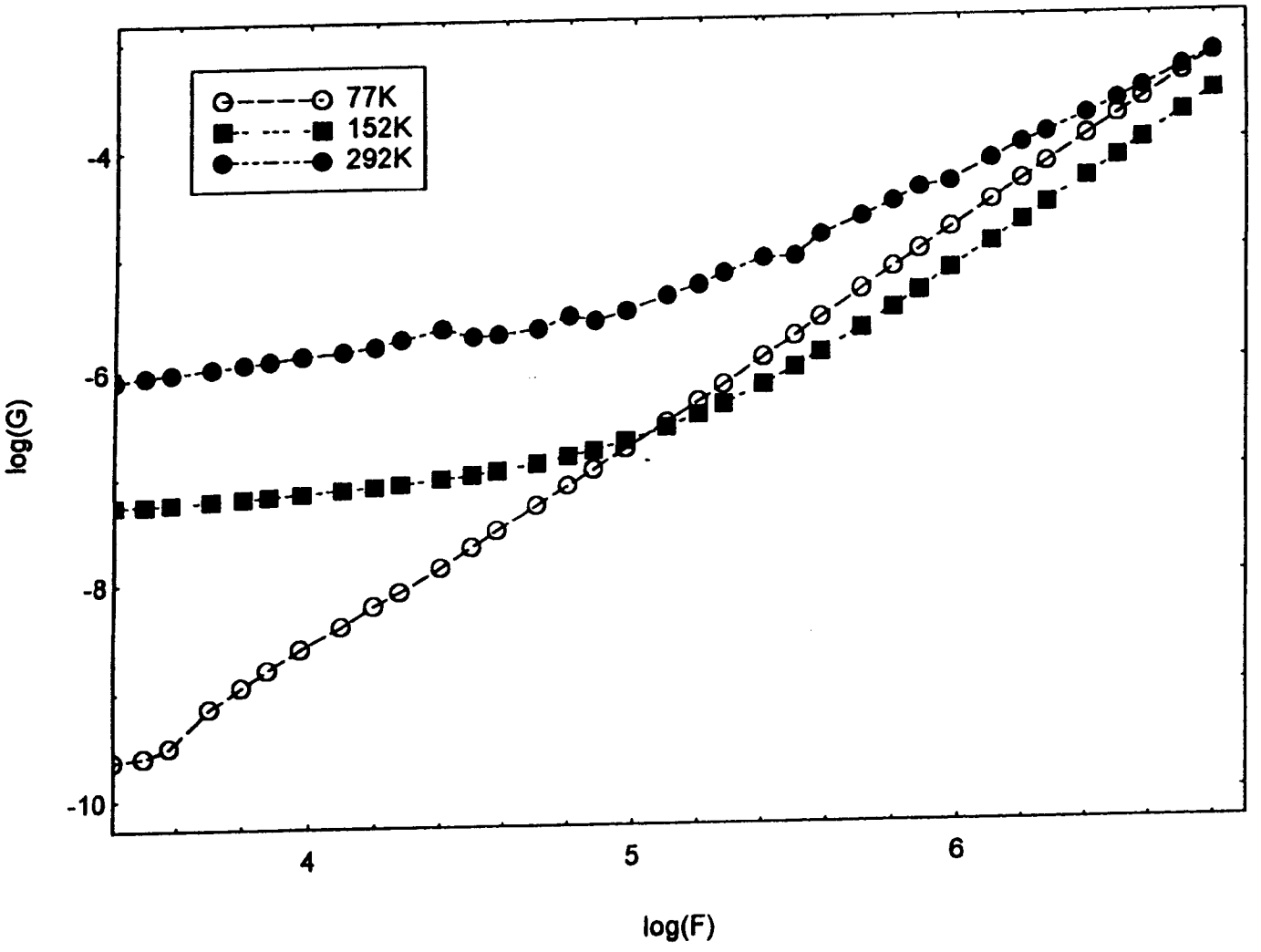

5.92. Log (G) vs. log (F) for FCrPc at various temperatures

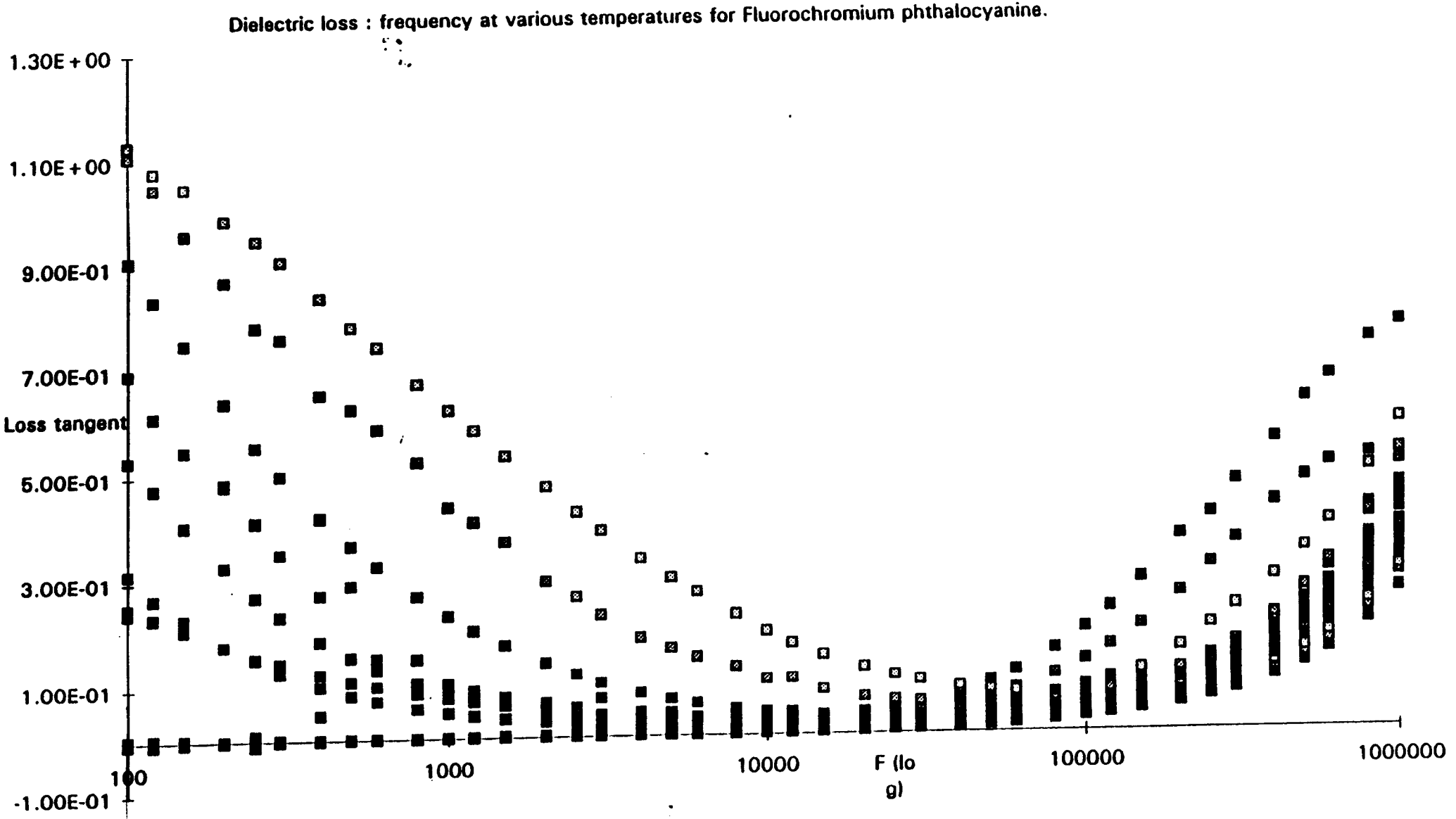

5.93 Plot of D vs. F for FCrPc at various temperatures

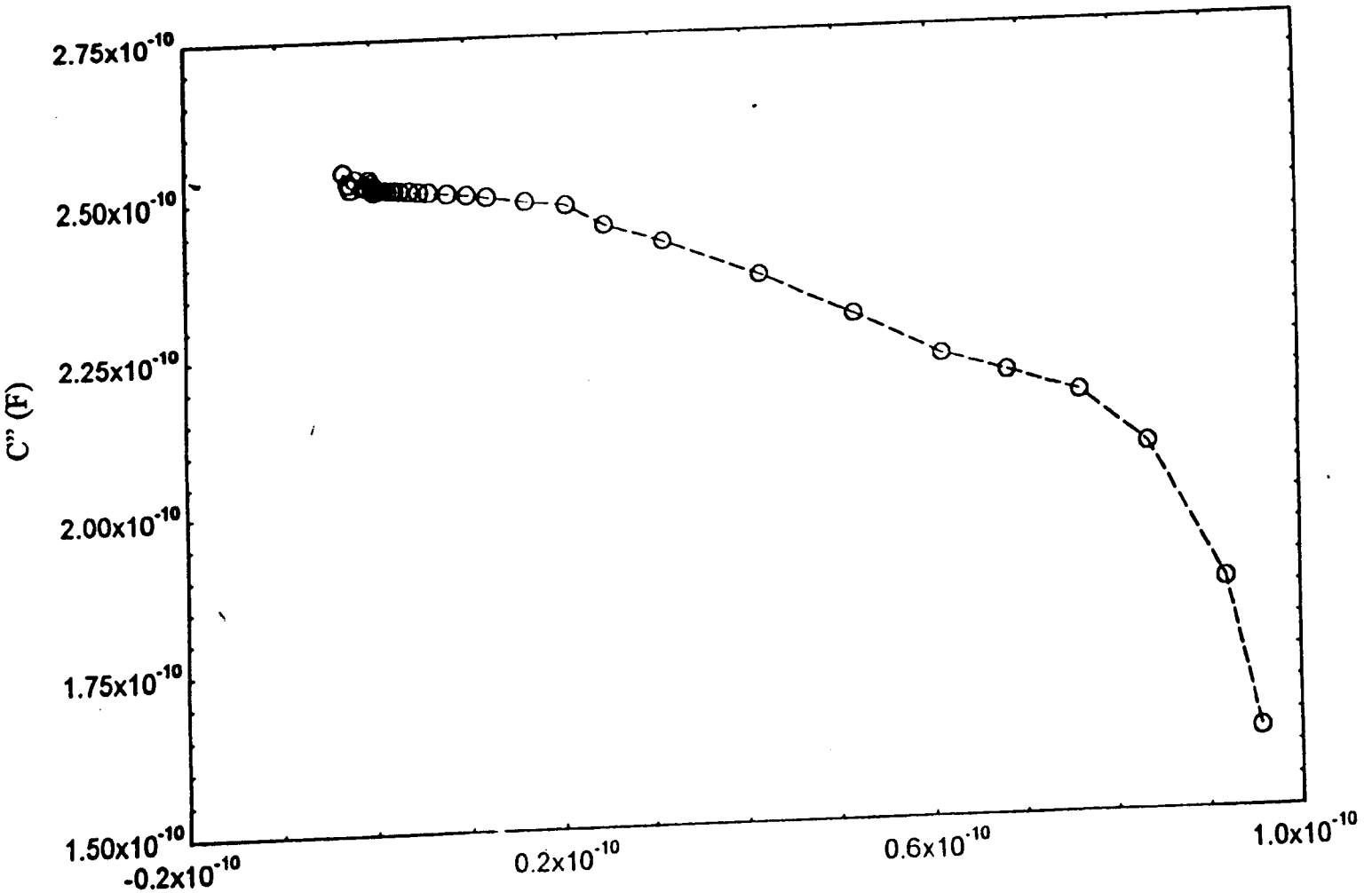

5.95 Cole-Cole plot for FCr(pc) at 77K.

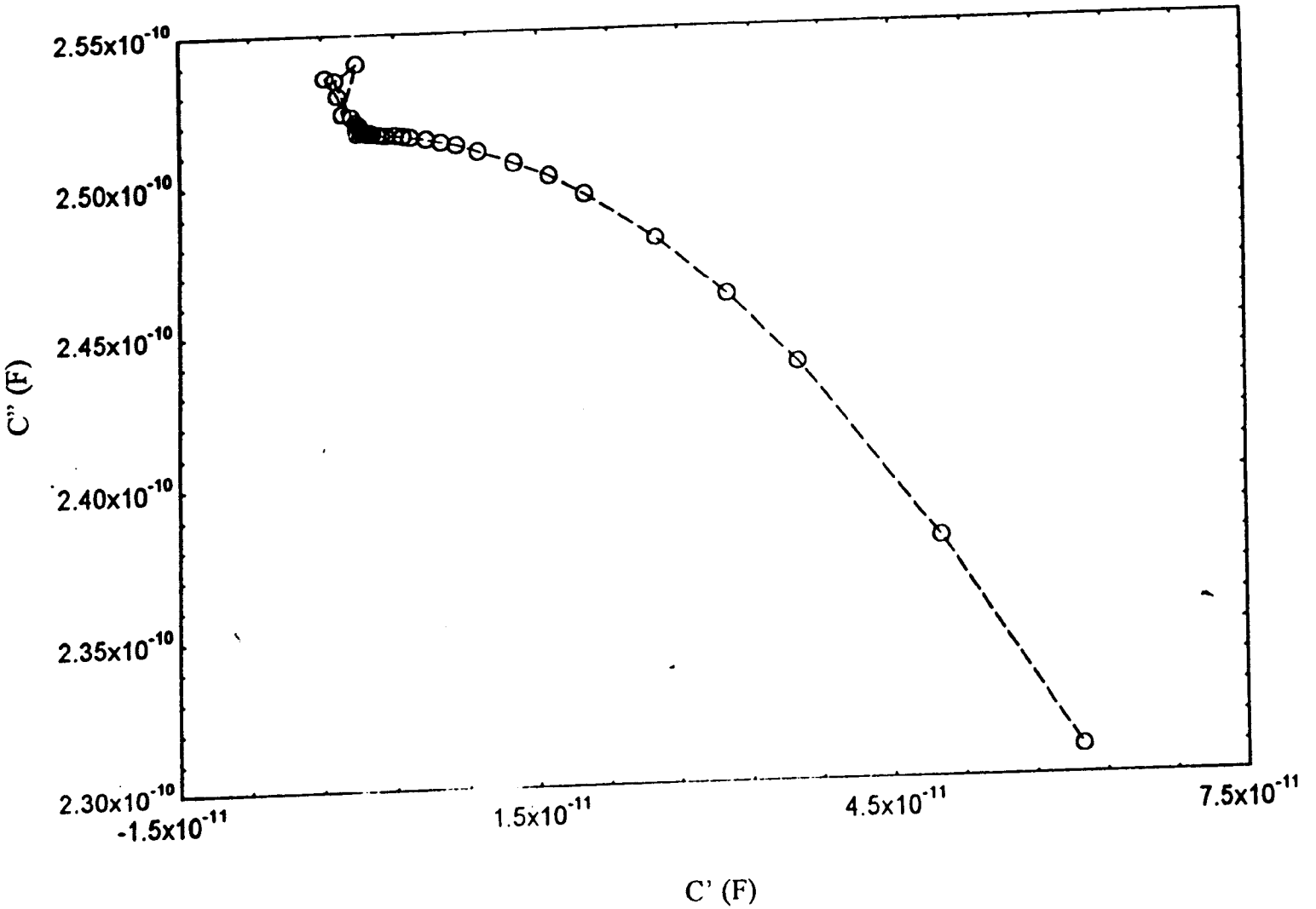

5.96 Cole-Cole plot for FCr(pc) at 102K.

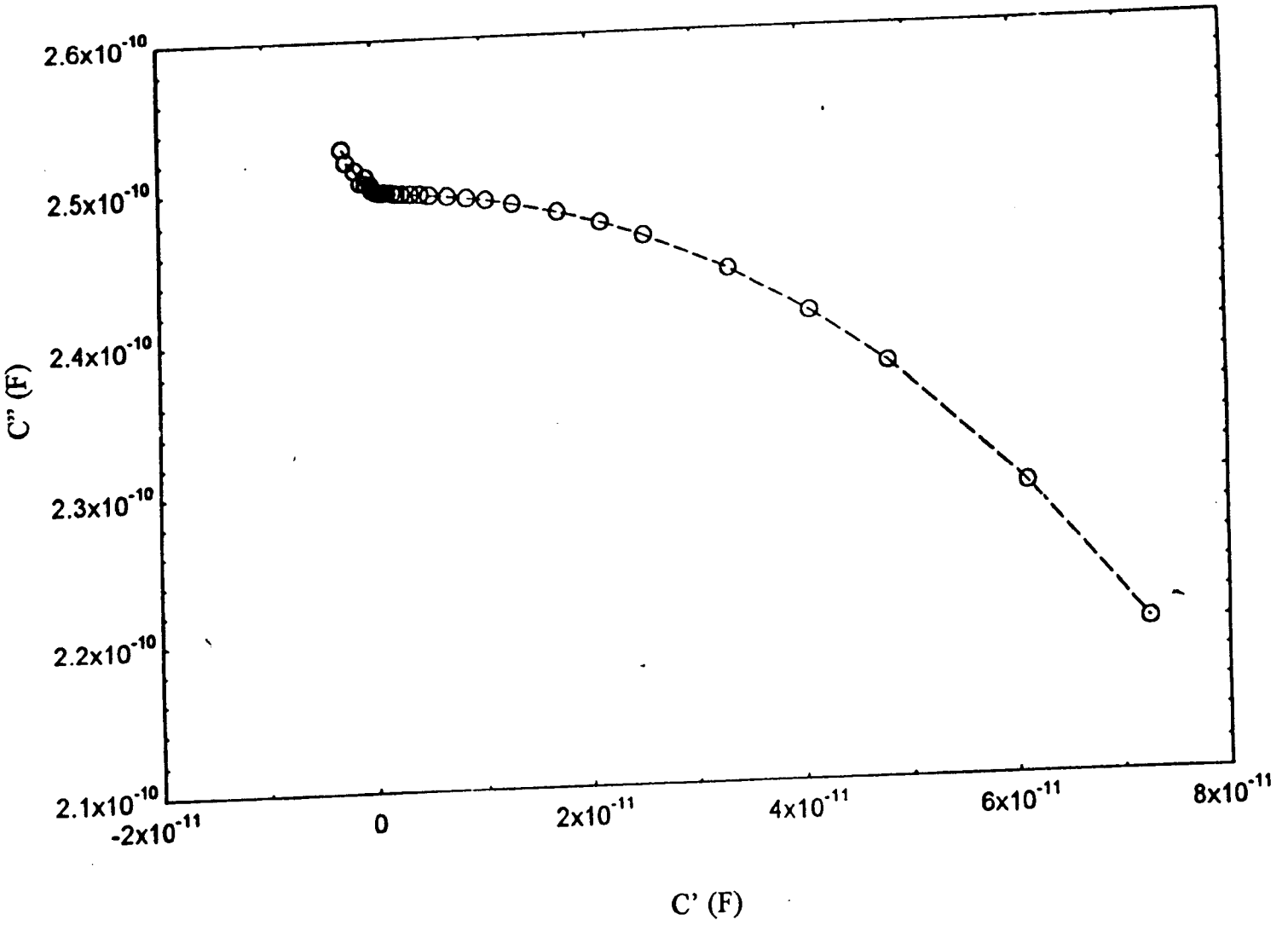

5.97 Cole-Cole plot for FCr(pc) at 152K

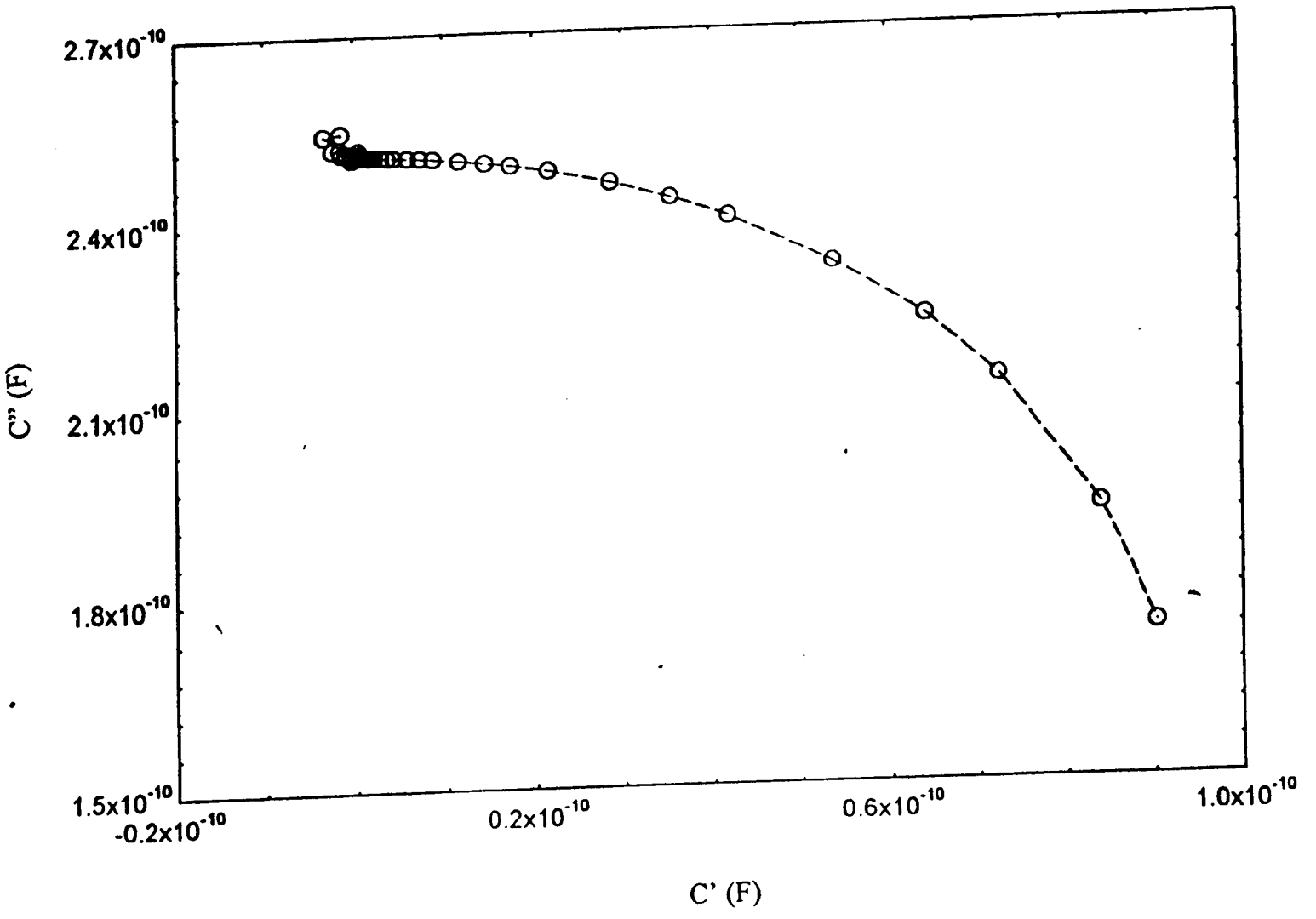

5.98 Cole-Cole plot for FCr(pc) at 202K

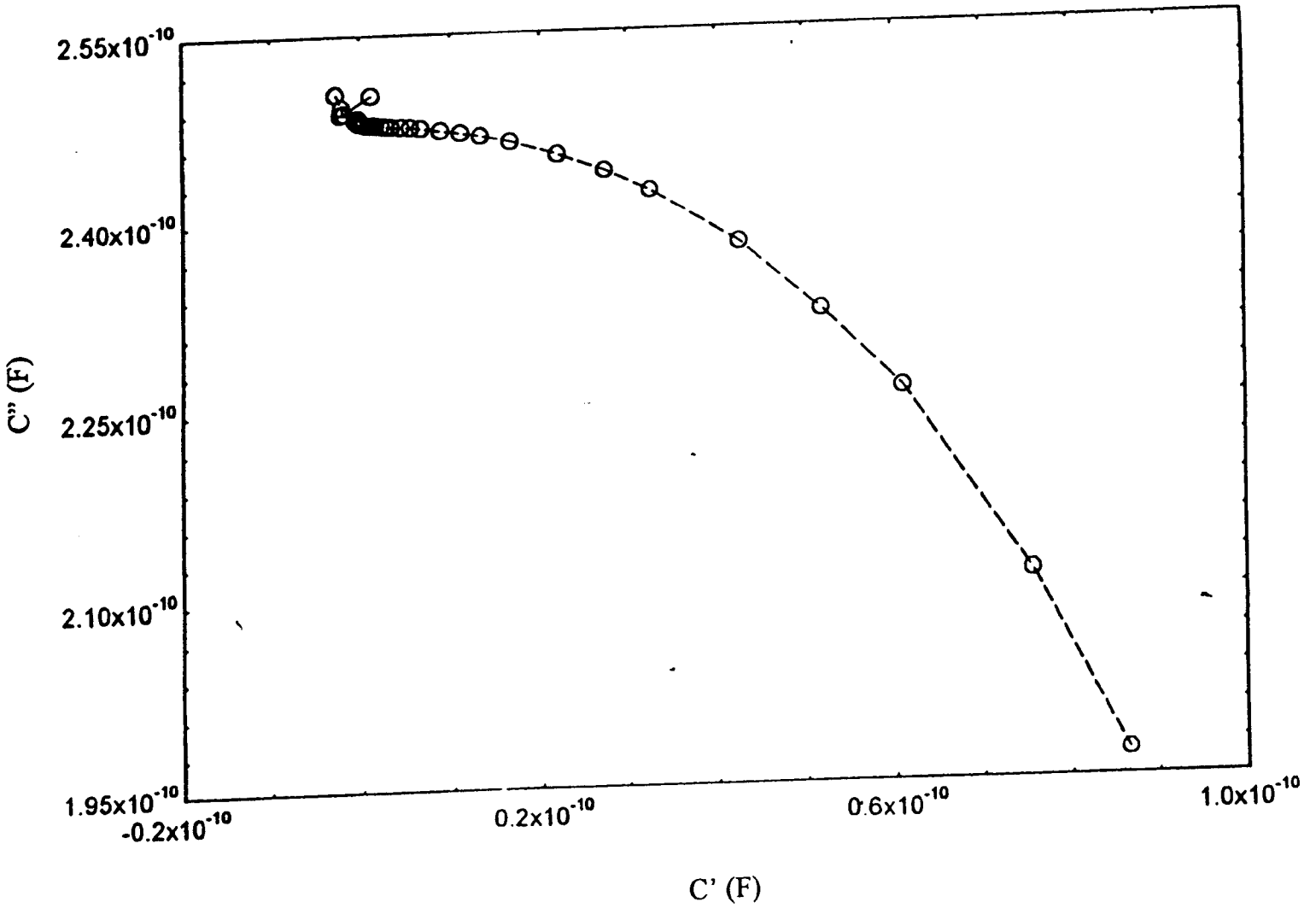

5.99 Cole-Cole plot for FCr(pc) at 262K

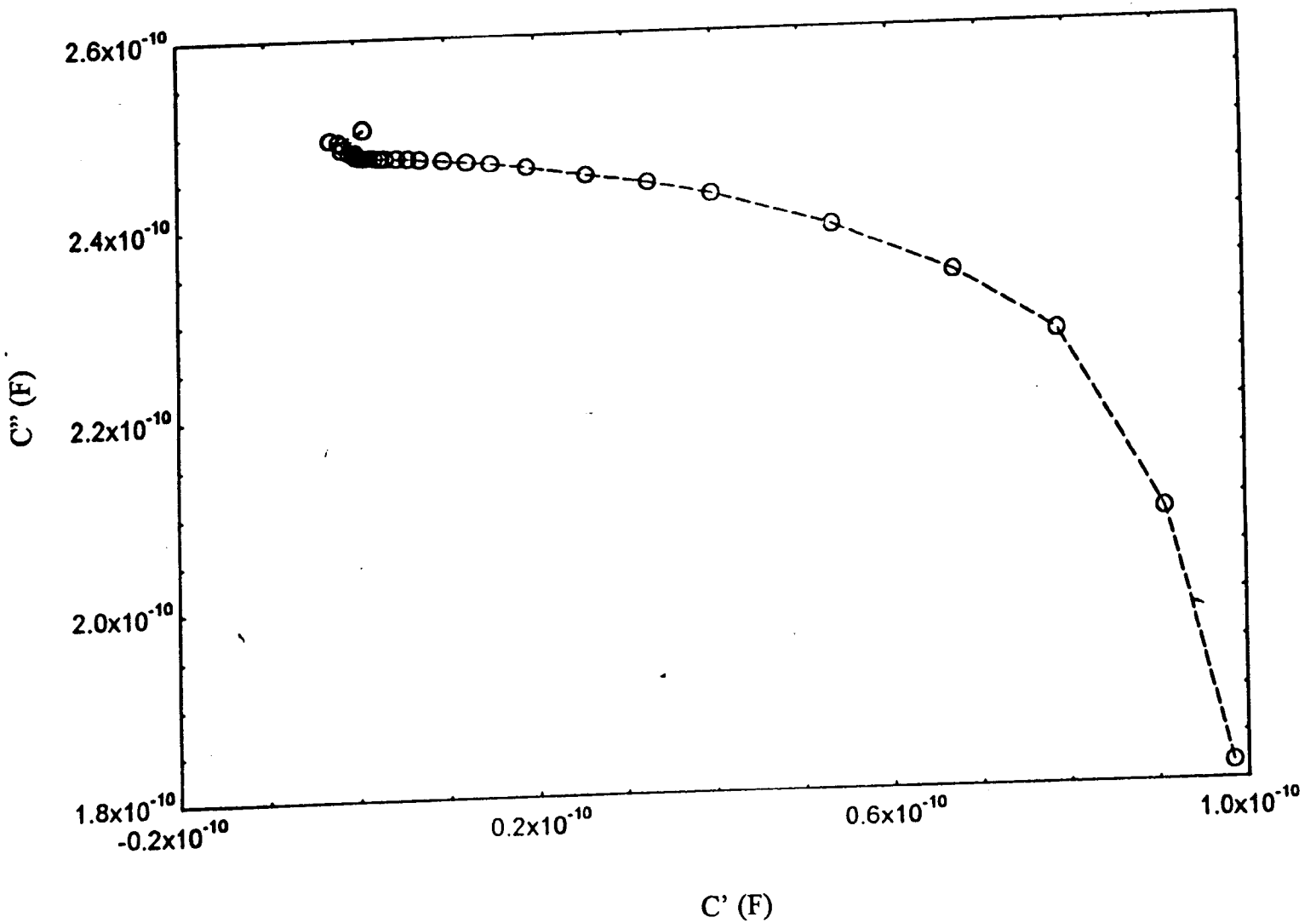

5.100 Cole-Cole plot for FCr(pc) at 292K

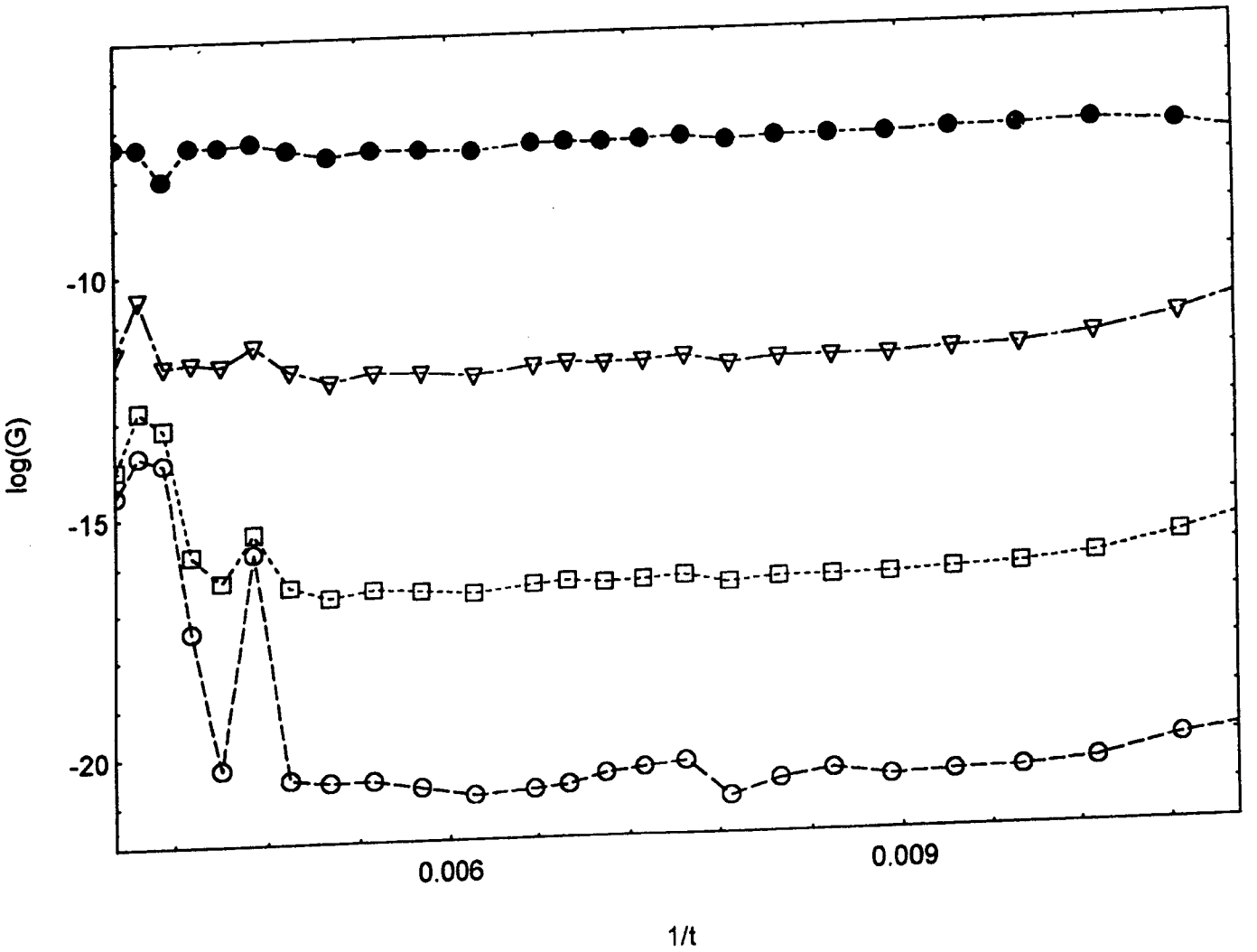

5.101 Activation energy plot for FCrPc at varying frequencies : top to bottom 1Mhz, 500kHz, 100kHz, 50kHz

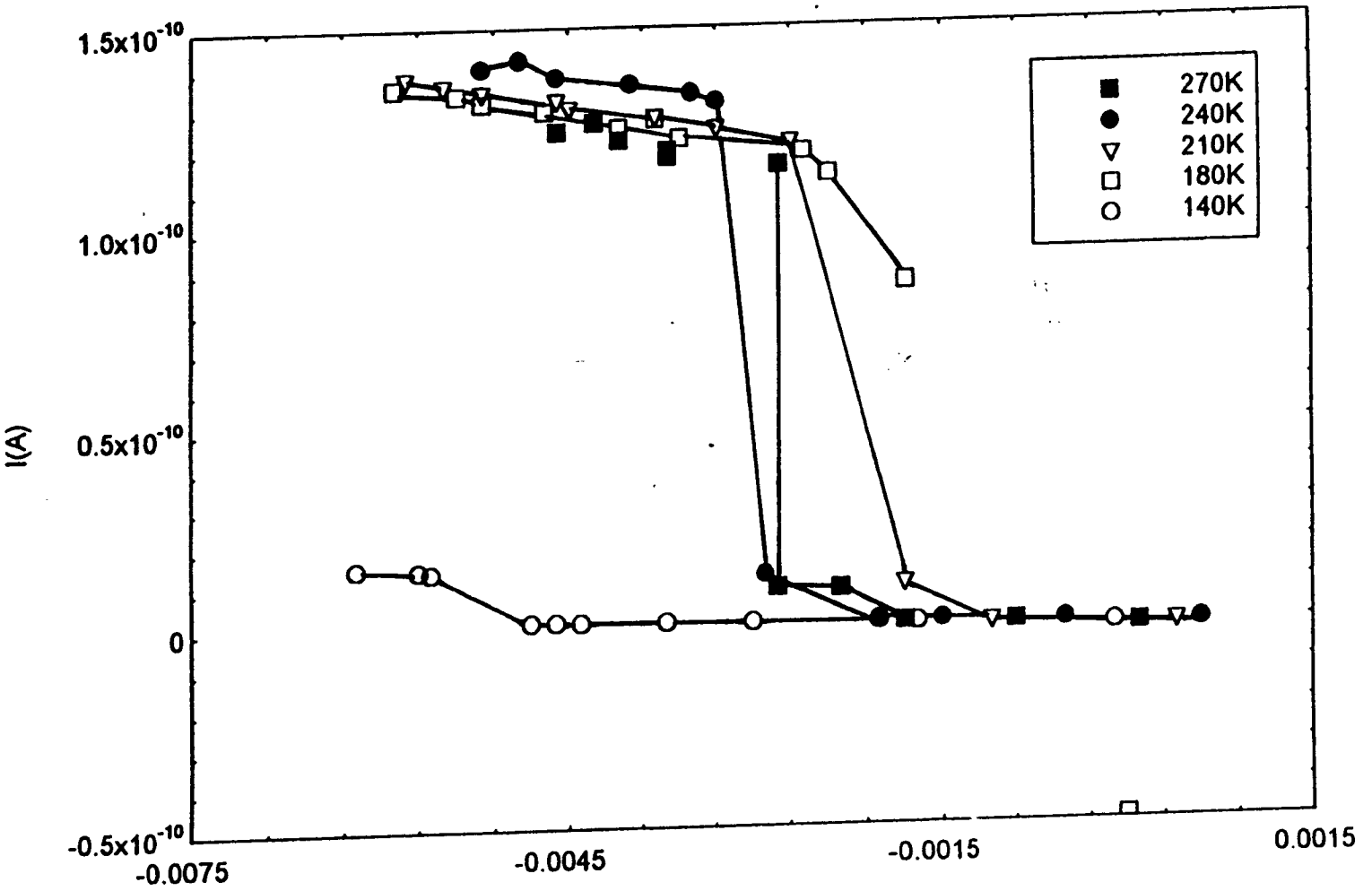

5.102. Dark current - voltage characteristic from 4-point method for FCrPc.

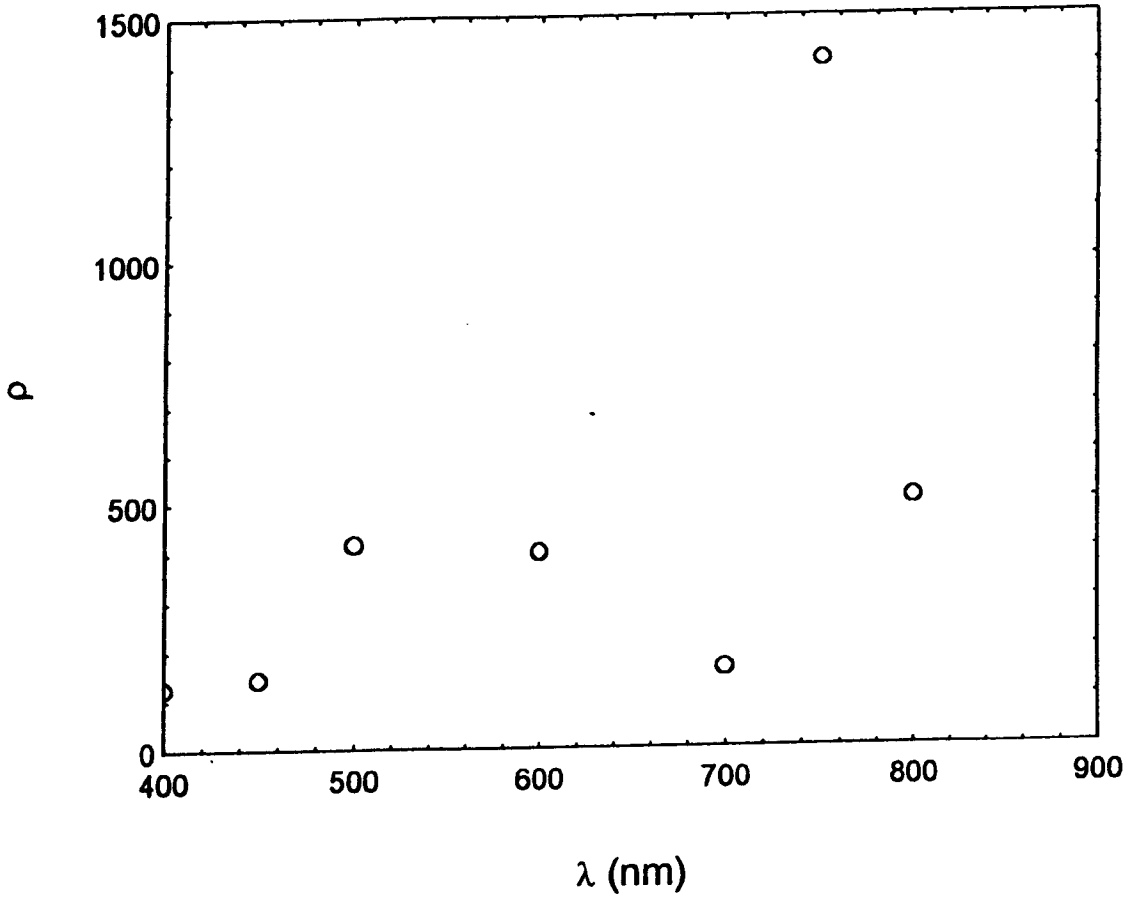

5.103 Resistivity versus incident wavelength for FCrPc at 100K

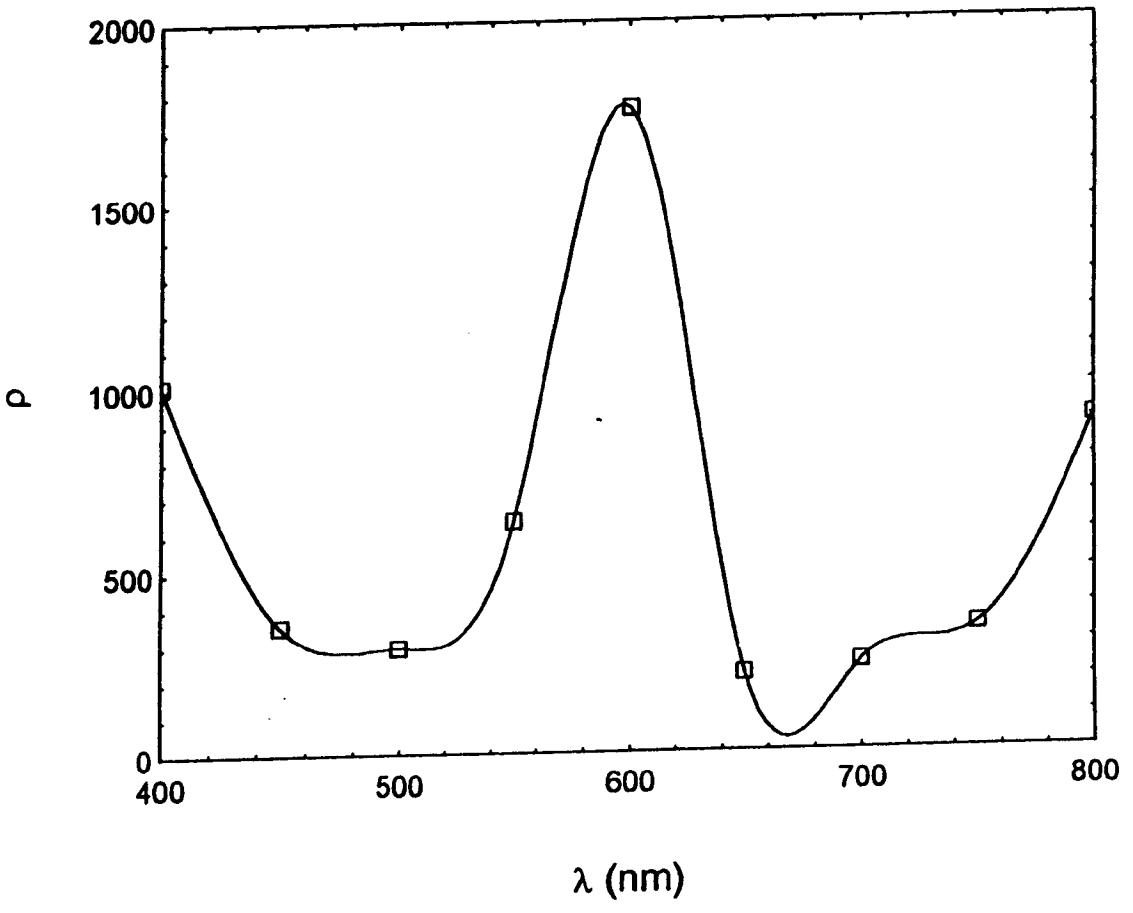

5.104 Resistivity versus incident wavelength for FCrPc at 140K

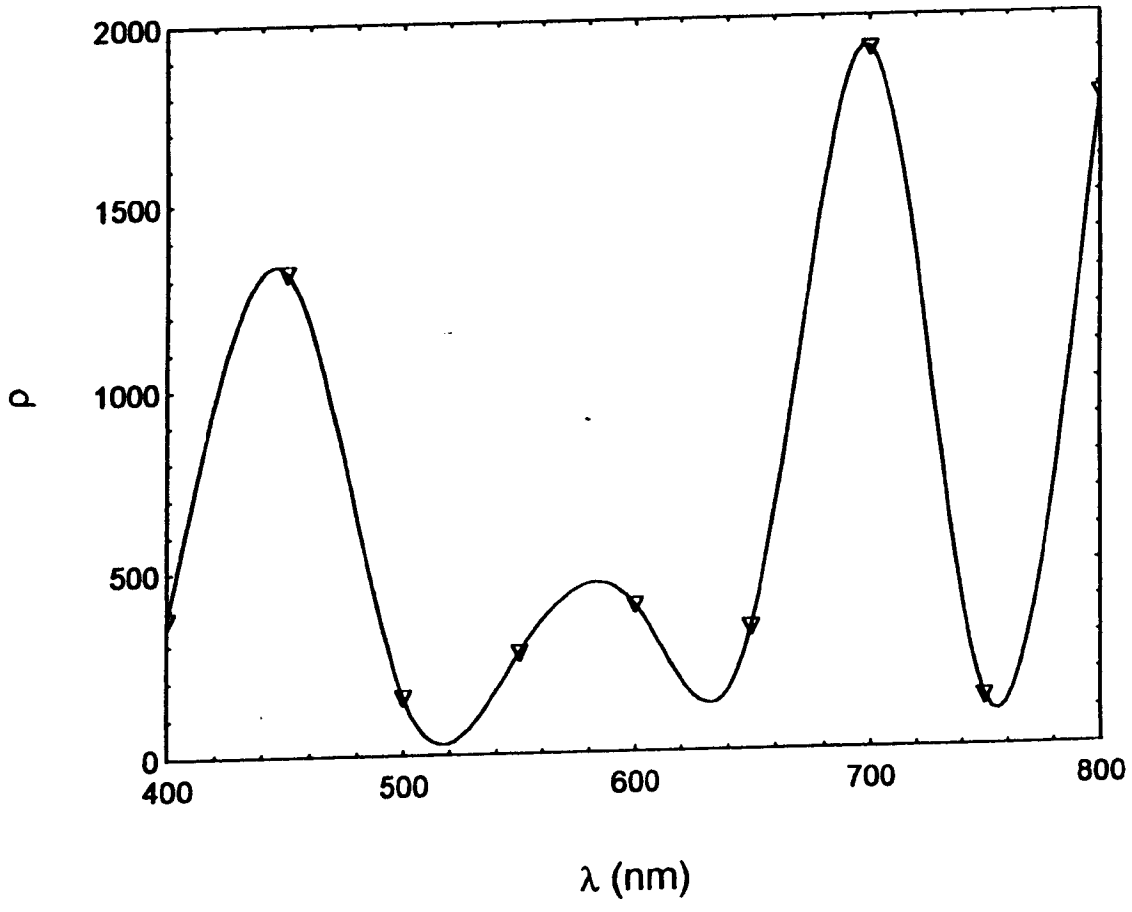

5.105 Resistivity versus incident wavelength for FCrPc at 180K

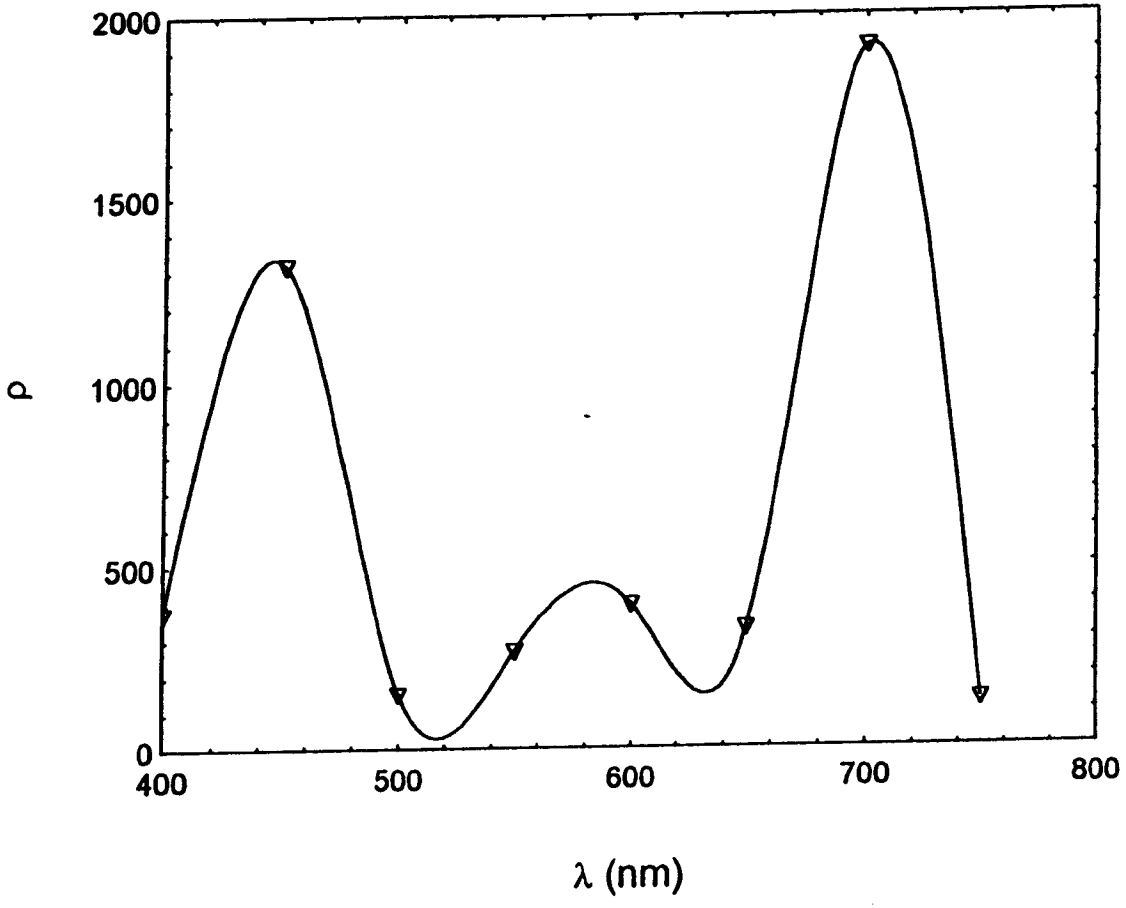

5.106 Resistivity versus incident wavelength for FCrPc at 210K

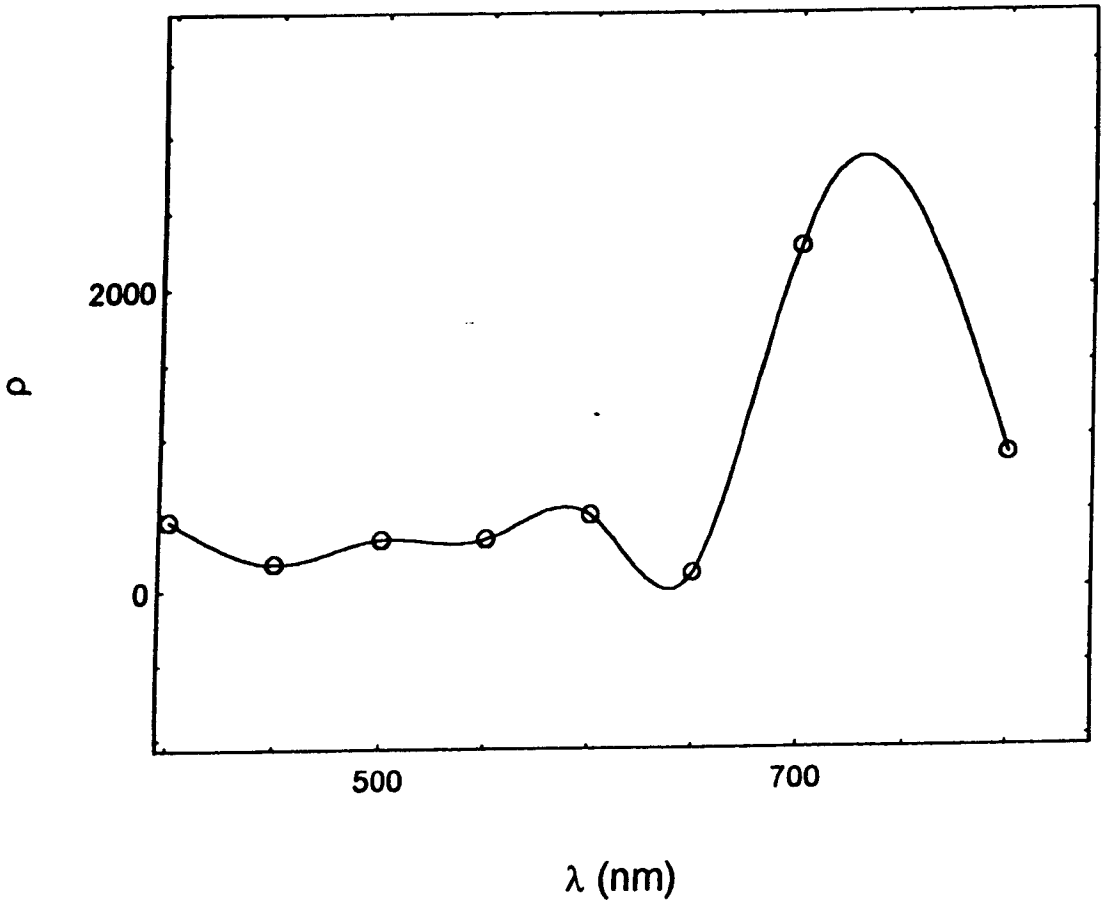

5.107 Resistivity versus incident wavelength for FCrPc at 240K

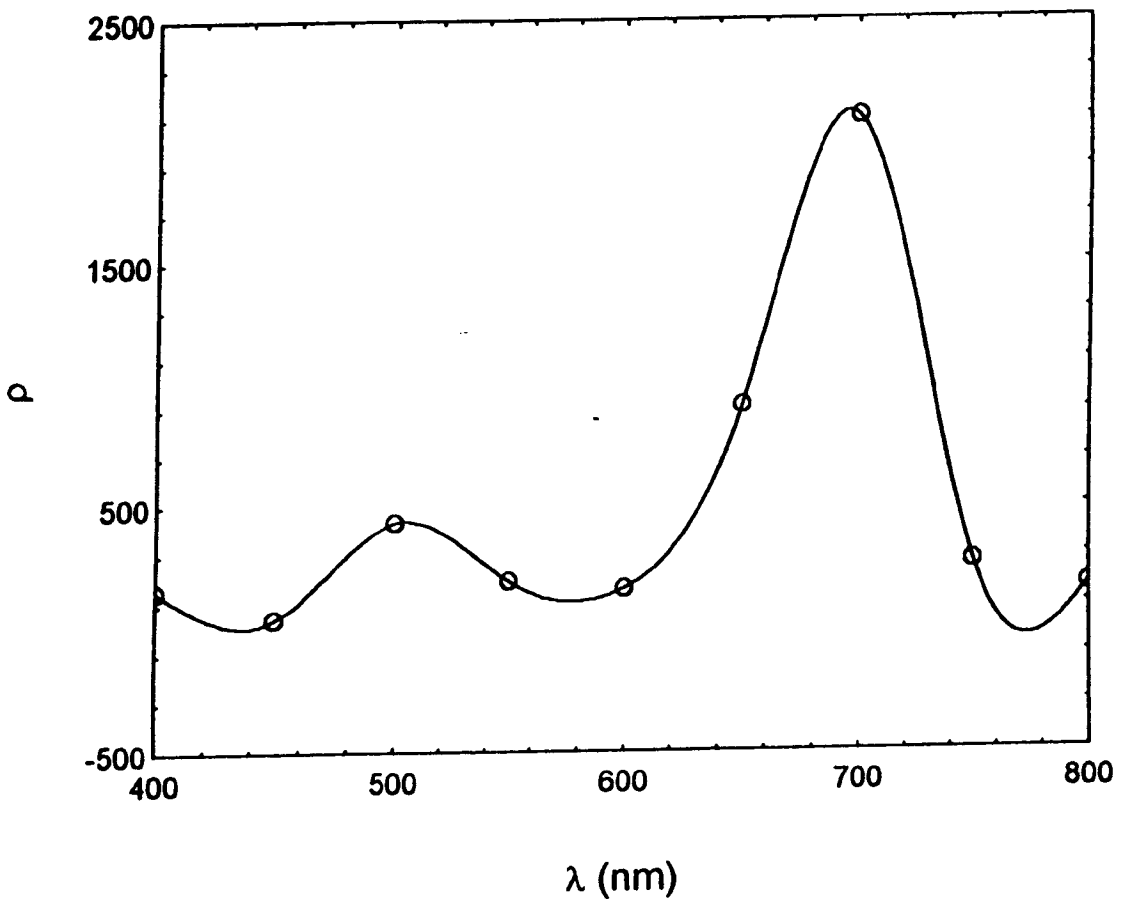

5.108 Resistivity versus incident wavelength for FCrPc at 270K

Chapter 6.

Conclusions and Suggestions for Further Work

By examining the combined results of our experiments and analysis, we are able to make some suggestions as to the electronic mechanisms occurring in the materials we have studied, and postulate advantages and possible applications of such properties in "real" devices for future use in the commercial and domestic arena.

The optical absorption data obtained for heavy fraction, thulium and gadolinium bisphthalocyanines suggest to us that the voltage cycling processes previously employed upon the samples tested do not cause a great degree of permanent change in the film oxidation state, and therefore it is possible that application of these materials as colour display elements may be carried out. Given that each material is capable of use as a red, green or blue filter to white light according to the applied potential, a matrix of small elements may be used to produce a backlit colour display. Whether this could find use in scenarios where fast switching is required depends upon the temporal susceptibility of the material oxidation state to a step change of applied voltage, a parameter outside the scope of our investigations here. Also, the expected lifetime of the material in terms of the number of switching cycles undertaken before visible degradation is an important factor.

We have established also from our optical data that the effect of the material structure within the films promotes obvious changes in the absorption spectrum and the associated optical parameters, the process being due to modification of the optical band energy centres primarily as a result of change in the intermolecular forces. It would be appropriate in further investigation to ascertain whether it is possible to exploit this property, for example whether adsorption of oxygen or other gases causes sufficient change to the film to be detectable in the refractive index or absorption spectrum. Should

this be viable, the necessity of electrical connection to the film itself would be obviated. As we have also established that the materials are of very low conductance, several distinct advantages are apparent for optical rather than electrical interrogation of the film; firstly, that noise produced by the effects of external electromagnetic influence becomes considerably less of a problem, since a photodetector would run at a current several orders of magnitude greater than that through a phthalocyanine film, greatly increasing the signal-to-noise ratio of the overall system. Secondly, the temperature effects upon the optical parameters are rather less pronounced than those affecting conductivity. Disadvantages, however, are that the complete system would have to be physically larger owing to an increase in the number of transducers present, and would for the same reason have a greater power requirement.

Establishment of the parameters for both ac and dc conduction in films of [HF(pc)(pc*)], [Lu(pc)(pc*)] and FCrPc have enabled us to offer predictions of the behaviour of such films over a wide range of temperatures and operational parameters, thus providing successive experimenters with the raw data for these novel materials necessary for future production of a model for their response to electrical excitation. This will obviate a great deal of time-consuming characterisation prior to the introduction of other parameters such as ambient effects. Our data suggest which theoretical models, and with what parameters, should be applied to conduction in the films.

The bisphthalocyanines tested, whilst not showing true ohmic conduction with gold electrodes, exhibit reproducible and symmetrical characteristics under vacuum. Conductivity changes resulting from humidity changes and oxygen adsorption were apparent, however, and degassing of the samples under high vacuum was necessary

before these reproducible data were recorded. Reproducible control of these parameters above vacuum ambient was however outside the scope of our measurement equipment. This reproducibility under controlled conditions is, however, a vital factor in any sensor or transducer application.

The photoresponse of fluorochromium phthalocyanine at all the measured temperatures from 100K to room temperature has offered promising results. Further characterisation of this material is advised on the grounds of our data, as it appears that the films are of particularly high photogeneration efficiency even at the low electric field strengths associated with the large interelectrode distance used in the van der Pauw sheet resistivity measurement. We have shown that this method is applicable for measurement of resistivity changes occurring as a result of photon excitation.

The computer controlled measurement system developed specifically for characterisation of these materials now covers all eventualities in this type of work, and will see considerable further use in the testing of similar materials.

Hence in summary, we have provided data concerning the effects of heating and voltage cycling on the optical parameters of the materials, showing that the structure and oxidation states cause visible effects on these. We have provided electronic band and conduction details for both alternating and direct current, and shown that for one of our materials (FCrPc) much promise is shown as a photoconducting medium. Also, the means for future experimenters to carry out similar work with ease has been provided during the course of the programme of work. We have shown that behaviour of the materials, although they possess novel substitutions, is in agreement with previously

published theoretical and empirical data, thus showing that the "family" resemblance of phthalocyanines and bisphthalocyanines is not simply restricted to structural factors, and hence it will be possible to gain some foreknowledge about the behaviour of further newly-synthesised compounds of the same type.

References

References

T.G. Abdel-Malik, A.M Abdeen, *phys. stat. sol.* (a) **72** (1982) 99-104

T G Abdel-Malik, A M Abdeen, H M El-Labany, A A Aly, *phys. stat. sol.* **72** (1982), 99-104

T G Abdel-Malik and G A Cox, *J Phys. C: Solid State Phys.*, **10** (1977), 63-74

S. N. Al-Refaie, *Appl. Phys. A* **51** (1990), 419-422

K Arshak and R Perrem, *J Phys D: Appl Phys.* **26** (1993), 1098-1102

H Austin Taylor, N Thon, *Symposium on Chemisorption of Gases and Solids*, proceedings, 1951.

S. Baker, Prof. G.G. Roberts, M.C. Petty, *IEE Proceedings*, **130**,1:5 (1983)

I Bedja, S Hotchandani, R Carpentier, K Vinodgopal, P V Kamat, *Thin Solid FIlms* **247** (1994), 195-200

D. Bélanger, J.P. Dodelet, L.H. Dao, B.A. Lombos, *J.Phys.Chem.* **88** (1984), 4288-4295

K B Blodgett, *J Am Chem Soc* **57**, 1007 (1935)

K B Blodgett and I Langmuir, *Phys. Rev.* **51**, 964 (1937)

J P Borgogno, F Flory, P Roche, B Schmitt, G Albrand, E Pelletier, H A Macleod. *Applied Optics* **23**,20 3567-3570 (1984)

E Brynda, L Kalvoda, I Koropecky, S Nespurek and J Rakusan, *Synthetic Matls* **37** (1990), 327-333

E. Brynda, L. Kalvoda, I. Koropecky, S. Nespurek, J Rakusan, *Thin Solid Films* **199** (1991), pp. 375-384

E Brynda, I Kminek, S Nespurek, *J.Mat. Sci.* **24** (1989) 4164-4167

E Brynda, I Koropecky, L kalvoda and S Nespurek, *Thin Solid Films* **199** (1992) 375-384

K.S. Cole, R. H. Cole, *J. Chem Phys.* **9** (1941), 341

A. Cole, R.J. McIlroy, S.C. Thorpe, M.J. Cook, J. McMurdo and A.K. Ray, *Sensors and Actuators B*, **13-14** (1993) 416-419

R A Collins, A Krier and A K Abass, *Thin Solid Films* **229,** 113 (1993) .

R A Collins, A Krier, A K *Thin Solid Films*, 1993. Accepted for publication

R A Collins, K Mohammed, *Thin Solid Films* **145** (1986), 133-145

M Cook, A J Dunn, *Thin Solid Films* **159** (1988) 395-404

M J Cook, J McMurdo, D A Miles, R H Poynter, J M Simmons, S D Haslam, R M Richardson, K Welford, *J Mater Chem.* **4(8)** (1994), 1205-1213

A. Das, A K Tripathi, A P Srivastava, *Indian J. Phys* **57a** (1983), 343-347

E. A. Davis and N. F. Mott, *Phil. Mag.* **22** (1970) 903.

S R Elliott, *Advances in Physics* **36** no. **2,** 138 (1987)

J Exley, A K Ray, M T Ahmet, J Silver, *J Mat. Sci: Materials in Electronics* **5** (1994), 180-184

A Fejfar, I H Biedermann, *Int J. Electronics* **73** (1992), 1051-1053

C.S. Frampton, J. N. O'Connor, J. Peterson and J. Silver, *Displays Tech. Appl.* **9** (1988) 174.

W Fulop, R Ginige, *Electronics Letters* **21** (1985) 439-441

A.K. Ghosh, D.L. Morel, T. Feng, R.F. Shaw, C.A. Rowe Jr., *J. Appl. Phys.* **45,1** (1974) 230-235

A. Gieren and W. Hoppe, *J. Chem. Soc. Chem. Comm.* **8** (1971) 413.

R D Gould, *J Appl Phys.* **53** (1982), 3353-3355

R D Gould, *J Phys D: Appl Phys.* **9** (1986) 1785-1790

R.D. Gould, A. K. Hassan,*Thin Solid Films* **223** (1993) 334-340

P Gupta, B Maiti, A B Maity, S Chaushuri, A K Pal, *Thin Solid Films* **260** (1995), 75-85

K.J. Hall, J.S. Bonham, L.E. Lyons, *Aust. J. Chem* **31** (1978) 1661-1677

C Hamann, *phys. stat. sol.* (a) **10.83** (1972), 83-90

C Hamann and A Mrwa, *Int J Electronics* **73** (1992), 1039-1040

R Hill, *J Phys. C: Solid State Physics* **7** (1974), 521-525

Z. Z. Ho, C. Y. Ju and W. M. Hetherington III, *J. Appl. Phys.* **62**, 716 (1987).

L. Honeybourne, J. O'Donnell, *RSC Analytical Division, Proceedings of Cardiff Symposium*, 1991

Y.L. Hua, M.C. Petty and G,.G. Roberts, *source obscured.* Published 1987.

T Ishida, S Wako and S Ushio, *Thin Solid Films* **39** (1976), 227-235

B B Ismail and R D Gould, *phys. stat. sol. (a)* **115** (1989), 237-245

S.A. James, A.K Ray, J. Silver, *phys. stat. sol. (a)* **129** (1992) 435

M Jaros, A W Beavis, P J Hagon, R J Turton, A Miloszewski, K B Wong, *Thin Solid Films* **222** (1992), 205-208

Jiang, A.D. Lu, X.M. Pang and Y.L. Hua, *Thin Solid Films* **199** (1991) 173-179

T A Jones, B Bott, *Sensors and Actuators* **9** (1986), 27-37

R Jones, R H Tredgold, P Hodge and A Hoorfar, *Thin Solid Films* **113** (1984), 115-128

A K Jonscher, *Dielectric Relaxation in Solids*, Chelsea Dielectrics Press, 1983.

L Kalvoda, E Brynda, *Thin Solid Films* **232** (1993) 120-125

Steven T Kirsch, *Applied Optics.* **20:12** 2085-2089 (1981)

N Koda, *Japanese Journal of Applied Physics*, **26** (1987), 182-183

S B Krupanidhi, M Sayer and A Mansingh, *Thin Solid Films* **113** (1984), 173-184

C M Lampert, *Thin Solid Films* **236** (1993), 6-13

I Langmuir, J *Am Chem Sci*, **39**, 1848 (1917)

X Lin, H Wang, K Lin, Y Yu and S Fu, *Thin Solid Films* **237** (1994), 310-313

Y Lin, H Shigeara, A Yamada, Thin Solid Films 179, 303 (1989)

J Liu and L Feng, *Thin Solid Films* **235** (1993), 76-7

Y. Liu, K. Shigehara, M. Hara and A. Yamada, J. Am. Chem. Soc. **113** (1991) 440.

J.P Lloyd, C. Pearson and M.C.Petty, *Thin Solid Films* **160** (1988) 431-443

E D Lucia and F D Verderame, *J Chem Phys.*, **48** (1968), 2674-2684

B. Lukas, D.R. Lovett and J. Silver, *Thin Solid Films*, **210/211** (1992) 213.

R Mach, P Flögel, L G Suslina, A G Areshkin, J Maege and G Voigt, *phys. stat. sol. (b)* **109** (1982), 607-615

M Maitrot, G Guillaud, B Boudjems, J J Andre and J Simon, *J Appl Phys.* **60** (1986), 2396-2399

J C Manifacier, J Gasiot, J P Fillard . *J. Phys. E : Scientific Instruments* 9 (1976) 1002-1004

P Mark, W Helfrich, *J App Phys* **33** (1962), 205-215

E Márquez, J Ramírez-Malo, P Villares, R Jiménez-Garay, P J S Ewen and A E Owen. *J Phys.D, Applied Physics*, **25** (1992) 535-541

P. N. Moskalev and I. S. Kirin, *Opt. Spectrosc.* **29** (1970) 220.

T.S. Moss, G.J. Burrell and B. Ellis, *Semiconductor Opto-electronics*, (Butterworth, London 1973), p.10

N F Mott and E A Davis, *Electronic processes in Non-crystalline Materials*, Claredon Press, Oxford 1979, p. 291.

S Mukhopadhyay, *PhD thesis*, 1990

S Mukhopadhyay and A K Ray, *Int J Electronics* **73/5** (1992), 1055-1058

V Nagesh, H G Grimmeiss, H Presting, H Kibbel and E Kasper, *Thin Solid Films* **222** (1992), 265-268

H. S. Nalwa, P. Vasudevan, *J. Mat. Science Letters* **2** (1983) 22-24

M M Nicholson, in Chapter 2 of *Phthalocyanines, Properties and Applications* (ed. C C Leznoff and A B P Lever. VCH Publishers, NewYork 1993) Vol 3 Chapter 2 p. 77 .

Nima Technology Ltd. *Trough Operating System Manual,* private publication (1987)

J. O'Donnell, Ph.D thesis, Bristol Polytechnic1990

M. Petty, D. R. Lovett and J. M. O'Connor, *Thin Solid Films*, **179** (1989) 387.

M Petty, D R Lovett, J R Miller and J Silver, *J Mater. Chem.* **1**, 971 (1991) .

M Petty, D R Lovett, J M O'Connor and J Silver, *Thin Solid Films* **79,** 387 (1989).

M Petty, D R Lovett, P Townsend, J M O'conor and J Silver, *J Appl. Phys.* **22,** 1604 (1989).

A Pockels, *Nature* **43** (1891) 437

A A Ramadan, R D Gould, A Ashour, *Thin Solid films* **239** (1994), 272-275

A K Ray, S Mukhopadhyay and M J Cook, *personal communication.* (1992)

A. K. Ray, S. Mukhopadhyay and M. J. Cook, *Phys. Stat. Sol. (a)*, 1992, **134**, K73.

A K Ray and C A Hogarth, *Int J Electronics* **73/5** (1992), 1027-1037

J.M Robertson, *J. Chem. Soc.* 1935, 615

M. L. Roderiguez-Mendez, R. Aroca, J. A. DeSaja, *Chem. Mater.*, **4** (1992) 1017.

A.M. Saleh, R. D. Gould, A.K. Hassan, *phys. stat. sol. (a)* **139** (1993) 379-389

T S Shafah and R D Gould, *Int J Electronics* **69** (1990), 3-9

U Seiferheld, H Bässler, B Movaghar, *Physical Review Letters* **51** (1983), 813-816

J Silver, *New Scientist*, 30 th September 48, (1989)

J. Silver, P. Lukes, P. Hey and M.T. Ahmet, *J. Mater. Chem.*, **2** (1992) 841.

J. Silver, P. Lukes, A. Houlton, S. Howe, P. Hey and M.T. Ahmet, *J. Mater. Chem.*, **2** (1992) 849.

J. Silver, P. Lukes, S. D. Howe and B. Howlin, *J. Mater. Chem.* **1** (1991) 29.

J. Simon and J.J. Andre, *Molecular Semiconductors*, Springer Verlag, Berlin, 1984, 124.

S A Song, J M O'Connor, D J Barber and J Silver, *J Crystal Growth* **88,** 477 (1988).

J Souto, R Aroca and J A Desaja, *J Raman Spectroscopy* **22,** 349 (1991) .

Y Sripathi, G B Reddy, L K Malhotra, *J Mat Sci: Materials in Electronics* **2** (1991), 109-111

M. J. Stillman and T. Nyokong, in *Phthalocyanines-Properties and applications*, ed. C.C. Lenznoff and A.P.B. Lever, VCH Publishers, Inc., New York, 1989, p.133.

A Sussman, *J Appl Phys.* **38** (1967), 2738-2747

R Swan, A K Ray and C A Hogarth, *Phys. Stat. Sol(a)* **127,** 555 (1991).

J Sworakowski, S Nespurek, *J Appl Phys.* **65(4)** (1989), 1559-1565

T Tagaki, I Yamada, A Saaski, *J Vac Sci Technol.* **23** (1975) 1128

J Takada, H. Awaji, M. Koshiolka, A. Nakajima, W.A. Nevin, *App. Phys. Lett.* **61**(18) (1992)

J. Tauc, in *The optical properties of solids*, ed. F. Abeles, North-Holland, Amsterdam, 1970, p.277.

T A Temofonte and K F Schoch, *J Appl Phys* **65** (1989), 1350-1355

S Tutihasi, G G Roberts, R C Keezer and R E Drews, *Physical Review* **177.3** (1969), 1143-1150

A J Twarowski, *J Chem Phys.* **76(5)** (1982), 2640

H Valerian and S Nespurek, *J Appl Phys.* **73** (1993), 4370-4377

L J van der Pauw, *Philips Research Reports* **13**, (1958) 1-9

Y A Vidadi, L Rozenshtein, E A Chistyakov, *Soviet Physics-Solid State* **11** (1969), 173-175

P.S. Vukusic and J.R. Sambles, *Thin Solid Films* **221** (1992) 311-317

C.R. Westgate and G. Warfield, *J. Chem. Phys.* **46:1** (1967) 94-97

A Wilson, R Collins, phys. stat. sol. (a) **98** (1986) 633-644

M Yamamoto, T Sugiyama, M Tanaka. *Japan. J. App. Phys.* **24**, 305 (1985)

M Yoneyama, M Sugi, M Saito, K Ikegami, S Kuroda and S Lizima, *Japanese Journal of Applied Physics*, **25** (1986), 961-965

Appendix A.
QBASIC Program for Control of Instrumentation for Electrical Measurements - INST.BAS (Developed by the author)

Listing of the program used to collect measurement data, together with associated variables.

Global Variables

Variable	Meaning
cvlo	C:V voltage lower limit
cvhi	C:V voltage upper limit
lv1	I:V lower V limit for regime 1
hv1	I:V upper V limit for regime 1
s1	Voltage step for regime 1
lv2	I:V lower V limit for regime 2
hv2	I:V upper V limit for regime 2
s2,	Voltage step for regime 2
lv3	I:V lower V limit for regime 3
hv3	I:V upper V limit for regime 3
s3	Voltage step for regime 3
meastype	flag for type of measurement
wflag	toggle for temperature warning
oflag	optical van der Pauw flag
sett	set temperature
t	temperature
ovpvol	optical van der Pauw applied voltage
vvl	van der Pauw voltage lower limit (sets current)
vvh	van der Pauw voltage upper limit (sets current)
td	delay between temperature change and measurement (minutes)
md	delay between measurement points (seconds)
md$	string of md
td$	string of td
sv	set voltage for van der Pauw
nd$	file name for saving previous directories data
flag1	on/off setting for I/V sequence 1
flag2	on/off setting for I/V sequence 2
flag3	on/off setting for I/V sequence 3
fio$	filename
f	frequency
cvf	C:V fixed frequency

```
DECLARE SUB cvchange ()
DECLARE SUB cvmeas ()
DECLARE SUB smeas ()
DECLARE SUB rmeas ()

DECLARE SUB phvdp ()
DECLARE SUB switch (meastype!)
DECLARE SUB optcal ()
DECLARE SUB cd ()
DECLARE SUB auto ()
DECLARE SUB diode ()
DECLARE SUB paramchange ()
DECLARE SUB VDP (vvl!, vvh!, sv!)
COMMON SHARED cvlo, cvhi
COMMON SHARED lv1, hv1, s1, lv2, hv2, s2, lv3, hv3, s3, f, meastype, wflag, ovpvol, oflag
COMMON SHARED sett, t, vvl, vvh, td, md, md$, td$, sv, nd$, flag1, flag2, flag3, fio$, cvf
```

```
DECLARE SUB ivm ()
DECLARE SUB SVARS ()
DECLARE SUB iv (VMIN, VMAX, STP)
DECLARE SUB lcr ()
DECLARE SUB MENU ()
DECLARE SUB init ()
DECLARE SUB tempcon ()
DECLARE SUB changet (nt!)
REM start
CALL init
CALL MENU

Data for frequency points of LCR Meter
100
DATA 20,25,30,40,50,60,80,100,120,150,200,250,300,400,500,600,800,1000,1200
DATA 1500,2000,2500,3000,4000,5000,6000,8000,10000,12000,15000,20000,25000
DATA 30000,40000,50000,60000,80000,100000,120000,150000,200000,250000,300000
DATA 400000,500000,600000,800000,1000000

Data for temperature points
500
DATA 77,82,87,92,97,102,107,112,117,122,127,132,137,142,147,152
DATA 162,172,182,192,202,212,222,232,242,252,262,272,282,292

SUB auto (this performs fully automatic control of temperature and measurement sequences)

lcrflag = 7
vdpflag = 7
ivflag = 7
cvflag = 7
CLS
COLOR (7)
LOCATE 27, 35: PRINT "RUNNING"


FOR count = 1 TO 30
cur = count
RESTORE 500
FOR r = 1 TO (cur - 1) (sets temperatures)
READ t: NEXT
READ t
nt = t
sett = t
CALL changet(nt)
td: TIME$ = "00:00:00"

400 pr$ = INKEY$ (stop/go keyboard inout)
22
PRINT #3, "R1" + CHR$(10) (write set temperature to serial port for ITC4)
INPUT #3, t$
IF LEFT$(t$, 1) <> "R" THEN GOTO 22
nowt = (VAL(RIGHT$(t$, LEN(t$) - 1))) / 10
COLOR (14)
LOCATE 3, 24: PRINT "Set Temperature is "; sett; " K    "
LOCATE 5, 23: PRINT "  Temperature is "; nowt; " K    "
COLOR (7)
LOCATE 13, 25: PRINT "Time delay is "; td; " minutes."
```

```
LOCATE 15, 28: PRINT "Time now is "; TIME$
COLOR (15)
LOCATE 25, 15: PRINT "Press N to measure NOW, or P to pause/continue"
LOCATE 19, 27: COLOR (vdpflag): PRINT "VDP measurements : "; (toggle measurement types on/off)
IF vdpflag = 7 THEN PRINT "OFF" ELSE PRINT " ON"
LOCATE 20, 27: COLOR (ivflag): PRINT "I/V measurements : ";
IF ivflag = 7 THEN PRINT "OFF" ELSE PRINT " ON"
LOCATE 21, 27: COLOR (lcrflag): PRINT "LCR measurements : ";
IF lcrflag = 7 THEN PRINT "OFF" ELSE PRINT " ON"
LOCATE 22, 27: COLOR (cvflag): PRINT "C/V measurements : ";
IF cvflag = 7 THEN PRINT "OFF" ELSE PRINT " ON"

COLOR (7)
LOCATE 23, 27: PRINT "C/V/I/L to trigger on/off"
IF pr$ = "v" AND vdpflag = 7 THEN vdpflag = 14: pr$ = ""
IF pr$ = "v" AND vdpflag = 14 THEN vdpflag = 7: pr$ = ""
IF pr$ = "i" AND ivflag = 7 THEN ivflag = 14: pr$ = ""
IF pr$ = "i" AND ivflag = 14 THEN ivflag = 7: pr$ = ""
IF pr$ = "l" AND lcrflag = 7 THEN lcrflag = 14: pr$ = ""
IF pr$ = "l" AND lcrflag = 14 THEN lcrflag = 7: pr$ = ""
IF pr$ = "c" AND cvflag = 7 THEN cvflag = 14: pr$ = ""
IF pr$ = "c" AND cvflag = 14 THEN cvflag = 7: pr$ = ""


(The next section switches in the correct instrument via the Farnell switching unit and then calls the appropriate measurement subroutine)
IF pr$ = "q" THEN GOTO esa
IF pr$ = "p" THEN GOSUB pause
IF (TIME$ <> td$) AND (pr$ <> "n") THEN 400
IF (nowt <> (sett - 2) OR nowt > (sett + 2)) AND wflag = 14 THEN GOTO warning
IF lcrflag = 14 THEN meastype = 3: CALL switch(meastype): CALL lcr: meastype = 0: CALL switch(meastype)
IF ivflag = 14 THEN meastype = 2: CALL switch(meastype): CALL ivm: meastype = 0: CALL switch(meastype)
IF vdpflag = 14 THEN meastype = 1: CALL switch(meastype): CALL VDP(vvl, vvh, sv): meastype = 0: CALL switch(meastype)
IF cvflag = 14 THEN meastype = 3: CALL switch(meastype): CALL cvmeas: meastype = 0: CALL switch(meastype)

NEXT
GOTO esa

pause:
pt$ = TIME$
998
COLOR (15)
LOCATE 27, 35: PRINT "WAITING"
co$ = INKEY$: IF co$ <> "p" THEN 998
TIME$ = pt$
COLOR (7)
LOCATE 27, 35: PRINT "RUNNING"
RETURN

warning: (option to give audible warning if temperature drifts)
CLS
pt$ = TIME$
9980 co$ = INKEY$
SOUND 0, 9
SOUND 1560, 9
987 PRINT #3, "R1" + CHR$(10)
INPUT #3, t$
IF LEFT$(t$, 1) <> "R" THEN GOTO 987
nowt = (VAL(RIGHT$(t$, LEN(t$) - 1))) / 10
COLOR (14)
```

```
LOCATE 3, 24: PRINT "Set Temperature is "; sett; " K    "
LOCATE 5, 23: PRINT "  Temperature is "; nowt; " K    "
COLOR (15)
pa$ = INKEY$: IF pa$ = "q" THEN GOTO esa
LOCATE 15, 12: PRINT "TEMPERATURE WARNING : PAUSED : CHECK LEVEL AND FLOW"
IF nowt <> (sett - 2) OR nowt > (sett + 2) THEN GOTO 9980
TIME$ = pt$
COLOR (7)
CLS
LOCATE 27, 35: PRINT "RUNNING"
GOTO td

esa:
END SUB
```

(Previous directories are stored in a file, and any one of the last ten used may be recovered)

```
SUB cd
CLS
COLOR (15)
OPEN "c:\gpib-pc\prevdirs.dat" FOR INPUT AS #10
FOR n = 1 TO 9
INPUT #10, dir$
PRINT n; " "; dir$
NEXT
CLOSE #10
PRINT

PRINT "(Number to select, or 0 for new directory.)"
999 s$ = INKEY$: IF s$ = "" THEN 999
IF s$ = "0" THEN 1000
OPEN "c:\gpib-pc\prevdirs.dat" FOR INPUT AS #10
FOR n = 1 TO VAL(s$)
INPUT #10, dir$
NEXT n
CLOSE #10
CHDIR dir$
nd$ = dir$
GOTO escd
1000
INPUT "New directory (full name)... ", nd$
MKDIR nd$
OPEN "newdir.dat" FOR OUTPUT AS #11
OPEN "c:\gpib-pc\prevdirs.dat" FOR INPUT AS #10
INPUT #10, dir$
FOR n = 1 TO 8
INPUT #10, dir$
PRINT #11, dir$
NEXT
CLOSE #10
PRINT #11, nd$
CLOSE #11
OPEN "newdir.dat" FOR INPUT AS #11
OPEN "c:\gpib-pc\prevdirs.dat" FOR OUTPUT AS #10
FOR n = 1 TO 9
INPUT #11, dir$
PRINT #10, dir$
NEXT
CLOSE #10
CLOSE #11
KILL "newdir.dat"
```

```
escd:
END SUB

(This subroutine has the variable NT [new temperature] passed to it and sets the controller accordingly)
SUB changet (nt)
nt = INT(10 * nt)
se$ = RIGHT$(STR$(nt), LEN(STR$(nt)) - 1)
do$ = "T+" + se$
PRINT #3, do$
INPUT #3, ru$
END SUB


(This creates a submenu of PARAMCHANGE enabling the operator to select voltage limits and frequencies for the C:V measurement)
SUB cvchange
9011 CLS
PRINT "                    C/V Measurement Parameters"
PRINT
PRINT "L : Change Lower  Voltage Limit, presently "; cvlo; " mV"
PRINT "H : Change Higher Voltage Limit, presently "; cvhi; " mV"
PRINT "F : Change Fixed Frequency, presently "; cvf; " Hz."
PRINT : PRINT "Q : Return to Previous Menu"

9012 cvc$ = INKEY$: IF cvc$ = "" THEN 9012
IF cvc$ = "l" THEN INPUT "New value ? ", cvlo
IF cvc$ = "h" THEN INPUT "New value ? ", cvhi
IF cvc$ = "f" THEN INPUT "New value ? ", cvf
IF cvc$ = "q" THEN 9013

GOTO 9011


9013 END SUB

(This performs C:V measurements on the LCR meter)
SUB cvmeas
CLS
PRINT "Frequency is set to "; cvf; " Hz."
PRINT #1, "remote 4"
PRINT #1, "output 4;func:imp cpg" (set LCR meter to measure parallel capacitance and conductance)
PRINT #1, "output 4;trig:imm"

f$ = RIGHT$(STR$(cvf), LEN(STR$(cvf)) - 1)

do$ = "Freq " + f$ + "Hz"
PRINT #1, "output 4;" + do$ (set frequency)

fb$ = "t_" + RIGHT$(STR$(sett), LEN(STR$(sett)) - 1) + ".cvm" (open file for data, with automatically selected file name)
OPEN fb$ FOR OUTPUT AS #7

FOR osv = 10 TO 500 STEP 10
op$ = "VOLT" + STR$(osv) + " mv"
PRINT #1, "output 4;" + op$ (set voltage)

PRINT #1, "output 4;trigger;fetch?" (collect reading)
PRINT #1, "enter 4"
INPUT #2, cap$, dil$
PRINT #7, STR$(osv) + " " + cap$
NEXT osv
```

```
CLOSE #7


END SUB

SUB diode (under development)

END SUB


(initialisation of remotely controlled instruments. Sets up the GPIB board, and makes certain all the machines are ready to listen)
SUB init
OPEN "GPIB0" FOR OUTPUT AS #1
OPEN "GPIB0" FOR INPUT AS #2
PRINT #1, "ABORT"
PRINT #1, "REset"
OPEN "com1:9600,n,8,2" FOR RANDOM AS #3
FOR rty = 0 TO 1000: NEXT
PRINT #3, "C1"
FOR rty = 0 TO 1000: NEXT
PRINT #3, "A1"
FOR rty = 0 TO 1000: NEXT
PRINT #3, "A1" + CHR$(10)
lv1 = 0: hv1 = 1: s1 = .05
lv2 = 1.2: hv2 = 5: s2 = .2
lv3 = 6: hv3 = 10: s3 = 1
vv1 = 0: vvh = 10: sv = 2
wflag = 7
md = 10: td = 10   'sec... min...
md$ = "00:00:" + RIGHT$(STR$(md), LEN(STR$(md)) - 1)
td$ = "00:" + RIGHT$(STR$(md), LEN(STR$(md)) - 1) + ":00"

PRINT md$, td$
flag1 = 14: flag2 = 14: flag3 = 14
END SUB

(performs current:voltage measurements between the limits defined by the global variables VMIN and VMAX, with step size STP)
SUB iv (VMIN, VMAX, STP)
inc = STP
PRINT #1, "remote 8"
PRINT #1, "output 8;Z1XC0XG1XF1XO1X"
FOR v = VMIN TO VMAX STEP inc
vs$ = "V" + STR$(v) + "X"
PRINT #1, "output 8;" + vs$
TIME$ = "00:00:00"
4 sto$ = INKEY$: IF sto$ = "q" THEN CLOSE #4: GOTO esiv
IF TIME$ <> md$ THEN 4
PRINT #1, "enter 8"
INPUT #2, da$
PRINT #4, STR$(v) + " " + da$
LOCATE 10, 34: PRINT "Voltage = "; v; " V      "
LOCATE 12, 30: PRINT "Current = "; da$; " A      "

NEXT

esiv:
CLS
```

```
END SUB

SUB ivm (selects values from the measurement parameters table and passes them to SUB IV)
CLS
PRINT "                Current/Voltage Measurements"
PRINT
PRINT
fil$ = "t_" + MID$(STR$(sett), 2) + ".IVM"
OPEN fil$ FOR OUTPUT AS #4
IF flag1 = 14 THEN CALL iv(lv1, hv1, s1)
IF flag2 = 14 THEN CALL iv(lv2, hv2, s2)
IF flag3 = 14 THEN CALL iv(lv3, hv3, s3)
PRINT #1, "output 8;OOX"
CLOSE #4
END SUB

(performs C:F, G:F and D:F measurements, file names T_*.cap, .con and .dil)
SUB lcr
CLS
PRINT "                LCR meter running..."
fa$ = "t_" + RIGHT$(STR$(sett), LEN(STR$(sett)) - 1) + ".cap"
PRINT #1, "remote 4"
PRINT #1, "output 4;func:imp cpg"
PRINT #1, "output 4;trig:imm"
RESTORE 100
fb$ = "t_" + RIGHT$(STR$(sett), LEN(STR$(sett)) - 1) + ".con"
OPEN fa$ FOR OUTPUT AS #6
OPEN fb$ FOR OUTPUT AS #7
FOR I = 1 TO 48
READ f
LOCATE 12, 28: COLOR (12): PRINT "Measuring C and G."
LOCATE 14, 28: COLOR (15): PRINT "Frequency "; f; " Hz."
f$ = RIGHT$(STR$(f), LEN(STR$(f)) - 1)
do$ = "Freq " + f$ + "Hz"
PRINT #1, "output 4;" + do$
TIME$ = "00:00:00"

220 sto$ = INKEY$: IF sto$ = "q" THEN CLOSE #6: CLOSE #7: GOTO eslc
IF TIME$ <> md$ THEN 220
PRINT #1, "output 4;trigger;fetch?"
PRINT #1, "enter 4"
INPUT #2, cap$, con$
LOCATE 16, 28: PRINT "G = "; con$; " S"
LOCATE 18, 28: PRINT "C = "; cap$; " F"
PRINT #6, STR$(f) + " " + cap$
PRINT #7, STR$(f) + " " + con$
NEXT
CLOSE #6
CLOSE #7

PRINT #1, "remote 4"
PRINT #1, "output 4;func:imp cpd"
PRINT #1, "output 4;trig:imm"

RESTORE 100
fb$ = "t_" + RIGHT$(STR$(sett), LEN(STR$(sett)) - 1) + ".dil"
OPEN fa$ FOR OUTPUT AS #6
OPEN fb$ FOR OUTPUT AS #7
CLS
PRINT "                LCR meter running..."
```

```
FOR I = 1 TO 48
LOCATE 12, 28: COLOR (12): PRINT "Measuring C and D"
LOCATE 14, 28: COLOR (15): PRINT "Frequency "; f; " Hz."
READ f
fS = RIGHT$(STR$(f), LEN(STR$(f)) - 1)
do$ = "Freq " + fS + "Hz"
PRINT #1, "output 4;" + do$
TIME$ = "00:00:00"
210 sto$ = INKEY$: IF sto$ = "q" THEN CLOSE #6: CLOSE #7: GOTO eslc
IF TIME$ <> md$ THEN 210
PRINT #1, "output 4;trigger;fetch?"
PRINT #1, "enter 4"
INPUT #2, cap$, dil$
LOCATE 16, 28: PRINT "D = "; dil$
LOCATE 18, 28: PRINT "C = "; cap$; " F"

PRINT #6, STR$(f) + " " + cap$
PRINT #7, STR$(f) + " " + dil$
NEXT
CLOSE #6
CLOSE #7

eslc:
CLS
END SUB

SUB m

END SUB

Generates main menu for the program)
SUB MENU
20 CLS
SCREEN 12

COLOR (14)
PRINT "          Variable Temperature Measurements"
COLOR (7)
PRINT
PRINT "              Directory : "; nd$
PRINT
COLOR (15)
PRINT : PRINT : PRINT
PRINT "S :                    Change Directory"
PRINT : PRINT "C :            Change Parameters for Measurements"
PRINT "T :                    Set Temperature"
PRINT "J :                    C/V Measurements"
PRINT "V :                    Van der Pauw Measurements"
PRINT "L :                    A.C. Measurements"
PRINT "D :                    Diode Measurements"
PRINT "I :                    I/V Measurements"
PRINT : PRINT "A :                    Automatic Measurements"
PRINT : PRINT "O :                    Optical Spectrum Calibration"
PRINT "P :            Photoelectric van der Pauw measurements"
PRINT : PRINT "E :                    Return to DOS"
10 op$ = INKEY$
IF op$ = "" THEN 10
IF op$ = "c" THEN fs = 1: CALL paramchange
IF op$ = "v" THEN fs = 1: meastype = 1: CALL switch(meastype): CALL VDP(vvl, vvh, sv): meastype = 0: CALL switch(meastype)
IF op$ = "I" THEN fs = 1: meastype = 3: CALL switch(meastype): CALL lcr: meastype = 0: CALL switch(meastype)
```

```
IF op$ = "d" THEN fs = 1: CALL diode
IF op$ = "i" THEN fs = 1: meastype = 2: CALL switch(meastype): CALL ivm: meastype = 0: CALL switch(meastype)
IF op$ = "a" THEN fs = 1: CALL auto
IF op$ = "t" THEN fs = 1: CALL tempcon
IF op$ = "e" THEN fs = 1: SYSTEM
IF op$ = "s" THEN fs = 1: CALL cd
IF op$ = "o" THEN fs = 1: CALL optcal
IF op$ = "p" THEN fs = 1: CALL phvdp
IF op$ = "j" THEN fs = 1: CALL cvmeas
IF fs = 1 THEN fs = 0: GOTO 20

GOTO 10
END SUB

SUB now

END SUB
```

(This uses the optical power meter to measure incident light at a range of wavelengths from 380nm to 900nm)

```
SUB optcal
CLS
PRINT "Optical Power Calibration Correction : Apply Sensor to Source and Press Key.."
444 pr$ = INKEY$: IF pr$ = "" THEN 444
PRINT #1, "gpibeos out cr lf"
PRINT #1, "gpibeos in cr lf"
PRINT #1, "remote 7"
PRINT #1, "output 7;C0"
OPEN "spec.dat" FOR OUTPUT AS #30
FOR n = 380 TO 900 STEP 5
f$ = "W0" + RIGHT$(STR$(n), LEN(STR$(n)) - 1)
PRINT #1, "output 7;" + f$
PRINT #1, "output 7;F2"
PRINT #1, "enter 7"
LINE INPUT #2, en$
po$ = RIGHT$(en$, 5)
PRINT #30, STR$(n) + " " + po$

LOCATE 14, 27: PRINT "Wavelength : "; n; " nm"
LOCATE 16, 26: PRINT "Power : "; po$; " microwatt"

NEXT
CLOSE #30

END SUB
```

(This allows the parameters and limits for all types of measurements to be customized, recalled or saved.)

```
SUB paramchange
40 CLS
PRINT "                Parameter Changes Menu"
PRINT
COLOR (flag1)
PRINT "X : I/V Sequence 1 is ";
IF flag1 = 14 THEN PRINT " ON" ELSE PRINT "OFF"
COLOR (15)
PRINT "1 : Lower Voltage Limit 1 for I/V, presently "; lv1; " V."
PRINT "2 : Upper Voltage Limit 1 for I/V, presently "; hv1; " V."
PRINT "3 : Step  Voltage  Size 1 for I/V, presently "; s1; " V."
PRINT
COLOR (flag2)
```

```
PRINT "Y : I/V Sequence 2 is ";
IF flag2 = 14 THEN PRINT " ON" ELSE PRINT "OFF"
COLOR (15)
PRINT "4 : Lower Voltage Limit 2 for I/V, presently "; lv2; " V."
PRINT "5 : Upper Voltage Limit 2 for I/V, presently "; hv2; " V."
PRINT "6 : Step  Voltage  Size 2 for I/V, presently "; s2; " V."
PRINT
COLOR (flag3)
PRINT "Z : I/V Sequence 3 is ";
IF flag3 = 14 THEN PRINT " ON" ELSE PRINT "OFF"

COLOR (15)
PRINT "7 : Lower Voltage Limit 3 for I/V, presently "; lv3; " V."
PRINT "8 : Upper Voltage Limit 3 for I/V, presently "; hv3; " V."
PRINT "9 : Step  Voltage  Size 3 for I/V, presently "; s3; " V."
PRINT
PRINT "A : Lower Voltage Limit for Van der Pauw, presently "; vvl; " V."
PRINT "B : Upper Voltage Limit for Van der Pauw, presently "; vvh; " V."
PRINT "C : Step  Voltage  Size for Van der Pauw, presently "; sv; " V."
COLOR (13)
PRINT "F : C/V Measurement Parameters (separate menu)"
COLOR (15)
PRINT
PRINT "M : Measurement Delay (Seconds), currently "; md
PRINT "T : Temperature Change Delay (Minutes), currently "; td
PRINT : PRINT "W : Temperature Warning is ";
COLOR (wflag)
IF wflag = 14 THEN PRINT " ON" ELSE PRINT "OFF"
COLOR (15)
PRINT : PRINT "Q : return; R/S : recall/save measurement regime"
50 pc$ = INKEY$
IF pc$ = "" THEN 50
IF pc$ = "x" AND flag1 = 14 THEN flag1 = 7: pc$ = ""
IF pc$ = "x" AND flag1 = 7 THEN flag1 = 14: pc$ = ""
IF pc$ = "y" AND flag2 = 14 THEN flag2 = 7: pc$ = ""
IF pc$ = "y" AND flag2 = 7 THEN flag2 = 14: pc$ = ""
IF pc$ = "z" AND flag3 = 14 THEN flag3 = 7: pc$ = ""
IF pc$ = "z" AND flag3 = 7 THEN flag3 = 14: pc$ = ""
IF pc$ = "w" AND wflag = 7 THEN wflag = 14: pc$ = ""
IF pc$ = "w" AND wflag = 14 THEN wflag = 7: pc$ = ""
IF pc$ = "r" THEN CALL rmeas
IF pc$ = "s" THEN CALL smeas

PRINT

IF pc$ = "1" THEN INPUT "New Value "; lv1
IF pc$ = "2" THEN INPUT "New Value "; hv1
IF pc$ = "3" THEN INPUT "New Value "; s1
IF pc$ = "4" THEN INPUT "New Value "; lv2
IF pc$ = "5" THEN INPUT "New Value "; hv2
IF pc$ = "6" THEN INPUT "New Value "; s2
IF pc$ = "7" THEN INPUT "New Value "; lv3
IF pc$ = "8" THEN INPUT "New Value "; hv3
IF pc$ = "9" THEN INPUT "New Value "; s3
IF pc$ = "a" THEN INPUT "New Value "; vvl
IF pc$ = "b" THEN INPUT "New Value "; vvh
IF pc$ = "c" THEN INPUT "New Value "; sv
IF pc$ = "f" THEN CALL cvchange
IF pc$ = "m" THEN GOSUB mdchange
```

```
IF pc$ = "t" THEN GOSUB tdchange



IF pc$ = "q" THEN GOTO es2
GOTO 40

tdchange:
INPUT "New Value "; td
td$ = "00:"
IF md < 10 THEN td$ = td$ + "0"
td$ = td$ + RIGHT$(STR$(td), LEN(STR$(td)) - 1) + ":00"
RETURN

mdchange:
INPUT "New Value "; md
md$ = "00:00:"
IF md < 10 THEN md$ = md$ + "0"
md$ = md$ + RIGHT$(STR$(md), LEN(STR$(md)) - 1)
RETURN

es2:
END SUB

(measures resistivity of a sample with a particular wavelength of incident light.)
SUB phvdp
oflag = 1
FOR wl = 380 TO 900 STEP 10
CLS : LOCATE 15, 20: PRINT " Set Wavelength to "; wl; " nm and press a key."
1234 wa$ = INKEY$: IF wa$ = "q" THEN GOTO esph
IF wa$ = "" THEN GOTO 1234
to$ = RIGHT$(STR$(sett), LEN(STR$(sett)) - 1)
wo$ = RIGHT$(STR$(wl), LEN(STR$(wl)) - 1)
fio$ = "T" + to$ + "W" - wo$
meastype = 1: CALL switch(meastype): CALL VDP(vvl, vvh, sv): meastype = 0: CALL switch(meastype)
NEXT
oflag = 0
esph:
CLS
END SUB

(load measurement parameters from disc)
SUB rmeas
REM params  flag1,lv1,hv1,s1 ...2...3 ,vvl,vvh,sv,ovpvol,md,td,wflag
CLS
PRINT " Please enter a file name to load the measurement regime..."
INPUT mss$
OPEN mss$ FOR INPUT AS #36
INPUT #36, flag1, lv1, hv1, s1, flag2, lv2, hv2, s2, flag3, lv3, hv3, s3, vvl, vvh, sv, cvf, cvlo, cvhi, md, td, wflag
CLOSE #36
CLS

END SUB

(save measurement parameters to disk)
SUB smeas
REM params  flag1,lv1,hv1,s1 ...2...3 ,vvl,vvh,sv,ovpvol,md,td,wflag
CLS
PRINT " Please enter a file name to save the measurement regime..."
INPUT mss$
```

```
OPEN mss$ FOR OUTPUT AS #36
PRINT #36, flag1, lv1, hv1, s1, flag2, lv2, hv2, s2, flag3, lv3, hv3, s3, vvl, vvh, sv, cvf; cvlo, cvhi, md, td, wflag
CLOSE #36
CLS
END SUB
```

(connects the reqiured instrument to the sample via the switching unit, according to the type of measurement used (global MEASTYPE))

```
SUB switch (meastype)

'                       meastype :
'                       1 : van der Pauw
'                       2 : I/V
'                       3 : LCR
'                       uses block F


IF meastype = 1 THEN PRINT #1, "output 14; d22f11"
IF meastype = 2 THEN PRINT #1, "output 14; d00f00"
IF meastype = 3 THEN PRINT #1, "output 14; d00f22"
IF meastype = 0 THEN PRINT #1, "output 14; d00f00"


END SUB
```

(collect new temperature value via the keyboard)

```
SUB tempcon
CLS
PRINT #3, "R1": INPUT #3, t$
COLOR (15)
PRINT "      Press 'T' to change temperature or any other key to proceed"
1 g$ = INKEY$
IF g$ = "" THEN 1
IF g$ <> "t" THEN 2
PRINT
INPUT "                  New temperature : ", nt
sett = nt
CALL changet(nt)
2 END SUB
```

(performs four-point probe resistivity measurement)

```
SUB VDP (vvl, vvh, sv)
inc = sv
CLS
PRINT "              Van der Pauw running... Please Wait"
PRINT #1, "remote 8"
PRINT #1, "output 8;Z1XC0XG1XF1XO1X"
PRINT #1, "REMOTE 13"
PRINT #1, "OUTPUT 13;U3M0I3R3T1"

LOCATE 3, 38: COLOR (15): PRINT "I"; : COLOR (12): PRINT "a"; : COLOR (14): PRINT "b"; : COLOR (14)
IF oflag = 0 THEN fil$ = "t_" + MID$(STR$(sett), 2) + ".IAB" ELSE fil$ = fio$ + ".iab"
OPEN fil$ FOR OUTPUT AS #4
PRINT #1, "REMOTE 14": PRINT #1, "OUTPUT 14;D00"
GOSUB MEAS
CLOSE #4
LOCATE 3, 38: COLOR (15): PRINT "I"; : COLOR (12): PRINT "a"; : COLOR (9): PRINT "d"; : COLOR (14)

IF oflag = 0 THEN fil$ = "t_" + MID$(STR$(sett), 2) + ".IAD" ELSE fil$ = fio$ + ".iaD"
OPEN fil$ FOR OUTPUT AS #4
PRINT #1, "REMOTE 14": PRINT #1, "OUTPUT 14;D11"
```

```
GOSUB MEAS
CLOSE #4
PRINT #1, "output 8;O0X"
PRINT #1, "output 14;d00"
GOTO es

(subsection of VDP to drive meters)
MEAS:
FOR v = vvl TO vvh STEP sv
vs$ = "V" + STR$(v) + "X"
PRINT #1, "output 8;" + vs$
TIME$ = "00:00:00"
sto$ = INKEY$: IF sto$ = "q" THEN CLOSE #4: GOTO es
6 IF TIME$ <> md$ THEN 6
PRINT #1, "enter 8"
INPUT #2, da$
PRINT #1, "ENTER 13"
INPUT #2, db$
db$ = LEFT$(db$, 10)
LOCATE 15, 20: PRINT " I = "; da$; "A;  V = "; db$; " V."
PRINT #4, (db$ + " " + da$)
NEXT
RETURN
es:
END SUB
```

The program offers all the types of data collection which are at present required by the various operators of the measurement system, although by virtue of the structured nature of the QuickBASIC language, any further development is simply a matter of adding a further subroutine and changing the main menu to accommodate it. This has been brought to bear in addition of routines requested by other users of the system:

(1) to provide capacitance:voltage measurements at fixed frequencies,

and (2) to perform high curent measurements on other samples using a larger power supply.

Appendix B.

Refereed Paper

JOURNAL OF MATERIALS SCIENCE: MATERIALS IN ELECTRONICS 5 (1994) 180–184

Electrical and optical properties of sublimed films of heavy-fraction rare-earth-element bisphthalocyanines

J. EXLEY, A. K. RAY
Physical Electronics and Fibre-optics Research Group, School of Engineering Information Technology, Sheffield Hallam University, City Campus, Pond Street, Sheffield, S1 1WB, UK

M. T. AHMET, J. SILVER
Department of Chemistry and Biological Chemistry, University of Essex, Wivenhoe Park, Colchester, Essex, CO4 3SQ, UK

Steady-state electrical measurements and optical-absorption experiments were performed on 50 nm thick samples of sublimed heavy-fraction rare-earth-element bisphthalocyanines films. From the Arrhenius plot of $\ln \sigma(T)$ (where $\sigma(T)$ is the conductivity at temperature T it was found that two conduction regimes existed. The activation energy of 0.18 eV at high temperatures ($T > 162$ K) relates to the distance of singlet states below the conduction band. The low-temperature activation energy of 4 meV indicates hopping conduction between localized states close to the Fermi level. Visible optical spectra in both absorption and transmission modes were obtained for the sample. The absorption data were analysed in terms of a well-known power law, and a value of 2.3 eV was found for the optical gap, E_0. Estimates of the refractive indices and the dielectric constants were made over the visible spectrum.

1. Introduction

The spectroelectrochemical properties of rare-earth-element bisphthalocyanine complexes have been extensively studied because of their potential applications in multicolour electrochromic devices [1–5]. Electrochromism is observed when samples of bisphthalocyanine derivatives are subjected to reduction or oxidation processes through a series of voltage cycling. The neutral compounds are generally green but they turn red on oxidization in which the loss of one electron per molecule takes place. When the compounds are reduced, they become blue on the addition of one electron per molecule. Further addition of an electron per molecule induces a change in colour to purple. The samples are generally prepared by depositing sublimed [6, 7] or Langmuir-Blodgett [8, 9] films of bisphthalocyanines onto transparent conducting electrodes such as indium tin oxide (ITO) glass substrates.

The purpose of this paper is to report on the results for electrical measurements of, and optical absorption in, heavy-fraction rare-earth bisphthalocyanine, [HF(pc)(pc*)] (where pc is a phthalocyanato dianion, pc* is a phthalocyanato monoradical cation, HF is a mixture of heavy-fraction rare-earth elements as found in partially refined heavy fractions or as in previously reported compounds [10]. This paper is divided into four sections. Section 2 is devoted to a description of the experimental techniques employed. The results from the measurements are presented in Section 3. Since the colour change is due to the occurrence of optical absorption at different frequencies, knowledge of the dispersion of optical constants such as the complex refractive index, N, and the dielectric constant, ε^*, is basic to an understanding of electrochromic behaviour. Using the one-electron theory, electrical and optical properties are then evaluated from the experimental data, and a full discussion is given in Section 4. Finally, Section 5 deals with the conclusions reached from treatments of the experimental results.

2. Experimental details

Heavy-fraction bisphthalocyanine [HF(pc)(pc*)] molecules were vacuum sublimed in an Edwards coater onto the surfaces of glass substrates. Using a Rank Taylor Hobson Form Talysurf instrument, the thickness of the deposited film was determined by obtaining the surface profile of the sample over the interface region between the film/glass substrate. A correction factor was introduced in order to compensate for the slight deviation of the sample surface from the horizontal.

For electrical characterizations, insulating substrates were used. A pattern of electrodes was generated by the vacuum deposition of copper through an all-steel mask onto the [HF(pc)(pc*)] film surface. The electrodes were approximately 1 mm in diameter. During the electrode deposition, the substrate was kept cooled at liquid-nitrogen temperature. Direct current (d.c.) measurements were made on the samples

0957–4522 © *1994 Chapman & Hall*

in planar configurations in a vacuum of the order of 10^{-4} Pa inside an Oxford Instruments liquid-nitrogen cryostat. Leads were attached to the sample electrodes by means of silver paint. With the help of a Keithley 617 digital electrometer in a microprocessor-controlled instrumentation system, the in-plane circulating current, I, was monitored as a function of the d.c. bias potential, V, at various temperatures from 77 to 300 K. The sample was maintained under an environment of nitrogen gas throughout the investigation, so as to avoid the formation of ice on the sample and to prevent any possible influence of adsorbed oxygen on the material properties. Using a Phillips PU8720 ultraviolet/visible spectrophotometer, optical absorption and transmission spectra were obtained for [HF(pc)(pc*)] compounds at room temperature in air between 1.4 and 4 eV. For these investigations, these films were prepared on ITO glass substrates. An uncoated substrate was used as a reference in the single-beam spectrophotometer, so that the output was solely in terms of the transmission characteristics of the films.

3. Results

Electrical measurements were performed on untreated [HF(pc)(pc*)] bisphthalocyanine film in planar configurations, and a characteristic material parameter, such as the d.c. activation energy, was deduced. The optical data were analysed in order to obtain information regarding the dispersion of the refractive index, the tails of localized states and the optical gaps. The film thickness was found to be 50 nm.

3.1. Electrical measurements

The circulating current, I, was measured for [HF(pc)(pc*)] films as the applied bias potential, V, was varied up to 100 V, both in the forward and the reverse directions. Fig. 1 displays a family of curves showing the typical variation of the current as a function of the applied d.c. voltage at five different temperatures from 77 to 297 K. The $I(V)$ characteristics were reproducible and symmetrical in both the forward and the reverse directions. This implies that the field due to the applied potential is symmetrically distributed in the bulk of the film. This conduction is not strictly ohmic, but at a given temperature, T, the current was found to have a power-law dependence on the potential, V, of the form

$$I = \rho V^s \qquad (1)$$

where the coefficient ρ and the index s are both temperature-dependent quantities. The value of s varied from 0.7 at 77 K to 1.1 at room temperature. ρ, on the other hand, had the values 7.2 $k\Omega^{-1} V^{0.3}$ and 21 $\Omega^{-1} V^{-0.1}$ at corresponding temperatures. The temperature of transition from the dependence with $s < 1$ to that with $s > 1$ is believed to be 162 K in which the $I(V)$ characteristic is found to be truly ohmic. As expected, the conduction generally increased with the rise in temperature, but the rate of the rise in conductivity was not as large at temperatures below 127 K as at temperatures above 127 K.

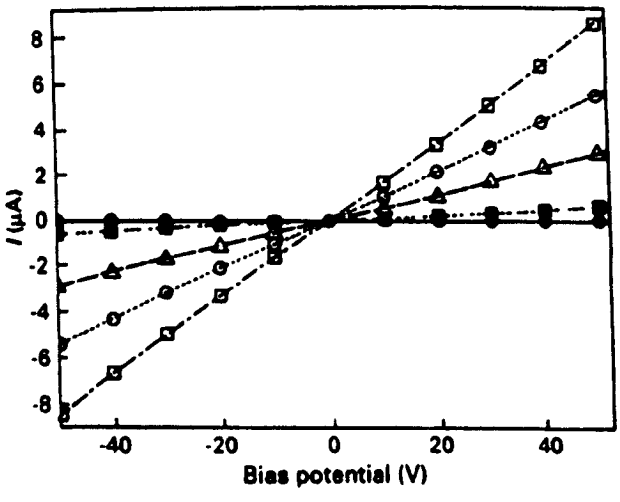

Figure 1 A set of five curves showing the variation of the circulating current through a 50 nm thick heavy-fraction bisphthalocyanine [HF(pc)(pc*)] film as a function of the applied bias potential up to ± 50 V, at different temperatures: (□) 297 K, (○) 267 K, (△) 247 K, (■) 207 K, and (●) 77 K. The device structure was planar; aluminium electrodes were used.

3.2. Optical measurements

Fig. 2 displays the absorption and transmittance spectra within the visible optical frequency range. The reflectivity, R, is also shown as a function of photon energy, $h\nu$. As expected, $R + T + A = 1$, where the absorption, A, and the transmittance, T, are given in terms of I_0 and I_t, the input and output optical intensities, respectively. Values of $[\ln(I_0/I)/t]$ are calculated for α as a function of the photon energy, $h\nu$, since the absorption coefficient, α, for [HF(pc)(pc*)] films of thickness t is defined by the condition that the energy in the wave falls to a value of exp(− 1) in a distance α^{-1}. Like monophthalocyanines, [HF(pc)(pc*)] films are found to be strongly absorbing materials, with α of the order of 10^7 m^{-1}. Fig. 3 shows typical features of absorption in bisphthalocyanine molecules in the visible region; the absorption rising to the Q-band peak at about 1.9 eV is probably due to a_{1u}–e_g type transitions [9]. There is also a noticeable

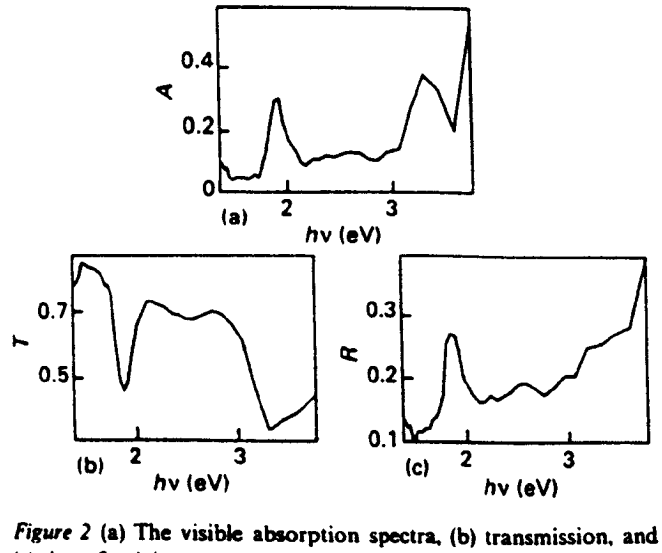

Figure 2 (a) The visible absorption spectra, (b) transmission, and (c) the reflectivity spectra.

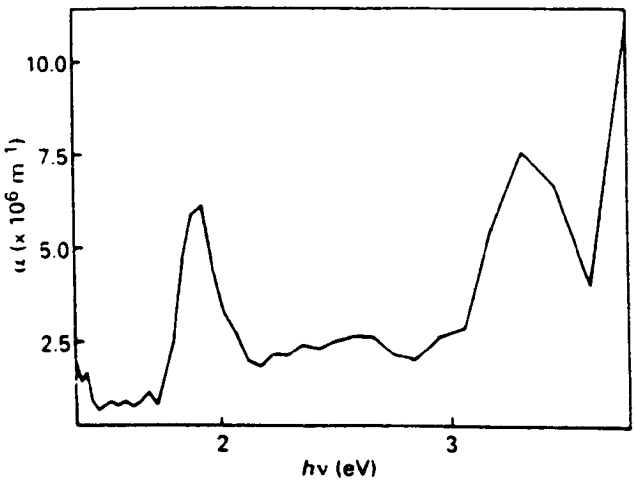

Figure 3 The variation of the absorption coefficient with the incident photon energy for a 50 nm thick [HF(pc)(pc*)] film.

broadening of the Q-band, which may be due to the interaction of molecules in the solid phase. In vapour spectra of these materials, it is normally possible to identify five bands Q, B, N, L and C; these are characteristic of the phthalocyanine ring. The B-band is seen to be located at approximately 3.0 eV. The N-, L- and C-bands have been noted to occur between 4 and 6 eV; and they were therefore outside the scope of our measurements. In sublimed films of monophthalocyanine complexes, the minimum of the transparent band usually occurs at $h\nu \approx 2.4$ eV [11]. For [HF(pc)(pc*)] films, an extra peak is observed within the energy window 2.2–2.4 eV. This peak is referred to as a radical band and has been shown to be present only in neutral and oxidized [M(pc)(pc*)] materials [12].

4. Discussion

In order to understand the conduction processes involved, values of ln I_c are plotted in Fig. 4 against the inverse of temperature, T^{-1}, where I_c is the circulating current at a bias potential of 50 V. For a given geometry of the device, the circulating current at a constant potential may be taken as a measure of the conductivity, σ, therefore, the resulting curve may be regarded as being an Arrhenius variation of the conductivity with temperature in the usual form:

$$\sigma = \sigma_0 \exp\left(-\frac{E_a}{kT}\right) \qquad (2)$$

The symbol E_a represents the activation energy. σ_0 is the value of the conductivity, σ, as $T \to \infty$. It can be observed from Fig. 3 that the activation energy, E_a, is a temperature-dependent quantity. For the high-temperature regime (that is, $T \geq 162$ K), the activation energy is estimated to be 0.18 eV. The activation energy for the low-temperature region was found to be very small, of the order of 7 meV. A tentative band diagram for electronic transport is given for phthalocyanines in [13]. The intrinsic band gap is normally believed to be 2.0 eV. Although this value is likely to vary, depending upon the nature of the central metal atom, the two values obtained for E_a are considered too small to excite carriers from the valence band to the conduction band. Singlet states, S_1, which lie in the energy-band gap of a phthalocyanine film are believed to be involved with the conduction at high temperatures, since the activation energy of 0.18 eV in this temperature regime compares well with the value of 0.21 eV for the approximate distance of the singlet state from the conduction-band edge. The low-temperature activation energy, on the other hand, is thought to be associated with hopping of carriers between localized states close to the Fermi level. The existence of these states is consistent with the non-crystalline nature of sublimed films.

The optical absorption data were analysed within the framework of the one-electron theory for molecular solids in order to obtain information on the density of localized states and the optical band gap. It was observed that, for the range of incident photon energies between 1.66 and 1.9 eV, there was a sharp increase in the values of the absorption, α. From the linear variation of the logarithm of α with the photon energy, $h\nu$, given in Fig. 5, this increase is found to be exponential and in the form of the Urbach relation

$$\alpha(\nu) = \alpha_0 \exp[(h\nu/\Delta) - b] \qquad (3)$$

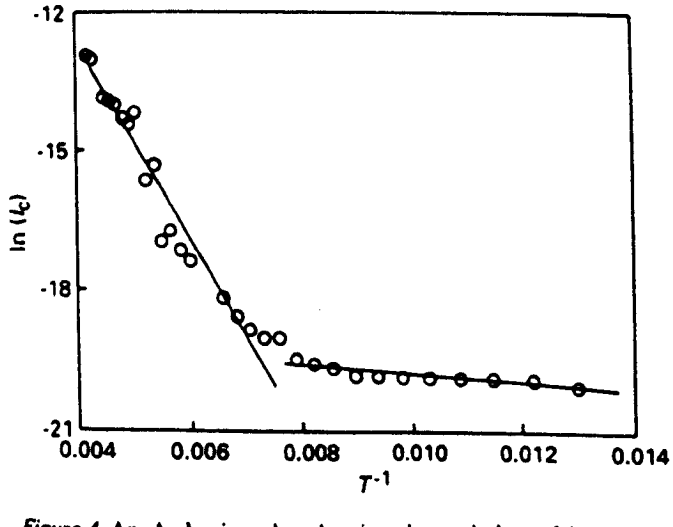

Figure 4 An Arrhenius plot showing the variation of ln I_c as a function of the inverse of temperature, T^{-1}, where I_c is the current (measured in μA) at a bias potential of 50 V.

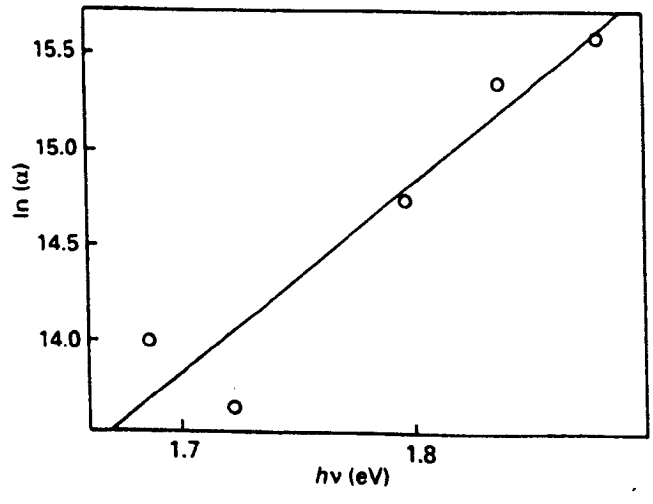

Figure 5 The exponential dependence of the absorption coefficient, α, on the incident photon energy, $h\nu$, for the energy range 1.66 eV $\leq h\nu \leq$ 1.90 eV.

where α_0 and h are constants at a given temperature [14]. The value of Δ is estimated to be 0.10 eV from the gradient of the graph. Although several amorphous semiconductors are known to exhibit a similar law for $\alpha \approx 10^6\ m^{-1}$, very little information is available for Urbach tails in molecular-solid-type materials. Our value for Δ agrees well with a value recently obtained for Langmuir–Blodgett films of substituted copper amphiphilic phthalocyanine molecules [15]. In some analyses, the quantity Δ can be interpreted as the tail widths of localized states in the band gaps, the densities of which are assumed to fall off exponentially with energy [16]. Davis and Mott [17], however, have pointed out that electronic transitions between the states in the band tail are not a plausible proposition in the light of the extremely small variation in the value of Δ between 0.05 and 0.06 eV. X-ray studies show that the molecular structure consists of two nearly parallel phthalocyanine ligands with the metal atom at the centre [18]. It is believed that the van der Waals force between the chemiphores gives rise to the Gaussian distribution of random fields yielding an exponential absorption edge.

At the lower energy range ($h\nu \leq 2.2$ eV), the absorption coefficient α decreases sharply with increasing photon energy. The absorption edge at the higher energy end ($h\nu \geq 2.8$ eV) is believed to be related to an interband transition. For direct band-to-band transitions, the absorption coefficient, α, is given in the form

$$\alpha(\nu) = (B/h\nu)[h\nu - E_0]^x \qquad (4)$$

where E_0 is the optical gap. The coefficient B can be determined from the conductivity of the film. The index x takes on a value of 1/2 for allowed transitions [13]. For the energy range $2.84\ eV \leq h\nu \leq 3.4$ eV, Fig. 6 gives a plot of $(\alpha h\nu)^2$ as a function of the photon energy, $h\nu$. Using the least-squares technique, the best straight line was drawn. From the ratio of intercepts on the ordinate to their respective slopes, the value 2.3 eV was determined for the optical gap, E_0. For a similar energy range, a modified form of Equation 4 was recently used to analyse the optical absorption edge for sublimed films of lead phthalocyanine [11], and a value of 2.4 eV was obtained for E_0.

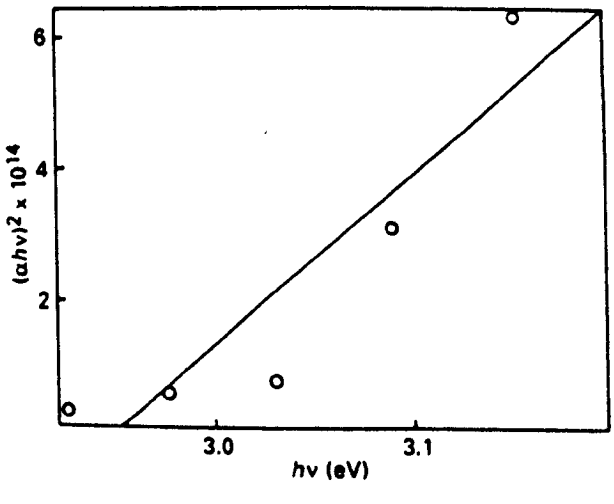

Figure 6 The power-law dependence of the absorption coefficient, α, (measured in units of m^{-1}), on the incident photon energy, $h\nu$, for the energy range of $2.84\ eV \leq h\nu \geq 3.4$ eV.

The optical properties of a bisphthalocyanine film are characterized by its complex refractive index, $N(= n - j\kappa)$, and its complex dielectric constant $\varepsilon^*\ (= \varepsilon_1 - j\varepsilon_2)$.

The extinction constant, κ, is given in the form

$$\kappa = \frac{\alpha\lambda}{4\pi} \qquad (5)$$

where λ is the wavelength. On the other hand, the real part, n, of the refractive index, N, represents the propagation constant and it may be found from the reflectivity, R, of an absorbing medium in air for normal incidence using the expression [19]

$$R = \frac{(n-1)^2 + \kappa^2}{(n+1)^2 + \kappa^2} \qquad (6)$$

The two components, ε_1 and ε_2, of the dielectric constant ε^* are related to n and κ by the following equations

$$\varepsilon_1 = n^2 - \kappa^2, \qquad \varepsilon_2 = 2n\kappa \qquad (7)$$

Using values of the absorption coefficient, α, and the reflectivity, R, from Fig. 2, the components n and κ of the complex refractive index, N, are plotted in Fig. 7 as a function of the photon energy. The variations of the dielectric constant ε^* are shown in Fig. 8. The variation of κ is found to be symbatic with the absorption spectrum. Overall, n increases as the photon energy, $h\nu$, decreases, and it appears to follow the properties indicated by the simple oscillator dispersion model. Peaks in n are observed in the vicinity of the peak absorbance values for the material. The propagation constant, n, falls from the peak value as the photon energy decreases further; it is to be expected that this fall in n on the low-energy side of the peak would be characterized by the Cauchy dispersion formula

$$n = A + \frac{B}{\lambda^2} + \frac{C}{\lambda^4} \qquad (8)$$

where A, B and C are constants peculiar to the

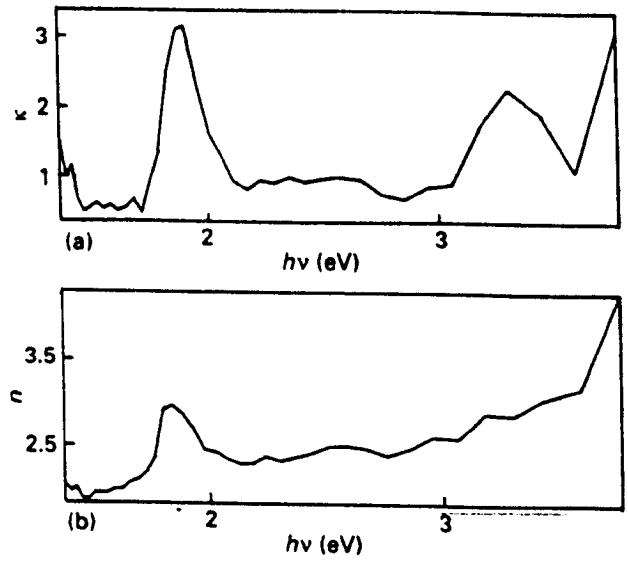

Figure 7 The variations of (a) the extinction coefficient, κ, and (b) the optical propagation constant, n (the real component of the refractive index) with respect to the incident photon energy for the 50 nm [HF(pc)(pc*)] sample.

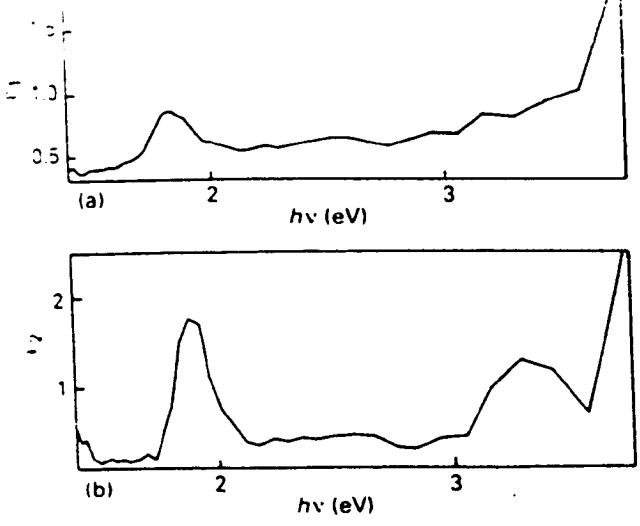

Figure 8 The dependence of both (a) the real component ε_1, and (b) the imaginary component, ε_2, of the dielectric constant, ε, for the 50 nm [HFtpcuPc*] sample.

material. λ is the wavelength at a given photon energy. The values of A, B and C are estimated to be 10.3, -1.05×10^{-11} m^2 and 3.35×10^{-24} m^4.

5. Conclusion

Nearly linear $I(V)$ characteristics were obtained for 50 nm thick samples of rare-earth-element bisphthalocyanine complexes in planar configurations with aluminium electrodes. The activation energy was found to be 0.18 eV and 7 meV at high and low temperatures, respectively; and the excitation to a singlet state below the conduction edge was associated with the conduction process at high temperatures, while the carrier transport between localized states was the dominant mechanism at a low temperature. The increase in the values of the absorption, α, for the range of incident photon energies between 1.66 and 1.9 eV was found to be exponential in the form of an Urbach relation, giving a value of 0.10 eV for the tail width, Δ, of localized states in the band gap. Optical absorption in the range of $2.84\ \text{eV} \leq h\nu \leq 3.4\ \text{eV}$ was, on the other hand, attributed to the allowed band-to-band transitions.

The authors are grateful to their colleagues for their encouragement and fruitful discussions. One of us (JE) thanks the Science and Engineering Research Council, UK for his studentship.

References

1. P. N. MOSKALEV and I. S. KIRIN, *Opt. Spectrosc.* **29** (1970) 220.
2. M. PETTY, D. R. LOVETT and J. M. O'CONNOR, *Thin Solid Films* **179** (1989) 387.
3. Y. LIU, K. SHIGEHARA, M. HARA and A. YAMADA, *J. Amer. Chem. Soc.* **113** (1991) 440.
4. B. LUKAS, D. R. LOVETT and J. SILVER, *Thin Solid Films* **210/211** (1992) 213.
5. J. SILVER, P. LUKES, P. HEY and M. T. AHMET, *J. Mater. Chem.* **2** (1992) 841.
6. J. SILVER, P. LUKES, A. HOULTON, S. HOWE, P. HEY and M. T. AHMET, *ibid.* **2** (1992) 849.
7. Y. LIU, K. SHIGEHARA and A. YAMADA, *Thin Solid Films* **179** (1989) 220.
8. M. L. RODERIGUEZ-MENDEZ, R. AROCA and J. A. DeSAJA, *Chem. Mater.* **4** (1992) 1017.
9. M. J. STILLMAN and T. NYOKONG, in "Phthalocyanines – properties and applications", edited by C. C. Lenznoff and A. P. B. Lever (VCH Publishers, New York, 1989) p. 133.
10. C. S. FRAMPTON, J. N. O'CONNOR, J. PETERSON and J. SILVER, *Displays Tech. Appl.* **9** (1988) 174.
11. R. A. COLLINS, A. KRIER and A. K. ABASS, *Thin Solid Films* **229** (1993) 113.
12. J. SILVER, P. LUKES, S. D. HOWE and B. HOWLIN, *J. Mater. Chem.* **1** (1991) 29.
13. J. SIMON and J. J. ANDRE, "Molecular semiconductors" (Springer Verlag, Berlin, 1984) p. 124.
14. N. F. MOTT and E. A. DAVIS, "Electronic processes in non-crystalline materials" (Clarendon Press, Oxford, 1979) p. 291.
15. A. K. RAY, S. MUKHOPADHYAY and M. J. COOK, *Phys. Status. Solidi (a)*, **134** (1992) k73.
16. J. TAUC, in "The optical properties of solids", edited by F. Abeles (North-Holland, Amsterdam, 1970) p. 277.
17. E. A. DAVIS and N. F. MOTT, *Phil. Mag.* **22** (1970) 903.
18. A. GIEREN and W. HOPPE, *J. Chem. Soc. Chem. Comm.* **8** (1971) 413.
19. T. S. MOSS, G. J. BURRELL and B. ELLIS, "Semiconductor opto-electronics" (Butterworth, London, 1973) p. 10.

Received 9 July
and accepted 27 August 1993